



# **Asphalt Research Consortium**

## **Quarterly Technical Progress Report April 1 – June 30, 2009**

July 2009

Prepared for  
Federal Highway Administration  
Contract No. DTFH61-07-H-00009

By  
Western Research Institute  
Texas A&M University  
University of Wisconsin-Madison  
University of Nevada-Reno  
Advanced Asphalt Technologies

[www.westernresearch.org](http://www.westernresearch.org)  
[www.ARC.unr.edu](http://www.ARC.unr.edu)

# TABLE OF CONTENTS

INTRODUCTION .....	1
GENERAL CONSORTIUM ACTIVITIES .....	3
PROGRAM AREA: MOISTURE DAMAGE.....	5
Category M1: Adhesion.....	5
Category M2: Cohesion .....	23
Category M3: Aggregate Surface .....	40
Category M4: Modeling.....	48
Category M5: Moisture Damage Prediction System .....	53
PROGRAM AREA: FATIGUE.....	57
Category F1: Material and Mixture Properties .....	57
Category F2: Test Method Development.....	87
Category F3: Modeling .....	103
PROGRAM AREA: ENGINEERED MATERIALS.....	127
Category E1: Modeling.....	127
Category E2: Design Guidance.....	165
PROGRAM AREA: VEHICLE-PAVEMENT INTERACTION.....	185
Category VP1: Workshop .....	185
Category VP2: Design Guidance .....	185
Category VP3: Modeling .....	190
PROGRAM AREA: VALIDATION.....	199
Category V1: Field Validation.....	199
Category V2: Accelerated Pavement Testing .....	200
Category V3: R&D Validation .....	201
PROGRAM AREA: TECHNOLOGY DEVELOPMENT.....	217
PROGRAM AREA: TECHNOLOGY TRANSFER.....	219
Category TT1: Outreach and Databases .....	219



## **INTRODUCTION**

This document is the Quarterly Report for the period of April 1 to June 30, 2009 for the Federal Highway Administration (FHWA) Contract DTFH61-07-H-00009, the Asphalt Research Consortium (ARC). The Consortium is coordinated by Western Research Institute with partners Texas A&M University, the University of Wisconsin-Madison, the University of Nevada Reno, and Advanced Asphalt Technologies.

The Quarterly Report is grouped into seven areas, Moisture Damage, Fatigue, Engineered Paving Materials, Vehicle-Pavement Interaction, Validation, Technology Development, and Technology Transfer. The format of the report is based upon the Research Work Plan that is grouped by Work Element and Subtask.

This Quarterly Report summarizes the work accomplishments, data, and analysis for the various Work Elements and Subtasks. This report is being presented in a summary. The Quarter of April 1 to June 30, 2009 is first quarter of the Year 3 contract year. Reviewers may want to reference the Year 3 Work Plan and perhaps the Revised Year 2 Work Plan in order to obtain background information on specific areas of research. The more detailed information about the research such as approaches to test method development, data collection, and analysis will be reported in research publications as part of the deliverables. The Year 3 Work Plan and the Revised Year 2 Work Plan, as well as many other documents are posted on the ARC website, [www.ARC.unr.edu](http://www.ARC.unr.edu). Reviewers may also want to reference the Year 3 Work Plan as some plans have been modified based on research findings to date.

The previous quarterly reports, Year 1, Revised Year 2, and Year 3 Work Plans, and other related documents and information about the Asphalt Research Consortium can be found at the ARC website, [www.ARC.unr.edu](http://www.ARC.unr.edu).

## **SUPPORT OF FHWA AND DOT STRATEGIC GOALS**

The Asphalt Research Consortium research is responsive to the needs of asphalt engineers and technologists, state DOT's, and supports the FHWA Strategic Goals and the Asphalt Pavement Road Map. More specifically, the research reported here supports the Strategic Goals of safety, mobility, and environmental stewardship. By addressing the causes of pavement failure and thus determining methods to improve asphalt pavement durability and longevity, this research will provide the motoring public with increased safety and mobility. The research directed at improved use of recycled asphalt pavement (RAP), warm mix asphalt, and cold mix asphalt supports the Strategic Goal of environmental stewardship.



## **GENERAL CONSORTIUM ACTIVITIES**

### **PROGRESS THIS QUARTER**

A substantial amount of time and effort was spent by Consortium members during the quarter preparing additional information on modeling timelines, relationships of different models, model deliverables, validation efforts, and other material requested as part of the review of the Year 3 Work Plan. The Year 3 Work Plan was submitted to FHWA Co-AOTR's Dr. Jack Youtcheff and Mr. Eric Weaver on January 30, 2009 followed by presentation at the ETG meetings in February 2009, and review by ETG members and FHWA personnel.

ARC members, Dr. Hussain Bahia, Dr. Elie Hajj, and Michael Harnsberger, attended the RAP Expert Task Group meeting in Manchester, New Hampshire on April 22 & 23, 2009 that was being hosted by New Hampshire DOT and the University of New Hampshire. Dr. Hussain Bahia of the University of Wisconsin Madison and Dr. Elie Hajj of the University of Nevada Reno presented an update on the RAP research being conducted by the ARC.

Dr. Peter Sebaaly attended the 7<sup>th</sup> International RILEM Symposium on Advanced Testing and Characterization of Bituminous Materials (ACTBM09) May 27-29, 2009 in Rhodes, Greece and presented an update on the research of the effect of non-standard heavy load vehicles. Dr. Sebaaly also attended the Warm-Mix Asphalt & Recycling Symposium, June 8-10, 2009 in Sacramento, CA.

### **WORK PLANNED FOR NEXT QUARTER**

ARC members will attend the Fundamental Properties & Advanced Models, Binder, and Mix & Construction ETG meetings in San Antonio, Texas in mid-September.



## PROGRAM AREA: MOISTURE DAMAGE

### CATEGORY M1: ADHESION

#### Work Element M1a: Affinity of Asphalt to Aggregate (UWM)

##### Work Done This Quarter

The research team focused on conducting tack test measurements in the Dynamic Shear Rheometer (DSR). Results from the tack test under dry and wet conditions, presented in the previous quarterly report, indicated good repeatability and consistency. The next step in the testing plan was to evaluate the possibility of running tack test measurements using rock disks. This was intended to offer insight into the effect of moisture damage over binder-aggregate bond strength. The results were to be correlated with those from the Bitumen Bond Strength (BBS) tests performed on the new Pneumatic Adhesion Tensile Testing Instrument (PATTI) Quantum Gold<sup>®</sup> instrument.

The tack test is performed using the 8-mm-diameter parallel-plate geometry system in the DSR. Since it is impractical to obtain 8-mm-diameter rock disks, the decision was made to use one 25-mm-diameter rock disk, similar to the rock disks used for the stress sweep test, and one 8-mm-diameter metal plate. One plate is kept to the 8-mm dimension because of the normal force limitation on the testing instrument, which prevents the research team from running tack tests on 25-mm-diameter plates. The metal plate-rock disk system has proved to be successful in other tests such as BBS and stress sweep tests. That data are presented in previous quarterly reports.

##### Significant Results

Samples were conditioned prior to testing for 6 hours, in both dry and wet conditions, at 40 °C. Tests were performed in isothermal conditions, at 24 °C, with a minimum of two replicates.

Table M1a.1. Tack test results for FH neat binder on granite substrate.

	Wet	Run	Tack Factor (N*s)	Average	Standard Deviation	Coefficient of Variation	Testing Temp. (°C)	Maximum Stress (psi)
		FH Neat (Granite)	1	164.52	133.77	43.49	32.5%	24
2	103.02		24	14.4				
FH Neat (Granite)	Dry	1	298.09	296.58	2.14	0.7%	24	31.7
		2	295.06				24	37.5
		3	328.28				24	43.3

Noticeable from table M1a.1 is the high coefficient of variation for the tests performed on the wet-conditioned samples. Similar testing was performed on different binders to eliminate the

possibility that this behavior was related to the type of binder tested. Typical results are shown in table M1a.2. There is no significant difference between the two binders in terms of repeatability of data, which indicates that the binder type has minimal effect on these results and cannot be the cause for the lack of consistency in the data.

Table M1a.2. Tack test results for two neat binders on granite substrate after wet conditioning.

		Run	Tack Factor (N*s)	Average	Standard Deviation	Coefficient of Variation	Testing Temp. (°C)	Maximum Stress (psi)
FH Neat (Granite)	Wet	1	164.52	108.19	40.69	37.6%	24	23.68
		2	67.48				24	18.21
		3	103.02				24	14.4
		4	97.74				24	23.52
CRM Neat (Granite)	Wet	1	190.62	168.41	70.16	41.66%	24	16.94
		2	224.78				24	24.53
		3	89.84				24	17.2

Tackiness tests were conducted at iso-stiffness conditions—varying the testing temperature such that the tested materials have the same stiffness equal to 5 MPa—in an attempt to understand the reason for this inconsistency. Table M1a.3 shows typical results for these tests.

Table M1a.3. Tack test results obtained in iso-stiffness conditions.

		Run	Tack Factor (N*s)	Average	Standard Deviation	Coefficient of Variation	Testing Temp. (°C)
FH Neat (Granite)	Wet	1	199.4	202.9	53.5	26.4%	25
		2	258.0				25
		3	151.2				25
	Dry	1	453.0	435.3	21.2	4.9%	25.4
		2	411.8				25.4
		3	441.1				25.4

Results for the tackiness tests conducted in iso-stiffness conditions show a similar trend with those conducted in isothermal conditions (shown in table M1a.1).

Significant Problems, Issues and Potential Impact on Progress

Data collected from tackiness tests performed after wet conditioning on mineral substrates show great difficulties in obtaining consistent, meaningful results. This could be the result of several factors, including difficulties in trimming an 8-mm-diameter sample on a 25-mm-diameter bottom plate, and moisture damage that is too severe for such a small sample on a mineral

substrate. The research team will look into this further; before the end of the next quarter, the team will decide whether to keep the tackiness test on mineral substrates as part of this work element. Minimal or no delays are expected because of the need for additional tests.

#### Work Planned Next Quarter

Next quarter, the research team will test binders in stress sweep according to the approved testing matrix. Results will be correlated and compared with those obtained from BBS tests in work element M2c. The team will also investigate reasons for the poor repeatability of the tackiness test results on mineral substrates, and make a decision about the future of this test as part of this work plan.

### **Work Element M1b: Work of Adhesion Based on Surface Energy**

#### ***Subtask M1b-1: Surface Free Energy and Micro-Calorimeter Based Measurements for Work of Adhesion (TAMU)***

#### Work Done This Quarter

The main goal of this subtask is to provide material property inputs required in other work elements as required. Any data obtained from this subtask will be included in the material properties database.

#### Work Planned Next Quarter

Work on this subtask will be conducted in conjunction with and as required by other work elements.

#### ***Subtask M1b-2: Work of Adhesion at Nano-Scale using AFM (WRI)***

#### Background

**Lubrication Theory.** Dynamic wetting of asphalt thin-films, which differ for asphalts derived from different crude sources, have recently been investigated based on models derived from lubrication theory. This theory was recently adopted to model the wetting properties of asphalt thin-films prepared by spin coating techniques for the final purpose of imaging and surface energy analyses conducted by atomic force microscopy techniques. Asphalt thin films are conveniently prepared in this fashion by spin casting very small volumes of asphalt-solvent (usually toluene) solutions onto spinning glass microscope slides. Lubrication theory (Emslie et al. 1958; Boatto et al. 1993; Oron et al. 1997; Khomenko and Yushchenko 2003; Diez et al. 2000; Schwartz and Roy 2004; Brenner 1993) may be used to describe the physics of dynamic wetting of a “flat” solid substrate (e.g., a glass microscope in the present case) by a Newtonian fluid (e.g., a dilute asphalt-toluene solution) when modeled in terms of a balance of forces. The system, in the present case, is described by a small volume (usually a couple of microliters) of

asphalt-solvent solution that is deposited onto a spinning glass microscope slide, where the angular velocity of rotation of the glass slide is varied between 300 and 1000 rpm.

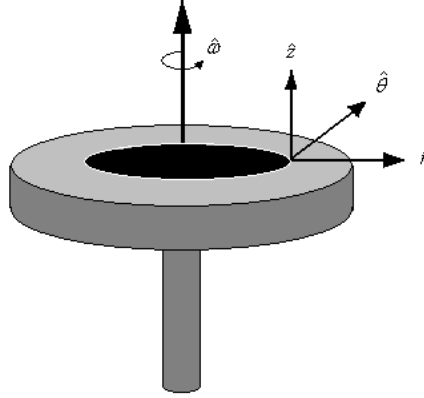


Figure M1b-2.1. Diagram of a wetting film of asphalt, spin cast onto a spinning substrate, defining the cylindrical polar coordinates  $(\hat{r}, \hat{\theta}, \hat{z})$  in vector-component notation, which define the frame of reference of the liquid once deposited on the spinning substrate, spinning at an angular velocity,  $\omega$ , with vector component,  $\hat{\omega}$ .

Emslie et al. (1958) originally proposed that a simple balance of forces between the viscous force of a fluid,  $\eta \nabla_z^2 v$ , as it resists a centrifugal force,  $\rho \omega^2 r$ , describes the process of dynamic contact line wetting of a spinning substrate by a viscous fluid, thus, an energy balance equation may be expressed as

$$0 = \rho \omega^2 r + \eta \frac{\partial^2 v}{\partial z^2} \quad (\text{M1b-2.1})$$

Equation M1b-2.1 is essentially derived from the Navier-Stokes equation for the general case of modeling flow phenomena. Equation M1b-2.1 may be used to evaluate the change in thickness, or height  $h$  of a wetting film, derived as a function of the viscosity,  $\eta$ , density,  $\rho$ , angular velocity,  $\omega$ , with vector component,  $\hat{\omega}$ , and fluid front velocity,  $v$ , in terms of cylindrical polar coordinates,  $(\hat{r}, \hat{\theta}, \hat{z})$ , which define the frame of reference of the liquid once deposited on the spinning substrate, figure M1b-2.1.

The film thickness at any time,  $t$ , may be described by the following expression

$$h(t \rightarrow t_\infty) = \frac{h_0}{\sqrt{1 + \frac{4\rho\omega^2 h_0^2 t}{3\eta}}} \quad (\text{M1b-2.2})$$

as the film approaches its final thickness. This solution has been referred to as the outer product solution, and constitutes an expression for relating changes in angular velocity, viscosity and

initial film thickness ( $h$ -height) to the final thickness of the film,  $h$  (@  $t = \infty$ ). Figure M1b-2.2a depicts a schematic drawing of a thin-film liquid “wave-front” flowing out from the center of a substrate, starting with an initial film thickness of  $h_0$ . This transverse wave of “wetting fluid” is described by a wetting layer spreading out in front of the wave, defined by the wetting height,  $h_w$ , (figure M1b-2.2b).

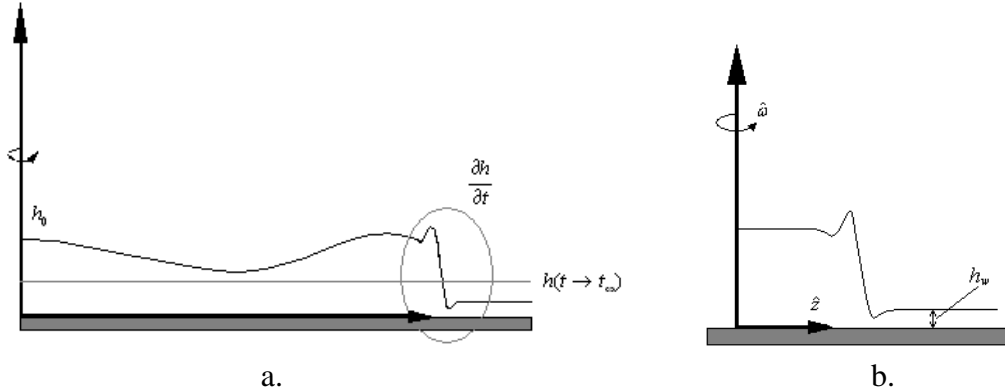


Figure M1b-2.2. Schematic drawing of a thin-film liquid “wave-front” flowing out from the center of a substrate, starting with an initial film thickness of  $h_0$ . b. Schematic drawing of the transverse wave of “wetting fluid” described by a wetting layer spreading out in front of the wave, defined by the wetting height,  $h_w$  [Moriarty et al. 1991].

Since the time of the seminal paper reported by Emslie et al. (1958), dozens of publications have become available expounding on the topic of lubrication theory. To date, most authors agree that additional forces must be accounted for in order to better define the phenomena of the wetting layer associated with the two-phase contact line. Usually these forces include gravitational forces (Frayssé and Homay 1994; Schwartz and Roy 2004; Schwartz 1989; Moriarty et al. 1991; Oron et al. 1997; Dandapat et al. 2003), in the case of spreading drops on inclined planes for example, frictional forces and shear [Yanagisawa 1987; Eres et al. 2000], Laplace pressure (Moriarty et al. 1991; Oron et al. 1997; Wilson et al. 2000; Neto et al. 2003; Dandapat et al. 2003; Schwartz and Roy 2004; Hwang and Ma 1989; Kim et al. 1990, 1992; Eres et al. 2000; Zhang and Lister 1999; Hocking 1992; Spaid and Homay 1996, 1997], which entails surface tension and disjoining pressure terms, in addition to evaporation [Meyerhofer 1978; Stillwagon and Larson 1990; Oron et al. 1997; Middleman 1987; Danov et al. 1998] and temperature effects [Oron et al. 1997; David et al. 1999; Kitamura 2001], all of which influence the physical phenomenon of both Newtonian and non-Newtonian fluids wetting either smooth or rough surfaces. For example, if the Laplace pressure,  $P$ , is taken into account, equation M1b-2.1 may be re-written as

$$0 = \rho\omega^2 r + \eta \frac{\partial^2 v}{\partial z^2} - \frac{\partial P}{\partial r} \quad (\text{M1b-2.3})$$

where the Laplace pressure is defined as the product of the surface tension,  $\gamma$ , of the liquid that is deposited, times the curvature,  $\kappa$ , plus the disjoining pressure,  $\Pi$ , expressed as

$$P = \kappa\gamma + \Pi \quad (\text{M1b-2.4})$$

The curvature may be derived in terms of cylindrical polar coordinates as

$$\kappa = - \left\{ \frac{\partial^2 h}{\partial r^2} + \frac{1}{r} \frac{\partial h}{\partial r} \left[ 1 + \left( \frac{\partial h}{\partial r} \right)^2 \right] \right\} \left[ 1 + \left( \frac{\partial h}{\partial r} \right)^2 \right]^{-3/2} \quad (\text{M1b-2.5})$$

where  $r$  defines the radius of curvature at the contact line interface. For the sake of simplifying the derivation in equation M1b-2.3, and in order to obtain a second equation in the change in thickness, or height,  $h$ , of the film as a function of time, the disjoining pressure term in equation M1b-2.4 may be ignored, and the surface tension is considered to be a constant material property (i.e., the dependence of temperature upon surface tension is taken to be constant if all samples are spun at the same temperature). Equation M1b-2.3 may then be re-written as

$$-\eta \frac{\partial^2 v}{\partial z^2} = \rho \omega^2 r \left( \kappa \frac{\partial}{\partial r} \gamma + \gamma \frac{\partial}{\partial r} \kappa + \frac{\partial}{\partial r} \Pi \right) \quad (\text{M1b-2.6})$$

Hwang and Ma (1989) have shown, by ignoring  $\Pi$ , that equation M1b-2.6 may be derived as

$$\frac{\partial h}{\partial t} = \frac{-1}{3\eta r} \frac{\partial}{\partial r} \left( \rho \omega^2 r^2 h^3 + \gamma r h^3 \frac{\partial}{\partial r} \left( \frac{1}{r} \frac{\partial}{\partial r} \left( r \frac{\partial h}{\partial r} \right) \right) \right) \quad (\text{M1b-2.7})$$

Exhaustive solutions have been proposed, employing the use of dimensionless quantities to arrive at a general solution to equation M1b-2.3, but to date the problem remains essentially unsolved.

**Dynamic Wetting and Observation of Fingering Instabilities.** Figure M1b-2.3 depicts a photographic image of solvent spin cast films “developed” for SHRP core asphalt AAD-1, spin cast at six different speeds (i.e., angular frequency;  $\omega = 300, 400, 500, 600, 700,$  and  $800$  rpm). Figure M1b-2.4 depicts a plot of film thickness (film thickness,  $h$  (nm) determined by a Filmetrics F20 analysis versus angular velocity.

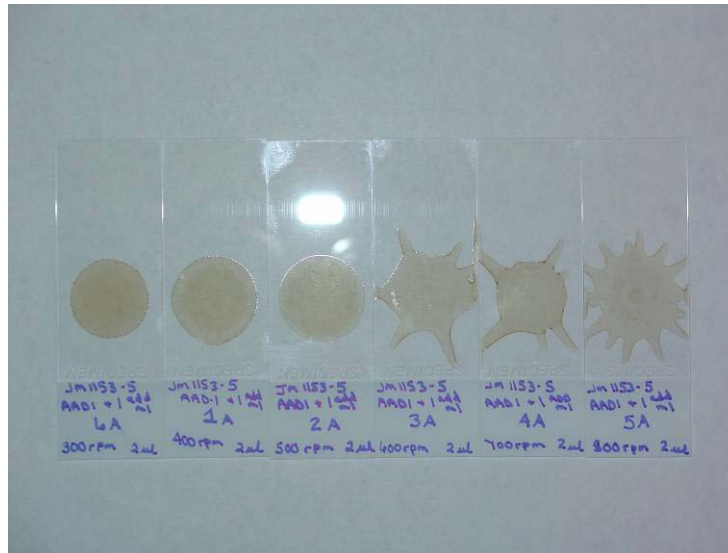


Figure M1b-2.3. Photographic image depicting spin cast films “developed” for SHRP core asphalt AAD-1 spin cast at six different speeds (angular frequency,  $\omega = 300, 400, 500, 600, 700,$  and  $800$  rpm).

It is readily observed in figure M1b-2.3 that as a film is spin cast at increasingly faster speeds, the film becomes less and less uniform (non-circular), and little “fingers” begin to develop at the edges of the film. This phenomenon is referred to as a fingering instability, as will be discussed.

Inspection of equation M1b-2.2 suggests that as the final film thickness is approached, film thickness,  $h$ , is found to be inversely proportional to the viscosity of the fluid that is initially deposited onto a substrate, but is directly proportional to the angular velocity at which the fluid is spun onto the substrate. In other words, if a set of asphalt solutions, given a set of test asphalts which differ significantly by viscosity, are prepared at the same concentration, the highest viscosity materials should be expected to develop into thicker films as compared to less viscous materials. Furthermore, thinner films should be expected to develop for a given material as the material, in solution, is spun at incrementally increasing speeds.

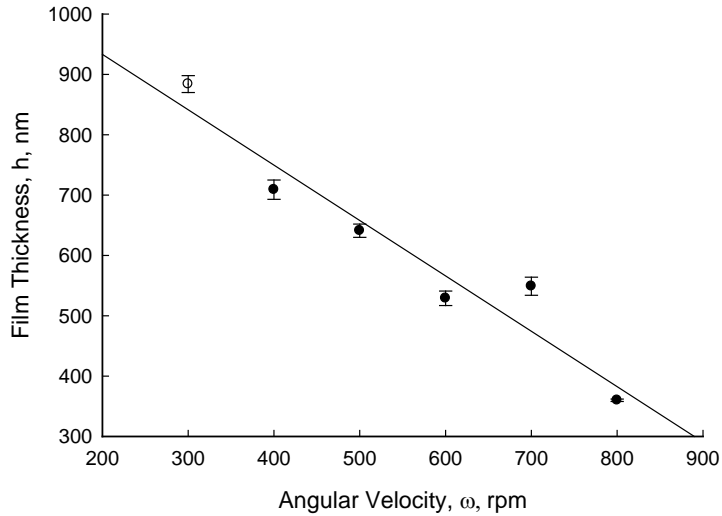


Figure M1b-2.4. Plot of film thickness (film thickness,  $h$  (nm) determined by Filmetrics F20 analysis, versus angular frequency for SHRP asphalt AAD-1, corresponding to photographic images depicting spin cast films “developed” for SHRP core asphalt AAD-1 in figure M1b-2.3.

One important consequence of the lubrication model is the observation of fingering instabilities (figure M1b-2.3). Fingering occurs when the centrifugal force “over powers” the line tension or disjoining pressure forces at the leading edge of the fluid wave-front. When this occurs, the flowing film is observed to “break over the levee”, as it were, at the leading edge of the transverse wave-front of the moving film, effectively spilling out past the front of the film in the form of a “finger”, thus, constituting a fingering instability in the spin-cast film. Fraysse and Homsy (1994) have suggested that a count of the number of fingers,  $N_{finger}$ , produced per film is inversely proportional to the surface tension,  $\gamma$ , of the liquid, according to the following expression

$$N_{finger} \cong \frac{\pi}{7} r_c^2 \left( \frac{\pi \rho \omega^2}{\gamma V_{drop}} \right)^{1/3} \quad (M1b-2.8)$$

In equation M1b-2.8,  $r_c$  is the critical radius of the fluid at the contact line where the fluid wave-front contacts the substrate,  $\rho$ , is the fluid density,  $\omega$  is the angular velocity of the spinning substrate, and  $V_{drop}$ , is the volume of the drop of liquid initially deposited onto the substrate.

### Work Done This Quarter

#### **Spin Casting of MN-Rochester Asphalts and SARA Fractions from Toluene Solutions**

Solutions of neat asphalts, iso-octane soluble maltenes, and polar aromatic SARA fractions, derived from **MN-Rochester** asphalts, were prepared as 1-g/10-mL toluene solutions, and spin cast on glass microscope slides as a function of angular speed (figure M1b-2.5). In figure M1b-2.5, each sample displays a slightly different set of "fingering" patterns, radii, and "tint".

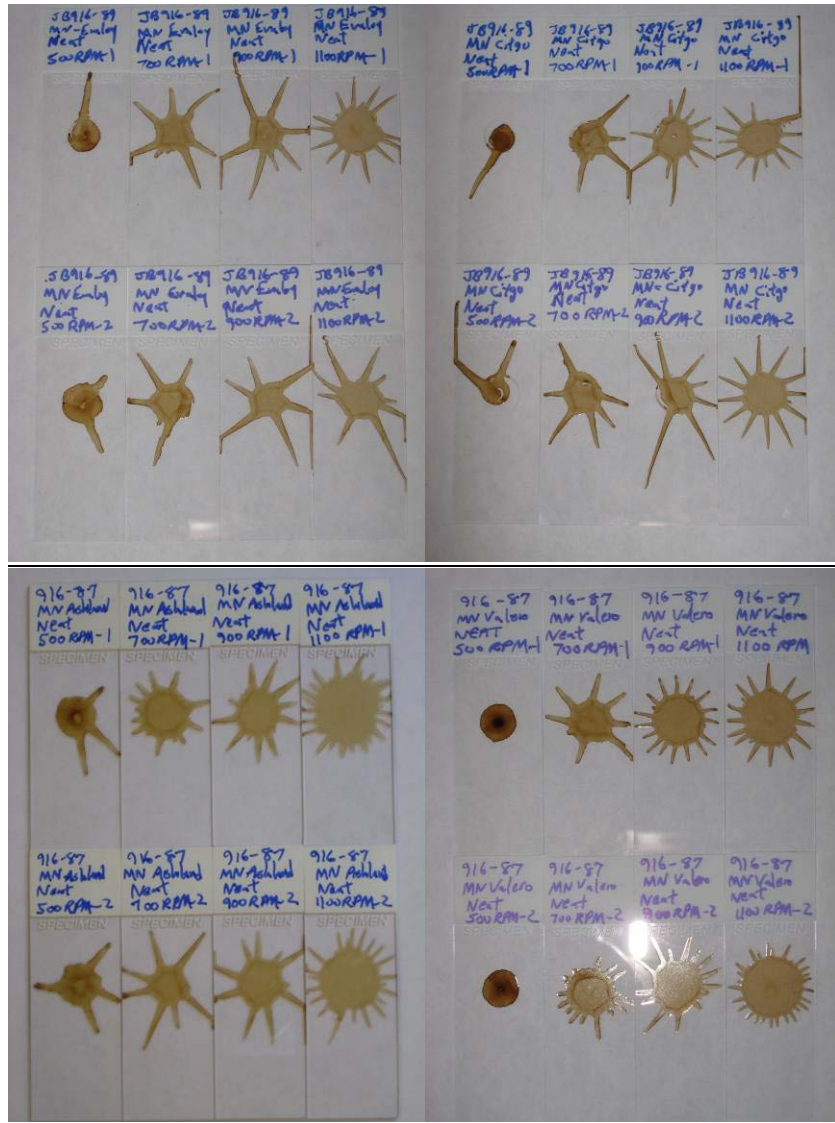


Figure M1b-2.5. Top-to-bottom, L-to-R; Evaloy modified, Citgo, Ashland, and Valero.

Additionally, if an asphalt is fractionated into "chemically-different" classes, SARA fractions for example, more dramatic differences in "film patterns" may be observed. In figure M1b-2.6, for example, notable differences in "fingering" patterns, radii, and "tint" are readily observed.

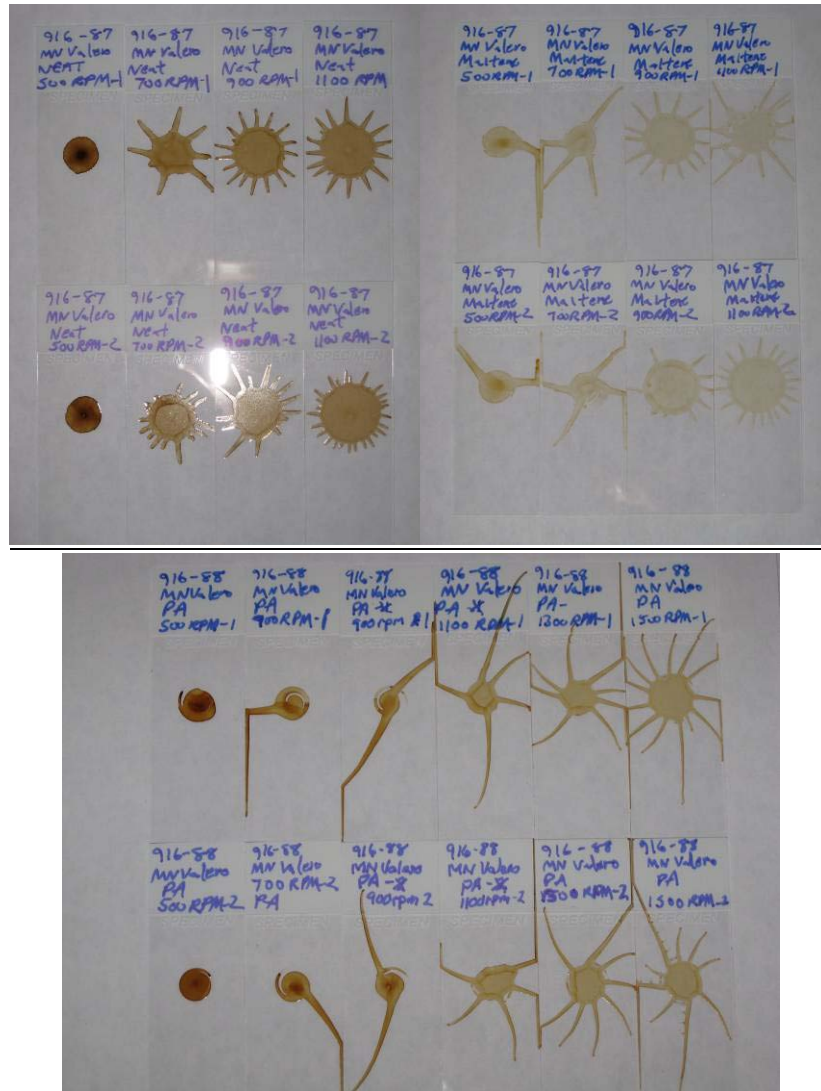


Figure M1b-2.6. Top, L-to-R; Valero, neat asphalt, iso-octane maltenes, SARA-PA's.

In the present case, possibly the most interesting trend in film patterning may be the differences observed between the films prepared with polar aromatic fraction, as compared to the films prepared with neat asphalt and maltene fractions. Here, radial fingering for neat asphalt solutions spun-out at 500, 700, 900 and 1100 rpm's is symmetrical, and the fingers develop "late", resulting in many short fingers. The polar aromatics, by contrast, develop early and produce long, skinny and curved fingers. Furthermore, spin casting of the polar aromatic solutions also requires an increase in angular velocity of 50% to produce a similar number of fingers compared

to the neat material. It is presently unknown which force, whether viscous,  $F_{vis} = \eta \frac{\partial^2 v}{\partial z^2}$  or

capillary,  $F_{cap} = \kappa \frac{\partial}{\partial r} \gamma + \gamma \frac{\partial}{\partial r} \kappa + \frac{\partial}{\partial r} \Pi$ , dominates. In future studies, more painstaking

experiments will be conducted to decouple the wetting forces from viscous forces in systems such as this in order to further study this phenomena.

### Significant Results

None.

### Significant Problems, Issues and Potential Impact on Progress

Manufacturers of high-speed video cameras are presently being contacted to submit cost estimates for this piece of the equipment.

### Work Planned Next Quarter

**Confined-Space Spin Casting Dynamics.** To develop very accurate thin films, Zhang et al., [2005] have suggested that wetting of a substrate within a confined space is given by the following derivation; Given a no slip boundary condition for a film flowing in one direction,

$$v_x = 0 \text{ @ } z = 0,$$

the force balance between viscosity and wetting/disjoining pressure of a wetting film is derived as

$$\eta \frac{\partial^2 v_x}{\partial z^2} = \frac{\partial(p + \Phi)}{\partial x}$$

where

$$\frac{\partial(p + \Phi)}{\partial z} = 0$$

assuming a zero shear at a LV-interface

$$\frac{\partial v_x}{\partial z} = 0 \text{ @ } z = h$$

Thus, with  $h = h(z, t)$  being the local film thickness, the total film pressure may be derived as

$$P = p + \Phi = -\gamma \frac{\partial^2 h}{\partial x^2} + \Pi(h)$$

where the Disjoining Pressure is given as

$$\Pi(h) = \frac{A_H}{12\pi h_3}$$

where  $A_H$  is the Hamaker constant

$$\eta \frac{\partial^2 v_x}{\partial z^2} = \frac{\partial}{\partial x} \left[ -\gamma \frac{\partial^2 h}{\partial x^2} + \frac{A_H}{12\pi h_3} \right]$$

$$\langle v_x \rangle = \frac{1}{h} \int_0^h v_x dz = -\frac{h^2}{3\eta} \left[ -\gamma \frac{\partial^2 h}{\partial x^2} + \frac{A_H}{12\pi h_3} \right]$$

Continuity equations may then be expressed as

$$\frac{\partial h}{\partial t} = -\frac{\partial}{\partial x} (h \langle v_x \rangle)$$

$$\frac{\partial h}{\partial t} = \frac{\partial}{\partial x} \left( \frac{h^3}{3\eta} \left[ -\gamma \frac{\partial^2 h}{\partial x^2} + \frac{A_H}{12\pi h_3} \right] \right)$$

with  $h = h_0$  @  $x = 0$

$$h = h_0$$

A schematic diagram of a confined space wetting process is shown in figure M1b-2.7.

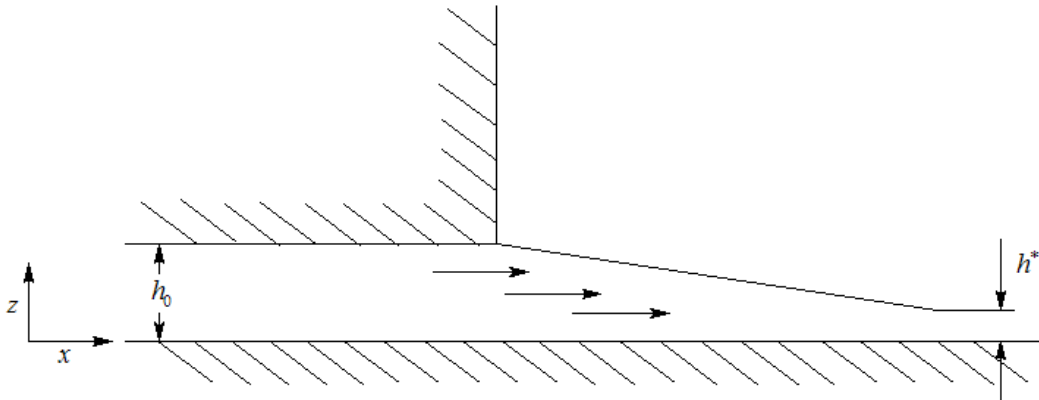


Figure M1b-2.7. Diagram of confinement space pertaining to a dynamic wetting apparatus, used to better control, measure and quantify wetting kinetics of asphalt solutions spin cast on glass slides.

## Test Plan

Tests will be conducted employing a robotic wetting apparatus. Figures M1b-2.8 and M1b-2.9 depict photographs of the present apparatus. A confined space will exist between a precision micro-syringe traveling across the surface of a spinning glass microscope slide as solution is dispensed at nano-droplet precision to derive films of well defined thickness. Experimental variables, such as angular velocity of the spinning slide, the dispensing rate of the solution from the syringe, the confinement distance between the syringe tip and glass slide, the translation rate of the syringe from the center to edge of the slide, and known concentrations and viscosities, will all be considered. The goal will then be to decouple the viscous force from the cohesive and wetting pressure forces when comparing between asphalts which differ by crude source by studying the differences in wetting kinetic phenomena of asphalt chromatographic fractions.



Figure M1b-2.8. Robotic arm, nano-syringe pump, a high speed digital camera demonstration unit, and spin caster.



Figure M1b-2.9. Controllers for robotic arm and nano-syringe pump.

### ***Robotically Controlled Spin Casting Apparatus***

A robotic arm assembly, nano-syringe, and high speed video camera (demo unit) have been assembled for the automated spin casting apparatus and are presently being tested to conduct dynamic wetting experiments. The images displayed in figures M1b-2.10 and M1b-2.11 are high speed video images from the demonstration unit. The high speed images aid in studying the instability of the films as they are cast. Manufacturers of high-speed video cameras are presently being contacted to submit cost estimates for this piece of the equipment.

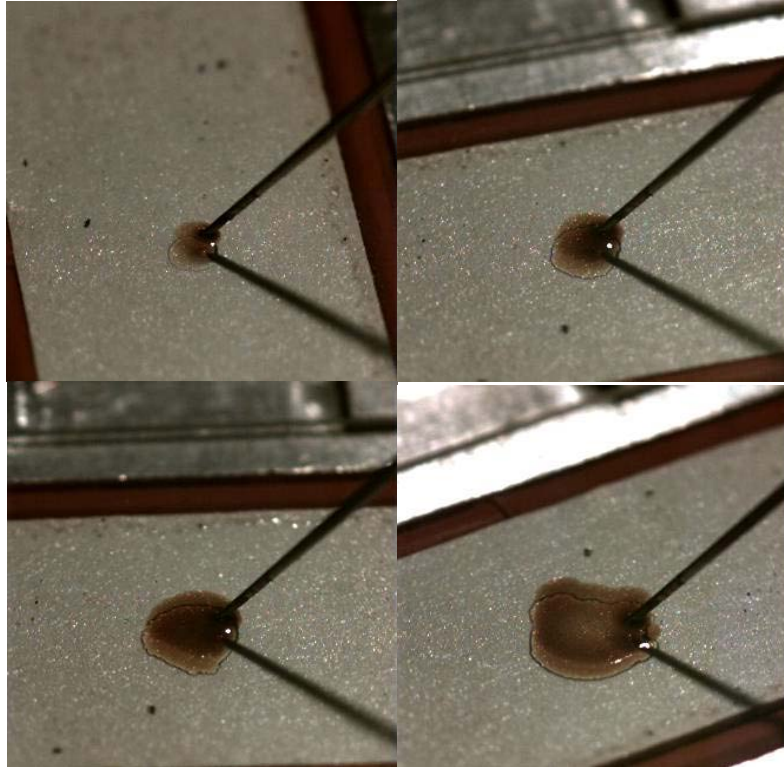


Figure M1b-2.10. High speed video images showing the time lapse of a developing spin cast film as fingering instability develops (early).



Figure M1b-2.10 cont. High speed video images showing the time lapse of a developing spin cast film as fingering instability develops (late).

### References

Boatto, S., L. P. Kadanoff, and P. Olla, 1993, Traveling-wave Solutions to Thin-film Equations. *Physical Review E*, 48(6): 4423-4431.

Brenner, M., 1993, Spreading of Droplets on a Solid Surface. *Physical Review Letters*, 71(4); 593-596.

Dandapat, B. S., P. Daripa, and P. C. Ray, 2003, Asymptotic Study of Film Thinning Process on a Spinning Annular Disk. *Journal of Applied Physics*, 94(6): 4144-4151.

Danov, K. D., N. Alleborn, H. Raszillier, and F. Durst, 1998, The Stability of Evaporating Thin Liquid Films in the Presence of Surfactant. I. Lubrication Approximation and Linear Analysis. *Physics of Fluids*, 10(1): 131-143.

David, M. B., Y. Zvirin, and Y. Zimmels, 1999, Determination of the Quench Velocity and Rewetting Temperature of Hot Surfaces: Formulation of a Nonisothermal Microscale Hydrodynamic Model. *Physical Review E*, 59(6): 6687-6698.

Derjaguin, B. V., V. M. Muller, and Y. P. Toporov, 1975, Effect of Contact Deformations on the Adhesion of Particles. *Journal of Colloid Interface Science*, 50: 314-326.

- Diez, J. A., L. Kondic, and A. Bertozzi, 2000, Global Models for Moving Contact Lines. *Physical Review E*, 63(011208): 1-13.
- Emslie, A. G., F. T. Bonner, and L. G. Peck, 1958, Flow of a Viscous Liquid on a Rotating Disk. *Journal of Applied Physics*, 29(5): 858-861.
- Eres, M. H., L. W. Schwartz, and R. V. Roy, 2000, Fingering Phenomena for Driven Coating Films. *Physics of Fluids*, 12(6): 1278-1295.
- Frayse, N., and G. M. Homsy, 1994, An Experimental Study of Rivulet Instabilities in Centrifugal Spin Coating of Viscous Newtonian and Non-Newtonian Fluids. *Physics of Fluids*, 6(4), 1491-1504.
- Hocking, L. M., 1992, The Influence of Intermolecular Forces on Thin Fluid Layers. *Physics of Fluids A*, 5(4): 793-799.
- Hwang, J. H., and F. Ma, 1989, On the Flow of a Thin Liquid Film Over a Rough Rotating Disk. *Journal of Applied Physics*, 66(1): 388-394.
- Israelachvili, J., 1992, *Intermolecular & Surface Forces*, 2<sup>nd</sup> Ed., Academic Press Limited, Academic Press Inc., San Diego, CA.
- Khomenko, A. V., and O. V. Yushchenko, 2003, Solid-Liquid Transition of Ultrathin Lubricant Film. *Physical Review E*, 68(036110): 1-6.
- Kim, S., J. S. Kim, and F. Ma, 1990, On the Flow of a Thin Liquid Film Over a Rotating Disk. *Journal of Applied Physics*, 69(4): 2593-2601.
- Kim, S., J. S. Kim, and F. Ma, 1992, Topographic Effect of Surface Roughness on Thin-Film Flow. *Journal of Applied Physics*, 72(1): 422-428.
- Kitamura, A., 2001, Thermal Effects on Liquid Film Flow During Spin Coating. *Physics of Fluids*, 13(10): 2788-2794.
- Meyerhofer, D., 1978, Characteristics of Resist Films Produced by Spinning. *Journal of Applied Physics*, 49(7): 3993-3997.
- Middleman, S., 1987, The Effect of Induced Air-Flow on the Spin Coating of Viscous Liquids. *Journal of Applied Physics*, 62(6): 2530-2532.
- Moriarty, J. A., L. W. Schwartz, and E. O. Tuck, 1991, Unsteady Spreading of Thin Liquid Films with Small Surface Tension. *Physics of Fluids A* 3(5): 733-742.
- Neto, C., K. Jacobs, R. Seemann, R. Blossey, J. Becker, and G. Grün, 2003, Correlated Dewetting Patterns in Thin Polystyrene Films. *Journal of Physics: Condensed Matter*, 15: S421-S426.

Oron, A., S. H. Davis, and S. G. Bankoff, 1997, Long-Scale Evolution of Thin Liquid Films. *Reviews of Modern Physics*, 69(3): 931-980.

Schwartz, L. W., 1989, Viscous Flows Down an Inclined Plane: Instability and Fingering Formation. *Physics of Fluids A* 1(3): 443-445.

Schwartz, L. W., and R. V. Roy, 2004, Theoretical and Numerical Results for Spin Coating of Viscous Liquids. *Physics of Fluids*, 16(3): 569-584.

Spaid, M. A., and G. M. Homsy, 1996, Stability of Newtonian and Viscoelastic Dynamic Contact Lines. *Physics of Fluids*, 8(2): 460-478.

Spaid, M. A., and G. M. Homsy, 1997, Stability of Viscoelastic Dynamic Contact Lines: An Experimental Study. *Physics of Fluids*, 9(4): 823-832.

Stillwagon, L. E., and R. G. Larson, 1990, Leveling of Thin Films Over Uneven Substrates During Spin Coating. *Physics of Fluids A* 2(11): 1937-1944.

Wilson, S. K., R. Hunt, and B. R. Duffy, 2000, The Rate of Spreading in Spin Coating. *Journal of Fluid Mechanics*, 413: 65-88.

Yanagisawa, M., 1987, Slip Effect for Thin Liquid Film on a Rotating Disk. *Journal of Applied Physics*, 61(3): 1034-1037.

Zhang, W. W., and J. R. Lister, 1999, Similarity Solutions for van der Waals Rupture of a Thin Film on a Solid Substrate. *Physics of Fluids*, 11(9): 2454-2462.

Zhang X., S. Saritha, and P. Neogi, 2005, Wetting Kinetics of a Thin Film on a Solid Surface Pinned to a Slot. *Ind. Eng. Chem. Res.* 44, 1204-1208.

***Subtask M1b-3: Identify Mechanisms of Competition Between Water and Organic Molecules for Aggregate Surface (TAMU)***

Work Done This Quarter

This sub task is investigating the mechanisms responsible for adhesion and debonding of model organic compounds (representing functional groups in asphalt binder) to minerals and representative aggregates. We are measuring the heat of reactions of the chemical mechanisms using a dual-mode flow adsorption calorimeter. Differences in molar heats of reaction of different organics bonding to the same absorbent are indicative of differences in the bonding strength of each absorbate with the absorbent of interest.

Work during this quarter focused on continued development of the instrument. We are currently conducting studies to validate the ability of the instrument to differentiate between bonding characteristics of materials produced under different conditions. These materials are known to have variable surface properties depending on the temperature of formation and other

environment conditions. Currently we are evaluating the instrument ability to accurately measured changes in surface characteristics as a function of the pH of the aqueous environment.

### Significant Results

There are no significant results for this quarter as we focused on aggregate characterizations.

### Significant Problems, Issues and Potential Impact on Progress

There are no significant issues.

### Work Planned Next Quarter

We plan on initiating flow through experiments to measure the molar heat of reaction of the adhesion of model organic compounds that represent asphalt to minerals and aggregates, as well as the molar heats of reactions of water adsorption to organic-coated minerals and aggregates.

Adhesion will be modeled in the flow-through calorimeter by organic sorption from nonaqueous phase solvents. Experimental variables include the chemistry of the model organic, single versus mixtures of model organics, ionic salt content of the nonaqueous phase solvent, and the surface chemistry of the mineral or aggregate.

Competition of water and the model organics for the mineral or aggregate surfaces will be characterized through flow-through experiments that introduce small amounts of water to the systems created during the adhesion studies above.

## **Work Element M1c: Quantifying Moisture Damage Using DMA (TAMU)**

### Work Done This Quarter

The research team selected one asphalt mixture from Texas to produce a Fine Aggregate Mixture (FAM) for the DMA test. The FAM was produced with and without moisture damage treated agents (lime and anti-stripping agents). The test protocol will include different modes; stress-controlled and strain-controlled at different conditions; dry and wet. This mixture has already been tested using the AASHTO T 283 test. The results from this test are given in table M1c-1 for the full asphalt mixture.

As part of this task, we are working on refining the method for preparing the FAM specimens for DMA testing. The FAM specimens should be properly fabricated to represent the composition and structure of the fine portion of the mixture. Three fine asphalt mixtures produced with different aggregates, and binders are being evaluated. Loose asphalt mixtures are prepared and sieved into different sizes. The ignition oven is then used to determine the percent binder for each size. FAM specimens were fabricated with different percent binders including the one that was determined using the ignition oven. The proposed procedure will correlate the appropriate percent binder with the aggregate gradation and its characteristics. The Aggregate Imaging

Measurement System (AIMS) is used to study the aggregate characteristics; angularity, texture, and form of the aggregates.

Table M1c-1. Performance results using AASHTO T 283 Test.

State		Untreated	Liquid treated	Lime-treated
Texas	Unconditioned Tensile Strength, psi	159	112	155
	Conditioned Tensile Strength, psi	98	112	153
	Tensile Strength Ratio, %	61	100	98

Significant Results

During the second year of the ARC project, a method was developed to prepare FAM specimens and test them in the DMA.

Significant Problems, Issues and Potential Impact on Progress

None

Work Planned Next Quarter

The FAM specimen preparation and mixture design protocol will be completed and the DMA tests will be in progress.

**CATEGORY M2: COHESION**

**Work Element M2a: Work of Cohesion Based on Surface Energy**

*Subtask M2a-1: Methods to Determine Surface Free Energy of Saturated Asphalt Binders (TAMU)*

Work Done This Quarter

No activity was planned for this quarter.

Work Planned Next Quarter

Work on this task is anticipated to start in year 4 of the project.

## ***Subtask M2a-2: Work of Cohesion Measured at Nano-Scale using AFM (WRI)***

### Work Done This Quarter

A nano-positioning stage has been installed and tested with the existing AFM equipment. This accessory allows for independent movement of both cantilever and sample for conducting metrology experiments including nano-rheology and nano-indentation.

### Significant Results

None.

### Significant Problems, Issues and Potential Impact on Progress

A vacuum chamber with inert gas purge will be assembled around the AFM system to control environment conditions, specifically to reduce water condensation on sample films and cantilever during cooling down of samples to sub-zero temperatures..

### Work Planned Next Quarter

It is well established, at least in brittle fracture, that the stress to form a crack is given as

$$\sigma = \sqrt{\frac{2\gamma E}{\pi a_c}} \quad (\text{M2a-2.1})$$

given the work of cohesion,  $W = 2\gamma$ , crack length,  $a_c$ , and Young's modulus,  $E = \sigma / \epsilon$ . If on the other hand it is assumed that plastic deformation occurs in the material, which could account for dissipation of energy at the crack tip, equation M2a-2.1 may be re-written as

$$\sigma = \sqrt{\frac{\mathcal{G}_c E}{\pi a_c}} \quad (\text{M2a-2.2})$$

where

$$\mathcal{G}_c = W + \mathcal{G}_p \quad (\text{M2a-2.3})$$

$\mathcal{G}_c$  is then referred to as the critical strain energy, which is expressed as a sum of both the surface energy term,  $W = 2\gamma$ , and a plastic deformation energy term  $\mathcal{G}_p$ . Thus, in materials which exhibit ductility,  $\mathcal{G}_p$  could be observed to be orders of magnitude greater than  $W$ .

In asphalt pavements as the asphalt approaches colder temperatures, near the glass transition temperature of the asphalt for example,  $W = 2\gamma$  increases to some maximum surface energy, while at the same time  $\mathcal{G}_p$  decreases, possibly low enough to be of the same order of magnitude

as the surface energy, where the asphalt film would most likely shows its greatest tendency to fracture. Conversely, as the temperature of a pavement is increased, equation M2a-2.2 becomes more relevant, given the increasing potential for the material to relax due to the lowering of the viscosity. At this point, the asphalt film is expected to soften, and become tacky.

Hence, it may be possible to study a ductile-brittle transition (temperature) in asphalt thin film specimens by employing a coupled “temperature-dependent” nanoindentation/pull-off adhesion force experiment. In this test procedure, a spin cast asphalt film (1-5 micrometers thick), which is thermally annealed prior to testing, is cooled to sub-ambient temperatures followed by hardness testing with nanoindentation. This is then followed by a pull-off of the cantilever tip from the film surface. In this case, it is anticipated that the indent hole will be well defined in shape (i.e., relative to the shape of the indentation tip), where only a small capillary pull-off force would be detected. It is then anticipated that as the temperature of the asphalt film is increased, indentation forces will decrease and the indent hole will become "less" well defined in shape, where the pull-off adhesion force is expected to increase. Thus, by conducting this type of test as a function of temperature, a transition temperature may be defined at which the adhesion “pull-off” force "crosses" or approaches that of the indent force.

### Theory

#### *Force-Distance AFM Microscopy (Pull-off Capillary Adhesion Force Measurements)*

In fundamental contact mechanics models, contact between two surfaces is often described by a frictionless interaction between a spherical surface brought into contact with a flat surface, followed by a pull-away of the two surfaces by a Hertzian load ( $P_{Hertz}$ ) (Shull 2002). A Hertzian contact load, in turn, is defined in terms of the reduced bulk modulus,  $E^*$ , the contact area,  $a^3$ , and the radius of curvature of the contacting surfaces,  $R$ , as

$$P_{Hertz} = \frac{4E^* a^3}{3R} \quad (M2a-2.4)$$

The contact displacement (figure M2a-2.1) is then defined in terms of the contact radius  $a$ , as

$$\delta_{hertz} = \frac{a^2}{R} \quad (M2a-2.5)$$

where the radius of curvature is defined in terms of the radii of both surfaces (1-spherical tip, 2-flat surface) as

$$\frac{1}{R} = \frac{1}{R_1} + \frac{1}{(R_2 \rightarrow \infty)} \rightarrow \frac{1}{R_1} \quad (M2a-2.6)$$

where the reduced bulk modulus is defined for both surfaces as

$$\frac{1}{E^*} = \frac{(1-\nu_1^2)}{E_1} + \frac{(1-\nu_2^2)}{E_2} \quad (M2a-2.7)$$

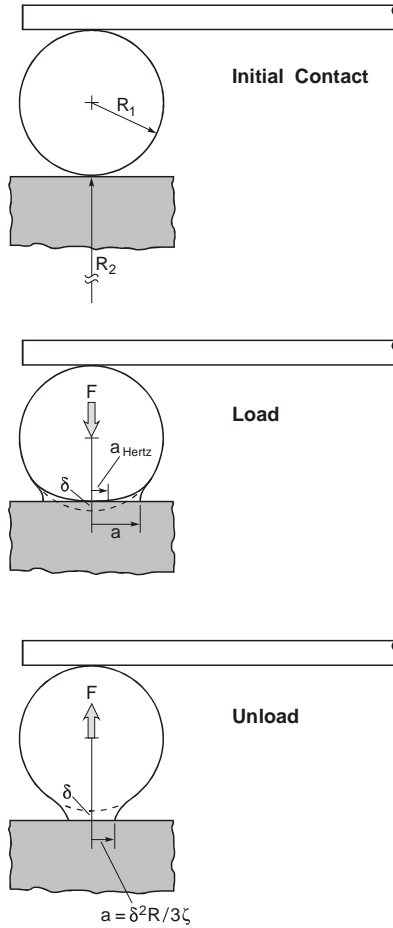


Figure M2a-2.1. Depiction of contact between a glass micro-bead cantilever tip and a glass slide surface during loading and unloading of the system.

Here,  $\nu_i$ 's are values of Poisson's ratio, and  $E_i$ 's are values of Young's modulus. The fracture energy release rate,  $G$ , may then be derived as

$$G = \frac{\left( \frac{4E^* a^3}{3R} - P \right)^2}{8\pi E^* a^3} = \frac{(P_{Hertz} - P)^2}{8\pi E^* a^3} = W_{12} \quad (\text{M2a-2.8})$$

and is shown to approximate the work of adhesion of the system.  $P_{Hertz}$  and  $P$  are the frictionless load and the actual applied load, respectively. The fracture energy release rate is equivalent to the work of adhesion in this case since the surfaces are at the point of separation, or "cracking." The work of adhesion is then simply twice the surface energy.

With viscoelastic materials where the stiffness of one or the other or both of the surfaces are shear rate and temperature dependent, the contact area that is measured may result in a transition in the contact area corresponding to either the JKR or DMT model in order to interpret the actual work of adhesion. It is then assumed that the load,  $P$ , approaches zero at a contact corresponding to the equilibrium work of adhesion, where equation M2a-2.8 may then be solved for in terms of the bulk modulus to find that a limiting contact area (Carpick et al. 1999),  $A = l/\zeta$ , exists, where

$$E^* = \frac{9\pi\gamma_{12}a}{\delta^2} \quad (\text{M2a-2.9})$$

and where

$$\frac{1}{\zeta} = A \quad (\text{M2a-2.10})$$

Depending on the compliance of the two surfaces (i.e., rigid sphere contacting rigid flat surface, rigid sphere contacting deformable flat surface, deformable sphere contacting rigid flat surface, deformable sphere contacting deformable flat surface), different models will apply. The JKR-load limit corresponds to contact between compliant surfaces where weak adhesive forces, and a high radius of curvature exists,

$$P_{JKR} = \lim_{\zeta \rightarrow 3a/\delta^2 R} \frac{E^*}{\zeta} = 3\pi\gamma_{12}R \quad (\text{M2a-2.11})$$

and the DMT-load limit corresponds to contact between stiff surfaces where strong adhesive forces, and a lower radius of curvature exist,

$$P_{DMT} = \lim_{\zeta \rightarrow 9a/4\delta^2 R} \frac{E^*}{\zeta} = 4\pi\gamma_{12}R \quad (\text{M2a-2.12})$$

AFM “pull-off” force measurements are conducted when a cantilever tip is retracted, after initially contacting the surface of a sample thin-film, when enough stress is applied which exceeds the adhesive/cohesive strength of the contact and the joint (contact between the cantilever-tip and sample) fails, and constitutes a measure of the work of adhesion of the system. In addition to providing a measure of the work of adhesion, analysis of the shapes of the various sections of the force curves potentially reveal a great deal about the mechanical properties of the material at the microscopic, and nanoscopic level. Figure M2a-2.2 depicts a typical force curve with labeled force regions.

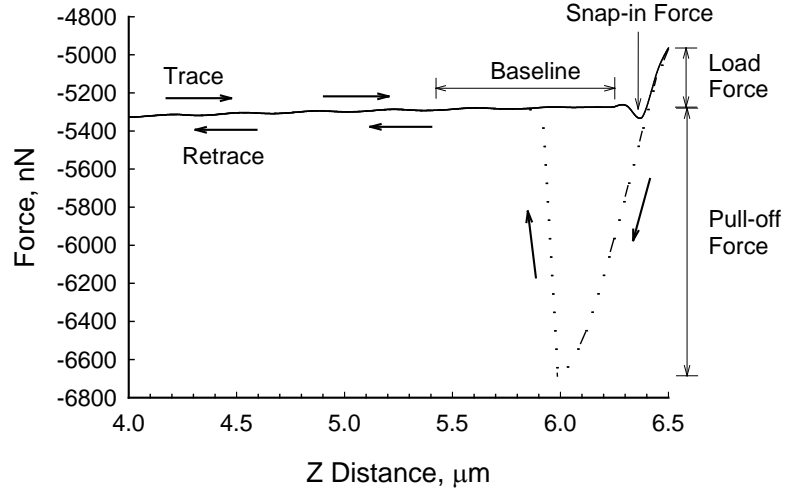


Figure M2a-2.2. Force curve plot depicting the applied load force, the snap-in force, the pull-off-force, and the baseline.

### ***Nanoindentation Measurements***

In contrast to pull-off force measurements, nanoindentation experiments measure the stiffness and creep relaxation properties of thin-films. (Bhushan 2005; Fisher-Cripps 2004; Geng et al. 2005; Huang and Lu 2006; Liu et al. 2006; Zhou and Komvopoulos 2006). In nanoindentation (i.e., nano-penetration testing) a small cantilever-indenter is loaded,  $P$ , into the surface of a material thin film coating at a constant loading rate, quantitatively expressed as

$$\frac{dP}{dt} = \frac{P_{\max}}{t_{\text{unload}}} \quad (\text{M2a-2.13})$$

so that the maximum load,  $P_{\max}$ , is defined at the unloading time,  $t_{\text{unload}}$ , (Figures M2a-2.3 and M2a-2.4).

The stiffness,  $\mathcal{S}(h_{\max})$ , at maximum contact depth,  $h_{\max}$  is then derived as

$$\mathcal{S}(h_{\max}) = \frac{dP(h = h_{\max})}{dh} = \frac{2}{\sqrt{\pi}} E_r \sqrt{A_c(h_{\max})} \quad (\text{M2a-2.14})$$

where

$$\frac{1}{E_r} = \frac{1 - (\nu_{\text{sample}})^2}{E_{\text{sample}}} + \frac{1 - (\nu_{\text{tip}})^2}{E_{\text{tip}}} \quad (\text{M2a-2.15})$$

is a reduced modulus, derived based on the bulk modulus and Poisson's ratio of both the sample and tip, and  $A_c$  is the indentation area. The Oliver-Pharr equation,

$$P = b(h - h_f)^m \quad (\text{M2a-2.16})$$

may then be conveniently used to evaluate load-displacement curves, as depicted in Figure M2a-2.3 derived from experiment. Here,  $h_f$  is the final position of the cantilever just after unloading.

The contact depth,  $h_c$ , is then calculated as

$$h_c = h_{\max} - \varepsilon \frac{P_{\max}}{\mathcal{S}} \quad (\text{M2a-2.17})$$

given that the contact stiffness is derived as

$$\mathcal{S} = \frac{dP(h = h_{\max})}{dh} = mb(h_{\max} - h_f)^{m-1} \quad (\text{M2a-2.17})$$

with fitting parameters  $\varepsilon$ ,  $m$  and  $b$ .

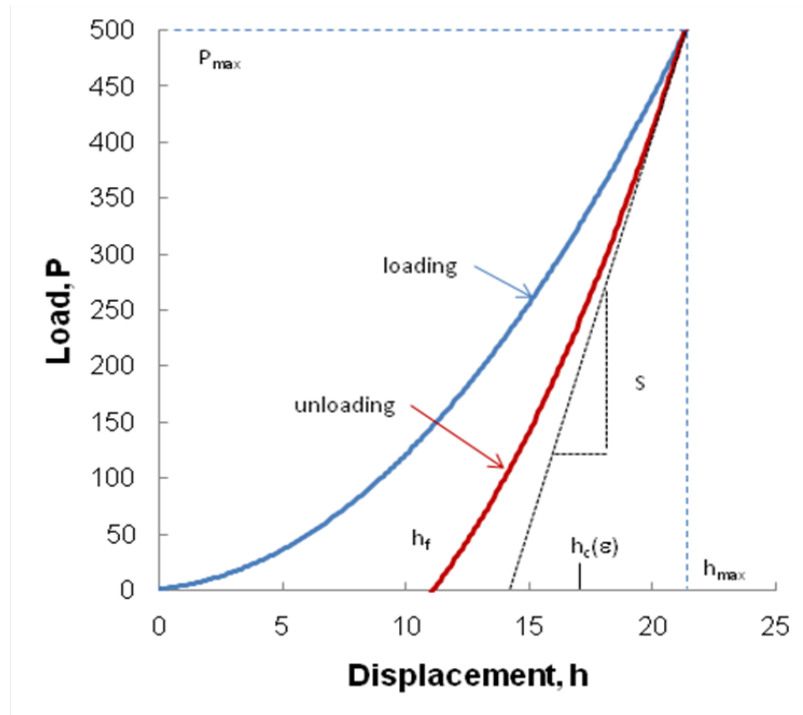


Figure M2a-2.3. Load-versus-indentation depth plot.

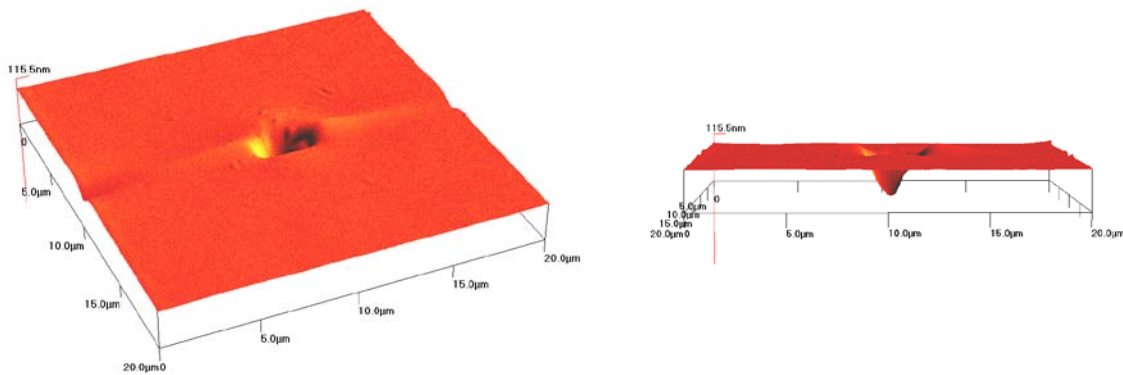


Figure M2a-2.4. AFM (WaveMode) images of a nano-indentation "hole".

### Test Plan

Asphalt films, 1-5 micrometers in thickness, will be prepared on glass substrates via solvent spin casting followed by thermal annealing in an inert gas atmosphere. Samples will then be tested by conducting rate and temperature dependent nano-indentations, followed directly by a pull-off action to record penetration depth, from which hardness and adhesion-capillarity interactions with the film are calculated. Indentation cantilevers will be selected based on reported stiffness's of asphalts at very cold temperatures increasing to near ambient conditions. Tests will be run by starting at a low temperature and increasing the temperature of the film until a transition is observed. Thus, the change in stiffness transitioning to “stickiness” will be evaluated to determine the temperature (range) at which these transitions take place as a function of crude source. In addition, tests will be performed at different locations on the surface of the film where notable differences in the surface morphology are subsequently observed. In this since, a stiffness map of the surface of the film will also be obtained. Correlations will then be sought to compare between the data gathered from these tests and rheological and mechanical test data related to stiffness (relaxation), fracture temperature and healing rates.

### References

- Bhushan, B., 2005, *Nanotribology and Nanomechanics An Introduction*, Springer-Verlag, Germany.
- Buxton, G. A., and A. C. Balazs, 2004, Modeling of Dynamic Fracture of Polymer Blends Processed Under Shear. *Phys. Rev. B.*, 69, 054101.
- Carpick, R. W., D. F. Ogletree, and M. Salmeron, 1999, A General Equation for Fitting Contact Area and Friction vs Load Measurements. *Journal of Colloid and Interface Science*, 211: 395-400.
- Fisher-Cripps, A. C., 2004, A Phenomenological Approach to Nanoindentation Creep. *Mater. Sci. Eng A*, 385, 74-82.

Geng, K., F. Yang, T. Druffel, and E. A. Grulke, 2005, Nanoindentation Behavior of Ultrathin Polymeric Films. *Polymer*, 46, 11768-11772.

Huang, G., and H. Lu, 2006, Measurements of Young's Relaxation Modulus Using Nanoindentation. *Mech. Time-Depend Mater*, 10, 229-243.

Liu, C-K, S. Lee, L-P Sung, and T. Nguyen, 2006, Load-Displacement Relations for Nanoindentation of Viscoelastic Materials. *J. Appl. Phys.*, 100, (033503)1-9.

Shull, K. R., 2002, Contact Mechanics and the Adhesion of Soft Solids. *Materials Science and Engineering R.*, 36: 1.

Zhou, J., and K. Komvopoulos, 2006, Surface and Interface Viscoelastic Behaviors of Thin Polymer films investigated by Nanoindentation. *J. Appl. Phys.*, 100 (114329): 1-8.

## **Work Element M2b: Impact of Moisture Diffusion in Asphalt Mixtures**

### ***Subtask M2b-1: Measurements of Diffusion in Asphalt Mixtures (TAMU)***

#### Work Done This Quarter

Tests related to the measurement of moisture diffusion and hysteretic effect of moisture diffusivity has been completed using the FTIR. Three different asphalt binders were included in this study. Researchers are currently completing the remaining tests and analyzing the information. An outline of the key findings expected from this subtask is described in the sections below.

#### Significant Results

Significant results will be reported after the complete data set of results is available.

#### Work Planned Next Quarter

The work planned for next quarter is to complete any remaining tests and analysis pertaining to this subtask. We anticipate completing the tests, analysis and reporting all findings pertaining to this sub task within the next two quarters. An outline of the key findings expected from this subtask is presented below:

1. Measurement of diffusivity of water through thin films of asphalt binder using FTIR: This section will include a detailed description of the test procedure used to measure diffusivity of asphalt binders using FTIR. The procedure will include methods for sample preparation, collecting data and the approaches used to analyze the resulting data. Results will be compared to diffusivity measured for similar materials.
2. Gravimetric measurement of diffusivity of water through sand-asphalt specimens: This section will include an analysis of gravimetric measurement of diffusivity of water through sand-asphalt mixtures. These gravimetric measurements were carried out for

different combinations of binder and fine aggregates subjected to moisture diffusion for a period of up to 21 months under two different temperatures. The data will also demonstrate how moisture diffusion is accelerated under elevated temperatures. The data will also explain the gap between moisture transport through air voids versus moisture diffusion through thin films of asphalt binder.

3. Hysteretic effect of moisture diffusion in binder films: This section will demonstrate the hysteretic effect of moisture diffusion through thin films of asphalt binder. Moisture diffusion through binder is a very slow process and it can take several hours for dry thin films to be fully saturated. Such prolonged durations of exposure to moisture are rarely possible in the field. Tests on asphalt binders with cyclic wetting and drying demonstrate higher rates of moisture diffusion after the first wet-dry cycle.
4. Transport of moisture versus water: This section will discuss, with experimental data, the difference between transport of water vapor versus transport of liquid water through films of asphalt binder. Different researchers have used the term moisture and water transport and diffusion interchangeably. Some of the recent results based on the FTIR were used to distinguish between these two processes.

### ***Subtask M2b-2: Kinetics of Debonding at the Binder-Aggregate Interface (TAMU)***

#### Work Done This Quarter

Most of the work accomplished under subtask M2b-1 also directly relates to this subtask. The most significant difference in this subtask is that a portion of the binder-ATR window interface will be purposefully exposed to be in direct contact with the water. This will allow the water to diffuse through the film as well as propagate along the binder-ATR window interface.

#### Work Planned Next Quarter

Researchers plan to continue work with emphasis on M2b-1 before addressing the specifics of this subtask.

### **Work Element M2c: Measuring Thin Film Cohesion and Adhesion Using the PATTI Test and the DSR (UWM)**

#### Work Done This Quarter

The research team phased out the old Pneumatic Adhesion Tensile Testing Instrument (PATTI) device and shifted all testing to the new PATTI Quantum Gold<sup>®</sup> instrument. The second unit was shipped to the University of Stellenbosch, South Africa. Before shipping the second unit, both machines were tested at the University of Wisconsin–Madison and upgraded as follows:

- Reference marks have been added around the pressure rate control knob to help with the reproducibility of testing.

- The data acquisition software was upgraded to include custom pullout stub sizes like the one developed at UW–Madison (20-mm diameter; 0.4mm film thickness).
- The data acquisition software was upgraded to include the option of saving the raw data collected in a spreadsheet format.

The research team investigated the influence of factors such as pressure increase speed, testing surface, binder modification, and water conditioning time and temperature on test results.

### Significant Results

With the old PATTI instrument, film thickness was controlled by using 12.5-mm modified stubs to have a film thickness of 0.4 mm; an 8-mm trimmed mold was used to ensure that the same amount of binder was used in every sample. The rate of deformation proved to be very difficult to control for the old PATTI instrument. Since the pressure rate is much more controllable with the new PATTI device (PQ Gold), it was used to study the effect of two different rates of deformation for neat and modified binders.

Figures M2c.1 and M2c.2 show examples of neat binders tested at rate 3 (approximately 230 psi/s) in dry and wet conditions. Figures M2c.3 and M2c.4 show the same results collected at rate 5 (approximately 530 psi/s).

The results indicate that the PQ Gold device seems to allow for a consistent and repeatable rate of deformation, as proven by the percent coefficient of variation. The shape of the plots in figures M2c.1 through M2c.4 indicates that the research team's testing is obtaining very consistent pressure rate increases, in a linear fashion, as expected. The area under the curves—the Bitumen Bond Strength (BBS) factor—is representative of the energy needed to drive the material to failure, and shows good consistency and repeatability.

Tables M2c.1 and M2c.2 list the results for neat and modified binders at various rates in dry and wet conditions.

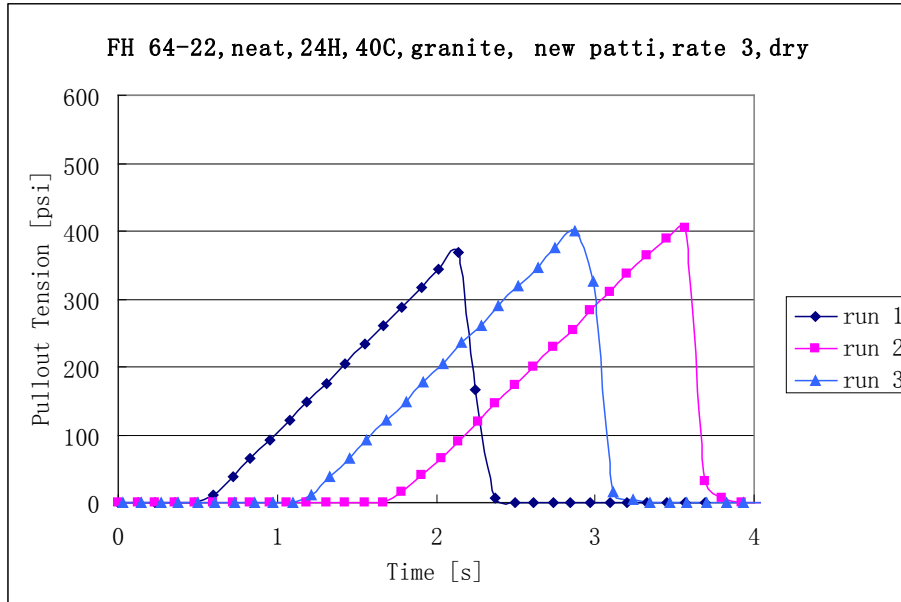


Figure M2c.1. Graph. BBS test results for FH PG 64-22 neat binder in dry conditions, on granite, during a 24-hour conditioning test at rate 3.

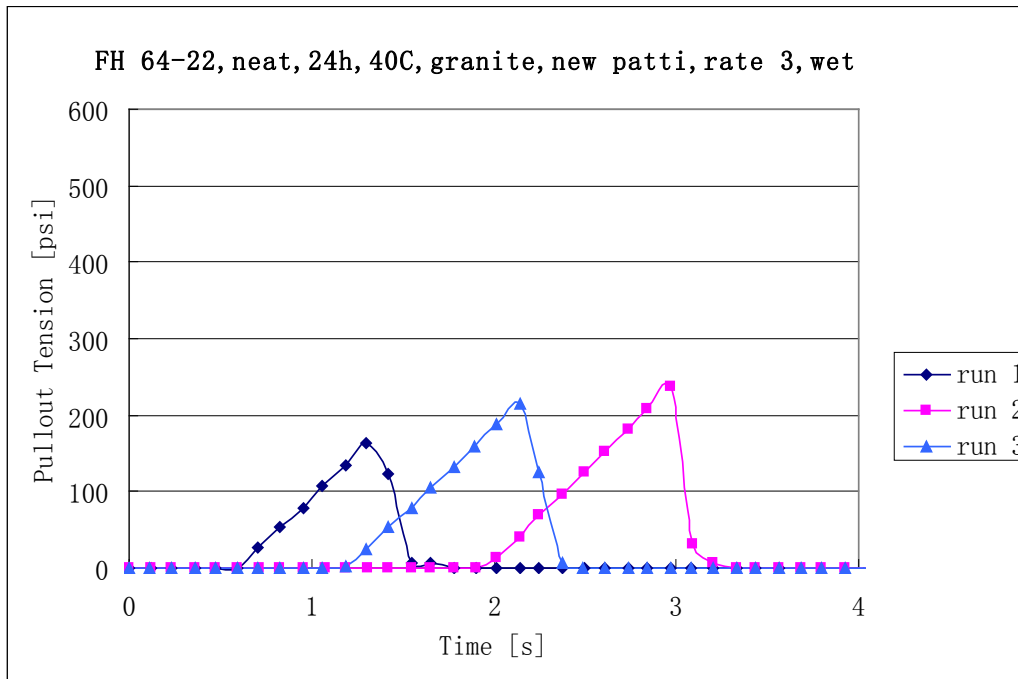


Figure M2c.2. Graph. BBS test results for FH PG 64-22 neat binder in wet conditions, on granite, during a 24-hour conditioning test at rate 3.

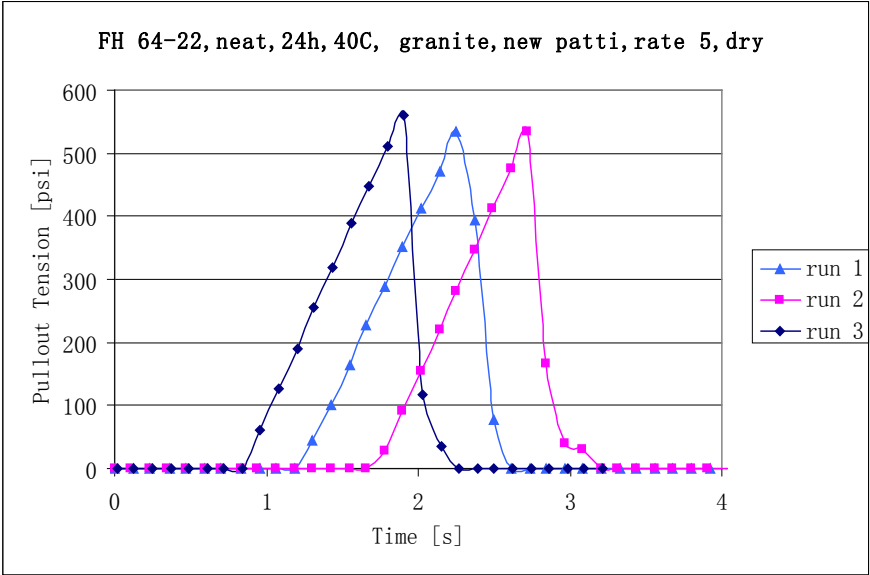


Figure M2c.3. Graph. BBS test results for FH PG 64-22 neat binder in dry conditions, on granite, during a 24-hour conditioning test at rate 5.

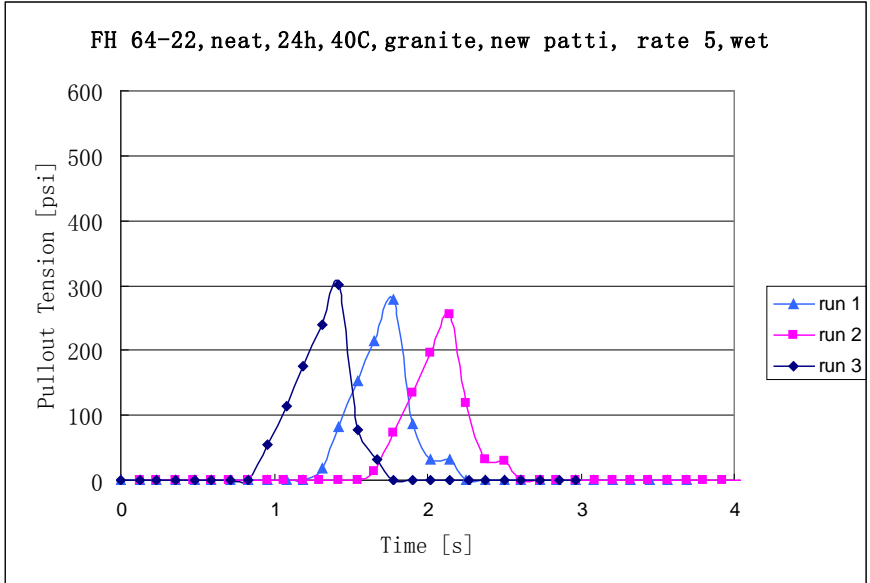


Figure M2c.4. Graph. BBS test results for FH PG 64-22 neat binder in wet conditions, on granite, during a 24-hour conditioning test at rate 5.

Table M2c.1 Summary of BBS test results for neat binders at rate 3.

Rate 3	Run		Temp (°C)		Failure Type	BBS Factor (psi*s)	Max Pullout Tension (psi)	Pullout Rate (psi/s)
FH neat	Granite	Dry	1	25.4	100% C	327.83	367.58	236.31
			2	25.3	100% C	407.73	404.62	228.88
			3	25.1	100% C	368.48	400.72	237.4
			average			368.0	391.0	234.2
			standard deviation			40.0	20.4	4.6
			% coefficient of variation			10.9%	5.2%	2.0%
	Granite	Wet	1	24.7	98% a, 2% c	73.8	163.85	231.1
			2	24.4	60% a, 40% c	136.0	236.96	235.83
			3	24.4	90% a, 10% c	121.3	214.54	224.64
			average			110.4	205.1	230.5
			standard deviation			32.5	37.5	5.6
			% coefficient of variation			29.5%	18.3%	2.4%
CRM neat	Granite	Dry	1	25.6	100% C	168.5	258.4	233.74
			2	25.4	100% C	171.9	259.38	234.15
			3	25.3	100% C	207.79	288.62	232.39
			average			182.7	268.8	233.4
			standard deviation			21.8	17.2	0.9
			% coefficient of variation			11.9%	6.4%	0.4%
	Granite	Wet	1	24.8	98% a, 2% c	151.78	244.76	223.07
			2	24.8	98% a, 2% c	155.2	249.63	228.71
			3	24.8	98% a, 2% c	143.56	238.91	234.09
			average			150.2	244.4	228.6
			standard deviation			6.0	5.4	5.5
			% coefficient of variation			4.0%	2.2%	2.4%

Table M2c.2. Summary of BBS test results for neat binders at rate 5.

Rate 5	Run		Temp (°C)		Failure Type	BBS Factor (psi*s)	Max Pullout Tension (psi)	Pullout Rate (psi/s)
FH neat	Granite	Dry	1	25.2	100%C	333.68	534.27	516.35
			2	25.1	100%C	309.46	533.3	540.71
			3	25.1	100%C	349.01	560.59	542.37
			average			330.7	542.7	533.1
			standard deviation			19.9	15.5	14.6
			% coefficient of variation			6.0%	2.9%	2.7%
	Granite	Wet	1	24.8	60%a,40%c	94.13	277.9	550.88
			2	24.5	80%a,20C	87.37	256.46	514.21
			3	24	60%a,40%c	108.82	301.3	514.99
			average			96.8	278.6	526.7
			standard deviation			11.0	22.4	20.9
			% coefficient of variation			11.3%	8.1%	4.0%
CRM neat	Granite	Dry	1	25.4	100%C	158.63	364.66	529.94
			2	25.2	100%C	133.47	329.56	531.15
			3	25.1	100%C	166.57	381.23	538.05
			average			152.9	358.5	533.0
			standard deviation			17.3	26.4	4.4
			% coefficient of variation			11.3%	7.4%	0.8%
	Granite	Wet	1	25.4	80%a,20C	98.07	273.03	522.21
			2	25.1	80%a,20C	72.27	232.09	473.3
			3	24.7	80%a,20C	84.87	245.73	538.52
			average			85.1	250.3	511.3
			standard deviation			12.9	20.8	33.9
			% coefficient of variation			15.2%	8.3%	6.6%

From the data shown in tables M2c.1 and M2c.2, both lower and higher rates of deformation give similar ranking of moisture damage on both neat and modified binders. Rate 5 is chosen because there is more clear moisture damage than rate 3. Also, the percent coefficient of variation for maximum pullout tension in rate 5 is smaller.

The procedure developed for testing using the new PQ Gold instrument is called the BBS test. A summary of the recommended BBS testing procedure is shown in table M2c.3.

Table M2c.3. Summary of BBS testing conditions.

Film Thickness (mm), small stub	0.4
Tank Pressure (psi)	100
Surface and Stub Temp (°C)	65
Binder Temp (°C)	150
Testing Temp (°C)	24-25
Testing Conditions	Oven and water bath
Water/Dry Conditioning (°C)	40 and 50
Flow Control	Rate 5

This procedure was used to test a number of modified binders in dry and wet conditions. Table M2c.4 shows the results of average maximum tension and pullout rate measured for the neat and modified binders. Results vary by the type of modification and water conditioning effects. The ratio of wet-to-dry pullout tension is shown in the far right column of table M2c.4. For this limited data set, the FH binder has lower values of the ratio compared to the CRM. The ratio, however, appears to vary by rate of loading, with higher rates giving reduced ratios. Both modifiers appear to improve moisture resistance, as shown by the increase in the pullout tension ratio. The polyphosphoric acid (PPA)-modified binder appears to resist water conditioning more than the styrene-butadiene-styrene (SBS)-modified binder.

The data set is too small to draw any main conclusions, but it is clear that the test procedure shows potential for measuring affinity between binders and mineral surface.

Table M2c.4. Summary of results for neat binders.

Binders	Substrata	Water Condition	Temp (°C)	Failure Type	Average BBS Factor (psi*s)	Max Pullout Tension (psi)	Pullout Rate (psi/s)	Dry to Wet Ratio (Tension)
<b>FH neat</b>	Granite	Dry	25.3	100% C	368.0	391.0	234	0.52
		Wet	24.4	90% A	110.4	205.1	230	
<b>CRM neat</b>	Granite	Dry	25.4	100% C	182.7	268.8	233	0.91
		Wet	24.8	98% A	150.2	244.4	229	
<b>FH neat</b>	Granite	Dry	25.1	100% C	330.7	542.7	533	0.51
		Wet	24.4	70% A	96.8	278.6	527	
<b>CRM neat</b>	Granite	Dry	25.3	100% C	152.9	358.5	533	0.70
		Wet	25.4	80% A	85.1	250.3	512	
<b>Modified Binders</b>								
<b>FH+1% PPA</b>	Granite	Dry	25.5	100% C	408.4	412.1	234	0.80
		Wet	24.7	75% A	267.0	327.9	231	
<b>CRM +2%LSBS</b>	Granite	Dry	25.4	100% C	218	292.8	226	0.81
		Wet	24.4	100% A	147.4	235.7	228	
<b>FH +1%PPA</b>	Granite	Dry	25.1	100% C	343.4	546.0	515	0.89
		Wet	24.7	100% A	284.9	487.5	518	
<b>CRM +2%LSBS</b>	Granite	Dry	25.4	100% C	236.3	439.4	507	0.63
		Wet	24.4	98% A	99.2	277.6	514	

Also notable is the failure type observed during this test. Without exception, the dry-conditioned materials failed in a cohesive manner (that is, bond failure within the binder layer). The water-conditioned materials, however, exhibited mostly adhesive-type failure (that is, failure occurred at the binder-aggregate interface). These preliminary results lead the research team to believe that the BBS test has great potential as a tool to examine the moisture damage susceptibility of asphalt binders, offering an easy-to-use, portable and inexpensive testing setup that provides reliable, repeatable results. Data collected from this test will be correlated with testing performed on the modified Dynamic Shear Rheometer (DSR) machine under the M1a work element.

Significant Problems, Issues and Potential Impact on Progress

None.

Work Planned Next Quarter

The research team will focus on refining the BBS testing procedure, continue investigating the effect of pullout rate on BBS test results, and decide on a testing rate.

To minimize the effect of the stub's geometry on testing results, the research team is preparing ½-inch-diameter stubs with built-in support feet of 0.4 mm in height. This will help correlate results with the E1c-2 work plan as well as simplify the testing procedure. The new stub configuration is designed to minimize sample flow-out at high temperatures and make it easier to maintain a constant film thickness during testing and conditioning.

### **CATEGORY M3: AGGREGATE SURFACE**

#### **Work Element M3a: Aggregate Surface Characterization (TAMU))**

##### Work Done This Quarter

Physical and chemical properties of aggregates at the macro and molecular scale influence the performance of asphalt mixes. These properties control the nature and durability of the bond between aggregates and asphalt in wet and dry conditions and its resistance to moisture induced damage and fatigue cracking. Recent research by Little and colleagues have shown that surface energy of the aggregate-asphalt interface is a reliable predictor of engineering properties of the asphalt mixture. Current understanding of the aggregate and bitumen properties that control and shape surface energy is limited, limiting our ability to *a priori* predict surface energy of any given aggregate-asphalt combination.

Current tasks are organized around the (1) characterization of the chemical composition of the surfaces of reference minerals and aggregates through electron beam spectroscopes, including electron microprobe, backscatter electrons and electron-dispersive spectroscopy (EDS), (2) the characterization of the surface energies of reference minerals and aggregates through the universal sorption device and microcalorimetry, (3) quantification of surface (upper 14 nm) atomic species and chemical state with an x-ray photoelectron spectroscope (XPS), and (4) surface topography characterization with scanning electron microscopy (SEM). The results from these tasks will support the development of a predictive model of aggregate surface energies based upon the surface energies of the minerals that compose the aggregate.

Tasks completed this quarter include additional BSE imaging of the basalt (RK) in order to more accurately calculate modal mineralogy, quantitative WDS analyses of the SAz-2 montmorillonite and Georgia kaolinite, image processing of X-ray elemental distribution maps of the aggregates and reference mineral samples, and compilation and organization of the quantitative WDS analyses. Specific accomplishments are highlighted in the tables below.

Surface energy measurements for quartz, microcline, labradorite, biotite, andesine, microcline, albite, augite, hornblende, hematite, siderite, dolomite, and calcite have been collected using the universal sorption device. The components of surface energy were calculated on replicates of the samples.

Sample preparation and aggregate surface characterization tasks completed this quarter are shown in the table below.

Table M3a.1. Status of tasks associated with mineralogical and chemical characterization of aggregates.

<b>SHRP</b>	<b>Name</b>	<b>Yr.Qtr</b>	<b>Thin Section Prep Status</b>	<b>Microprobe Analysis Status</b>
<b>RA</b>	Lithonia Granite	08.1	1 aggr sample prepared, 2 more in progress	1 set of X-ray maps, 1 set of BSE images, 1 preliminary set of WDS quant analyses
		08.2	2 more aggregate samples prepared	2 sets of X-ray maps, BSE images are not needed because of grain size
		09.1		WDS quant analyses of major minerals completed
<b>RC</b>	Limestone (higher absorption)	08.1	2 aggr samples prepared	1 set of X-ray maps, 1 set of BSE images, 1 preliminary set of WDS quant analyses
		08.2	-	No additional analyses
<b>RD</b>	Limestone (low absorp.)	08.1	4 aggr samples prepared,	4 sets of X-ray maps, 1 set of BSE images, 1 preliminary set of WDS quant analyses
		08.2	-	No additional analyses
<b>RK</b>	Basalt	08.1	2 aggr samples prepared, 1 more in progress	2 sets of X-ray maps, 1 set of BSE images, 1 preliminary set of WDS quant analyses
		08.2	1 sample in progress	3 additional sets of X-ray maps, 13 set of BSE images, 1 set of WDS quant analyses for pyroxene, olivine, amphibole
		09.1		WDS quant analyses of feldspar, pyroxene and clay completed.
		09.2		Additional BSE images of thin sections RK1a and RK1b acquired; image processing of X-ray maps in progress
<b>RL</b>	Gulf Coast Gravel	08.1	5 aggr samples prepared, 9 more in progress	4 sets of X-ray maps, 1 set of BSE images, 1 preliminary set of WDS quant analyses
		08.2	9 more in progress	9 sets of X-ray maps
		09.1		WDS quant analyses of mineral grains in 9 gravel particles completed.
		09.2		Image processing of X-ray maps in progress
<b>MM</b>	MM Sandstone	09.1	One 25mm aggr mount prepared with > 20 fragments	1 sets of X-ray maps acquired

Sample preparation and mineral surface characterization tasks completed this quarter are shown in the tables below.

Table M3a.2. Status of tasks associated with mineralogical and chemical characterization of mineral components of aggregates.

Mineral	Group	Yr.Qtr	(1) Acquisition Status (2) Microprobe Mount Status	Microprobe Analysis Status
Quartz	Silica Mineral	08.1	(1) > 200 grams acquired (Arkansas, RNG specimen) (2) Polished microprobe mount in preparation	In progress
		08.2	In progress	In progress
Microcline	Alkali Feldspar	08.1	(1) > 160 grams acquired (G&G collection, B0434) (2) Preliminary polished mount prepared	Preliminary homogeneity and quantitative chemical analysis acquired.
		08.2	In progress	In progress
Albite	Plagioclase Feldspar	08.1	(1) > 100 grams acquired (G&G collection, B0469) (2) Polished mount to be prepared	In progress
		08.2	In progress	In progress
Oligoclase	Plagioclase Feldspar	08.3	> 100 grams acquired (G&G collection, 008)	In progress
Andesine	Plagioclase Feldspar	08.1	(1) > 65 grams acquired (G&G collection, B0513) (2) Preliminary polished mount prepared	Preliminary homogeneity and quantitative chemical analysis acquired.
		08.2	In progress	In progress
Labradorite	Plagioclase Feldspar	08.1	(1) > 160 grams acquired (Naim, Labrador; RNG specimen) (2) Preliminary polished mount prepared	Preliminary homogeneity and quantitative chemical analysis acquired.
		08.2	In progress	In progress
Anorthite	Plagioclase Feldspar	08.1	Samples to be acquired	NA
		08.2	NA	NA

Table M3.a 2. Status of tasks associated with mineralogical and chemical characterization of mineral components of aggregates, (cont.)

Mineral	Group	Yr.Qtr	(1) Acquisition Status (2) Microprobe Mount Status	Microprobe Analysis Status
Hornblende	Amphibole	08.1	(1) > 350 grams acquired (G&G collection, B0545) (2) Preliminary polished mount prepared	Preliminary homogeneity and quantitative chemical analysis acquired.
		08.2	In progress	In progress
Hornblende	Amphibole	08.1	(1) > 70 grams acquired (G&G collection, Room 008) (2) Polished mount to be prepared	In progress
		08.2	In progress	In progress
		09.1	(2) Polished mount prepared	X-ray map acquired; WDS quant analyses completed.
Augite	Pyroxene	08.1	(1) > 0 (?) grams acquired (G&G collection, B1007) (2) Preliminary polished mount prepared	Preliminary homogeneity and quantitative chemical analysis acquired.
		08.2	In progress	In progress
Augite	Pyroxene	08.1	(1) > 80 grams acquired (G&G collection, Room 008) (2) Polished mount to be prepared	In progress
		08.2	In progress	In progress
		09.2		WDS quant analyses completed.
Forsteritic Olivine	Olivine	08.1	(1) > 280 grams acquired (San Carlos, AZ) (2) Polished mount to be prepared	In progress
		08.2	In progress	In progress

Table M3a.2. Status of tasks associated with mineralogical and chemical characterization of mineral components of aggregates, (cont.)

Mineral	Group	Yr.Qtr	(1) Acquisition Status (2) Microprobe Mount Status	Microprobe Analysis Status
Muscovite	Mica	08.1	(1) > 65 grams acquired (G&G collection, Room 008) (2) Polished mount to be prepared	Preliminary quantitative chemical analysis acquired.
		08.2	In progress	In progress
		09.1	(2) Polished mount prepared	X-ray map acquired; WDS quant analyses completed.
Biotite	Mica	08.1	(1) > 175 grams acquired (G&G collection, B0857) (2) Polished mount to be prepared	In progress
		08.2	In progress	In progress
		09.1		WDS quant analyses completed.
Biotite	Mica	08.1	(1) > 150 grams acquired (G&G collection, Room 008) (2) Polished mount to be prepared	Preliminary quantitative chemical analysis acquired.
		08.2	In progress	In progress
Calcite	Carbonate	08.1	(1) > 100 grams acquired (Mexico; RNG specimen) (2) Polished mount to be prepared	In progress
		08.2	In progress	In progress
Dolomite	Carbonate	08.1	Samples to be acquired	NA
		08.2	NA	NA
		09.1	(2) Polished mount prepared	X-ray map acquired; WDS quant analyses completed.
Siderite	Carbonate	09.1		WDS quant analyses completed.

Table M3a.2. Status of tasks associated with mineralogical and chemical characterization of mineral components of aggregates, (cont.)

Mineral	Group	Yr.Qtr	(1) Acquisition Status (2) Microprobe Mount Status	Microprobe Analysis Status
Hematite	Iron Oxide	08.1	Samples to be acquired	NA
		08.2	NA	NA
		09.1	(2) Polished mount prepared	X-ray map acquired; WDS quant analyses completed.
Magnetite	Iron Oxide	08.1	Samples to be acquired	NA
		08.2	NA	NA
Ilmenite	Iron Titanium Oxide	08.3	> 100 g sample (Ontario; RNG specimen)	NA
		09.1	(2) Polished mount prepared	X-ray map acquired; WDS quant analyses completed.
Goethite	Iron Oxyhydroxide	08.1	Samples to be acquired	NA
		08.2	NA	NA
Kaolinite (KGA-1B)	Clay Mineral	08.3	Samples acquired	NA
		08.2	Samples acquired	In progress
Kaolinite (Georgia)	Clay Mineral	08.3	Samples acquired	NA
		08.2	Samples acquired	In progress
		09.2	Unpolished flat mount prepared	WDS quant preliminary analyses completed
Montmorillonite (SAz-2)	Clay Mineral	08.3	Samples acquired	NA
		08.2	Samples acquired	In progress
		09.2	Unpolished flat mount prepared	WDS quant preliminary analyses completed
Chlorite	Clay Mineral	08.3	Samples acquired; ~25 g Calumet and New Melones (RNG)	NA
		08.2	Samples acquired	In progress

## Significant Results

### **Establishing a Surface Energy Predictive Model**

One of the first goals will be to establish a model for predicting aggregate bulk surface energies based on mineralogical composition. Improved prediction of aggregate bulk properties pertinent to moisture damage susceptibility can lead to better methods to measure material properties and moisture damage susceptibility of asphalt/aggregate mixes. Development of a simple visual field test of aggregate surface energy properties will aid in on-site evaluation of aggregate moisture damage susceptibility.

We expect the bulk/total surface energy of an aggregate to be a function of the component surface energies of its mineralogical constituents as:

$$Se_{aggregate} = \sum (Se_{Mineral} \cdot SA) + \sigma$$

where  $Se$  is surface energy,  $SA$  is surface area, and  $\sigma$  is the error term. A visual inspection of rock mineralogy based on percent of constituents can accurately predict total surface energy of the sample.

Methods –A Universal Sorption Device can be used to measure pure phase mineral surface energies by calculating the amount of a reference gas (water, hexane, and methylpropyl ketone in this case) sorbed to the mineral surface at various pressures. The adsorption isotherm for each reference gas is used to calculate equilibrium spreading pressure for each of the vapors along with the specific surface area (SSA) using the BET Equation. The equilibrium spreading pressure of each vapor is then used to calculate the three surface energy components using GvOC Equations. These values will then be used to establish an additive model of total surface energy for previously characterized rock samples based on percent of each constituent at the surface. The validity of the model will be tested by using the same Universal Sorption Device technique on the aggregate samples. A statistical analysis will be performed on the observed measurements versus predicted values.

Experiments – Although rock mineralogy has the capacity to be very complex it is dominated by a relatively small group of minerals of predictable variability in North America. The mineralogy of common aggregates used in hot asphalt mixes across America is outlined in the aggregate analysis data from the Strategic Highway Research Program's (SHRP) materials reference library. Pure phase minerals are being collected by Dr. Ray Guillemette based on the findings of the SHRP. These minerals are the dominant constituents in all major aggregates of the study. The chosen minerals are listed in table 1.

The surface energies of these pure phase minerals will be calculated using a Universal Sorption Device using three reference gases to determine spreading pressures. Each mineral will be crushed and passed through a number 10 sieve. Minerals will be washed with distilled water and heated for 24 hours at 80° Celsius in a Fisher Isotemp® Oven. Each reference gas will be used on a separate sample of each pure phase mineral. After the test is run each sample will be washed with distilled water and reheated at 80° C for future analysis.

After each of the pure phase mineral surface energies have been quantified the SHRP aggregate samples themselves will be crushed and analyzed on the Universal Sorption Device to statistically determine the linear additive model's validity

Data- The data gained from this experiment will be in  $erg / (cm)^2$  for each pure phase mineral and SHRP aggregate. In order to calculate mineral surface energy the isotherm for each reference gas must be calculated. To obtain a full isotherm, the aggregate is exposed to ten equal increments of partial probe vapor pressure from vacuum to saturated vapor pressure. At each stage the adsorped mass is recorded after it reaches equilibrium. The adsorped mass of each stage is then used to plot the isotherm. The measured isotherm for hexane is then used to calculate the specific surface area (SSA) using the Branauer, Emmett, and Teller BET equation:

$$A = \left( \frac{N_m N_0}{M} \right) \alpha$$

where  $N_0$ =Avogadro's number;  $M$ =molecular weight of the probe vapor;  $\alpha$  = projected area of a single molecule; and  $N_m$ =monolayer capacity of the aggregate surface. The specific surface area and each adsorption isotherm are then used to calculate three surface energy components using the GvOC equation:

$$W = 2\sqrt{\gamma_s^{lw}\gamma_v^{lw}} + 2\sqrt{\gamma_s^+\gamma_v^-} + 2\sqrt{\gamma_s^-\gamma_v^+}$$

where  $g^{Total}$  = total surface energy of the material;  $g^{lw}$  = Lifhsitz-van der Waals or dispersive component;  $g^{AB}$  = acid-base component;  $g^+$  = Lewis acid component, and  $g^-$  = Lewis base component.

## Current Results

In order to use the Universal Sorbtion Device as an appropriate measuring device for surface energy the reproducibility must first be known. In order to test the reproducibility one of the SHRP aggregates was chosen at random and the surface energy was measured on the sorption device. The aggregate was RD-7, a shaly limestone composed primarily of calcite. Hexane and methylpropyl ketone were run in triplicate and water vapor was tested four times. The results indicated that there was a good deal of internal consistency between the test runs, and the overall surface energy calculation was within a 95 percent confidence interval to previous study of the aggregate over two years ago. In total, testing of 12 minerals and two clays has either been completed or is in progress. All minerals will be tested in quadruplicate for each vapor. The results to date are included in the following chart.

		Mineral Surface Energy					
Mineral	SSA	LW	e- Acceptor	e- Donor	Polar Component	Fractional Polarity	Total
Quartz	0.10	51.42	0.00	399.58	0.65	0.01	52.07
Microcline	0.10	44.00	0.46	202.79	19.35	0.31	63.35
Calcite		41.67	0.09	153.71	7.43	0.15	49.10
Biotite	0.06	52.51	0.07	809.97	14.90	0.22	67.41
Labradorite	0.23	39.72	0.03	1062.51	11.55	0.23	51.27
Andesine	0.10	40.64	0.40	4953.93	89.24	0.69	129.88
Albite	0.19	51.57	0.22	501.69	21.22	0.29	72.79
Augite	0.03	52.67	8.69	6981.14	492.71	0.90	545.38
Siderite	0.07	61.39	1.59	789.63	70.80	0.54	132.18
Hematite	0.05	48.99	2.85	558.07	79.82	0.62	128.81
Dolomite	0.08	60.29	0.18	564.05	20.28	0.25	80.57
Hornblende	0.09	51.92	0.91	1338.86	69.70	0.57	121.63

### Significant Problems, Issues and Potential Impact on Progress

No significant problems at this time.

### Work Planned Next Quarter

Work planned in the next quarter includes continued analysis of the aggregates and minerals, with specific reference to surface energies.

## **CATEGORY M4: MODELING**

### **Work Element M4a: Micromechanics Model (TAMU)**

#### Work Done This Quarter

##### *Lattice Micromechanical Model*

The reader is referred the work element F3b.

##### *Cohesive Zone Micromechanical Model*

Recalling from previous reports, researchers at TAMU developed a coupled micromechanical model of moisture-induced damage in asphalt mixtures. The model integrates the effects of moisture on the mechanical properties of the microstructure in two different ways: 1) by making the viscoelastic material properties of the asphalt matrix to be dependent on the amount of moisture content (cohesive degradation), and 2) by making the strength and fracture toughness of

the aggregate-asphalt matrix interfaces to be a function of the amount of moisture in these zones (adhesive degradation). Adhesive fracture at the interfacial zones is achieved by applying the Cohesive Zone Modeling (CZM) technique. The micromechanical model has been implemented in the commercial finite element software Abaqus<sup>®</sup> using a two-steps sequentially coupling technique.

During this quarter, the researchers applied the micromechanical model to investigate the role of the air void phase on the mechanical performance of asphalt mixtures that are subjected to moisture diffusion and mechanical loading processes. The internal air void structure of asphalt mixtures plays a main role on the development of moisture-related deterioration processes. However, this phase is usually considered to be part of the fine aggregate matrix (FAM) of the mixture, and its actual contribution to damage is usually overlooked. In this quarter, researchers generated and explicitly included air voids structures as an independent phase within the mixture's microstructure.

Figure M4a.1 presents the 50mm by 50mm representative volume element (RVE) that was selected for this study, as well as its finite element implementation. The mixture was composed of 231 coarse aggregates embedded in a fine aggregate matrix (FAM).

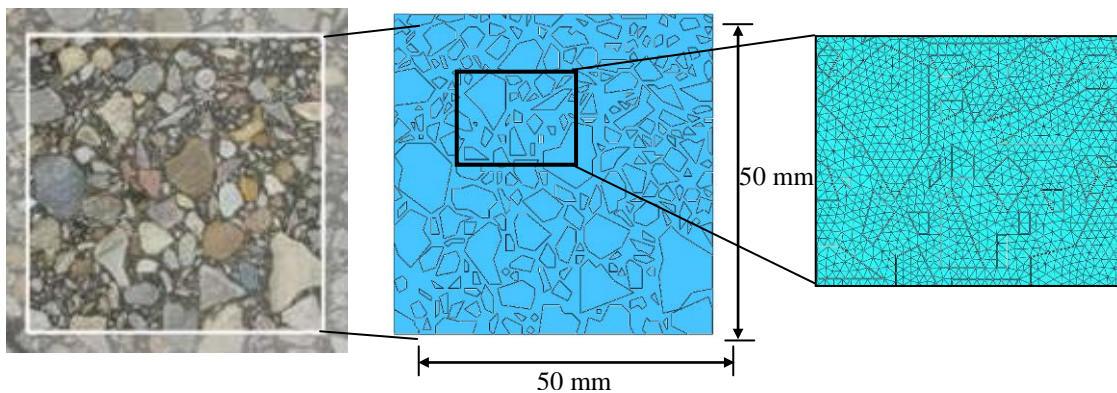


Figure M4a.1. Microstructure model used in the parametric analysis and its corresponding finite element implementation.

Circular voids were randomly generated using a log-normal probabilistic density function of the air void sizes. This distribution was obtained from measurements conducted in a dense-graded asphalt mixture by means of the X-Ray Computer Tomography technique. The location of the air voids within the microstructure was randomly determined. Three different levels of total air voids content were analyzed: 4%, 7% and 10%. Due to the uncertainty on the internal characteristics of the void structure, 10 different sets of air voids at each one of the three total levels were considered. Figure M4a.2 shows one example of the air voids structures generated at the three levels of air voids content.

The physical and mechanical material properties of the coarse aggregates and the bulk matrix (FAM), as well as the moisture dependency of their mechanical properties, were similar to those used in previous works (refer to previous quarterly reports). Air voids were assigned to a moisture diffusion coefficient of  $26\text{mm}^2/\text{s}$ , and they were considered to have zero-resistance during the mechanical simulations.

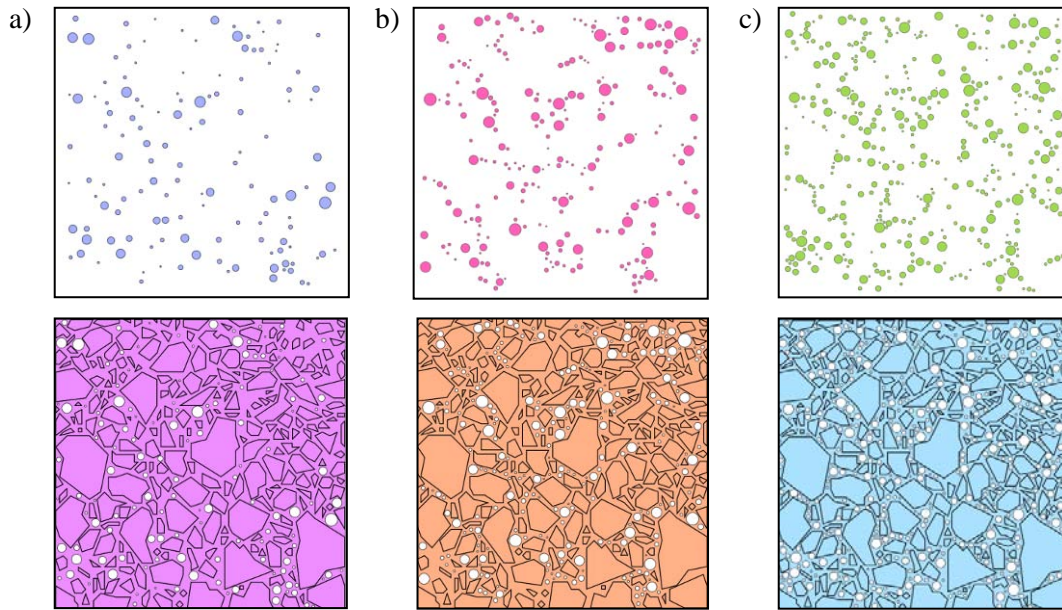


Figure M4a.2. Randomly created void structures and their correspondent microstructure models at three levels of air voids content: a) 4%, b) 7% and b) 10%.

The microstructures (30 in total) were initially subjected to a load-controlled mechanical test in *dry* condition. The mechanical test consisted of loading and unloading the material at a rate of  $0.16\text{ N/s}$  during a total of 30 seconds. Similar microstructures were subjected to a 10 days moisture diffusion period. The boundary conditions used for these simulations were uniformly distributed along the perimeter of the microstructure model, constant during the 10 days simulation period and equal to a normalized moisture concentration of the FAM (i.e., moisture content divided by the moisture at saturation) of 1.0. At the end of the 10 days period, the microstructures in *wet* condition were subjected to the same mechanical loading scheme previously described.

The total energy dissipated by the microstructures in *dry* and *wet* conditions (i.e., area within the load-displacement curves in the left hand side of figure M4a.3) and the overall stiffness of the mixtures (i.e., maximum load divided by maximum displacement in the same figure) were used to study the impact of the air void phase on the mechanical responses of the mixtures.

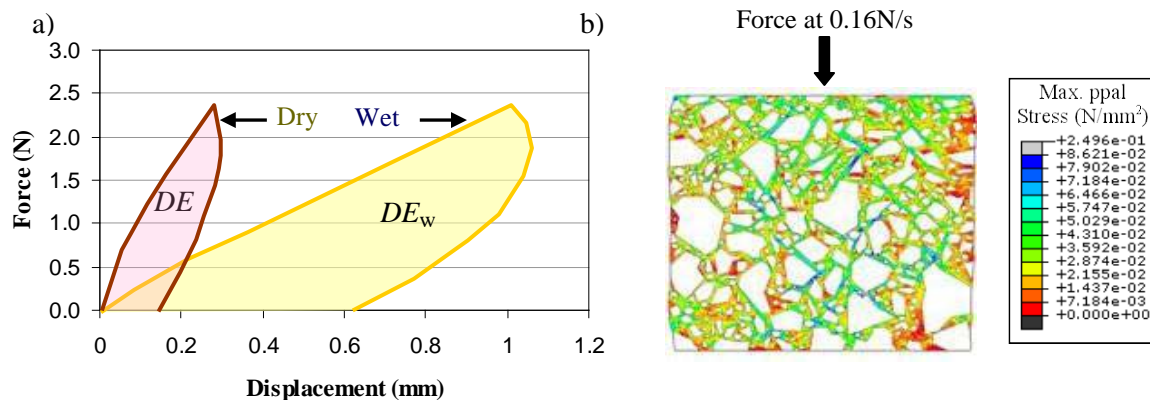


Figure M4a.3. a) typical force-displacement curve obtained for a structure containing 7% air voids content ( $DE$ : dissipated energy) and b) maximum internal deformations caused within the microstructure during the mechanical loading test (10% air voids).

The results from the study (figure M4a.4) showed that the air void phase highly influences the mechanical performance of asphalt mixtures. Mixtures with large amounts of air voids presented larger values of total dissipated energy and smaller values of stiffness—in both dry and wet states—than compared to mixtures with small percents of air voids. Besides, at any fixed level of total percent of air voids, the energy dissipated by a microstructure in wet state was always larger than the energy dissipated by the mixture in dry condition. This result is a direct consequence of the coupling effect that exists between the moisture diffusion profiles and the mechanical material properties of the components of the mixture.

A statistical sampling technique (i.e., bootstrapping) was used to determine the expected mean value of the total dissipated energy and overall stiffness in the moisture-conditioned mixtures. The results showed that a polynomial function of third order or higher can be used to describe the relationship between the amount of air voids (from 0% to 10%) and the expected mechanical performance of the mixture.

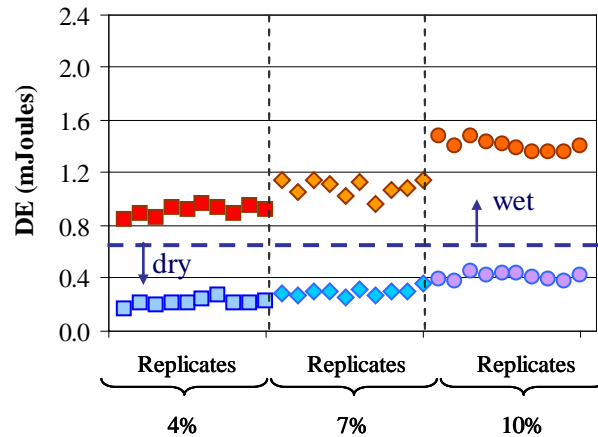


Figure M4a.4. Total dissipated energy ( $DE$ ) by the asphalt mixtures in dry and wet state.

### Significant Results

#### *Lattice Micromechanical Model*

The reader is referred the work element F3b.

#### *Cohesive Zone Micromechanical Model*

In the previous quarter, the micromechanical model was successfully applied to study the role of different physical and mechanical material properties of the mixture on its susceptibility to moisture damage. In this quarter, the model was further applied to study the role of the air void phase on the mechanical performance of the mixtures. A paper containing the main findings from this study (Analysis of the Effect of the Internal Air Void Structure on the Moisture Sensitivity of Asphalt Mixtures) is currently under development. Besides, it is noteworthy that this work used a highly complex microstructure, which overcomes one of the main challenges identified in previous reports.

### Significant Problems, Issues and Potential Impact on Progress

#### *Lattice Micromechanical Model*

The reader is referred the work element F3b.

#### *Cohesive Zone Micromechanical Model*

None

### Work Planned Next Quarter

#### *Lattice Micromechanical Model*

The reader is referred the work element F3b.

#### *Cohesive Zone Micromechanical Model*

The researchers found that studying the role of the air void phase is crucial when analyzing moisture-related degradation processes in asphalt mixtures. However, the generation and explicit addition of the air voids phases into the microstructure was found to be a complex and time-consuming task. Therefore, it was decided to explore other approaches that can be used to conduct similar analyses. During the next quarter, a stochastic methodology based on random field theory will be developed to indirectly include the effect of the air void phase within the microstructure of the mixture. The coupled micromechanical model of moisture-induced damage will be used to evaluate the expected mechanical performance of the mixtures.

### Journal Papers during This Quarter

Caro, S., Masad, E., Bhasin, A., and Little, D. (2009). "A Coupled Micromechanical Model of Moisture-Induced Damage in Asphalt Mixtures." *Journal of Materials in Civil Engineering* (ASCE), (in press).

Caro, S., Masad, E., Bhasin, A., Little, D., and Sanchez-Silva, M. (2009). "Analysis of the Effect of the Internal Air Void Structure on the Moisture Sensitivity of Asphalt Mixtures." *Journal of the Association of Asphalt Paving Technologists* (AAPT), (submitted for evaluation).

### **Work Element M4b: Analytical Fatigue Model for Mixture Design**

The initial development of this work element is the same as Subtask F3c-1. The development of a method to separate the viscoelastic response from fatigue damage and the development of a model to analyze resistance to fatigue cracking under both dry and wet conditions is provided under subtask F1b-1. See the progress reported under Work Element F3c.

### **Work Element M4c: Unified Continuum Model**

The reader is referred the Work Element F3c.

## **CATEGORY M5: MOISTURE DAMAGE PREDICTION SYSTEM**

This area is planned to start later in the project.

Moisture Damage Year 3		Year 3 (4/09-3/10)											
		4	5	6	7	8	9	10	11	12	1	2	3
<b>Adhesion</b>													
<b>M1a</b>	<b>Affinity of Asphalt to Aggregate - Mechanical Tests</b>												
M1a-1	Select Materials												
M1a-2	Conduct modified DSR tests												
M1a-3	Evaluate the moisture damage of asphalt mixtures							P					
M1a-4	Correlate moisture damage between DSR and mix tests							P					P
M1a-5	Propose a Novel Testing Protocol												P
<b>M1b</b>	<b>Work of Adhesion</b>												
M1b-1	Adhesion using Micro calorimeter and SFE							JP					
M1b-2	Evaluating adhesion at nano scale using AFM												
M1b-3	Mechanisms of water-organic molecule competition												
<b>M1c</b>	<b>Quantifying Moisture Damage Using DMA</b>												
<b>Cohesion</b>													
<b>M2a</b>	<b>Work of Cohesion Based on Surface Energy</b>												
M2a-1	Methods to determine SFE of saturated binders												
M2a-2	Evaluating cohesion at nano scale using AFM												
<b>M2b</b>	<b>Impact of Moisture Diffusion in Asphalt</b>												
M2b-1	Diffusion of moisture through asphalt/mastic films							JP			D		F
M2b-2	Kinetics of debonding at binder-aggregate interface												
<b>M2c</b>	<b>Thin Film Rheology and Cohesion</b>												
M2c-1	Evaluate load and deflection measurements using the modified PATTI test												
M2c-2	Evaluate effectiveness of the modified PATTI test for Detecting Modification												
M2c-3	Conduct Testing						JP						
M2c-4	Analysis & Interpretation											D	
M2c-5	Standard Testing Procedure and Recommendation for Specifications				D								
<b>Aggregate Surface</b>													
<b>M3a</b>	<b>Impact of Surface Structure of Aggregate</b>												
M3a-1	Aggregate surface characterization												
<b>Modeling</b>													
<b>M4a</b>	<b>Micromechanics model development</b>			2JP									JP
<b>M4b</b>	<b>Analytical fatigue model for use during mixture design</b>												
<b>M4c</b>	<b>Unified continuum model</b>			JP									JP
<b>M5</b>	<b>Moisture Damage Prediction System</b>												

**LEGEND**

**Deliverable codes**

- D: Draft Report
- F: Final Report
- M&A: Model and algorithm
- SW: Software
- JP: Journal paper
- P: Presentation
- DP: Decision Point
- [x]

-  Work planned
-  Work completed
-  Parallel topic

**Deliverable Description**

- Report delivered to FHWA for 3 week review period.
- Final report delivered in compliance with FHWA publication standards
- Mathematical model and sample code
- Executable software, code and user manual
- Paper submitted to conference or journal
- Presentation for symposium, conference or other
- Time to make a decision on two parallel paths as to which is most promising to follow through
- Indicates completion of deliverable x

Moisture Damage Year 2 - 5		Year 2 (4/08-3/09)				Year 3 (4/09-3/10)				Year 4 (04/10-03/11)				Year 5 (04/11-03/12)			
		Q1	Q2	Q3	Q4	Q1	Q2	Q3	Q4	Q1	Q2	Q3	Q4	Q1	Q2	Q3	Q4
<b>Adhesion</b>																	
<b>M1a</b>	<b>Affinity of Asphalt to Aggregate - Mechanical Tests</b>																
M1a-1	Select Materials		DP														
M1a-2	Conduct modified DSR tests		P		P												
M1a-3	Evaluate the moisture damage of asphalt mixtures				DP		P			P							
M1a-4	Correlate moisture damage between DSR and mix tests						P		P								
M1a-5	Propose a Novel Testing Protocol				P				P							JP, F	
<b>M1b</b>	<b>Work of Adhesion</b>																
M1b-1	Adhesion using Micro calorimeter and SFE						JP					JP,F					
M1b-2	Evaluating adhesion at nano scale using AFM							JP							JP		JP, F
M1b-3	Mechanisms of water-organic molecule competition				JP							JP	D	F			
<b>M1c</b>	<b>Quantifying Moisture Damage Using DMA</b>											JP	D	F			
<b>Cohesion</b>																	
<b>M2a</b>	<b>Work of Cohesion Based on Surface Energy</b>																
M2a-1	Methods to determine SFE of saturated binders														JP		
M2a-2	Evaluating cohesion at nano scale using AFM							JP						JP			JP, F
<b>M2b</b>	<b>Impact of Moisture Diffusion in Asphalt</b>																
M2b-1	Diffusion of moisture through asphalt/mastic films						JP	D	F		JP	D	F				
M2b-2	Kinetics of debonding at binder-agreagte interface										JP	D	F				
<b>M2c</b>	<b>Thin Film Rheology and Cohesion</b>																
M2c-1	Evaluate load and deflection measurements using the modified PATTI test	DP	JP	D	F												
M2c-2	Evaluate effectiveness of the modified PATTI test for Detecting Modification			D	DP,F												
M2c-3	Conduct Testing						JP										
M2c-4	Analysis & Interpretation				P				D			D, JP		F			
M2c-5	Standard Testing Procedure and Recommendation for Specifications					D							D	P,F			
<b>Aggregate Surface</b>																	
<b>M3a</b>	<b>Impact of Surface Structure of Aggregate</b>																
M3a-1	Aggregate surface characterization																
<b>Models</b>																	
<b>M4a</b>	<b>Micromechanics model development</b>				JP	2JP			JP					M&A	D	DP	F, SW
<b>M4b</b>	<b>Analytical fatigue model for use during mixture design</b>																M&A,D
<b>M4c</b>	<b>Unified continuum model</b>					JP			JP					M&A	D	DP	F, SW
<b>M5</b>	<b>Moisture Damage Prediction System</b>																

**LEGEND**

**Deliverable codes**

- D: Draft Report
- F: Final Report
- M&A: Model and algorithm
- SW: Software
- JP: Journal paper
- P: Presentation
- DP: Decision Point
- [x]

-  Work planned
-  Work completed
-  Parallel topic

**Deliverable Description**

- Report delivered to FHWA for 3 week review period.
- Final report delivered in compliance with FHWA publication standards
- Mathematical model and sample code
- Executable software, code and user manual
- Paper submitted to conference or journal
- Presentation for symposium, conference or other
- Time to make a decision on two parallel paths as to which is most promising to follow through
- Indicates completion of deliverable x



## **PROGRAM AREA: FATIGUE**

### **CATEGORY F1: MATERIAL AND MIXTURE PROPERTIES**

#### **Work Element F1a: Cohesive and Adhesive Properties**

##### ***Subtask F1a-1: Critical Review of Measurement and Application of Cohesive and Adhesive Bond Strengths (TAMU)***

###### Work Done This Quarter

The work on improving the white paper relating the ideal work of fracture to the practical work of fracture was continued. A paper was prepared that combines the results from this task and task Fa1-4 and it will be submitted to AAPT.

###### Significant Results

None

###### Significant Problems, Issues and Potential Impact on Progress

None

###### Work Planned Next Quarter

Improvements to this white paper will be made continually based on literature review. In addition, researchers plan to validate the findings from this paper in the context of bituminous materials by accomplishing the various subtasks in this work element.

##### ***Subtask F1a-2: Develop Experiment Design (TAMU)***

###### Work Done This Quarter

The experiment design was completed and reported in the last quarterly report.

###### Work Planned Next Quarter

At this time, researchers do not anticipate any changes to this experiment design. However, as the work progresses in this subtask and in the area of modeling, some refinement to the proposed experiment design may be required in future.

### ***Subtask F1a-3: Thermodynamic Work of Cohesion and Adhesion (Year 1 start)***

#### Work Done This Quarter

The objective of this subtask is to provide the surface free energy of asphalt binders that will be used in other subtasks as a material property input or for the comparison with results from other test methods. Based on the requirements from other tasks, tests under this subtask will be ongoing through the remainder of this project.

#### Work Planned Next Quarter

Based on the requirements from other tasks, tests under this subtask will be ongoing through the remainder of this project.

### ***Subtask F1a-4: Mechanical Work of Adhesion and Cohesion***

#### Work Done This Quarter

Data obtained from pull-off testing of thin asphalt samples between stainless steel plates was analyzed. The data included the surface free energy of stainless steel and asphalts, force and displacement data gathered during the tests, and images of failed samples. The force, displacement, and surface free energy data was utilized to determine the relationship between fracture energy and ideal work of fracture. Force and displacement measurements were used to calculate the energy required to fracture the sample as shown in the example in figure F1a.1.

The tested sample images, figure F1a.2, were analyzed using image analysis software to determine the percent of adhesive and cohesive failures. Figure F1a.3 displays the average gray level determined from a range of film thicknesses. The higher the gray level the greater the percent of adhesive failure. Combining the information in figure F1a.3 with the known bond energies for adhesive failure between the asphalt and steel and cohesive failure in the asphalt binder, an effective ideal bond energy was determined for each film thickness.

Using the effective ideal bond energy for each asphalt binder and film thickness in conjunction with the results from figure F1a.1, the relationship between fracture energy and effective ideal bond energy was determined. Figure F1a.4 displays the relationship between the effective ideal bond energy and fracture energy of the three tested asphalts at a film thickness of 15- $\mu\text{m}$ .

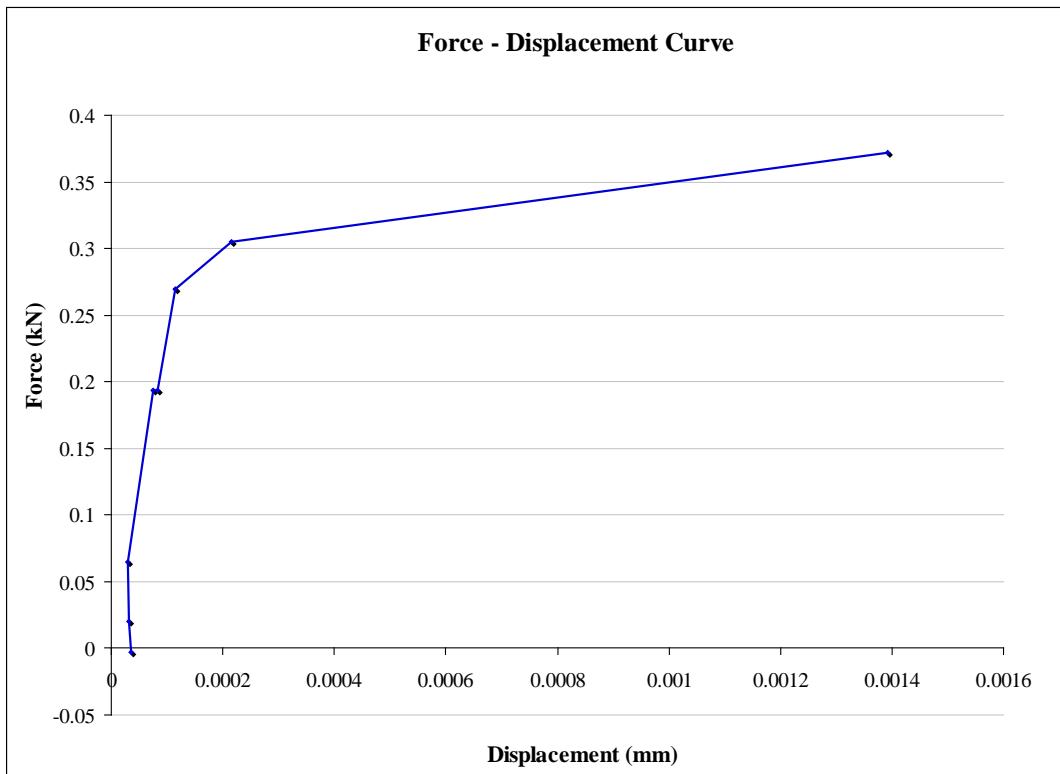


Figure F1a.1. Typical force displacement curve.

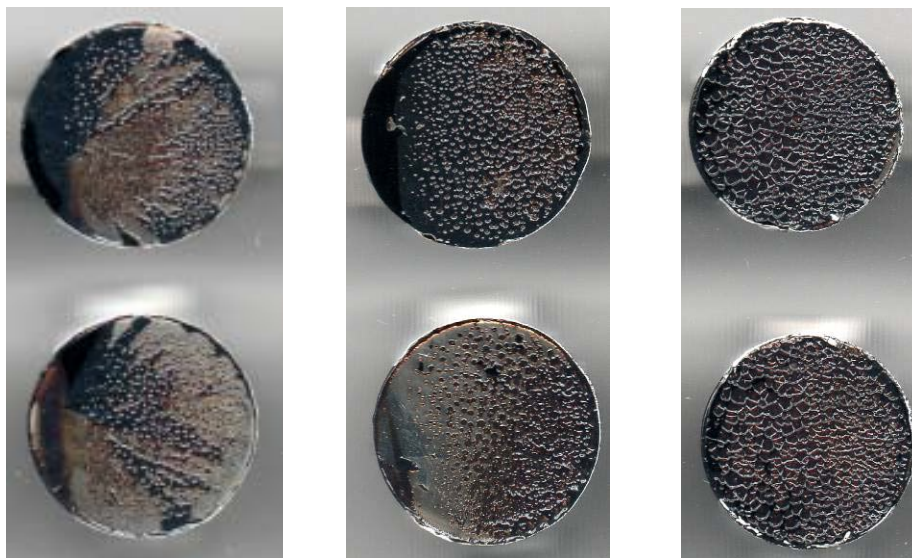


Figure F1a.2. Left: adhesive failure; center: mixed mode failure; right: cohesive failure.

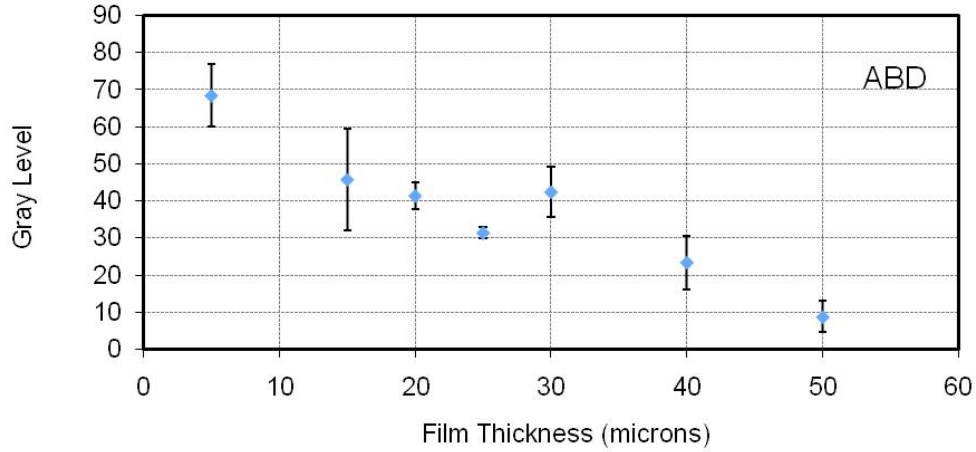


Figure F1a.3. Effective ideal bond energy of tested samples.

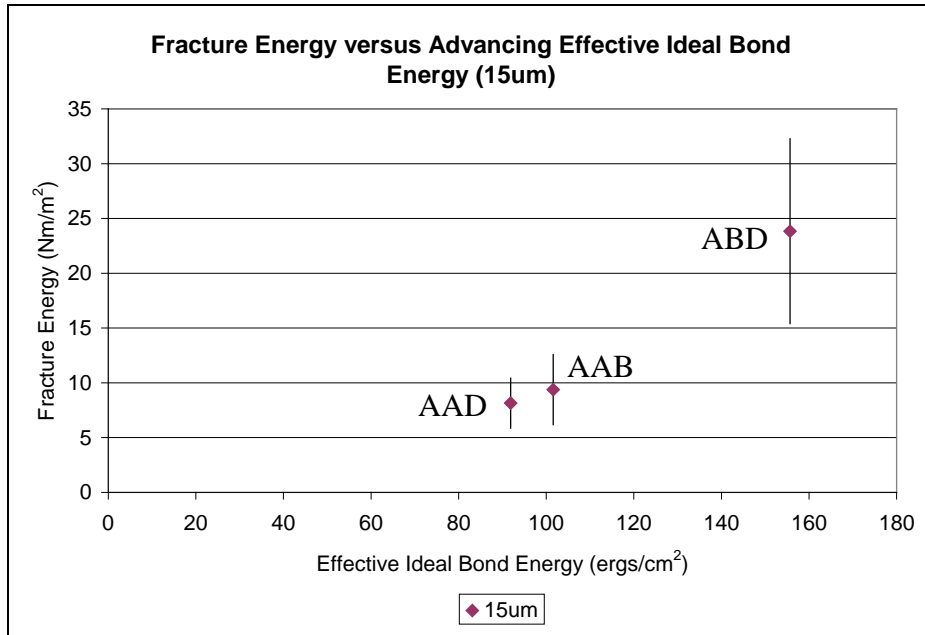


Figure F1a.4. Relationship between fracture energy and effective ideal bond energy (15- $\mu$ m).

Significant Results

The ideal bond energy, calculated using the surface free energy of the constituent materials, can be much smaller in magnitude than the practical fracture energy measured using mechanical tests. However, the results of this research show that despite the difference in magnitude, the ideal bond energy is important and directly related to the magnitude of the fracture energy.

### Significant Problems, Issues and Potential Impact on Progress

One problem that was encountered in this task was the variability in the displacement to fracture measured during the pull-off experiment. This variability was attributed to misalignments in the vertical orientation of the samples during testing.

### Work Planned Next Quarter

Tests will be conducted using sample holders constructed of aggregate instead of stainless steel. Two aggregate types will be used, limestone and river gravel, in conjunction with the three core asphalts. This testing will evaluate the effects of moisture on the bond strength of the asphalt/aggregate interface and the effect of changes in loading rate.

### ***Subtask F1a-5: Evaluate Acid-Base Scale for Surface Energy Calculations***

#### Work Done This Quarter

No activity was planned for this quarter.

#### Work Planned Next Quarter

Work on this subtask is planned in year 4 of this project.

### **Work Element F1b: Viscoelastic Properties (Year 1 start)**

#### ***Subtask F1b-1: Separation of Nonlinear Viscoelastic Deformation from Fracture Energy under Cyclic Loading (TAMU)***

#### Work Done This Quarter

The main objective of this task was to develop an approach to determine the following three main aspects of material response during cyclic loading:

- i) identify the limiting stress or strain amplitude that results in a nonlinear viscoelastic response without causing damage,
- ii) model and monitor the change in the nonlinear viscoelastic parameters with increasing number of load cycles, and
- iii) model and monitor the change in the nonlinear viscoelastic parameters within each cycle.

Researchers have made significant progress to achieve the first two steps that were reported in the previous quarterly reports. The last step is important because the researchers hypothesized that during each load cycle only specific portions of the load cycle contribute to damage. Also, in order to obtain accurate estimate of the dissipated energy due to fatigue damage, the non-linear

viscoelastic response and response due to damage must be accurately modeled and discounted for at each and every point within the load cycle.

In the previous quarterly report, we described the use of Schapery's nonlinear viscoelastic model to predict the nonlinear viscoelastic response of a material under dynamic loading. This model was used to demonstrate that the phase angle measured during dynamic loading was itself a function of time within each load cycle. During this quarter, we measured the response of some binders under dynamic loading. Preliminary results indicate that nonlinear viscoelastic response maybe more pronounced for modified binders as compared to unmodified binders. Based on the mathematical model for nonlinear response, it is expected that under controlled stress mode of loading the strain amplitude will not remain constant. Instead, the peak values of the strain response will follow a second harmonic. Results from the binder tests indicate some evidence of this second harmonic. However, we still need to conduct detailed analysis to validate that this observation is indeed due to the non-linear response of the binder.

#### Work Planned Next Quarter

In the next quarter, we will include tests on binders at lower temperatures as well as tests on typical FAM specimens. Results from a previous study indicate the nonlinear response of the material is more pronounced in the case of FAM specimens.

#### ***Subtask F1b-2: Separation of Nonlinear Viscoelastic Deformation from Fracture Energy under Repeated and Monotonic Loading***

#### Work Done This Quarter

A Weibull distribution model was developed for the air void/crack size in asphalt mixtures based on the dissipated Pseudo Strain Energy (DPSE) theory that was developed last quarter. In last quarter, the DPSE in an asphalt mixture was separated into two components: i)  $W_{R1}$ , the DPSE for developing cracking, and ii)  $W_{R2}$ , the DPSE for developing permanent deformation. In this quarter, the DPSE for developing cracking ( $W_{R1}$ ) was used to calculate the number and average size of air voids/cracks, which is detailed in Work Element F2c. In addition to determining the average size of air voids/cracks, an X-ray Computed Tomography (CT) system was used to detect the maximum air void size in an undamaged asphalt mixture specimen. The X-ray CT system also detected a minimum air void size and the average air void size over the interval between the detected maximum and minimum air void size in an undamaged asphalt mixture specimen. The minimum air void size detected by the X-ray CT system was not the "true" minimum because of the resolution limit and the arbitrarily chosen threshold gray intensity in the X-ray CT image analysis. Therefore, the X-ray CT system did not take into account the air voids smaller than the detected minimum air void size. As a result, the average air void size determined by the X-ray CT system was not the "true" average size.

In order to address the limitation of the X-ray CT system, the calculated average air void crack size by the DPSE theory together with the results from the X-ray CT system were used to determine the true distribution of the air void size in the range between 0 and the maximum air

void size. The probability density function of the air void size was defined as in Equation F1b-2.1.

$$f(x) = \begin{cases} 0 & x > c_{\max} \\ a\lambda^a x^{a-1} e^{-(\lambda x)^a} & 0 \leq x \leq c_{\max} \\ 0 & x < 0 \end{cases} \quad (\text{F1b-2.1})$$

where  $a$  and  $\lambda$  are the Weibull distribution parameters,  $c_{\max}$  is the maximum air void size detected by the X-ray CT system. The probability density function is qualitatively presented in figure F1b-2.1, in which  $c_R$  is the resolution limit of the X-ray CT system;  $c_{\min}$  is the minimum air void size detected by the X-ray CT system; and  $c_{\max}$  is the maximum air void size detected by the X-ray CT system. The solid curve in figure F1b-2.1 illustrates  $f(x)$  defined in Equation F1b-2.1, which is in fact a truncated Weibull distribution. This solid curve is extended to infinity along the dashed curve to present the complete probability density function of the Weibull distribution.

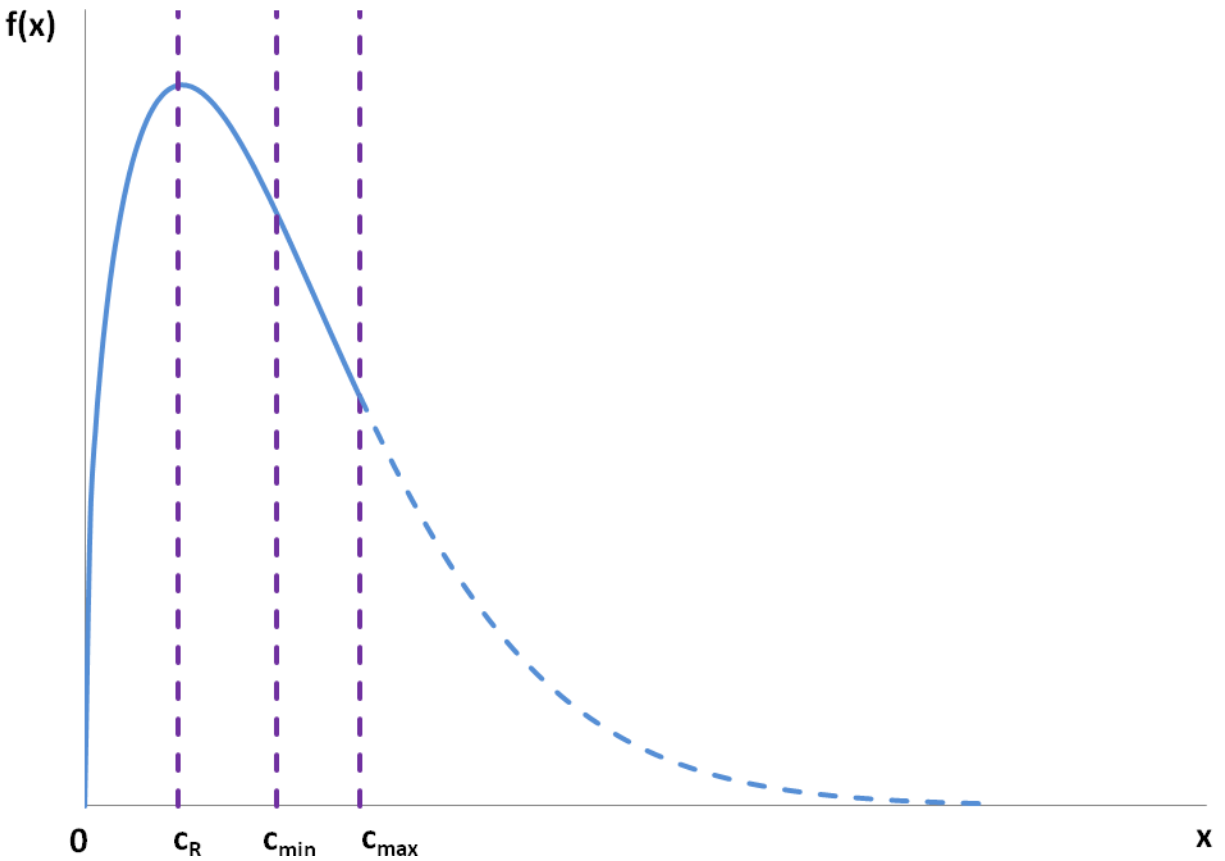


Figure F1b-2.1. Probability density function of the truncated Weibull distribution for air void/crack size.

In order to calculate  $E(X)$ , the integral of  $f(x)$  over the interval  $[0, c_{\max}]$  had to be normalized to 1. As a result,  $E(X)$  was calculated using the following integration:

$$E(X) = \int_0^{c_{\max}} x \frac{f(x)}{A_{c_{\max}}} dx = \frac{1}{A_{c_{\max}}} \int_0^{c_{\max}} x a \lambda^a x^{a-1} e^{-(\lambda x)^a} dx = \frac{1}{A_{c_{\max}}} \int_0^{c_{\max}} a (\lambda x)^a e^{-(\lambda x)^a} dx \quad (\text{F1b-2.2})$$

where  $A_{c_{\max}}$  is the area under  $f(x)$  in the interval  $[0, c_{\max}]$ ,  $A_{c_{\max}} = \int_0^{c_{\max}} f(x) dx = 1 - e^{-(\lambda c_{\max})^a}$ .

Let  $t = (\lambda x)^a$ , Equation F1b-2.2 is arranged as:

$$E(X) = \frac{1}{\lambda \left[ 1 - e^{-(\lambda c_{\max})^a} \right]} \int_0^{(\lambda c_{\max})^a} t^{\left(1 + \frac{1}{a}\right) - 1} e^{-t} dt = \frac{1}{\lambda \left[ 1 - e^{-(\lambda c_{\max})^a} \right]} \gamma \left[ 1 + \frac{1}{a}, (\lambda c_{\max})^a \right] \quad (\text{F1b-2.3})$$

where  $\gamma \left[ 1 + \frac{1}{a}, (\lambda c_{\max})^a \right]$  is a lower incomplete gamma function, which is defined to be:

$$\gamma(s, x) = \int_0^x t^{s-1} e^{-t} dt \quad (\text{F1b-2.4})$$

The expected value of the air void/crack size determined by Equation F1b-2.3 is the “true” expected value because it is the weighted average of all air voids/cracks. As a contrast, the average size of the air voids determined by the X-ray CT system is the weighted average of air void size between the minimum air void ( $c_{\min}$ ) and maximum air void ( $c_{\max}$ ) determined by the X-ray CT system. The expected value of air void size in the interval  $[c_{\min}, c_{\max}]$  can be formulated to be:

$$\begin{aligned} E_{X\text{-ray}}(X) &= \int_{c_{\min}}^{c_{\max}} x \frac{f(x)}{A_{c_{\max}} - A_{c_{\min}}} dx \\ &= \frac{1}{A_{c_{\max}} - A_{c_{\min}}} \int_{c_{\min}}^{c_{\max}} x a \lambda^a x^{a-1} e^{-(\lambda x)^a} dx \\ &= \frac{1}{A_{c_{\max}} - A_{c_{\min}}} \int_{c_{\min}}^{c_{\max}} a (\lambda x)^a e^{-(\lambda x)^a} dx \end{aligned} \quad (\text{F1b-2.5})$$

where  $A_{c_{\min}}$  is the area under  $f(x)$  in the interval  $[0, c_{\min}]$ ,  $A_{c_{\min}} = \int_0^{c_{\min}} f(x) dx = 1 - e^{-(\lambda c_{\min})^a}$ ; therefore,  $(A_{c_{\max}} - A_{c_{\min}})$  is the area under  $f(x)$  in the interval  $[c_{\min}, c_{\max}]$ . Let  $t = (\lambda x)^a$ , Equation F1b-2.5 is arranged as:

$$\begin{aligned}
E_{X-ray}(X) &= \frac{1}{\lambda \left[ e^{-(\lambda c_{\min})^a} - e^{-(\lambda c_{\max})^a} \right]} \int_{(\lambda c_{\min})^a}^{(\lambda c_{\max})^a} t^{\left(\frac{1}{a}\right)-1} e^{-t} dt \\
&= \frac{1}{\lambda \left[ e^{-(\lambda c_{\min})^a} - e^{-(\lambda c_{\max})^a} \right]} \left[ \int_0^{(\lambda c_{\max})^a} t^{\left(\frac{1}{a}\right)-1} e^{-t} dt - \int_0^{(\lambda c_{\min})^a} t^{\left(\frac{1}{a}\right)-1} e^{-t} dt \right] \\
&= \frac{1}{\lambda \left[ e^{-(\lambda c_{\min})^a} - e^{-(\lambda c_{\max})^a} \right]} \left\{ \gamma \left[ 1 + \frac{1}{a}, (\lambda c_{\max})^a \right] - \gamma \left[ 1 + \frac{1}{a}, (\lambda c_{\min})^a \right] \right\}
\end{aligned} \tag{F1b-2.6}$$

Equations F1b-2.3 and F1b-2.6 are two simultaneous equations with two unknowns,  $a$  and  $\lambda$ , the Weibull distribution parameters. To solve these two equations, the following parameters were obtained from Work Element F2c as input to the two equations to solve for  $a$  and  $\lambda$ :

- $E(X)$  determined by the DPSE theory;
- $E_{X-ray}(X)$  determined by the X-ray CT system;
- $c_{\max}$  determined by the X-ray CT system; and
- $c_{\min}$  determined by the X-ray CT system.

After solving Equations F1b-2.3 and F1b-2.6, the probability density function of the air void size in the tested undamaged asphalt mixture specimen was found to be:

$$f(x) = \begin{cases} 0 & x > 0.491 \text{ mm} \\ 4.974x^{0.403} e^{-3.546x^{1.403}} & 0 \leq x \leq 0.491 \text{ mm} \\ 0 & x < 0 \text{ mm} \end{cases} \tag{F1b-2.7}$$

For damaged specimens, only Equation F1b-2.3 was available since the X-ray CT system could not provide the instantaneous information on the crack sizes. Consequently, a perturbation analysis was conducted on the damaged specimen at every loading cycle based on the probability density function of the undamaged specimen. By doing the perturbation analysis, the distribution parameters were obtained for the probability density functions at all loading cycles. Figure F1b-2.2 shows the variation of  $a$ ,  $\lambda$  and  $c_{\max}$  with the number of loading cycles, and figures F1b-2.3 through F1b-2.5 illustrates the probability density functions at certain numbers of loading cycles.

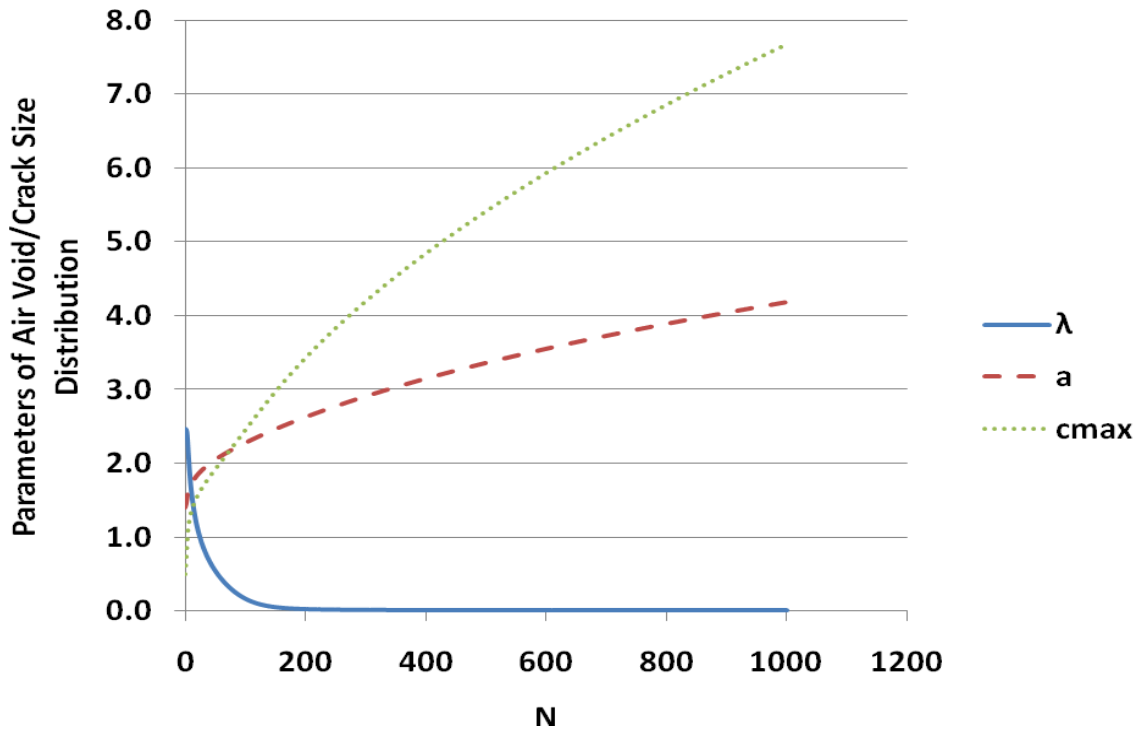


Figure F1b-2.2. Variation of parameters of air void/crack size distribution with number of loading cycles.

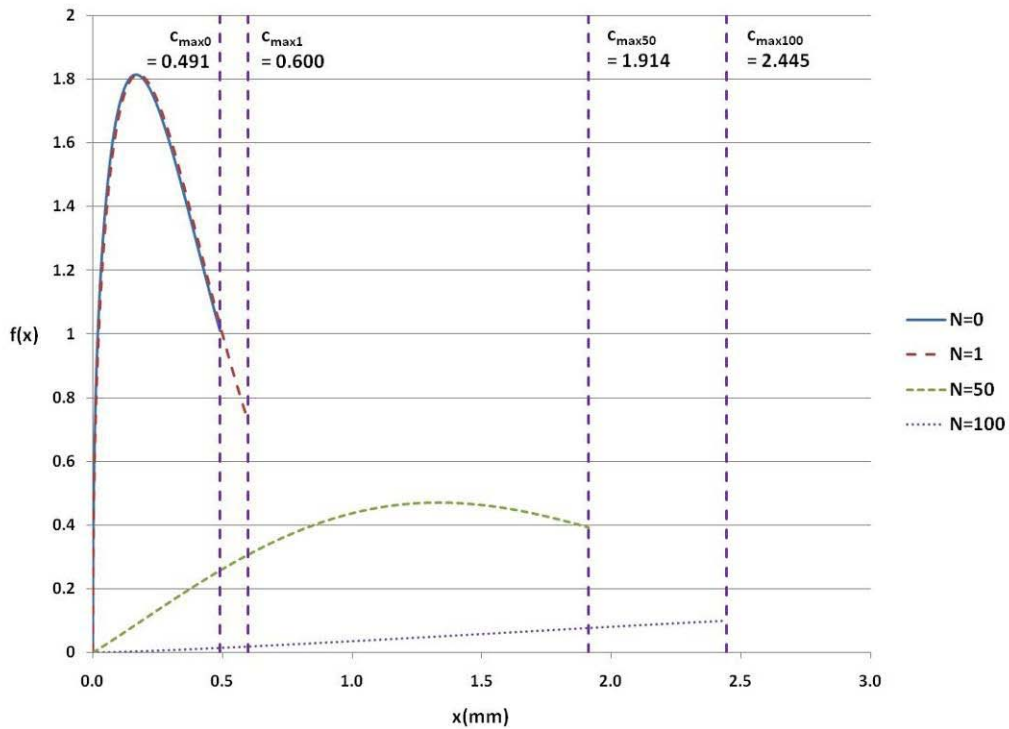


Figure F1b-2.3. Probability density functions of air void/crack size distribution at  $N = 0, 1, 50$  and  $100$ .

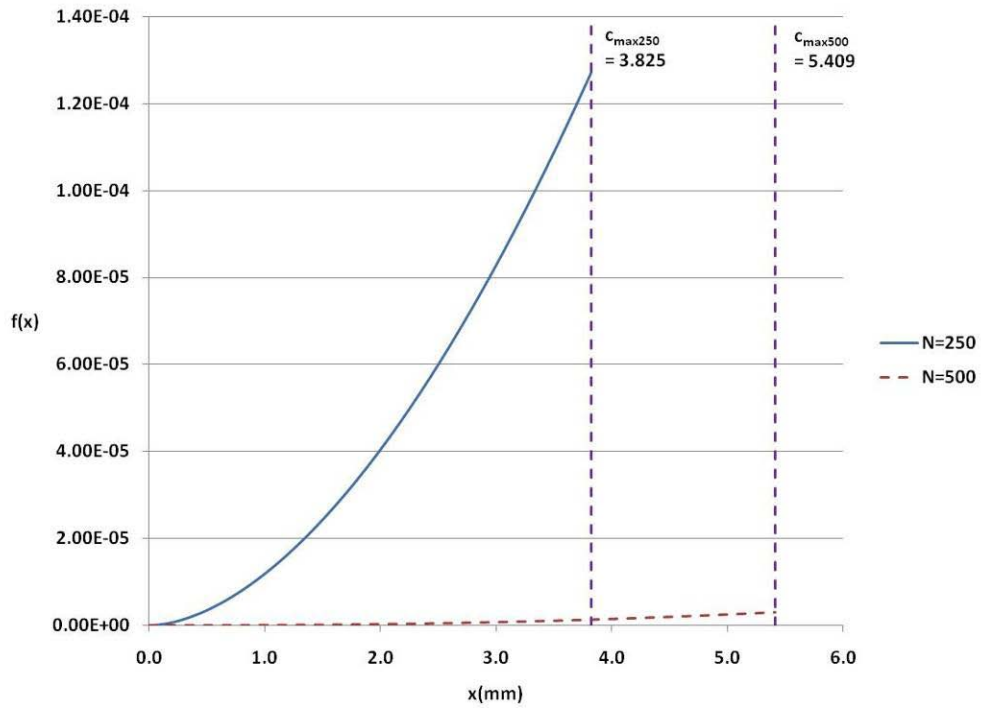


Figure F1b-2.4. Probability density functions of air void/crack size distribution at N = 250 and 500.

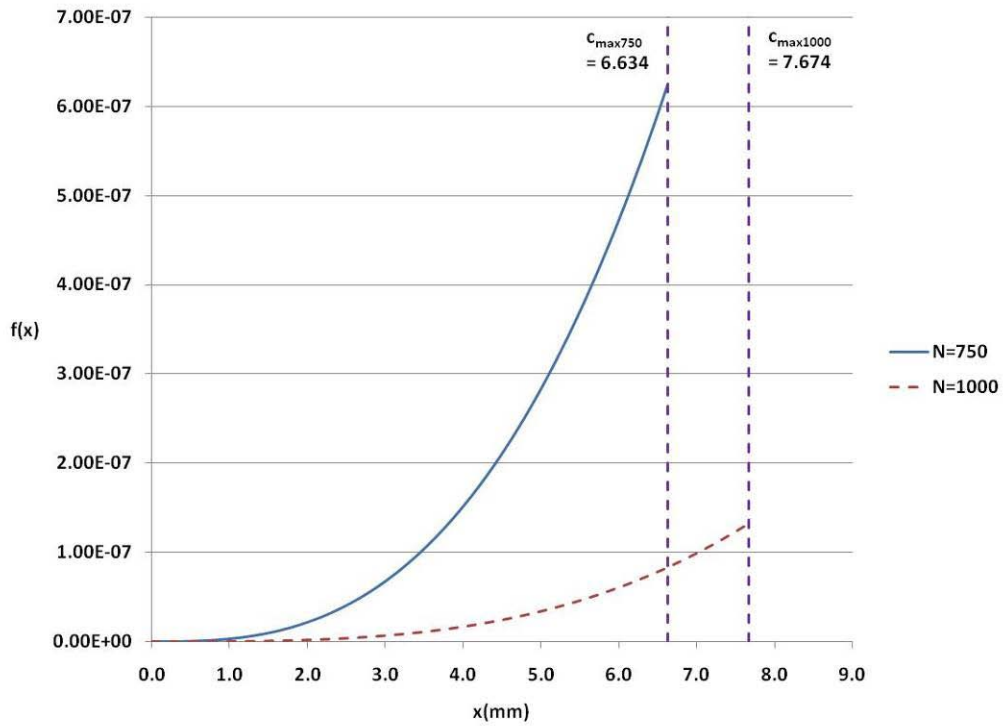


Figure F1b-2.5. Probability density functions of air void/crack size distribution at N = 750 and 1000.

Knowing  $f(x)$  for all loading cycles, the variance of the distribution was determined using Equation F1b-2.8 and was plotted in figure F1b-2.6. As shown in figure F1b-2.6,  $Var(X)$  increases approximately linearly as the number of loading cycles increases.

$$Var(X) = \frac{\gamma \left[ 1 + \frac{2}{a}, (\lambda c_{\max})^a \right] - \gamma^2 \left[ 1 + \frac{1}{a}, (\lambda c_{\max})^a \right]}{\lambda^2 \left[ 1 - e^{-(\lambda c_{\max})^a} \right]} \quad (F1b-2.8)$$

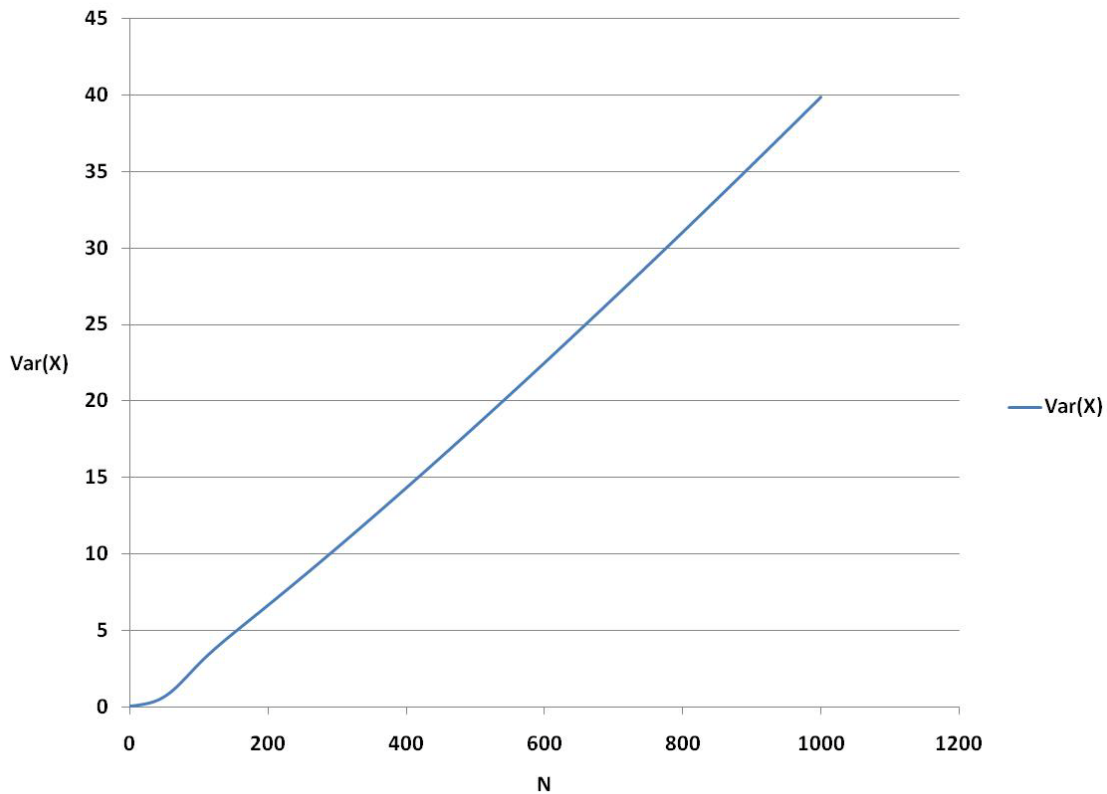


Figure F1b-2.6. Variation of variance of air void/crack size distribution with number of loading cycles.

### Significant Results

The experimental data obtained in Work Element F2c were used to develop a Weibull distribution model for the air void/crack size in asphalt mixtures. The calculated average size of air voids in an undamaged specimen together with the maximum air void size, minimum and average air void/size detected by the X-ray CT system were used to formulate two simultaneous equations with two unknown Weibull distribution parameters. These two simultaneous equations

were solved to obtain the probability density function of the air void size in the undamaged specimen. Then a perturbation analysis was conducted to obtain the probability density functions of crack size at all loading cycles.

#### Significant Problems, Issues and Potential Impact on Progress

- The new MTS machine availability for testing the pilot experiment samples with different air voids, binders, aggregates and aging;
- The reception of the aggregates and asphalts for the full experiment;
- The need to begin compressive testing to determine the undamaged and permanent deformation (plasticity) properties of different mixtures; and
- The availability of DMA equipment for testing for the effects of aging and moisture.

#### Work Planned Next Quarter

- Tests to be conducted on the pilot samples with different air voids, binders and aggregates;
- Analysis of initial air void sizes by X-ray CT and the fracture mechanics method;
- Determination of Paris' Law parameters  $A$  and  $n$  for each sample;
- Determination of the evolution patterns of  $a$ ,  $\lambda$ ,  $c_{\max}$  and  $\bar{c}$  as they depend on the mixture volumetrics and fundamental properties  $A$ ,  $n$ ,  $\Delta G_f$ ,  $E$ , % air void and film thickness; and
- Trial to see if healing model can resolve the difference in calculated final maximum crack size (using fracture mechanics) and that which can be observed after handling and scanning with the X-ray CT.

#### **Work Element F1c: Aging**

##### ***Subtask F1c-1: Critical Review of Binder Oxidative Aging and Its Impact on Mixtures (TAMU)***

#### Work Done This Quarter

There is no literature review work this quarter.

#### Work Planned Next Quarter

Review of previous work is an ongoing effort.

### ***Subtask F1c-2: Develop Experimental Design (TAMU)***

#### Work Done This Quarter

A draft experimental design was submitted last quarter. Final selection of materials (binder and aggregate) for testing has been determined.

#### Significant Results

The pilot experiment design was completed, and specimen fabrication (Subtask F1c-4) continued and was completed. Testing of the specimens has been delayed by equipment issues (Subtask F1c-4).

#### Significant Problems, Issues and Potential Impact on Progress

Further review of the core materials for use in the expanded experiment and of additional field sites for validation is needed.

#### Work Planned Next Quarter

Conducting the laboratory experiments of the experimental design that use the improved testing protocol (work element F2c) has been delayed by equipment difficulties but will begin in the next quarter. Also, additional field site cores for use in validation of the transport oxidation model and for evaluating the impact of binder oxidation on fatigue will be obtained from WRI.

### ***Subtask F1c-3: Develop a Transport Model of Binder Oxidation in Pavements (TAMU)***

#### Work Done This Quarter

Using the results of first order (fast-rate) reaction and zero-order (constant-rate) reaction experiments (section F1c-1), calculations were made using the previously-reported binder oxidation model for pavements. The carbonyl growth rate of the combined first order and constant-rate reactions can be described by:

$$r_{CA} = \frac{dCA}{dt} = (IJ - CA_0) \cdot k_f \cdot e^{-k_f t} + k_c$$

This reaction rate expression was implemented in the binder oxidation model, coupled with calculated pavement temperature profiles. The carbonyl growth of asphalt binders at three pavement depths and for two different climates, Texas and Minnesota, are shown in figures F1c-3. 1 and F1c-3 2, respectively.

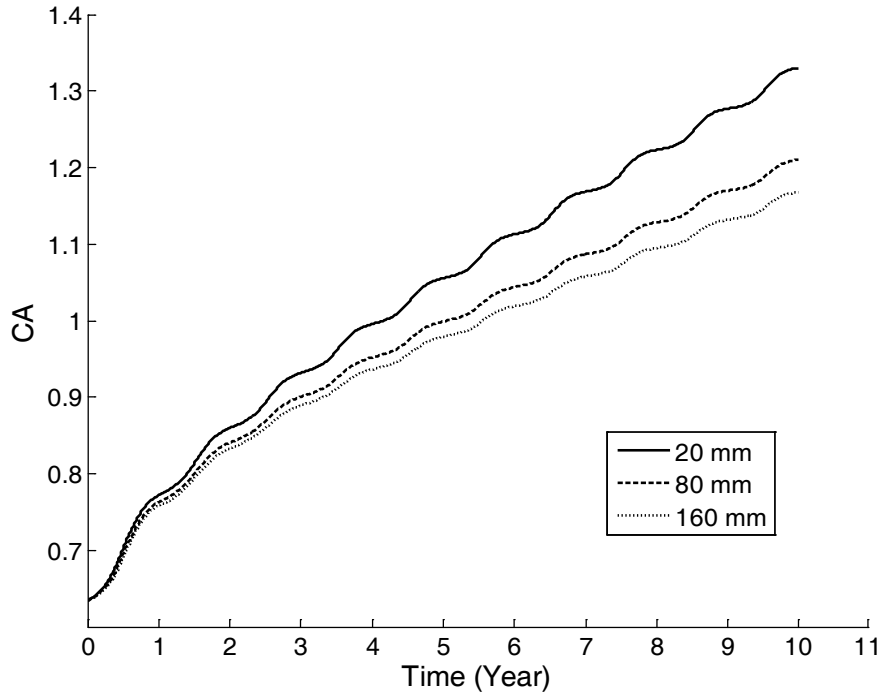


Figure F1c-3.1. Calculated carbonyl growth of Alon 64-22 in Texas climate using kinetics data for both first order and constant-rate reactions.

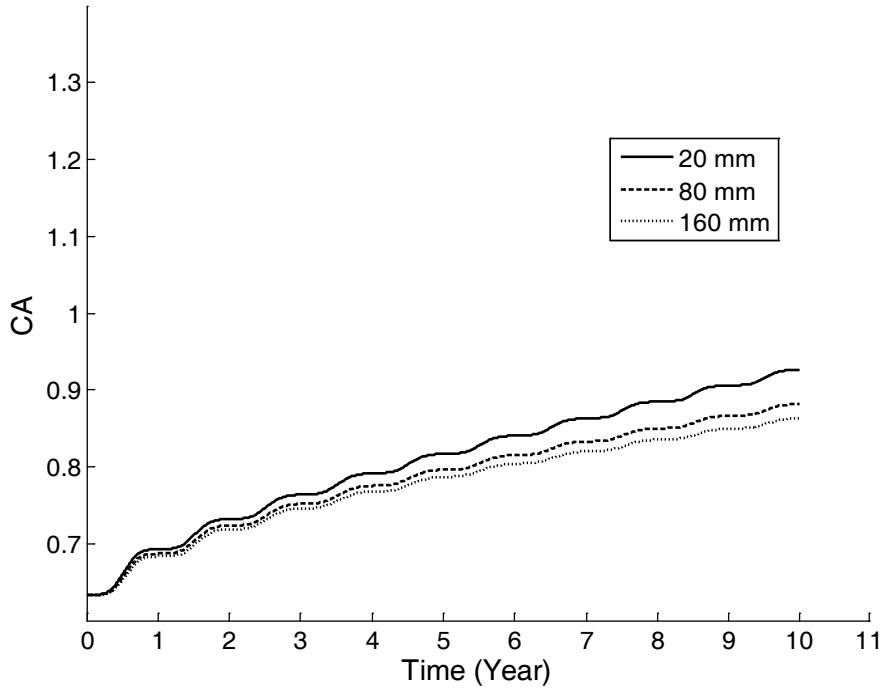


Figure F1c-3.2. Calculated carbonyl growth of Alon 64-22 in a Minnesota climate using kinetics data for both first order and constant-rate reaction.

As shown from the figures, the approximate times for this asphalt binder to reach the constant-rate period are estimated to be from 2 to 3 years in Texas and 4 to 5 years in Minnesota climates. This is the first effort to quantitatively model both the fast-rate and constant rate reaction periods to make estimates of binder oxidation in pavements.

### Significant Results

The ability to estimate binder oxidation in pavements as a function of time and depth, and in a full range of climates has been demonstrated. These estimates also now include the full range of binder oxidation over both the fast-rate and constant-rate periods. These calculations are essential for providing a foundation for mixture model calculations that include binder (and thus pavement) changes over time due to binder oxidation and thus an improved understanding of pavement durability.

### Significant Problems, Issues and Potential Impact on Progress

Further binder oxidation model validation is needed. More actual pavement aging rates need to be compared to model calculations. Pavement cores are available but ideally must be tested for physical properties (subtask F1c-4) before binder aging can be determined. Also, air void characteristic data for the corresponding pavements should be obtained or measured. Higher resolution X-ray CT scans are being evaluated for their ability to provide these air void data. If these air void characteristic data are not available, then parameter estimation methods will be employed.

Field cores are available for extraction and recovery of the binder to assess binder aging as a function of time and depth. However, an essential part of our research plan is to subject the mixture specimens to physical tests (fatigue, e.g.) before the destructive testing of air voids and extraction and recovery as a function of depth below the pavement core are conducted. The purpose of this specific protocol is to provide binder oxidation as a function of core age and depth on the very same cores as the mixture tests. In this way, the effects of binder oxidative hardening will be more closely matched to changes in the mixture physical properties due to this hardening. However, the delays in developing these mixture tests have prevented moving ahead with the air voids and binder testing. We are reassessing our protocol to allow obtaining air voids and binder properties independent of the mixture properties. Such a revised protocol would provide binder hardening on a core different than the sister core used for mixture testing, but hardening levels should be very comparable.

### Work Planned Next Quarter

For the study of fast-rate aging kinetics, work of this project will conduct binder oxidation experiments similar to those reported above (section F1c-1) using the core ARC binders. Neat binders will be aged in the POV apparatuses at three or more temperatures, as POV aging capability becomes available. Samples will be retrieved and tested for chemical and physical properties. Results will be analyzed for kinetics parameters and hardening susceptibilities from which both the fast-rate and constant-rate reaction kinetics and hardening parameters will be determined.

This quarter we will develop a modified protocol for field core testing that will allow us to proceed with mixture air voids and binder extraction and recovery independent of mixture testing (see the preceding section). We will then proceed with this testing on available field cores.

***Subtask F1c-4: The Effects of Binder Aging on Mixture Viscoelastic, Fracture, and Permanent Deformation Properties (TAMU)***

Work Done This Quarter

In this quarter, progress was made in three separate areas: determining the viscoelastic properties of aged field cores; determining the distribution of air void and crack sizes with repeated loading; and determining the fracture properties of mixes tested in repeated tension. The latter two developments are linked intimately together and it by using them that the characterization of the undamaged and damaged properties of the specimens fabricated for testing in the pilot experiment (Subtask F1c-2) will be accomplished. These specimens included 24 AAM samples and 24 AAD samples of unaged, and 24 AAM samples and 24 AAD samples of 6 months aged. The materials selected for the subsequent expanded experiment included two kinds of binder (Binder 1 and Binder 2) and four types of aggregate. They are Aggregate 1 (Limestone), Aggregate 2 (Granite), Aggregate 3 (Gravel), and Aggregate 4 (Andesite). Furthermore, a smaller experiment with Binder 1 and Aggregates 3 and 4 was designed to study the effect of aggregate type.

The fracture properties of mixtures is found using the  $W_{R1}$  dissipated pseudo-strain energy which was found to have an intercept,  $a$ , and a slope,  $b$ , when plotted linearly against the number of load cycles. It was found that the intercept varied inversely with the air void content and this fact plus fracture mechanics theory was used to determine the mean size (radius) of the air voids and the number of them. The only material properties that were used to determine this mean air void radius were the Surface Bond Energy, the Modulus, the asphalt film thickness, the undamaged phase angle and the phase angle after the first damaging load cycle, the intercept and slope of the dissipated pseudo-strain energy,  $W_{R1}$ , and the percent of air voids. This mean size was found to be smaller than the smallest air void radius observed in the X-Ray Computed Tomography scans of the same samples in the undamaged state. Use of truncated Weibull distributions for the fracture mechanics mean void size and the range of observable void sizes in the X-Ray CT scans together permitted the determination of the initial Weibull air void size probability density function parameters. The figure F1c-4.1 shows the initial Weibull distribution of air void radii that were determined by the combined use of these two measuring techniques. Also shown on the figure is the range of air void sizes between  $c_{min}$  and  $c_{max}$  that were detectable by the X-Ray CT method and the limit of resolution,  $c_r$  of that method. The initial maximum air void radius was 0.491 mm.

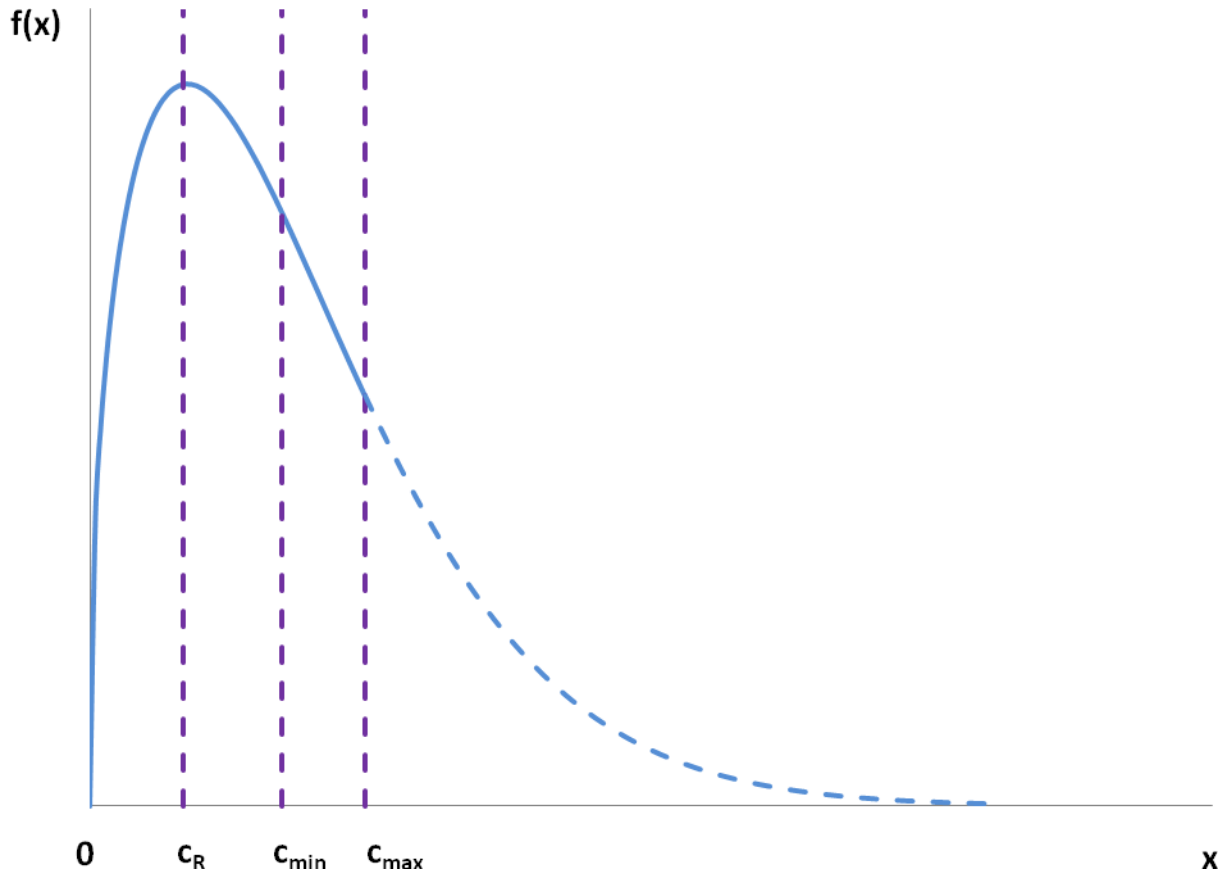


Figure F1c-4.1. Weibull distribution of initial air void radii.

This is an important step for the aging process for the prediction model uses as an input the original, undamaged air void radius. Having the complete Weibull distribution of the air void sizes makes it possible to take into account the effect of the air void size distribution on the process of oxidative aging. But the developments went several steps farther.

With repeated loads, the calculated mean air void/crack radii grew, the dissipated pseudo-strain energy  $W_{R1}$  increased linearly, the apparent modulus of the specimens decreased and the apparent phase angle increased. A formulation of the relation between the apparent modulus, phase angles, strain and stress and the actual modulus, phase, strain and stress together with the changing dissipated pseudo-strain energy was used to determine the Paris' Law parameters, commonly designated as  $A$  and  $n$ . This was used to predict the mean crack or air void radius as it grew with repeated loads. The predicted values of the mean crack radius corresponding to the values of the Paris' Law coefficients  $A$  and  $n$  are shown in figure F1c-4.2.

This growing mean crack radius together with the evolving Weibull distribution parameters was used to compute the maximum crack radius and the variance of the crack sizes. The Paris' Law parameters  $A$  and  $n$  were checked with values that had been calculated by other methods and were

found to match those values very well while being derived solely and entirely from the original test data.

The implications for this development are that as the cracks grow in size, the oxidative aging can proceed at a more rapid pace since with larger air void or crack sizes, more air can be made available to react with the mix. This couples the aging process to the fatigue-fracture process. The ability to predict the growth of the size and distribution of crack sizes also has implications for the availability of water vapor to evolve moisture damage. The changing Weibull distribution of the crack radii with increasing number of loading cycles is shown in figure F1c-4.3. Shown on that figure are the truncated Weibull distributions for  $N$  equal to 0, 1, 50 and 100. Beyond 100 loading cycles the Weibull distribution had only the rising portion of the curve and the final maximum crack radius after 1000 load repetitions was 7.674 mm. No measurement of the final crack radius was made with the X-Ray CT equipment because the time required to remove, handle and scan the sample would permit a considerable amount of healing and crack closure. However, this suggests a method of calibrating healing models, using the fracture mechanics model and the X-Ray CT method in tandem as was done with the initial air void size distribution.

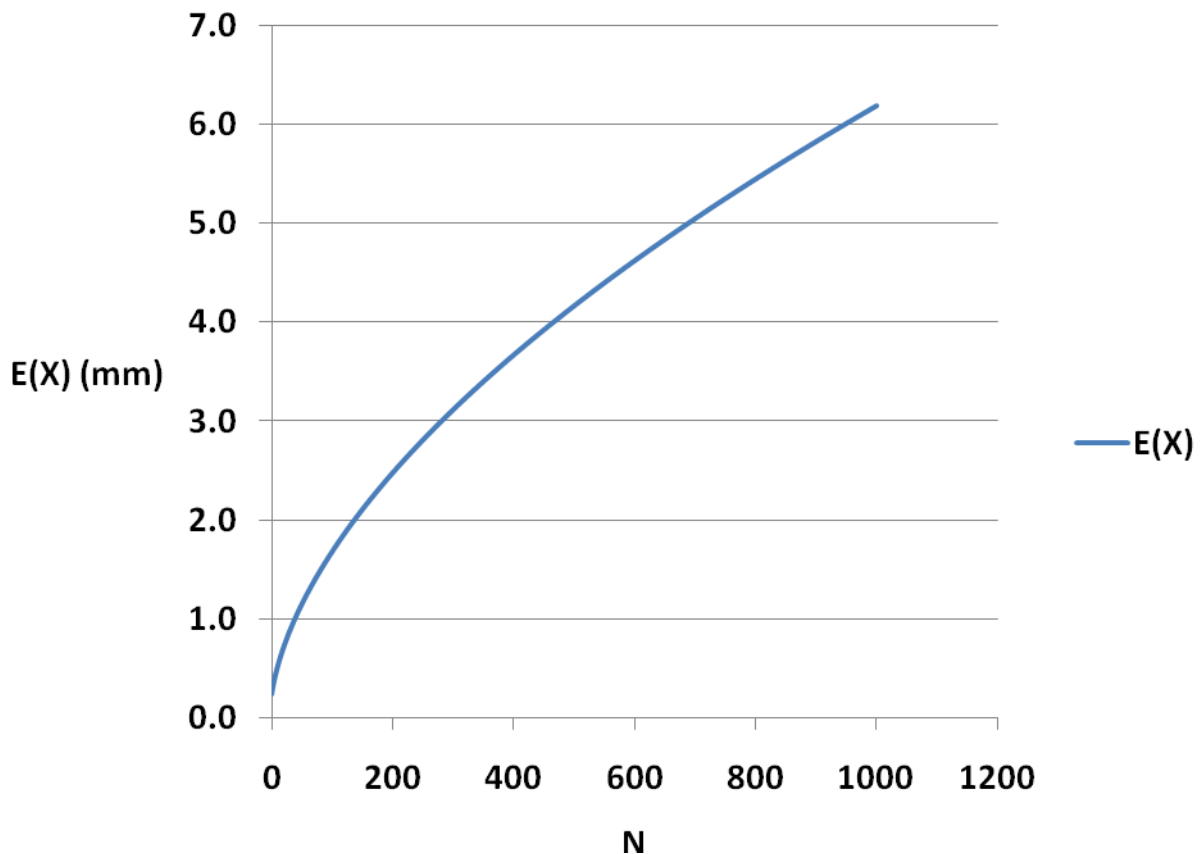


Figure F1c-4.2. Mean crack radius with number of loading cycles (Luo et al. 2009).

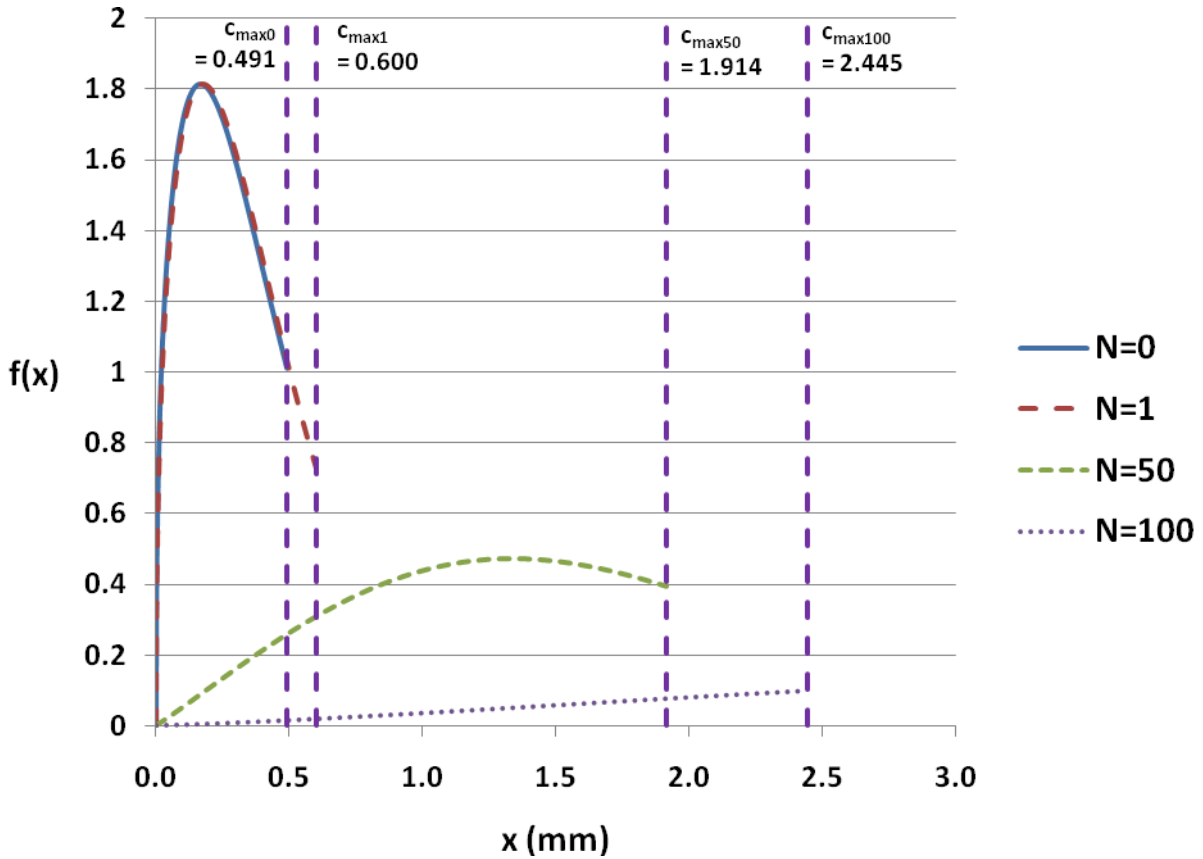


Figure F1c-4.3. Changing Weibull probability density functions of crack radii with increasing numbers of loading cycles (Luo et al. 2009).

It is necessary to connect these laboratory results to actual mixture properties of asphalt pavement surface layers in the field. Tests on core samples from the field have been complicated by several difficulties. Layers of a single mixture are rarely found to be more than a few inches thick. The surface of the asphalt is usually much stiffer than the mixture below. Typical 6-inch diameter cores are shown in figure F1c-4.4



Figure F1c-4.4. Typical cores of asphalt surface layers.

When this thin layer is tested in tension, the stiffer modulus induces an oscillation of the sample which has been hard to control and to predict. After considerable experimentation a tensile testing protocol was developed that produced oscillations that did not damage the specimen. An example of the microstrain measurements that were made on a thin, oscillating sample is shown in figure F1c-4.5. This shows that there were smaller oscillations on the top of the pavement surface where the mixture was stiffer.

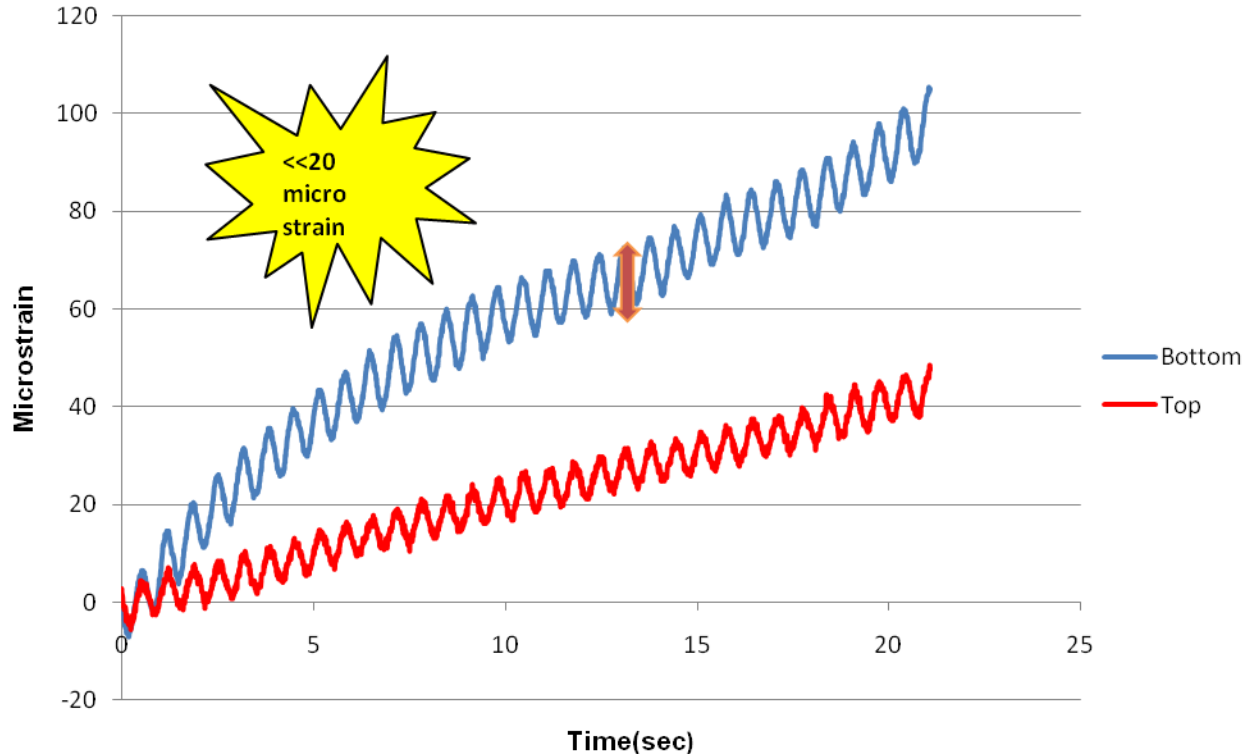


Figure F1c-4.5. Monotonic tensile microstrain measurements on the top and bottom surfaces of a pavement core.

An analytical approach was developed that predicts the stretching and oscillating that is commonly observed and has resulted in being able to determine the viscoelastic frequency-dependent characteristics of the mixture moduli at the surface and at the bottom of the surface layer. The results of this analysis of the test data are shown in figure F1c-4.6. The magnitude of the Complex Modulus is plotted against frequency in Hertz. The stiffness of the mixture on the surface of the pavement layer is stiffer at all levels of frequency. However, the values shown in that figure are for an unusually soft mixture. Not shown here are the results of the horizontal LVDT readings with which we are able to calculate the Viscoelastic Poisson's Ratio. It is possible to make the undamaged Viscoelastic Characterization (VEC) test at three temperatures on these field cores and to determine the mixture master curves of the magnitude and phase angles of the complex modulus and Poisson's Ratio at both the top and bottom of the sample.

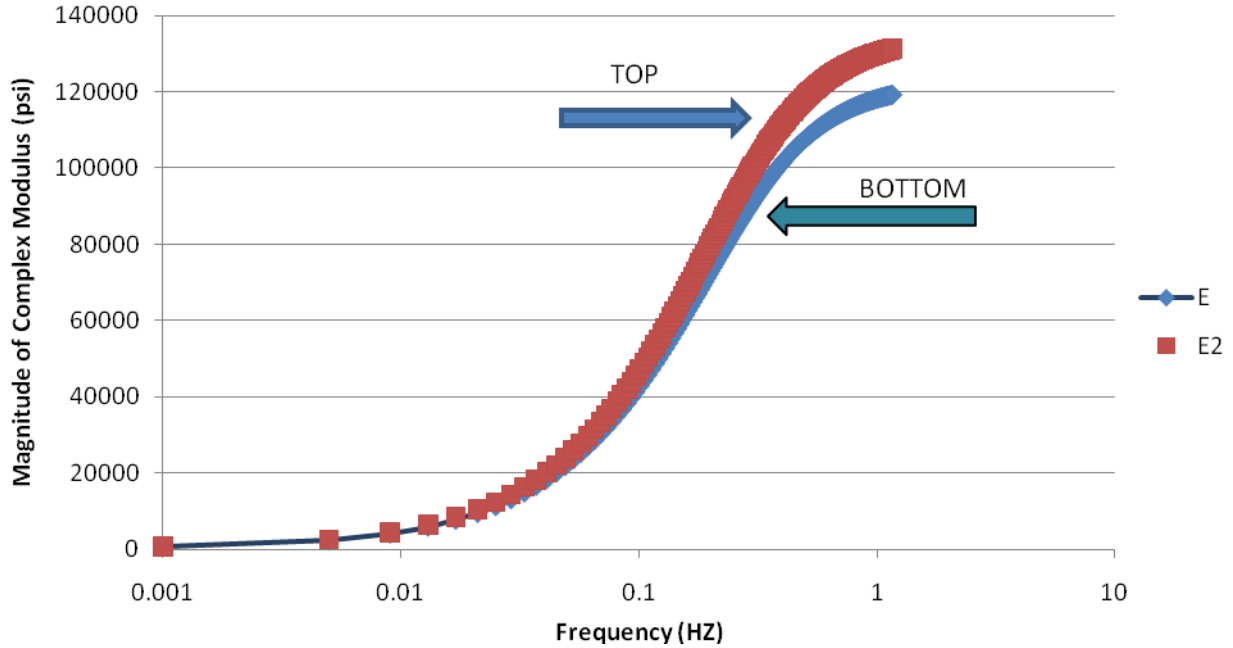


Figure F1c-4.6. Magnitude of the complex modulus of the mixture on the top and bottom surfaces of an asphalt surface layer.

More testing needs to be done to verify that the results are repeatable and accurate. If proven accurate, this provides the opportunity to observe the effect of aging on mixture and binder properties at different depths below the surface. If proven, this will provide the ability to compare actual measured viscoelastic properties with the predictions that can be made with laboratory samples and artificial aging protocols.

#### Significant Problems, Issues and Potential Impact on Progress

New Linear Variable Differential Transformers (LVDTs) with higher precision have been used since January 2009. The new MTS equipment was delivered in June 2009 and is still being tested and adjusted. No production tests have been run on it to this date but it is getting close. Dynamic Mechanical Analysis (DMA) testing is being held up by having only one such device available for the testing.

#### Work Planned Next Quarter

Testing on the pilot unaged specimens will be done and testing on the 6-month aged specimens will be begun. The new test protocols will be used to determine the properties of the unaged mixes. When the testing of the aged mixtures is begun, those samples will also be tested in the same way and we will then be able to determine the effect of aging on the viscoelastic, fracture, crack propagation and crack size distribution properties of mixtures. Materials will be received for molding the samples for the expanded experiment. Further work will be done on the protocol of how

to determine the anisotropic plasticity (permanent deformation) properties of a mixture making use of the  $W_{R2}$  dissipated pseudo-strain energy. More tests will be made to determine the original air void sizes of different mixes and subsequent growth of the crack sizes and evolution of the size distributions using the combination of fracture mechanics and X-Ray CT scans which has been described above. Tests to finalize the protocol for measuring the undamaged anisotropic compressive viscoelastic properties of a mixture will be made. It is the departure from these undamaged properties that compressive damage tests can be used to determine the plasticity properties of a mixture. These will also be affected by the aging. More tests will be run on field cores to verify the repeatability and accuracy of the test and analysis method that was developed in the last quarter to determine the viscoelastic properties of a field core mixture as it changes with depth from the surface downward.

### Publications

Luo, X., Luo, R., Lytton, R. L., Koochi, Y. (2009) “Characterization of Damage in Asphalt Mixture Using Dissipated Pseudo-Strain Energy.” To be submitted to *Journal of Transportation Engineering*, American Society of Civil Engineers.

Luo, R., and Lytton, R. (2009) “Distribution of Crack Size in Asphalt Mixtures.” To be submitted to *Journal of Transportation Engineering*, American Society of Civil Engineers.

### ***Subtask F1c-5: Polymer Modified Asphalt Materials (TAMU)***

#### Work Done This Quarter

No activity this quarter.

#### Significant Results

No activity.

#### Significant Problems, Issues and Potential Impact on Progress

No activity.

#### Work Planned Next Quarter

During the next quarter, polymer modified binders will be obtained for testing.

## **Work Element F1d: Healing**

### ***Subtask F1d-1: Critically Review Previous Work on Healing under FHWA Contracts DTFH61-C-92-00170 and DTFH61-C-99-00022 (TAMU)***

#### Work Done This Quarter

The literature review was continued in this quarter.

#### Work Planned Next Quarter

This is an ongoing subtask that will be continued through this project

### ***Subtask F1d-2: Select Materials with Targeted Properties (TAMU)***

#### Work Done This Quarter

Pending the sampling and collection of the core binders that will form the basis of the main test program, we are currently using locally available binders to develop the test method to validate the healing model.

#### Work Planned Next Quarter

For next quarter we plan to measure the properties related to the healing model for the core asphalt binders.

### ***Subtask F1d-3: Develop Experiment Design (TAMU)***

#### Work Done This Quarter

The healing model comprises a wetting function and an intrinsic healing function. Research from the previous quarters led to the development of a test method to measure the intrinsic healing properties using the DSR. The wetting function is defined by mechanical properties of the binder as well as properties such as the healing process zone. In this quarter researchers were able to develop an experiment design that will allow validating the healing model. This will be achieved in the following three main stages:

1. The intrinsic healing properties will be measured using the DSR in shear mode following the procedure developed earlier. The test will be conducted by applying different levels of normal force to the specimen. In addition, intrinsic healing rates will also be measured by applying a normal force to the specimen instead of applying a shear stress using the DMA.
2. Healing in FAM specimens will be measured by applying cyclic loads followed by rest periods. These tests will be in controlled strain mode of loading in direct tension. A triangular waveform will be used to apply and recede the strain in tension on the

specimen. It is hypothesized that varying the rate at which the strain recedes from its peak value can control the rate of wetting. A continuum approach will be used to quantify healing that occurs in the specimen during the rest periods.

3. The micromechanical model for healing will be verified by measuring the intrinsic healing function for the material, changing the different rates of wetting using a FAM specimen and then comparing results from the model to the measured healing on the FAM specimens.

#### Work Planned Next Quarter

Modifications to the work plan, if required, will be made after obtaining initial results.

#### ***Subtask F1d-4&5: Investigate Test Methods to Determine Material Properties Relevant to Asphalt Binder Healing (TAMU)***

#### Work Done This Quarter

The preliminary experiment design to validate the healing model was developed as described in F1d-3. Testing with asphalt binders following this test plan is underway.

#### Work Planned Next Quarter

The intrinsic healing function for different asphalt binders will be measured (step 1 described in F1d-3) for different asphalt binders using the DSR and the normal force methods.

#### ***Subtask F1d-5: Testing of Materials for model validation\* (TAMU)***

#### Work Done This Quarter

No work planned.

#### Work Planned Next Quarter

Work in this subtask is planned for later after completion of Subtask F1d-4. Summarily, step 3 of the outline presented in F1d-3 is for validation of the healing model.

#### ***Subtask F1d-6: Evaluate Relationship Between Healing and Endurance Limit of Asphalt Binders (UWM)***

#### Work Done This Quarter

Application of the reduced cycles concept for analysis of asphalt fatigue data (Christensen and Bonaquist 2009) was employed on existing binder time sweep data with promising results. The endurance limits calculated from the analysis were then compared with Accelerated Load Facility (ALF) fatigue performance data for the same binders with a reasonable correlation.

Binder time sweep data at multiple applied strain levels were required to perform the reduced cycle analysis. Data from previous research (Martono and Bahia 2008) that evaluated the fatigue performance of various binders used in an FHWA ALF experiment at multiple strain levels were thought to be an excellent candidate for the preliminary analysis using the reduced cycle concept. One unmodified and four modified binders were tested at levels ranging from 3% to 9% strain at 10 Hz and 19 °C.

The equations employed in the Christensen study on asphalt mixtures were left unchanged; however, the initial value of  $\alpha$  used during curve fitting was taken from previous research on these materials using more traditional viscoelastic continuum damage (VECD) concepts (Johnson et al. 2009; Wen and Bahia 2009). The reference applied strain was taken at 3%, the lowest level for the majority of binders in this data set.

### Significant Results

The plots shown in figure F1d-6.1 represent the original fatigue curves for the styrene-butadiene-styrene (SBS)-modified binder measured at 3%, 5% and 7% strain. Figure F1d-6.2 shows the shifted fatigue data using the equations introduced in the Christensen study.

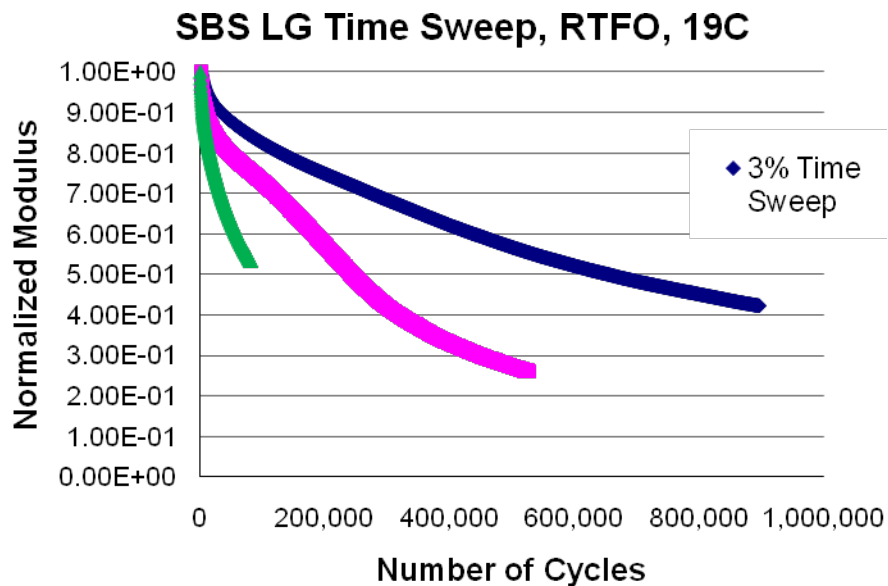


Figure F1d-6.1. Graph. Plots of the normalized modulus with number of cycles during time sweep testing. (RTFO = rolling thin film oven.)

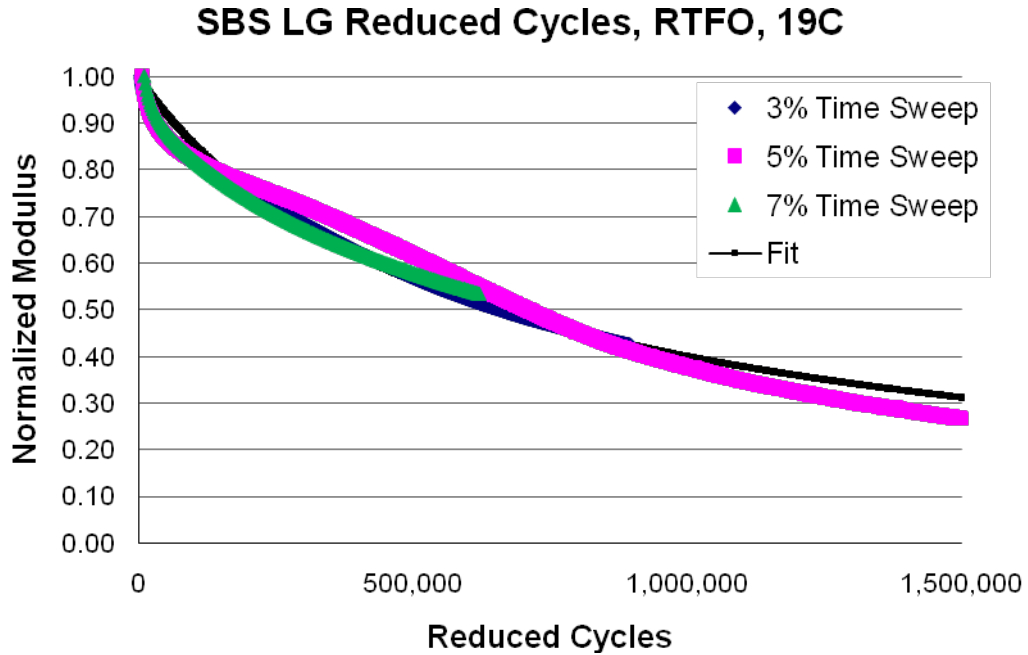


Figure F1d-6.2. Graph. Plots of normalized cycles versus reduced cycles for the SBS binder.

As shown in table F1d-6.1, endurance limit strain was determined through the process of curve fitting (based on the 3% reference strain).

Table F1d-6.1. Endurance limit strain determined from time sweep analysis.

Binder	Average Endurance Limit Strain
Control 70-22	5.97E-07
Air Blown	6.14E-03
CR TB	1.43E-02
SBS LG	1.74E-02

A reasonable correlation is observed when plotting endurance limit strain against the cracking experienced by the ALF test sections, as shown in figure F1d-6.3.

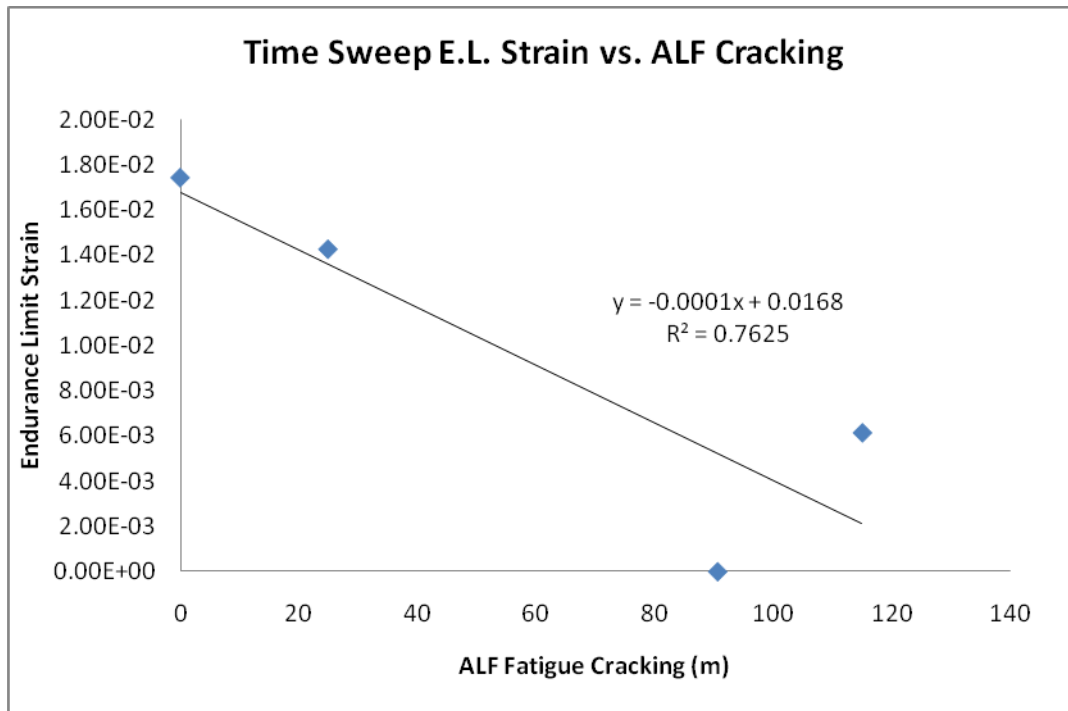


Figure F1d-6.3. Graph. Plot of endurance limit strain versus ALF fatigue cracking.

While the linear relation is not perfect, the general trend is intuitive, given the expectation that a material with a higher endurance limit strain will have a higher fatigue life.

Significant Problems, Issues and Potential Impact on Progress

None.

Work Planned Next Quarter

While calculation of endurance limits directly from binders may eventually prove to be useful, the question remains as to whether the calculated endurance limits are related to the materials' healing characteristics. Work next quarter will focus on attempting to use the test methods shown in previous quarterly technical progress reports to measure healing properties. The research team will also consult with consortium partners at the Texas Transportation Institute asphalt testing laboratory on the matter.

Cited References

Christensen, D. W., and R. Bonaquist, 2009, Analysis of HMA fatigue data using the concepts of reduced loading cycles and endurance limit. *Journal of the Association of Asphalt Paving Technologists*, 78.

Johnson, C. M., H. U. Bahia, and H. Wen, 2009, Practical application of viscoelastic continuum damage theory to asphalt binder fatigue characterization. *Journal of the Association of Asphalt Paving Technologists*, 78.

Martono, W., and H. U. Bahia, 2008, Developing a Surrogate Test for Fatigue of Asphalt Binders. The 87th Transportation Research Board Annual Meeting, Washington, D.C.

Wen, H., and H. U. Bahia, 2009, Characterizing Fatigue of Asphalt Binders Using Continuum Damage Mechanics. The 88th Transportation Research Board Annual Meeting, Washington, D.C.

***Subtask F1d-7: Coordinate with Atomic Force Microscopic (AFM) Analysis (WRI)***

Work Done This Quarter

None

Significant Results

None

Significant Problems, Issues and Potential Impact on Progress

None

Work Planned Next Quarter

Analysis of existing data will continue in the next quarter. In these analyses, morphological features observed in asphalt and asphalt chromatographic fraction thin films will prepared from validation site asphalts will be compared to performance data of the field site pavements.

***Subtask F1d-8: Coordinate Form of Healing Parameter with Micromechanics and Continuum Damage Models (TAMU)***

This subtask will be conducted in coordination with Work Elements F3b and F3c. The objective of this subtask will be to frame the healing property of asphalt binders and mastics, and if required the fine aggregate matrix, in a form that can be easily incorporated in the micromechanics model as well as the continuum fatigue model. This subtask will be critical to ensure that healing is appropriately incorporated along with other material properties as a part of these models.

## CATEGORY F2: TEST METHOD DEVELOPMENT

### Work Element F2a: Binder Tests and Effect of Composition (UWM)

#### Work Done This Quarter

The research team conducted fatigue tests, rheological measurements, material aging and production of new blends. In addition to the materials included in the original work plan, the research team added cross-linked materials to its materials inventory to provide a better comparison with modified binders produced in the field. The influence of cross-linking on fatigue performance of asphalt binder has been investigated in connection with Butafalt, a widely used cross-linking material.

Binder Yield Energy Tests (BYETs) for binders were conducted at 19 °C and at the temperatures of  $G^*\sin(\delta) = 500$  kPa. Results of binders with Butafalt were compared with the same binders without the cross-linker. Results of time sweep fatigue testing are being collected and analyzed using the viscoelastic continuum damage (VECD) procedure being developed as part of the F2e work element. All time sweep tests were performed at two temperatures (19 °C and intermediate true grade temperature) and at two stress levels to simulate different pavement structures.

#### Significant Results

The PG properties of cross-linked modified binders are shown in tables F2a.1, F2a.2 and F2a.3 for un-aged-, rolling thin film oven (RTFO)- and pressure aging vessel (PAV)-aged conditions, respectively.

Table F2a.1.  $G^*/\sin(\delta)$  original material.

	Original, $G^*/\sin(\delta)$ [kPa]			High Temp True PG Grade [°C]
	T, °C	Run 1	Run 2	
<b>FH + 2 LSBS + 0.123 BUT</b>	@70	1.55	1.51	<b>74.1</b>
	@76	0.82	0.81	
<b>FH + 4 LSBS + 0.246 BUT</b>	@82	1.15	1.19	<b>83.8</b>
	@88	0.67	0.70	
<b>CRM + 2 LSBS + 0.123 BUT</b>	@64	1.29	1.21	<b>66.8</b>
	@70	0.77	0.67	
<b>CRM + 4 LSBS + 0.246 BUT</b>	@76	1.00	1.01	<b>76.2</b>
	@82	0.64	0.66	

LSBS = linear styrene-butadiene-styrene. BUT = Butafalt.

Table F2a.2.  $G^*/\sin(\delta)$  RTFO-aged material.

	<b>RTFO, <math>G^*/\sin(\delta)</math> [kPa]</b>			<b>High Temp True Grade [°C]</b>
	T, °C	Run 1	Run 2	
<b>FH + 2 LSBS + 0.123 BUT</b>	@70	3.16	3.31	<b>73.4</b>
	@76	1.61	1.64	
<b>FH + 4 LSBS + 0.246 BUT</b>	@76	3.32	3.01	<b>79.9</b>
	@82	1.84	1.80	
<b>CRM + 2 LSBS + 0.123 BUT</b>	@64	2.30	2.43	<b>64.6</b>
	@70	1.27	1.28	
<b>CRM + 4 LSBS + 0.246 BUT</b>	@70	2.31	2.29	<b>70.5</b>
	@76	1.34	1.37	

Table F2a.3.  $G^*\sin(\delta)$  PAV-aged material.

	<b>PAV, <math>G^*\sin(\delta)</math> [kPa]</b>			<b>TG [°C]</b>
	T, °C	Run1	Run2	
<b>FH + 2 LSBS + 0.123 BUT</b>	@19	6961.4	6968.0	<b>21.7</b>
	@22	4759.3	4874.3	
<b>FH + 4 LSBS + 0.246 BUT</b>	@19	7157.1	6949.0	<b>21.9</b>
	@22	5084.8	4913.4	
<b>CRM + 2 LSBS + 0.123 BUT</b>	@16	6845.4	6536.2	<b>18.3</b>
	@19	4732.0	4554.2	
<b>CRM + 4 LSBS +0.246 BUT</b>	@13	6262.5	6276.6	<b>14.8</b>
	@16	4279.7	4381.0	
	@19	2840.7	2964.7	

The influence of cross-linking on BYET results is shown in figure F2a.1.

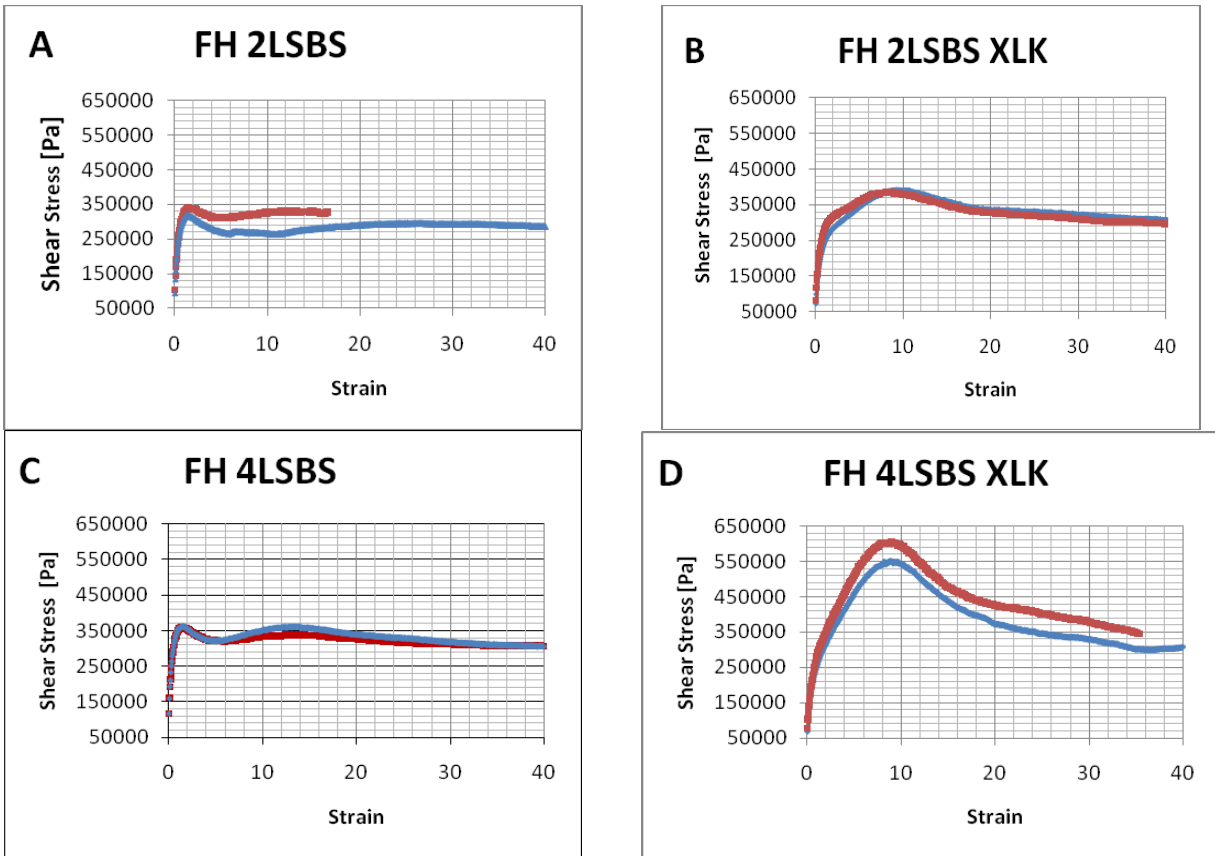


Figure F2a.1. Graphs. Effect of cross-linking of SBS on results of the BYET for the FH binder: (A) modification with 2% LSBS, no cross-linking; (B) modification with 2% LSBS, cross-linking (XLK); (C) modification with 4% LSBS, no cross-linking; and (D) modification with 4% LSBS, cross-linking.

Figure F2a.2 is a bar chart comparing the yield energy levels of the materials shown in figure F2a.1 with other binders modified with Elvaloy terpolymer (ELV). The results show that the cross-linked polymers give very comparable levels of the yield energy regardless of the modification level for styrene-butadiene-styrene (SBS), and the results are comparable to the 1.5% content of the terpolymer. However, the binders with no cross-linking and the binder with lower concentration of the terpolymer are at a much lower level of yield energy.

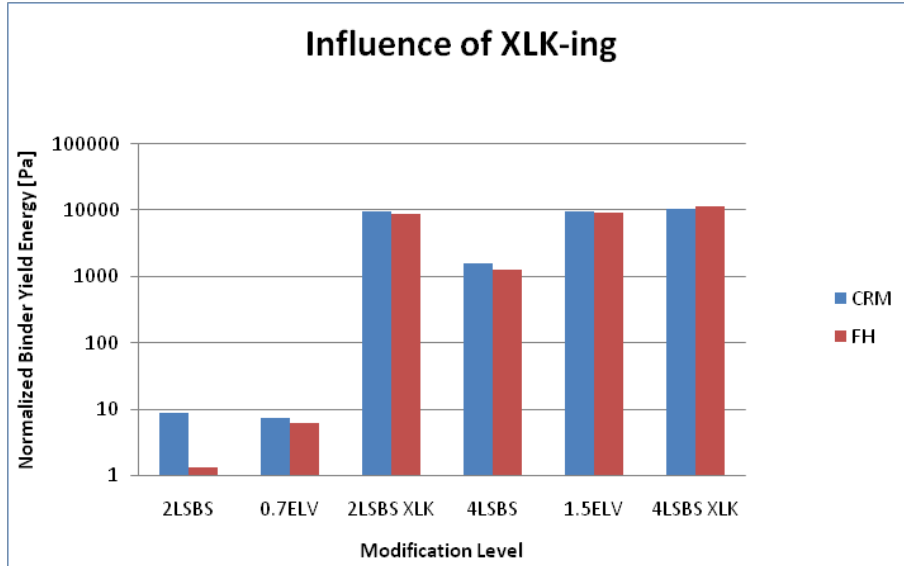


Figure F2a.2. Graph. Influence of cross-linking on BYET results versus modification level.

Figure F2a.3 shows the results of the time sweeps in terms of the number of cycles to crack propagation ( $N_p$ ) and number of cycles to 20% reduction in dissipated energy ( $N_{p20}$ ). The  $N_p$  and  $N_{p20}$  calculations follow the procedures outlined in NCHRP Report 459. As shown, there does not appear to be a similarity in trend with regard to the effect of cross-linking when comparing BYET and time sweep results. The 4% SBS appears to give less cycles to failure than the 2% SBS. The 2% and 4% cross-linked binders show very different results. This initial data lead the research team to believe that the BYET data are more of an indication of material composition rather than a direct correlation with fatigue properties. The time sweep test is known to show high potential for variability, and more replicates will be conducted to confirm the unexpected trends shown in figure F2a.3.

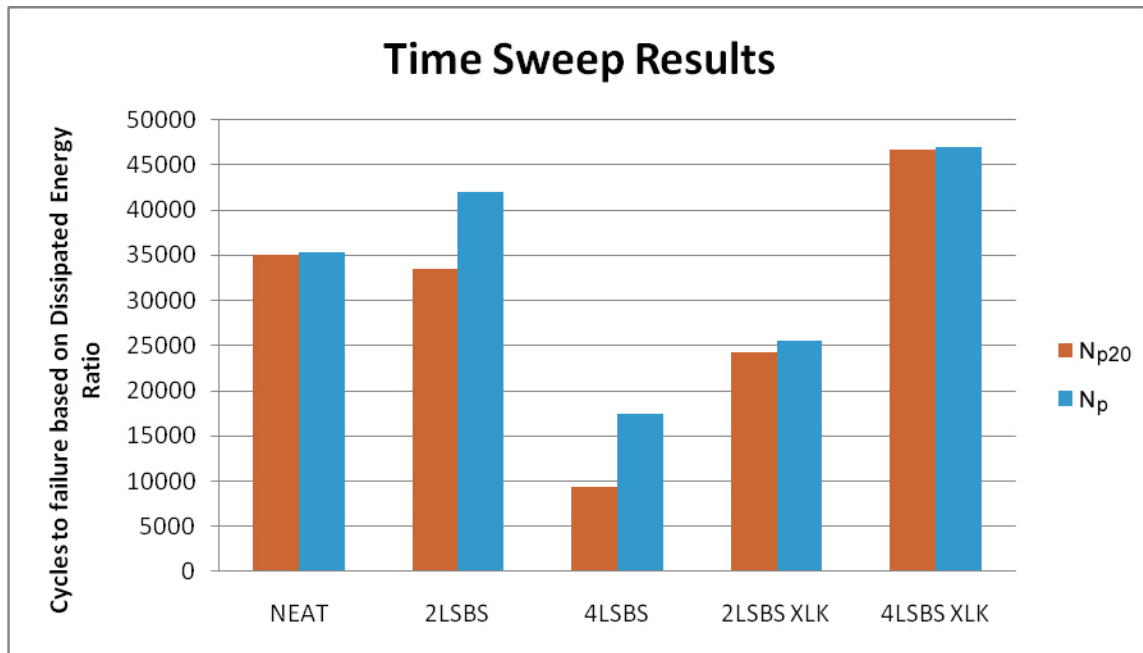


Figure F2a.3. Graph. Time sweep test results.

The data collected to date are not sufficient to draw significant conclusions. More analysis will be conducted to understand the relationship between the two tests and the effect of binder modification on fatigue.

#### Significant Problems, Issues and Potential Impact on Progress

The lack of correlation between the BYET results and the time sweep is a major concern since these tests are expected to rank materials similarly. Replicate testing and more elaborate analysis will be conducted to find the reasons for these differences.

#### Work Planned Next Quarter

Collection and analysis of data will continue, and the research team will investigate the relationship between the BYET and time sweep results. Similar tests will be performed for CRM-based binders.

#### Cited References

Bahia, H. U., D. I. Hanson, M. Zeng, H. Zhai, M. A. Khatri, and R. M. Anderson, 2001, *Characterization of Modified Asphalt Binders in Superpave Mix Design*. NCHRP Report 459.

## **Work Element F2b: Mastic Testing Protocol (TAMU)**

### Work Done This Quarter

Improvements to the test protocol to determine fatigue-cracking resistance of FAM specimens using the DMA were made in Subtask F1b-1. Further work on this subtask will be carried out in coordination with the technology development area. The tentative protocol was presented to the mixture ETG at the semi-annual meeting in Reno, NV in September 2008.

### Work Planned Next Quarter

Researchers will coordinate with the technology development work area to further develop the test protocols.

## **Work Element F2c: Mixture Testing Protocol (TAMU)**

### Work Done This Quarter

In this quarter, a test protocol and its analysis for characterizing the undamaged viscoelastic anisotropic compressive and tensile properties of an asphalt mixture were completed. Also, a method was developed for testing and analyzing the results of a repeated direct tension test to determine the initial radius of the air voids and the number of such air voids using the principles of fracture mechanics. The method went further using the fundamental material properties of modulus, surface bond energy, mean asphalt film thickness and the measured rate of change of dissipated pseudo-strain energy of fracture,  $W_{R1}$ , to determine the Paris' Law coefficients, A and n.

The test protocol on the properties of undamaged asphalt mixtures was further modified and improved to characterize the anisotropic viscoelastic properties of undamaged asphalt mixtures. The asphalt mixture behaves differently under compressive and tensile loading. Under compressive loading, the undamaged asphalt mixtures were described as transversely isotropic linear viscoelastic material which was interpreted using four parameters including i) the compressive complex modulus in the axial direction, ii) the compressive complex Poisson's ratio in the axial direction, iii) the compressive complex modulus in the radial direction, and iv) the compressive complex Poisson's ratio in horizontal plane. Under tensile loading, the undamaged asphalt mixture was characterized as an isotropic linear viscoelastic material using two parameters including i) the tensile complex modulus, and ii) the tensile complex Poisson's ratio. These six parameters were obtained by three nondestructive test scenarios: i) uniaxial compressive creep test, ii) uniaxial tensile creep test, and iii) indirect tensile creep test. The three test scenarios were completed using the Universal Testing Machine (UTM) and Material Testing Machine (MTS). Figures F2c.1 through 3 shows the set-up of the three tests. Because all three of the tests are nondestructive, they can be run on the same sample, thus reducing the sample-to-sample error that is common to most testing.

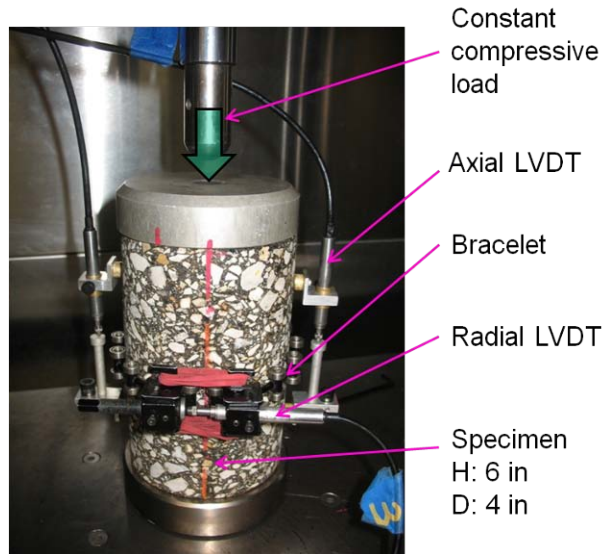


Figure F2c.1. Uniaxial compressive creep test.

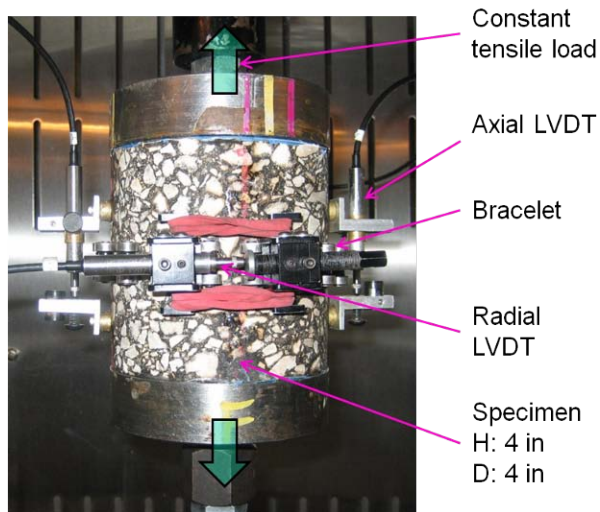


Figure F2c.2. Uniaxial tensile creep test.

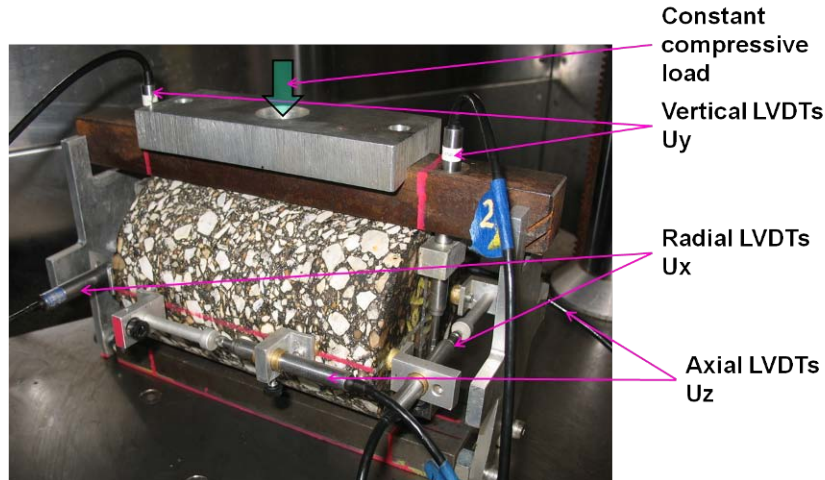


Figure F2c.3. Indirect tensile creep test.

In the uniaxial compressive creep test, a constant compressive axial load was applied to the asphalt mixture specimen whose diameter was 4 inches and height was 6 inches. The total loading time was 60 seconds. During the loading period, the axial strain and radial strain were measured, which were both functions of time. The uniaxial tensile creep test was similar to the uniaxial compressive creep test except that a constant tensile axial load, instead of compressive axial load, was used in the test and the height of the asphalt mixture specimen was cut into 4 inches so as to eliminate the effect of the non-uniform distribution of the air void on the tensile properties of the asphalt mixture. In the indirect tensile creep test, a constant compressive load was applied to the specimen along the radial direction. The deformation in the vertical direction, radial direction and the axial direction were recorded as a function of time. Based on the test data, a set of formulas was derived to determine the aforementioned anisotropic viscoelastic properties of the asphalt mixture. The Laplace Transform method for determining the frequency dependence of the complex moduli and Poisson's ratios was used to compute the viscoelastic properties.

In the last quarter, based on the previously developed test protocol for repeated direct tension (RDT) test, the process of damage accumulation has been characterized using dissipated pseudo strain energy (DPSE). During the test, two major damages, fatigue cracking and permanent deformation, can be determined by the two components of the DPSE,  $W_{R1}$  and  $W_{R2}$ , respectively. In this quarter, the focus was on applying  $W_{R1}$  to model fatigue cracking in the presence of repeated tensile loading. In the first place, the crack growth rate,  $dc/dN$ , was related to the pseudo J-integral in the form of simple power law as shown in Equation 1.

$$\frac{dc}{dN} = A(J_R)^n \quad (1)$$

where  $A$  and  $n$  = material constants and  $J_R$  = pseudo J-integral, which was based on the change of the DPSE as stated in the literature (Si et al. 2002; Walubita et al. 2006; Masad et al. 2007; Arambula 2007). However, instead of the DPSE,  $W_{R1}$  was used to determine  $J_R$ , considering the

true energy dissipation during the process of cracking rather than a global change of energy in the whole specimen. Consequently,  $J_R$  was given by Equation 2 as follows:

$$J_R = \frac{\partial W_{R1}}{\partial(\text{crack surface area})} \quad (2)$$

Substituting Equation 2 into 1 and conducting integration yielded the expression for the average crack radius of a growing crack:

$$c = \left[ (c_0)^{\frac{2n+1}{n+1}} + \left( \frac{2n+1}{n+1} \right) A^{\frac{1}{n+1}} \left( \frac{b}{4\pi M} \right)^{\frac{n}{n+1}} N \right]^{\frac{n+1}{2n+1}} \quad (3)$$

where  $c_0$  = the initial crack size;  $b$  = the slope of  $W_{R1}$  versus the number of load cycles;  $N$  = the number of load cycles; and  $M$  = the number of cracks. As shown in Equation 3,  $c_0$  was an essential input parameter to calculate crack growth. As a result, a further investigation was made to determine this parameter based on the concept of elastic pseudo strain energy (EPSE). EPSE was a newly defined energy analogous to elastic strain energy but replacing strain by pseudo strain. It was especially useful for asphalt mixtures because it allowed inferring a viscoelastic problem from a reference elastic case. With respect to the redistribution of EPSE during the process of cracking, a basic equation was established in the following way:

$$\begin{aligned} \text{measured EPSE} = & \text{EPSE of uncracked specimen} - \text{released EPSE due to cracking} \\ & + \text{stored surface energy on crack surfaces} \end{aligned} \quad (4)$$

Equation 4 was applied to two different material states, undamaged state and damaged state. In the undamaged state the crack size equaled to  $c_0$ ; in the damaged state the crack size equaled to  $c_0$  plus crack increment of  $\Delta c$ . Combination of these two states enabled one to achieve an equation for  $c_0$ , in which all variables can be obtained directly from measurement. Then an iterative method was used to find successive approximation to the solution for  $c_0$  and the number of voids,  $M$ . Additionally, X-ray Computed Tomography (CT) along with image analysis was performed to verify this calculated initial crack size. Because of the limit of resolution of the X-Ray CT equipment, the mean air void radius was found to be smaller than the minimum air void radius that was detected by the X-Ray CT equipment. These results are discussed more fully under the Work Element F1c-4 on aging, in which an accurate estimate of the mean air void radius is essential to the model of oxidative aging.

Once the initial void radius of the undamaged mixture was determined, repeated direct tension tests were run for 1000 loading cycles and the dissipated pseudo strain energy was calculated for each load cycle. These data were used, together with a formulation of the relation of the apparent pseudo-elastic modulus, phase angle, stress, and strain to the true values of the same quantities in the damaged material, to determine the values of the Paris' Law coefficients,  $A$  and  $n$ , using Equation 1. This requires an iterative procedure which converges on the final values in about 3

or 4 iterations. The values thus calculated match well with other published values that were calculated using Schapery's theory of crack growth in viscoelastic materials (e.g., Arambula, 2007 and Walubita, 2006).

### Significant Results

Test protocols were further developed to characterize the anisotropic viscoelastic properties of undamaged asphalt mixtures. A data analysis approach was proposed to determine six parameters including the compressive complex modulus in the axial direction, the compressive complex Poisson's ratio in the axial direction, the compressive complex modulus in the radial direction, the compressive complex Poisson's ratio in horizontal plane, as well as the tensile complex modulus, and the tensile complex Poisson's ratio. Tests results indicate that the undamaged asphalt mixture showed different properties in compressive and tensile loading. Specifically, the phase angle of the tensile complex modulus was significantly greater than that of the compressive complex modulus. And the undamaged asphalt mixture exhibited anisotropic properties in compressive loading. Comparison of the test results demonstrated that the magnitude of the compressive complex modulus in the axial direction was about two times larger than the magnitude of the compressive complex modulus in the radial direction.

The CMSE\* (Calibrated Mechanistic with Surface Energy) method was further developed to modeling fatigue cracking of asphalt mixtures using the RDT test protocol. From this single test, both the initial crack size and the average crack radius of a growing crack can be determined on the basis of measured material properties. Compared with the result from the X-ray CT scans, the analytical value of  $c_0$  was smaller. However, it may be more accurate due to its advantage of avoiding the resolution limit with the X-ray CT examination, which resulted in a lack of detection of the smaller microcracks. The method also determined the number of initial air voids which was a larger number than was counted by the X-Ray CT method for the same reason. It was also demonstrated that the analytical method using Equation 1 produces accurate, repeatable and realistic values of the Paris' Law fracture parameters.

### Significant Problems, Issues and Potential Impact on Progress

The availability of testing machine time may prove to be a problem in the coming quarter.

### Work Planned Next Quarter

The same test scenarios will be conducted at three temperatures (10°C, 20°C and 30°C) in order to construct the master curves of the magnitude and phase angle of the complex modulus and complex Poisson's ratio and assess the effect of the temperature on the anisotropy of the asphalt mixture in compressive loading.

The analytical method to determine the initial air void radius,  $c_0$ , the number of such air voids,  $M$ , and the essential Paris' Law parameters,  $A$  and  $n$ , for crack growth in Equation 1 will be applied to more mixtures with a variety of air voids, binders, and aggregates to verify that the method produces accurate, repeatable and realistic values of the fracture material properties.

## Cited References

Arambula, E. (2007). *Influence of Foundational Material Properties and Air Void Structure on Moisture Damage of Asphalt Mixes*. Ph.D. Dissertation, Texas A&M University, College Station, Texas.

Masad, E., V. Castelo Branco, D. Little, and R.L. Lytton (2007). "A Unified Method for the Analysis of Controlled-Strain and Controlled-Stress Fatigue Testing," *International Journal of Pavement Engineering*, Vol.00, No. 0, pp.1-14.

Si, Z. (2001). *Characterization of microdamage and healing of asphalt concrete mixtures*. Ph.D. Dissertation, Texas A&M University, College Station, Texas.

Walubita, L.F., A. Epps Martin, C.J. Glover, and R.L. Lytton. (2006). "Computation of Pseudo Strain Energy and Paris Law Fracture Coefficients from Surface Energy and Uniaxial Strain-Controlled Tension Test Data." *International Journal of Pavement Engineering*, Vol. 7, No. 3, pp. 167-178.

## **Work Element F2d: Tomography and Microstructural Characterization (TAMU)**

### Work Done This Quarter

The work done this quarter has been largely related to X-Ray tomography. This work has been conducted in conjunction with Subtask F1b-2. Please refer to Subtask F1b-2 for the work done, findings, and results.

### Work Planned Next Quarter

The work related to X-Ray tomography of asphalt mixtures and measurement of viscoelastic properties of the binder using the AFM will continue next quarter.

## **Work Element F2e: Verification of the Relationship between DSR Binder Fatigue Tests and Mixture Fatigue Performance (UWM)**

### Work Done This Quarter

In the previous quarter, work focused on comparing monotonic and cyclic testing methods to limited mixture data. The research team found that there are a number of options available when exploring possible failure criteria for fatigue testing. Challenges remain as to determining which binder test methodology is most indicative of fatigue performance, but the work this quarter has shown that there are many promising paths.

In this quarter, binder testing focused on four materials, shown in table F2e.1, which include one unmodified binder used as a control and three commercially produced modified binders. All four

materials were tested using a frequency sweep to create rheological master curves for determining the testing temperatures at which the materials have the same level of dissipated energy. Previous work by Shenoy and Santagata (Shenoy 2002; Santagata et al. 2009) used iso-stiffness fatigue testing to eliminate any possible effect of the initial stiffness on the fatigue results. For purposes of this study, and because of the body of work relating dissipated energy during cyclic loading to fatigue damage, all testing for this work was performed at iso-dissipated energy temperatures.

Table F2e.1. Description of binders.

Binder PG Grade	Modification Type	Testing Temperature (°C)
64 - 28	None	13.1
64 - 28	SBS	12.1
58 - 34	Ethylene terpolymer	8.6
64 - 34	Ethylene terpolymer	6.2

SBS = styrene-butadiene-styrene.

The binder tests under consideration are the time sweep, amplitude sweep and Binder Yield Energy Test (BYET). Testing conditions are:

- Time sweep: strain-controlled at 2.5% and 5% applied strain, 10 Hz.
- Amplitude sweep: strain-controlled, 100 cycles per strain level at 1% strain increments up to 20%, 10 Hz.
- BYET: constant shear rate of 0.01/s.

All binder tests were performed in strain-controlled mode; subsequent beam fatigue testing was also performed in strain control. Because of the limited number of available specimens, only one applied strain level was used—500 microstrain—to obtain two replicate runs.

### Significant Results

#### *Time Sweep Test Results*

The primary focus of this study is to evaluate current binder fatigue test methods with regard to the performance of the same materials subjected to four-point flexural fatigue testing. Time sweep tests are the most direct corollary to this type of loading. The plots of the complex modulus versus number of loading cycles at 2.5% applied strain are shown in figure F2e.1, with the corresponding  $N_{p20}$  values given in table F2e.2.

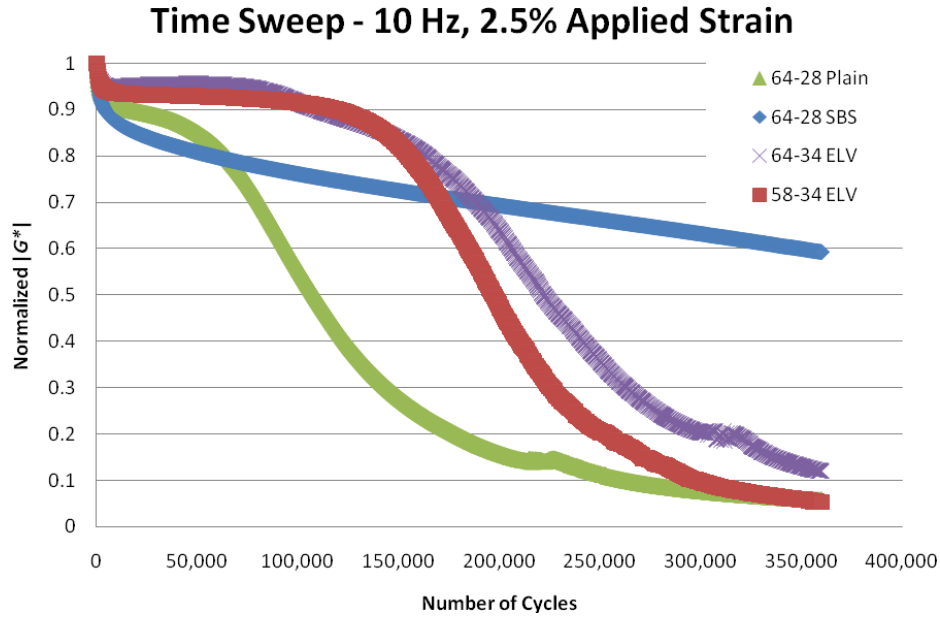


Figure F2e.1. Graph. Plot of time sweep results for binder at 2.5% applied strain. (ELV = Elvaloy.)

Table F2e.2. Binder time sweep test results.

Binder	$N_{p20}$ - 2.5% strain	$N_{p20}$ - 5.0% strain
64 – 28 Neat	80,100	24,900
64 – 28 SBS	360,000	123,100
58 – 34 ET	163,500	15,000
64 – 34 ET	175,800	32,400

**Note:** At 2.5% applied strain, the 64 – 28 SBS had reached only a 17.6% reduction in dissipated energy ratio (DER) after 10 hours of testing.

As can be seen in the results, the unmodified binder showed the fastest drop in modulus and subsequently resulted in the lowest value of  $N_{p20}$ . Alternatively, the SBS-modified binder showed a substantial resistance to fatigue damage. Recent work involving accelerated pavement testing has also shown that polymer-modified binders can enhance the fatigue performance of asphalt mixtures (Kutay et al. 2008). However, determining the specific material characteristic for this increase in performance has been challenging. Elastomeric polymers can affect the material by simultaneously increasing modulus and decreasing phase angle, both of which are significant in calculating dissipated energy.

### Binder Yield Energy Test Results

While applicability of the BYET to fatigue performance indication is still under investigation, it provides a novel ability to gain further insight into the differences in mechanical response between unmodified and polymer-modified binder. In figure F2e.2, the plots of the stress-strain response of the polymer-modified binders show a higher stress and strain tolerance under monotonic loading than the unmodified material. While not a cyclic test procedure, it can be hypothesized that there exists an energy threshold at which the material loses its ability to resist damage. This threshold can be reached either through cyclic or monotonic loading, although work on uniting the two is still in progress. The polymer-modified binders show a greater propensity to absorb applied energy, as denoted by the average Yield Energy (YE) values from two replicates shown in table F2e.3.

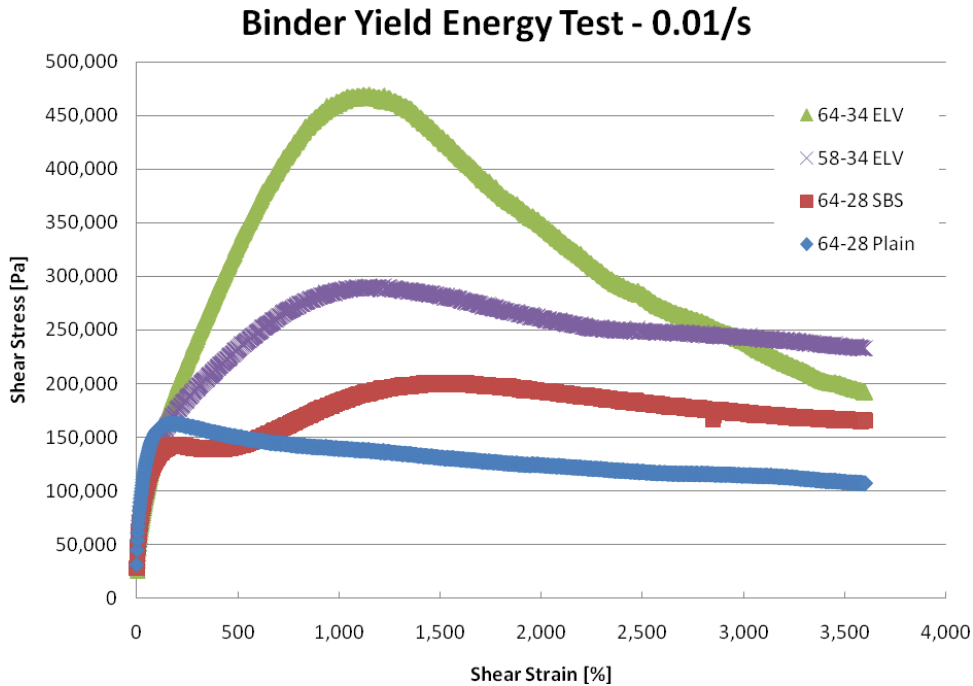


Figure F2e.2. Graph. BYET results at 1% shear strain per second.

Table F2e.3. Binder YE test results.

Binder	Average YE (Pa)	Average GTM (%)
64 – 28 Neat	239,801	176%
64 – 28 SBS	2,617,000	1,559%
58 – 34 ET	2,568,636	1,184%
64 – 34 ET	4,024,517	1,093%

GTM = gamma at tau max.

### Amplitude Sweep Results

The stress versus strain plots for the amplitude sweep test results are shown in figure F2e.3. Determining a failure criterion has always been challenging for this type of test. The research team decided to employ viscoelastic continuum damage (VECD) analysis to model the damage growth in the materials (Kim et al. 2006), and then use the amount of damage at a predetermined percentage of initial undamaged linear viscoelastic (LVE) complex modulus. In this case, the damage parameter D at a 25% complex shear modulus reduction was chosen to ensure a substantial level of damage had occurred in the specimens. Results are shown in table F2e.4.

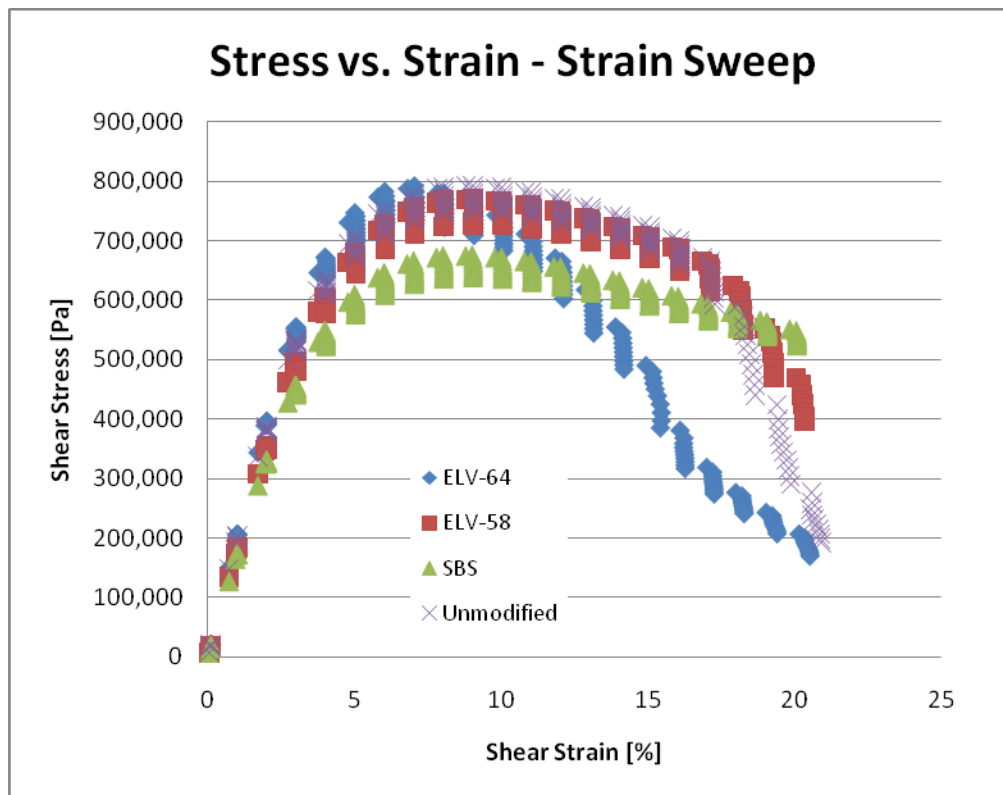


Figure F2e.3. Graph. Strain sweep results.

Table F2e.4. Results of VECD analysis of strain sweep data.

Binder	PG	Temp (°C)	Damage Parameter at 25% ( $G^*$ )
64 – 28 Neat	64-28	13.1	22,015
64 – 28 SBS	64-28	12.1	18,808
58 – 34 ET	58-34	8.6	21,654
64 – 34 ET	64-34	6.2	18,836

ET = ethylene terpolymer.

### *Flexural Beam Fatigue Results*

Beam fatigue results were only available for the modified binders, as the slab from which beams were cut for the unmodified binder had substantial damage during storage. Multiple failure criteria were employed. Using AASHTO T321, one beam had yet to achieve failure after 5 million cycles, so the team also considered normalized stiffness reduction. At 50% initial stiffness, the same beam still not had achieved failure. All beams experienced a reduction to 65% initial stiffness, so this was used for comparison to binder test results; results are shown in table F2e.5.

Table F2e.5. Four-Point Bend (4PB) fatigue results at  $N_f = 65\%$  stiffness reduction.

Binder Used in Mixture	Replicate 1 $N_f$	Replicate 2 $N_f$	Average $N_f$
64 – 28 SBS	25,000	40,000	32,500
58 – 34 ET	330,000	85,000	207,500
64 – 34 ET	N/A	35,000	35,000

### *Comparison Between Mixture and Binder Fatigue Results*

Work is currently under way to relate the results of the binder tests to mixture performance. Test results indicate that the SBS-modified binder showed substantially better resistance to fatigue damage in comparison to other materials during time sweep testing, but this performance was not seen in the beam fatigue data. Rankings of the three modified binders are shown in table F2e.6 with regard to the various test methods, with the strain sweep being the only procedure that gave the same ranking as the beam fatigue.

Table F2e.6. Ranking of binders using various fatigue tests.

Binder Used in Mixture	Beam Fatigue	Time Sweep 2.5%	Time Sweep 5.0%	BYET– YE	BYET– GTM	Strain Sweep– D@0.25M
64 – 28 SBS	C	A	A	B	A	C
58 – 34 ET	A	C	C	C	B	A
64 – 34 ET	B	B	B	A	C	B

### Significant Problems, Issues and Potential Impact on Progress

None.

### Work Planned Next Quarter

A testing program is currently under way in conjunction with TPF-5(146), “Evaluation of Modified Performance Grade Binders in Thin Lift Maintenance Mixes, Surface Mix and a Reflective Crack Relief Layer Mix” to evaluate the binder fatigue properties for the mixtures included in the study. Laboratory fatigue testing will also be performed on the mixtures, and the binder fatigue data will be further compared to mixture performance.

### Cited References

Kim, Y., H. J. Lee, D. N. Little, and Y. R. Kim, 2006, A Simple Testing Method to Evaluate Fatigue Fracture and Damage Performance of Asphalt Mixtures. *Journal of the Association of Asphalt Paving Technologists*, 75: 755-788.

Kutay, M. E., N. Gibson, and J. Youtcheff, 2008, Conventional and Viscoelastic Continuum Damage (VECD) Based Fatigue Analysis of Polymer Modified Asphalt Pavements. *Journal of the Association of Asphalt Paving Technologists*, 77.

Santagata, E., O. Baglieri, D. Dalmazzo, and L. Tsantilis, 2009, Rheological and Chemical Investigation on the Damage and Healing Properties of Bituminous Binders. *Journal of the Association of Asphalt Paving Technologists*, 78.

Shenoy, A., 2002, Fatigue Testing and Evaluation of Asphalt Binders Using the Dynamic Shear Rheometer. *Journal of Testing and Evaluation*, 30(4): 303-312.

## **CATEGORY F3: MODELING**

### **Work Element F3a: Asphalt Microstructural Model (WRI)**

#### Work Done This Quarter

A meeting was held in Delft in June during the same week in which the International Workshop on Chemo-Mechanics of Bituminous Materials was held. Jack Youtcheff (FHWA), Michael Greenfield (URI), Linbing Wang (VT), Troy Pauli (WRI), and the Delft Team; Tom Scarpas, Niki Kringos and Alexander Schmets, were in attendance. The focus of the meeting pertained to developing models and theories which would account for the physico-chemical and chemo-mechanical properties at different time (size) scales, and methodologies which would be needed to couple between these scales.

#### Significant Results

None.

## Significant Problems, Issues and Potential Impact on Progress

None.

## Work Planned Next Quarter

Members of the asphalt microstructure modeling team will begin/continue work in their respective subtasks. A preliminary outline of a model will be developed during the next quarter to show critical links between different time (size) scales, and approaches to couple these models.

## **Work Element F3b: Micromechanics Model (TAMU)**

### *Subtask F3b-1: Model Development*

#### **Lattice Micromechanical Model**

The new lattice modeling engine of multi-scale virtual fabrication and lattice modeling (MS-VFLM) developed in the last quarter is finalized with significant increase in computational efficiency. It has all the functionality of the previous lattice modeling software except the viscoelastic deformation. A sample output from the new MS-LFVM run is shown in the figure, which contains scaling up of fracture energies, sample crack patterns and final load-deflection curve at scale 1. Comparison of efficiency indicates that both tension (TEN) test and single-edge notch (SEN) tests require less than 8 times the previous implementation. The practical implication is that the result shown in the figure takes around 1.1 hours, as opposed to more than 9 hours it took with the previous implementation. This indicates that *virtual testing of laboratory scale specimen can now be done within a reasonable time*. Further reduction of computational cost is currently being investigated. In addition to the computational work, work has initiated on investigating the discrepancy in time-dependency between binder deformation and mastic deformation.

## Work Done This Quarter

In the previous quarter, the computational efficiency of the multi-scale virtual fabrication and lattice modeling (MS-VFLM) software was increased. The current quarter's efforts focused on further increasing the efficiency of the code as well as incorporating viscoelastic fracture. The new code is now 20 times faster than the original code, and accurate results may be obtained within one hour. With respect to viscoelastic fracture, a qualitative framework is developed and implemented (sample crack patterns resulting from this scheme are shown in figure F3b-1.1). Investigation is now started towards the understanding and characterization of the quantitative aspects of the model.

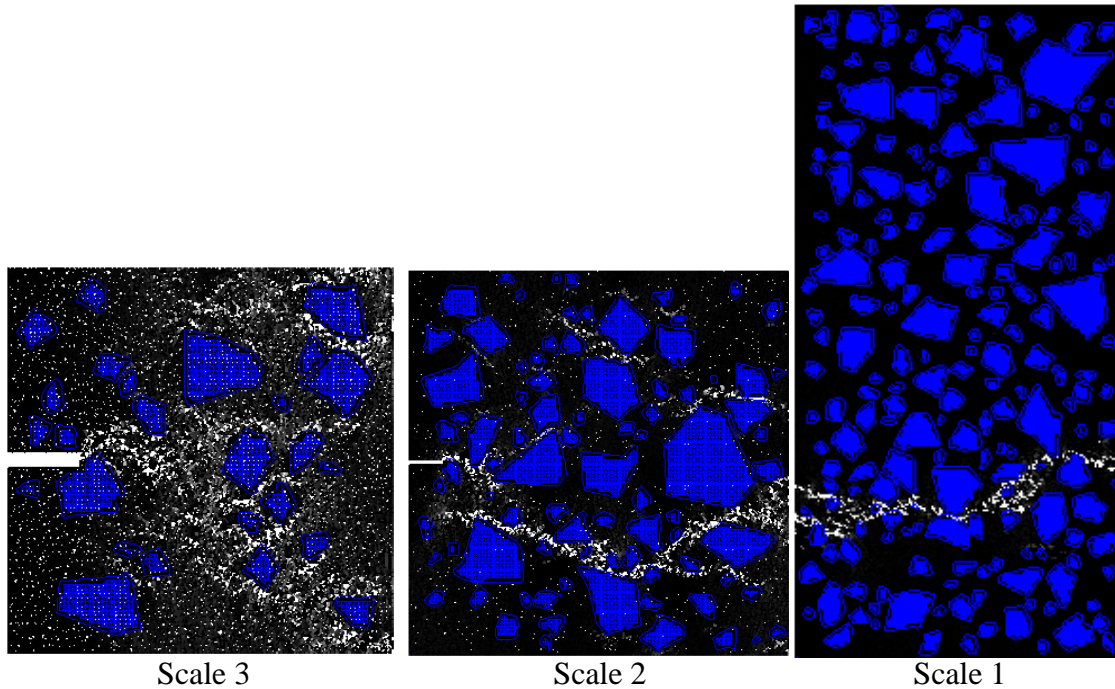


Figure F3b-1.1. Sample crack patterns obtained at different scales from MS-VFLM code after including viscoelastic fracture functionality (qualitative only). Quantitative model development is currently underway

### Significant Results

- The efficiency of MS-VFLM software is further increased and it is currently 20 times more efficient than original code.
- Preliminary model of viscoelastic fracture is included in lattice modeling. The simulation results appear qualitatively reasonable. Further work is underway with respect to more precise quantitative simulation of viscoelastic fracture.

### Significant Problems, Issues and Potential Impact on Progress

None

### Work Planned Next Quarter

Viscoelastic fracture modeling will be finalized and work will initiate on modeling air voids.

### **Cohesive Zone Model**

### Work Done This Quarter

During this quarter we have progressed towards multiple activities such as:

- Modeling of asphalt concrete mixtures at different loading rates to check the current intrinsic bilinear cohesive zone model for predicting fracture process of the mixtures;
- Identification of cohesive zone fracture properties of asphalt matrix phase by integrating experimental results from semi-circular bending (SCB) specimens and numerical simulations;
- Development of a modeling framework for the characterization of the dynamic modulus of HMA mixtures using the FEM micromechanics approach;
- Nano-indentation testing to measure elastic properties of mixture constituents particularly for aggregate particles and interfaces between particles and matrix phase; and
- Development of a testing-analysis protocol for mixing, compaction, and production of the asphalt matrix specimens that are used to produce model inputs (properties of matrix phase).

The outcomes of this quarter resulted in presentations in two conferences and submission of two journal papers and two conference papers as listed at the end of this report.

Work progress and significance of each activity can be summarized as follows.

- Modeling of asphalt concrete mixtures at different loading rates to check the current intrinsic bilinear cohesive zone model.

Two tensile strain rates (0.01  $\epsilon$ /sec and 0.001  $\epsilon$ /sec) were applied to asphalt concrete mixture specimens (figure F3b-1.2(a)) and their representative finite element mesh (figure F3b-1.2(b)) with the bilinear cohesive zone elements within asphalt matrix phase. Three independent cohesive zone parameters ( $T_{max}$ ,  $K_{eff}$ , and  $\delta$ ) in the model were found through a forward method comparing simulation results and performance test results.

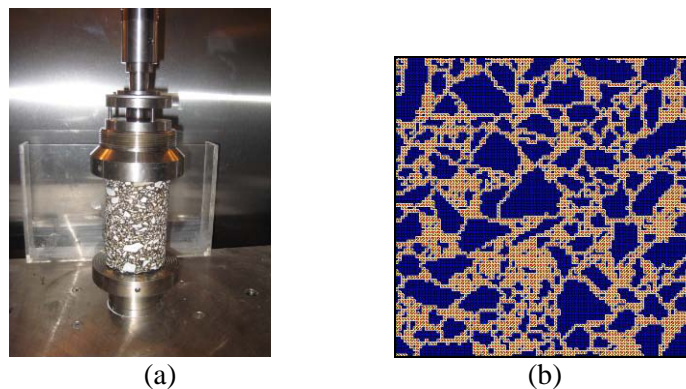


Figure F3b-1.2. (a)HMA mixture subjected to uniaxial tension; (b) finite element mesh of the mixture.

Figure F3b-1.2 shows the experimental and numerical results obtained from the two different strain rates applied to the specimens. Figure F3b-1.3 also includes a plot of the numerical predictions for a specimen subjected to 0.001  $\epsilon$ /sec by using the same cohesive zone parameters as those found for the 0.01  $\epsilon$ /sec case. The lower peak and the reduced initial stiffness observed from the slower rate simulation demonstrates that the model was able to capture the viscoelastic effect (rate-dependence) of the mixture to a certain extent; however, as the figure presents a mismatch between the simulation and the test results, the consideration of the viscoelasticity of the bulk asphaltic matrix is not sufficient to characterize the overall process of the mixture performance. A different set of cohesive zone properties is necessary to match with test results, which implies that the fracture process in viscoelastic media is also a rate-dependent phenomenon (Kim et al. 2007; Souza et al. 2004) and must be modeled accordingly. Rate-dependent models, such as a nonlinear viscoelastic fracture model proposed by Allen and his colleagues (Yoon and Allen 1999; Allen and Searcy 2001), a generalized fluid model (Kogan et al. 1996), or a viscoelastic cohesive zone model (Rahul-Kumar et al. 1999), need to be sought and implemented in the process.

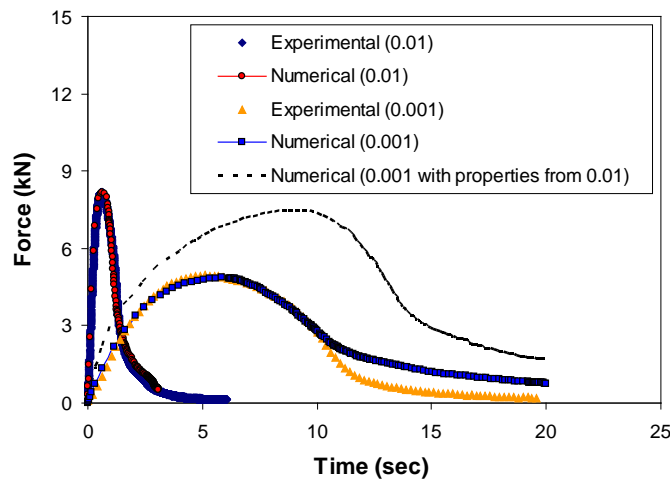


Figure F3b-1.3. Test results vs. model simulations.

- Determination of cohesive zone fracture properties of asphalt matrix phase.

A testing program currently under investigation is the use of semi-circular bend (SCB) specimens. Even if some limitations exist, such as the arching effect (Wagoner et al. 2005), several factors make this attempt an interesting and promising possibility to be investigated. The SCB testing is very simple to perform, and multiple testing specimens can be easily prepared by a routine process of mixing and Superpave gyratory compacting of asphalt mixtures.

Figure F3b-1.4(a) presents the current SCB testing set-up incorporated with the use of a digital image correlation (DIC) system that can monitor the displacement and strain fields on the overall surface of the specimen. The DIC analysis will help characterize fracture behavior more

realistically so that the determination of cohesive zone properties can be more effectively performed.

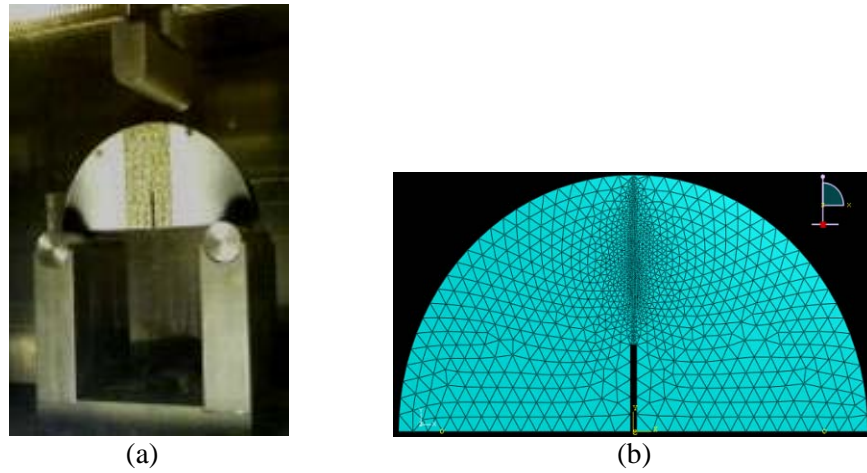


Figure F3b-1.4. (a) SCB testing set-up, and (b) its numerical modeling.

Figure F3b-1.5 presents the SCB test results by plotting the reaction force as the loading time increased at five different loading rates (5, 10, 25, 50, and 100 mm/min). Clearly, rate-dependent fracture behavior is observed. Slower loading rates produce more compliant responses than faster loading rates. Test results will be incorporated with numerical fracture simulations, as illustrated in figure F3b-1.4(b), to identify cohesive zone fracture properties based on the inverse analysis. The fracture properties are then used to model the fracture failure of general HMA mixtures.

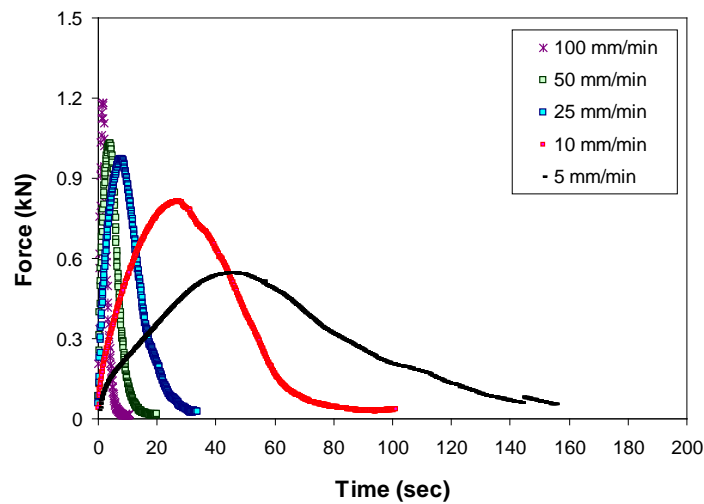


Figure F3b-1.5. SCB test results demonstrating rate-dependent fracture.

The development of the test will involve various investigations on the appropriate SCB specimen density and geometry. These issues will be one of main focuses for next quarters. For the determination of the optimized geometry, the proper geometry of the notch (length, width, and tip sharpness) and the specimen thickness will be investigated.

- Development of a modeling framework for the characterization of the dynamic modulus of HMA mixtures using the FEM micromechanics approach.

Along with the modeling with fracture, we have also attempted to model linear viscoelastic behavior of asphalt concrete mixtures by simulating the dynamic modulus which is a key material property to perform analysis and design of pavements (MEPDG 2004). Two-dimensional microstructure of the HMA mixtures was obtained through an image analysis process of the Superpave gyratory compacted (SGC) specimen. Figure F3b-1.6(a) shows a treated image of a HMA sample (100 mm width and 150 mm height). Figure 3b-1.6(b) shows the FEM mesh generated corresponding to the image shown in figure F3b-1.5(a). Boundary conditions imposed on the mesh is shown in figure F3b-1.6(c).

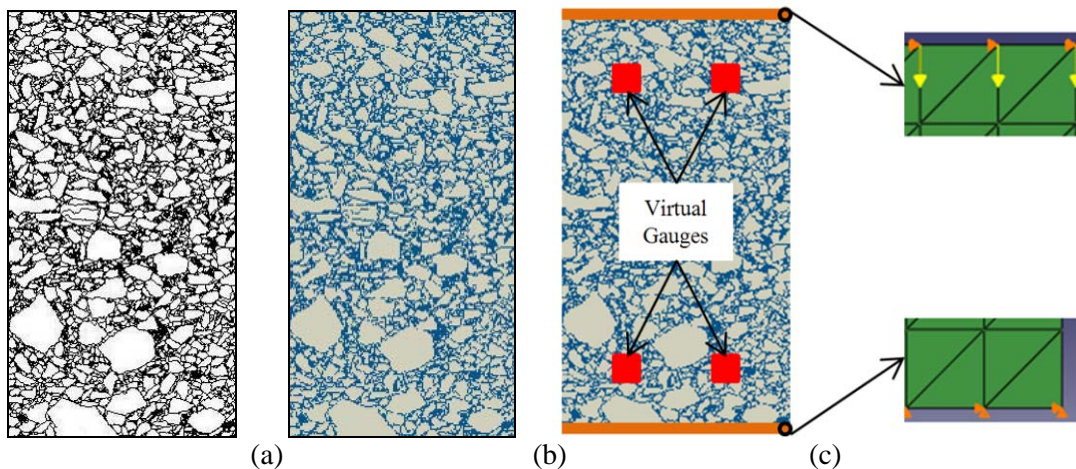


Figure F3b-1. 6. Two-dimensional microstructure of a HMA specimen: (a) a treated image, (b) FEM mesh, (c) boundary conditions posed.

With the mesh developed, boundary conditions were applied to simulate actual dynamic modulus tests. A compressive haversine load was evenly applied to the top nodes. To construct a dynamic modulus master curve, a wide spectrum of loading frequencies was simulated ( $10^{-4}$  to  $10^4$  Hz). Averaged vertical deformations from the two sets of virtual gauge points (in figure 6(c)) were used to calculate the dynamic modulus, defined simply as the ratio of the haversine stress amplitude to the haversine strain amplitude.

Figure F3b-1.7 shows the dynamic modulus comparisons between FEM numerical simulation results and experimental data (average of two samples). The comparisons revealed a very good agreement between the numerical and the experimental results. A relatively higher deviation was

observed at lower loading frequencies. Several factors may have caused the deviation including (a) no explicit consideration of air voids within the mixtures; (b) two-dimensional simplification of the three-dimensional problem; (c) lack of aggregate-aggregate contact due to the two-dimensional approximation; and (d) damage that may have occurred during the dynamic modulus testing at higher temperature conditions.

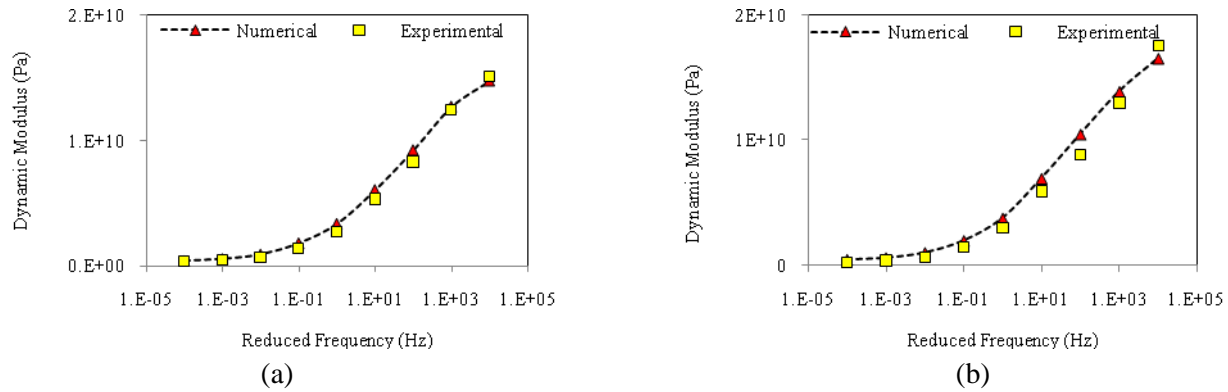


Figure F3b-1.7. Experimental and numerical dynamic modulus master curves at a reference temperature of 21°C - mixture with additional: (a) 1.0% hydrated lime, and (b) 1.5% hydrated lime.

- Nano-indentation testing to measure elastic properties of mixture constituents.

As proposed in the last quarter, we started evaluating the properties of mixture constituents (aggregates and asphalt matrices) using the nanoindentation technique. A Berkovich shaped indenter made of diamond was used to make indentations in nano scale at different locations of very finely polished aggregates (4 different types) and asphalt matrix samples. Test results are shown in figure F3b-1.8. Modulus of elasticity obtained from the matrix phase was found coherent with typical modulus values obtained from rheological tests of matrix specimens. The elastic moduli of aggregates were much greater than typical values found from handbooks or literature (Barksdale 1991; Zhou et al. 1995). We don't have any definite reasons to explain such a difference at this moment. We will investigate why the nano-indentation testing produced higher moduli of aggregate particles than typically-known values, around 30-60 GPa.

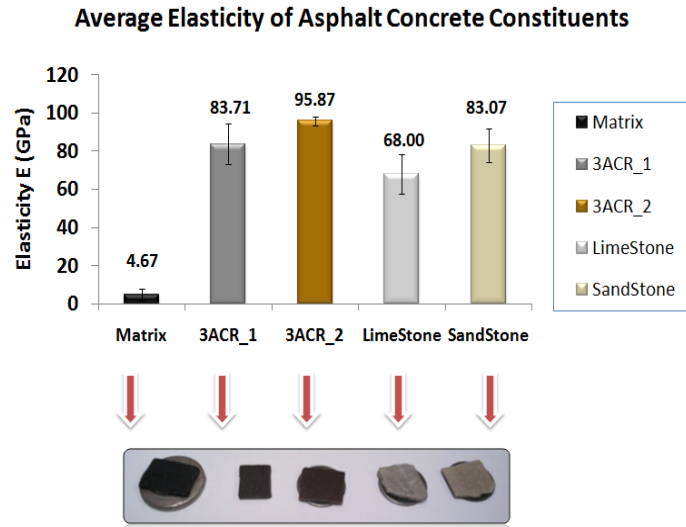


Figure F3b-1.8. Moduli of elasticity obtained from the nano-indentation test.

- Development of a testing-analysis protocol for mixing, compaction, and production of the asphalt matrix specimens.

This task is to develop a more articulate and scientific protocol in mixing and compaction of the asphalt matrix specimens which produce key material properties (viscoelastic properties and cohesive zone properties of matrix phase) to accomplish the micromechanical modeling. Advanced image analysis techniques (from Dr. Amit Bhasin at UTA) and finite element computational simulations (from Dr. Kim at UNL) will be incorporated with mechanical tests to finally develop the best protocol of asphalt matrix specimen fabrication. During the last quarter, we developed a mix design protocol that can account for absorption and coating of asphalt binder to aggregates. The matrix mix design now has a fixed binder percentage calculated for a selected asphalt mixture while its density changes to find an appropriate level of air voids in the matrix phase to model HMA mixtures. Several different densities of matrix phase have been tried to simulate different levels of air voids from a minimum (close to 0 %) to a maximum (4 %) as long as compaction is allowed. The Superpave gyratory compactor is used to compact matrix mixtures. Each compacted sample were sawn and cored to produce 45 mm long and 12 mm diameter cylindrical specimens to perform linear viscoelastic constitutive tests. Significant test results will be presented in the next quarter.

Significant Problems, Issues and Potential Impact on Progress

None.

Work Planned Next Quarter

The development of SCB fracture testing system and proper implementation of a cohesive zone model that can identify rate-dependent fracture behavior of HMA mixtures will be mainly

focused for the next quarter. Various rate-dependent cohesive zone models (Allen and Searcy 2001; Kogan et al. 1996; Rahul-Kumar et al. 1999) will be investigated.

The proper level of density (compaction) in the asphalt matrix phase will be determined in the next quarter. Test results will be incorporated with numerical simulations (such as the dynamic modulus simulation) and the advanced tomography study to establish a logical methodology for fabricating asphalt matrix mixtures that are used for the micromechanical model.

We will also start to evaluate properties of common materials (binders, matrix, aggregates, and mixtures) selected by ARC modeling teams (TAMU, NCSU, UTA, and UNL). Test results will then be incorporated into the model.

### Cited References

Allen, D. H. & Searcy, C. R. (2001). A micromechanical model for a viscoelastic cohesive zone. *International Journal of Fracture*, 107, 159-176.

Barksdale, R. D. (1993). *The aggregate handbook*. Washington, D.C. : National Stone Association.

Kim, Y. R.; Allen, D. H.; & Little, D. N. (2007). Computational Constitutive Model for Predicting Nonlinear Viscoelastic Damage and Fracture Failure of Asphalt Concrete Mixtures. *International Journal of Geomechanics*, 7 (2), 102-110.

Kogan, L., Hui, C.-Y., and Ruina, A. (1996). Theory of chain pull-out and stability of weak interfaces. *Macromolecules*, 28, 4090-4100.

NCHRP. "Guide for Mechanistic-Empirical Design of New and Rehabilitated Pavement Structures." Project 1-37A. Washington DC: National Cooperative Highway Research Program, Transportation Research Board, National Research Council, 2004.

Rahul-Kumar, P., Jagota, A., Bennison, S. J., Saigal, S., and Muralidhar, S. (1999). Polymer interfacial fracture simulations using cohesive elements. *Acta Materialia*, 47(15), 4161-4169.

Souza, F. V.; Soares, J. B.; Allen, D. H.; & Jr., F. E. (2004). A model for predicting damage evolution in heterogeneous viscoelastic asphaltic mixtures. *Transportation Research Record: Journal of the Transportation Research Board*, 1891, 131-139.

Yoon, C. & Allen, D. H. (1999). Damage dependent constitutive behavior and energy release rate for a cohesive zone in a thermoviscoelastic solid. *International Journal of Fracture*, 96, 56-74.

Wagoner, M. P.; Buttlar, W. G.; & Paulino, G. H. (2005). Disk-shaped compact tension test for asphalt concrete fracture. *Experimental Mechanics*, 45, 270-277.

Zhou, F. P., Lydon, F. D., and Barr, B. I. G. 1995. Effect of Coarse Aggregate on Elastic Modulus and Compressive Strength of High Performance Concrete. *Cement and Concrete Research*, 20, 177-186.

### Journal Papers, Conference Proceedings, and Presentations Produced during This Quarter

Y. Kim, J. Lee, and J. Lutfi. (2009). “Geometrical Evaluation and Experimental Verification to Determine Representative Volume Elements of Heterogeneous Asphalt Mixtures.” *Journal of Testing and Evaluation*, submitted.

F. Aragão, Y. Kim, and J. Soares. (2009). “Dynamic Modulus Prediction of Asphalt Concrete Mixtures through Various Methods: Analytical, Phenomological, and Numerical Methods.” *Transportation Research Record*, submitted.

F. Aragão and Y. Kim. (2009). “Modeling of Asphalt Mixtures Subjected to Nonlinear Viscoelastic Fracture.” *2010 GeoFlorida Conference: Advances in Analysis, Modeling, and Design*, submitted.

F. Aragão, Y. Kim, J. Lee, and J. Soares. (2009). “A Micromechanical Finite Element Model for Predicting the Dynamic Modulus of Heterogeneous and Rate-Dependent Asphalt Concrete Mixtures.” *2009 ABPv Conference*, accepted.

F. Aragão, Y. Kim, J. Lee, and D. H. Allen. “A Micromechanical Fracture Model for Heterogeneous and Rate-Dependent Asphalt Concrete Mixtures Using the Finite Element Method.” *10<sup>th</sup> U.S. National Congress on Computational Mechanics*, presented.

F. T. S. Aragão and Y. Kim. “Modeling Fracture and Failure of Nonlinear, Inelastic Asphalt Concrete Mixtures.” *2009 Joint ASCE-ASME-SES Conference on Mechanics and Materials*, presented.

### ***Subtask F3b-2: Account for Material Microstructure and Fundamental Material Properties***

#### Work Done This Quarter

No activity was conducted on this subtask.

### **Work Element F3c: Development of Unified Continuum Model (TAMU)**

#### Work Done This Quarter

The ARC researchers modified the selection of aggregates that will be used to produce test mixtures. The previous selection was logistically difficult to acquire. The modified ARC aggregates and core binders are presented in tables F3c-1 and F3c-2 consequently. Six binder-aggregate combinations will be used to produce mastic and fine asphalt mixtures, while three binder-aggregate combinations will be used to produce full asphalt mixtures as presented in table F3c-3. Among the three binder-aggregate combinations for full asphalt mixtures, one is selected for the first round of experiments to develop the model and fine tune the test protocol. This mixture will be designed using limestone (ARC AG 002) and NuStar Energy binder (ARC BI 001). The remaining two full asphalt mixtures

will be tested for further verification of the developed model. The needed amount of binders and aggregates from each ARC team was collected and compiled together as presented in table F3c-4.

Table F3c-1. Core aggregates for ARC.

Aggregate ID	Description	Source	Remarks
ARC AG 001	Siliceous Conglomerate	WY	The proposed source is from the same area as SHRP designation RJ; regarded as susceptible to moisture damage
ARC AG 002	Brownwood Limestone	TX	Good resistance to moisture damage
ARC AG 003	Andesite	NV	Highly moisture sensitive aggregate; presents challenge in establishing the Superpave mix design
ARC AG 004	Limestone	WI	This aggregate has poor moisture damage resistance
ARC AG 005	Watsonville Granite from the Granite Rock Company in California	CA	SHRP designation RB; regarded as resistant to moisture damage
ARC AG 006	Gravel	AR, also used in TX	Used in NCHRP 9-34; aggregate has poor moisture damage resistance as reported by field and 9-34 protocols but it has very high TSR (AASHTO T283)

Note: the ARC AG 001 and ARC AG 002 are the main core aggregates (table F3c-3). All the remaining core aggregates are for supplement studies.

Table F3c-2. Core binders for ARC.

Binder ID	Supplier	Reported Crude Source	Location
ARC BI 001	NuStar Energy	Paulsboro, NJ	Venezuelan
ARC BI 002	Montana Refining OR Exxon-Mobil*	Great Falls, MT OR Billings, MT	W. Canadian blend
ARC BI 003	Valero Refining	Benecia, CA	CA Valley & ANS
ARC BI 004	W.Texas Intermediate OR Saudi Arabian Medium/Heavy OR Gulf Coast*	Valero Refining OR another source	To be decided

\*WRI to pick one from the possible alternatives in this row

Table F3c-3. Binder-aggregate combinations of test mixtures.

<b>Binders</b>	<b>Aggregates</b>	<b>Mastic and Fine Asphalt Mixtures</b>	<b>Full Asphalt Mixtures</b>
ARC BI 001	ARC AG 001	X	X
	ARC AG 002	X	X
ARC BI 002	ARC AG 001	X	
	ARC AG 002	X	X
ARC BI 003	ARC AG 001	X	
	ARC AG 002	X	

Table F3c-4. Material quantities for ARC.

		<b>NCSU</b>	<b>TAMU</b>	<b>UTA</b>	<b>UNL</b>
<b>Material</b>		<b>Amount (kg)</b>	<b>Amount (kg)</b>	<b>Amount (kg)</b>	<b>Amount (kg)</b>
ARC BI 0001		164	938	60	60
ARC BI 0002		88	483	60	40
ARC BI 0003		12	68	60	20
ARC BI 0004		N/A	16	N/A	20
<b>Size 1*</b>	ARC AG 0001	800	3500	N/A	150
	ARC AG 0002	1600	7000	N/A	300
	ARC AG 0003	N/A	150	N/A	N/A
	ARC AG 0004	N/A	150	N/A	N/A
	ARC AG 0005	N/A	150	N/A	N/A
	ARC AG 0006	N/A	150	N/A	N/A
<b>Size 2*</b>	ARC AG 0001	570	2060	220	170
	ARC AG 0002	970	3860	220	230
	ARC AG 0003	N/A	75	N/A	100
	ARC AG 0004	N/A	75	N/A	100
	ARC AG 0005	N/A	75	N/A	100
	ARC AG 0006	N/A	75	N/A	100
<b>Size 3*</b>	ARC AG 0001	250	780	150	50
	ARC AG 0002	390	1425	150	70
	ARC AG 0003	N/A	40	N/A	30
	ARC AG 0004	N/A	40	N/A	30
	ARC AG 0005	N/A	40	N/A	30
	ARC AG 0006	N/A	40	N/A	30

\* Size 1: passing 19 mm and retained on #16, Size 2: passing #16 and retained on #200, and Size 3: passing #200

The three-dimensional constitutive model including the temperature and damage effects was implemented in finite element (FE) code. The temperature effect is considered by incorporating temperature shifted factor within both viscoelastic and viscoplastic model shown as Eqs. (1) and (2), respectively.

$$\varepsilon(t) = g_0 D_0 \sigma^t + g_1 \int_0^t \Delta D(\psi^t - \psi^\tau) \frac{d(g_2 \sigma^\tau)}{d\tau} d\tau \quad (1)$$

$$\dot{\varepsilon}_{ij}^{vp,\psi} = \Gamma \left( \frac{f(\sigma_{ij}^\psi, \varepsilon_e^{vp,\psi})}{\sigma_y^0} \right)^N \frac{\partial g^\psi}{\partial \sigma_{ij}^\psi} \quad (2)$$

where  $\psi^t = \int_0^t \frac{d\xi}{a_T}$

The experimental measurements from creep recovery tests at a reference temperature 20°C was selected to obtain the viscoelastic and viscoplastic material properties shown in tables F3c-5 and F3c-6, respectively. The time-temperature shifting with a reference temperature of 20°C is applied to obtain the temperature shifted factors  $a_T$  shown as figure F3c-1. The temperature shifted factors for each temperature are shown in table F3c-7. Figure F3c-2 shows the relationship between temperature and temperature shifted factors. The FE model with the material parameters (tables F3c-5, F3c-6 and F3c-7) is used to conduct inverse analysis by comparing the numerical results with the experimental measurements at different temperatures. The results for different temperature are shown in figure F3c-3. In general, the numerical results have reasonable predictions with the experimental measurements at low temperatures 10°C and 20°C. However, the prediction at high temperature 40°C is under estimated, since the time-temperature shifting for temperature 40°C does not shift well.

In terms of damage effect, several damage rules are investigated in order to find a damage rule which is proper for asphalt materials. The selected damage rule should be able to take into account the loading rate effect, the post peak behavior in strain control tests, and the tertiary creep behavior in constant load tests. Three models for damage rule are proposed and explained briefly and some results are included. The viscoelastic and viscoplastic parameters are determined for  $T = 20^\circ C$  from creep-recovery tests. The same material constants are used to model the constant load test for characterizing the damage law. The experimental results for the creep test under different stress levels are shown in figure F3c-4.

a) First proposed law:

$$\dot{\phi} = \left( \frac{Y}{(1-\phi)Y_0} \right)^c \quad (3)$$

where,  $Y = \bar{\tau} - \alpha \bar{I}_1$ ,  $\tau = \frac{\sqrt{J_2}}{2} \left(1 + \frac{1}{d} + \left(1 - \frac{1}{d}\right) \frac{\bar{J}_3}{\sqrt{J_2^3}}\right)$ , and  $Y_0$ , and  $C$  are material constants. The model parameters are found and compared with experiments in figure F3c-5.

**b)** Second proposed model:

The second proposed damage model is:

$$\dot{\phi} = \frac{1}{T_m} e^{N\varepsilon^{Tot}} (1 - \phi)^{-C_1} \quad (4)$$

where,  $T_m, N, C_1$  are material constants and  $\varepsilon^{Tot}$  is the total strain. This damage law is based on strain evolution. Comparisons between experimental results and model prediction are shown in figure F3c-6.

**c)** The third proposed law:

Figures F3c-5 and F3c-6 show that the predictions are not very accurate when the stress level is high. Parametric studies show that choosing different values for parameter  $T_m$  fit the experimental data at high stress levels. Hence, one may assume  $T_m$  to be stress dependent. In order to do that the following model is proposed:

$$\dot{\phi} = \frac{1}{T_m} e^{N\varepsilon^{Tot}} \quad (5)$$

where  $T_m$  is stress dependent:

$$T_m = \left(\frac{Y}{Y_0}\right)^{-q} T_0 \quad (6)$$

In equations (5) and (6)  $Y_0, T_0$  are reference values and  $q$  is the material parameter which could be calibrated from creep tests at several stress levels. The experiment and model results are shown in figure F3c-7. Figure F3c-7 shows that the proposed damage law can predict the creep behavior under different stress levels.

Table F3c-5. Linear viscoelastic coefficients at a reference temperature 20 °C.

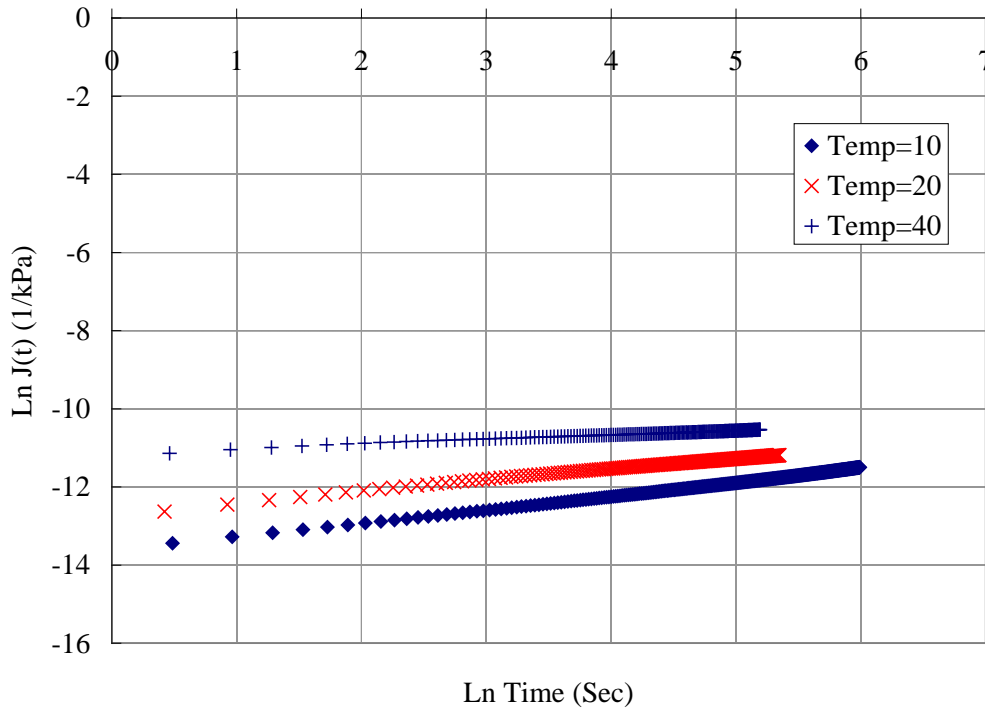
n	$\lambda_n$ (s <sup>-1</sup> )	D <sub>n</sub> (kPa <sup>-1</sup> )
1	1	1.77E-06
2	0.1	7.60E-7
3	0.01	1.23E-06
4	0.001	2.93E-06

Table F3c-6. The values of the viscoplastic parameters at a reference temperature 20 °C.

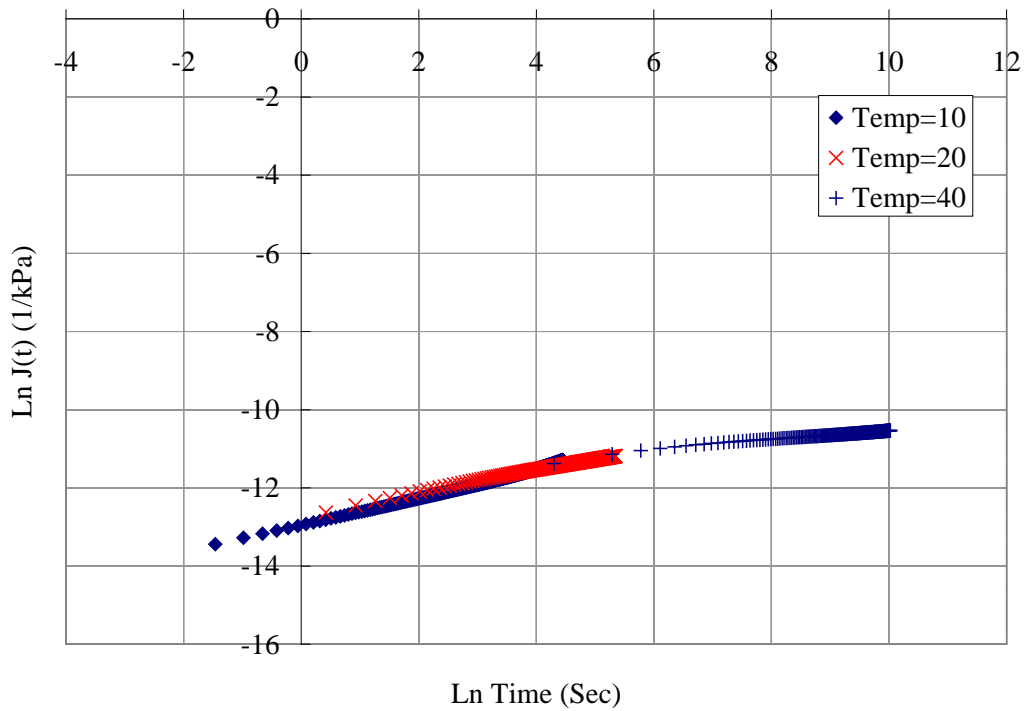
Viscoplastic parameters	
$\alpha$	0.30
$\beta$	0.15
$\Gamma$	8.0E-4
$N$	3.63
$\kappa_0$	35
$\kappa_1$	680
$\kappa_2$	175

Table F3c-7. The temperature shift factor for each temperature

Temp. (°C)	aT
10	7.0
20	1.0
40	0.008



(a) Before applying the temperature shift factor.



(b) After applying the temperature shift factor.

Figure F3c-1. Data before and after applying the temperature shift factor.

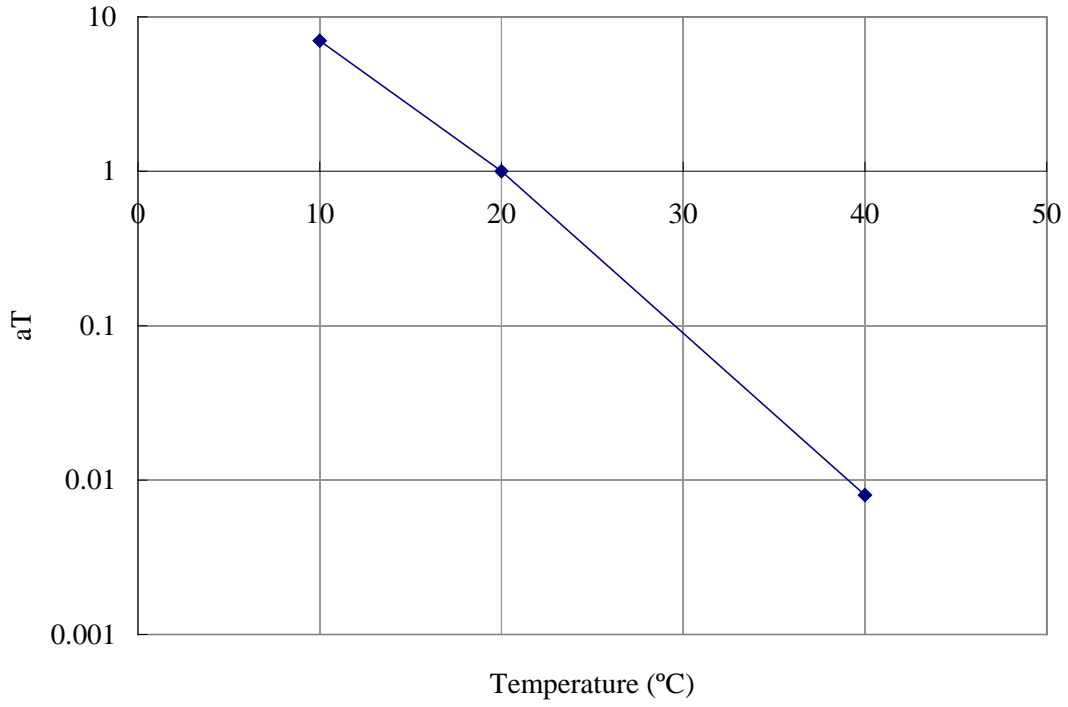
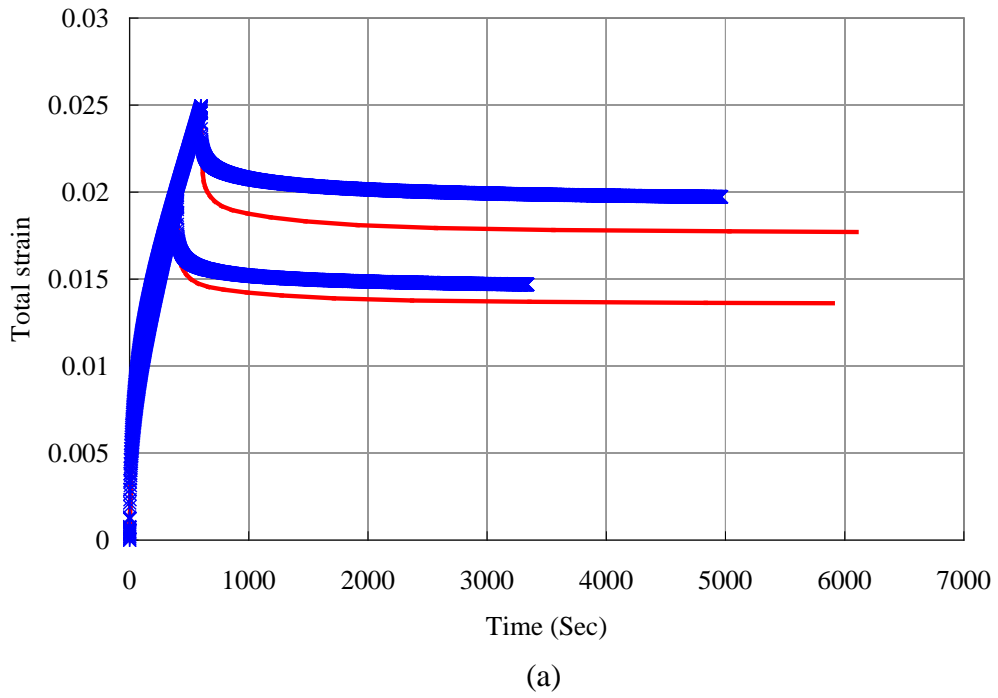
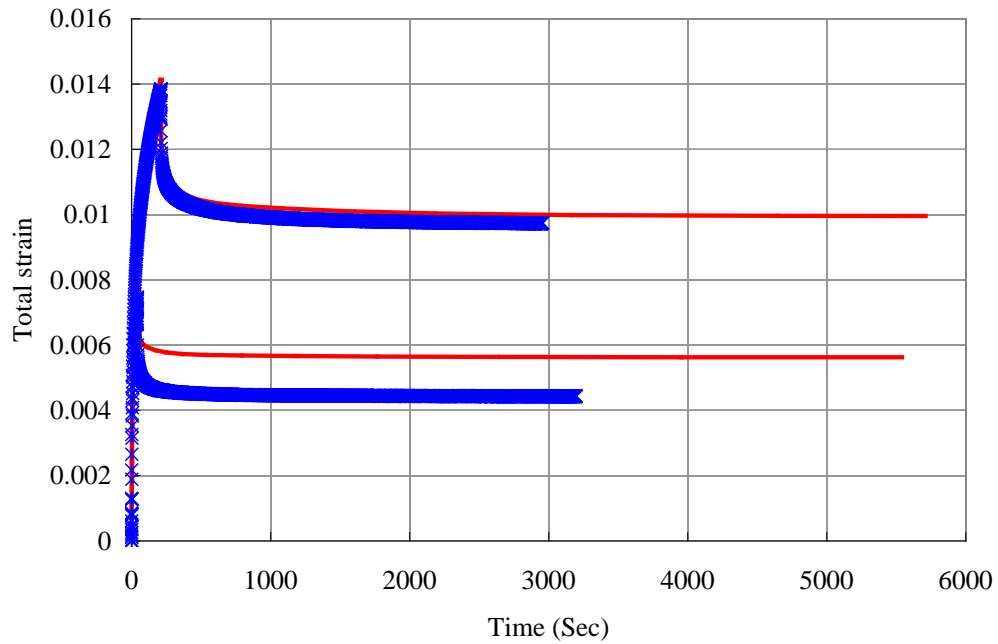
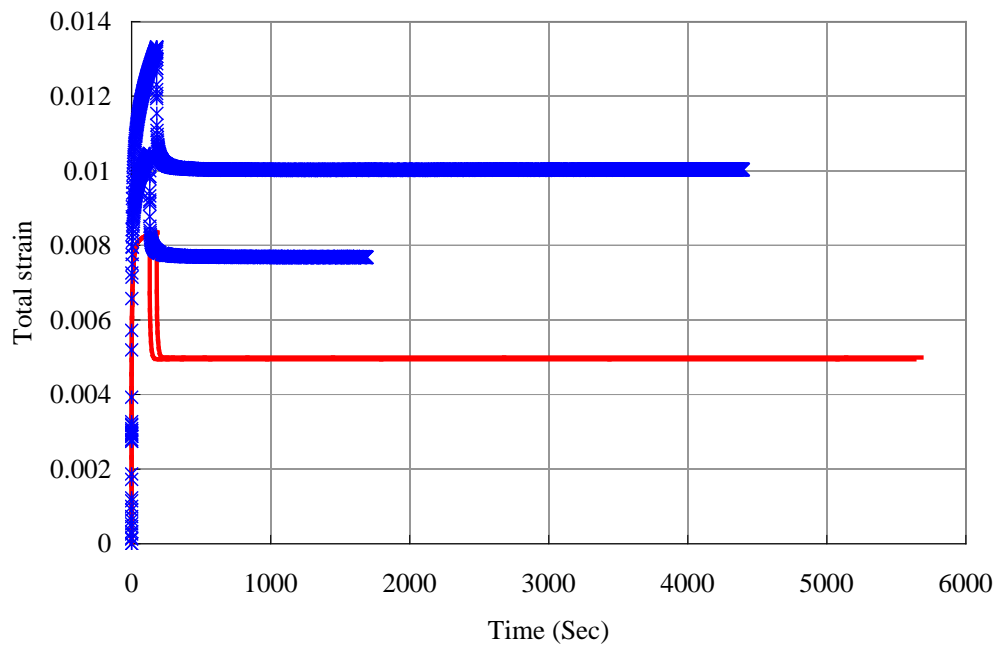


Figure F3c-2. The relationship between temperature shift factor ( $a_T$ ) and temperature.





(b)



(c)

Figure F3c-3. Comparison of between total strain measurements and finite element results at temperature (a) 10 °C, (b) 20 °C and (c) 40 °C.

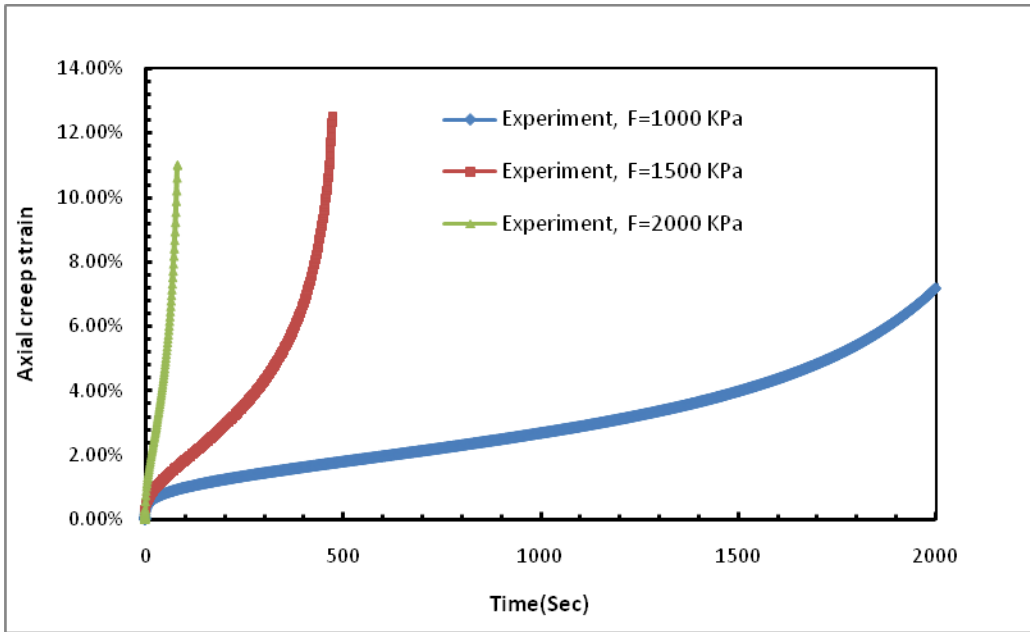


Figure F3c-4. Experimental results of creep test under different stress levels.

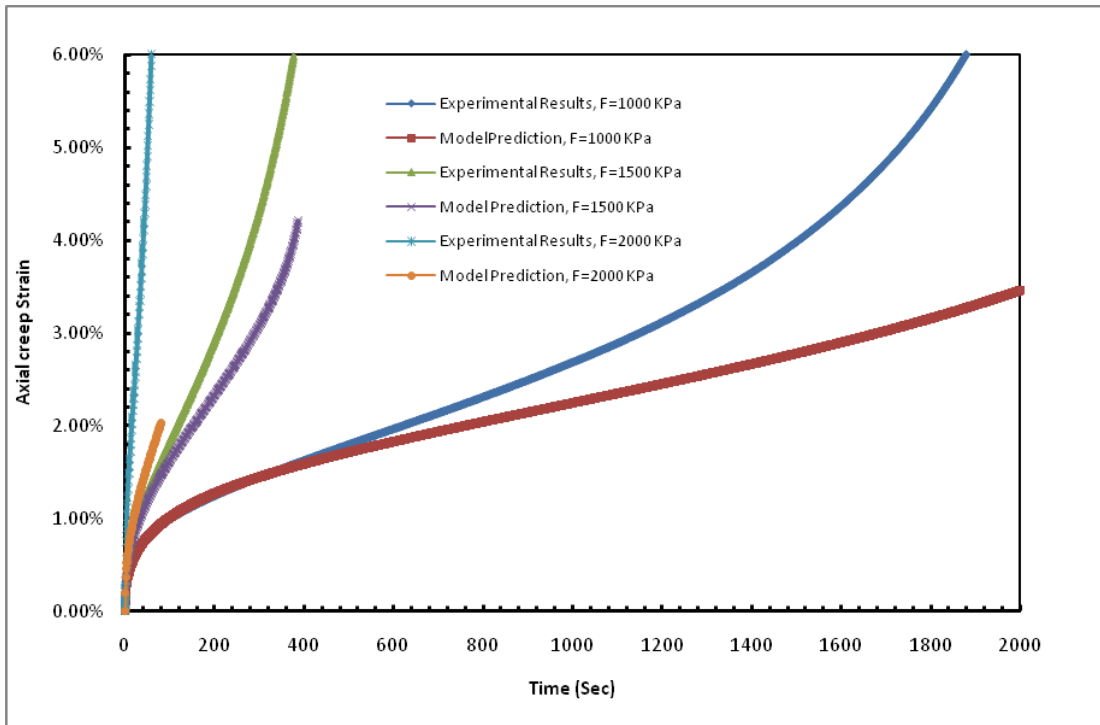


Figure F3c-5. Experimental Results and model prediction for the model proposed in equation (3).

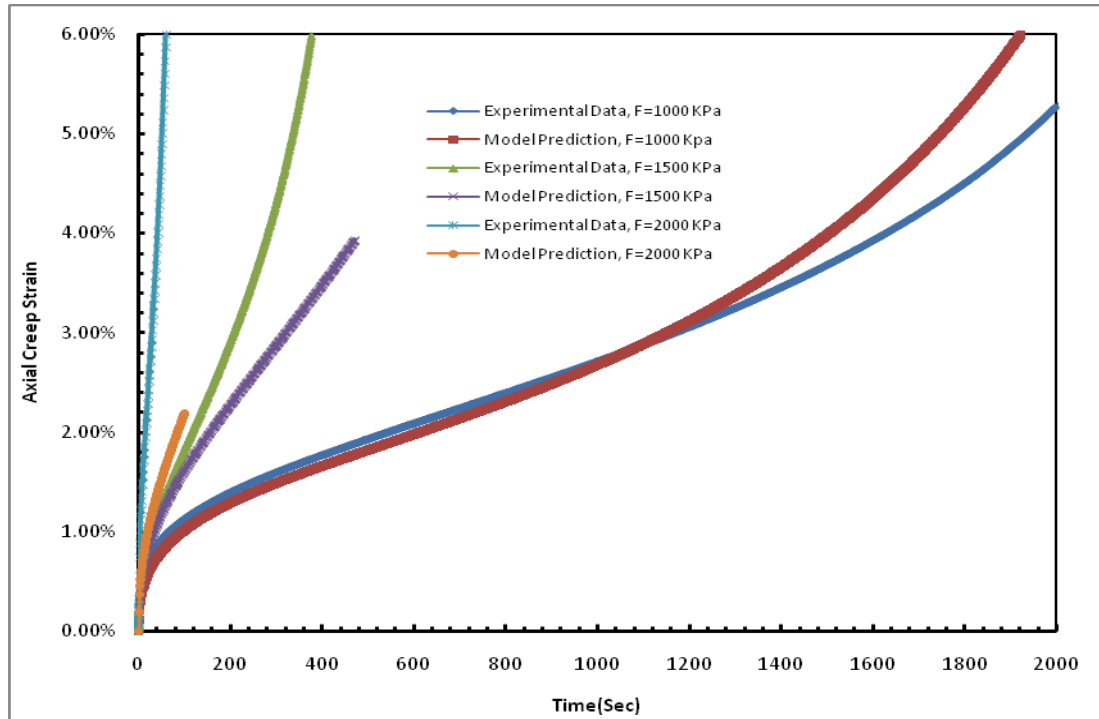


Figure F3c-6. Experimental Results and model prediction for the model proposed in equation (4).

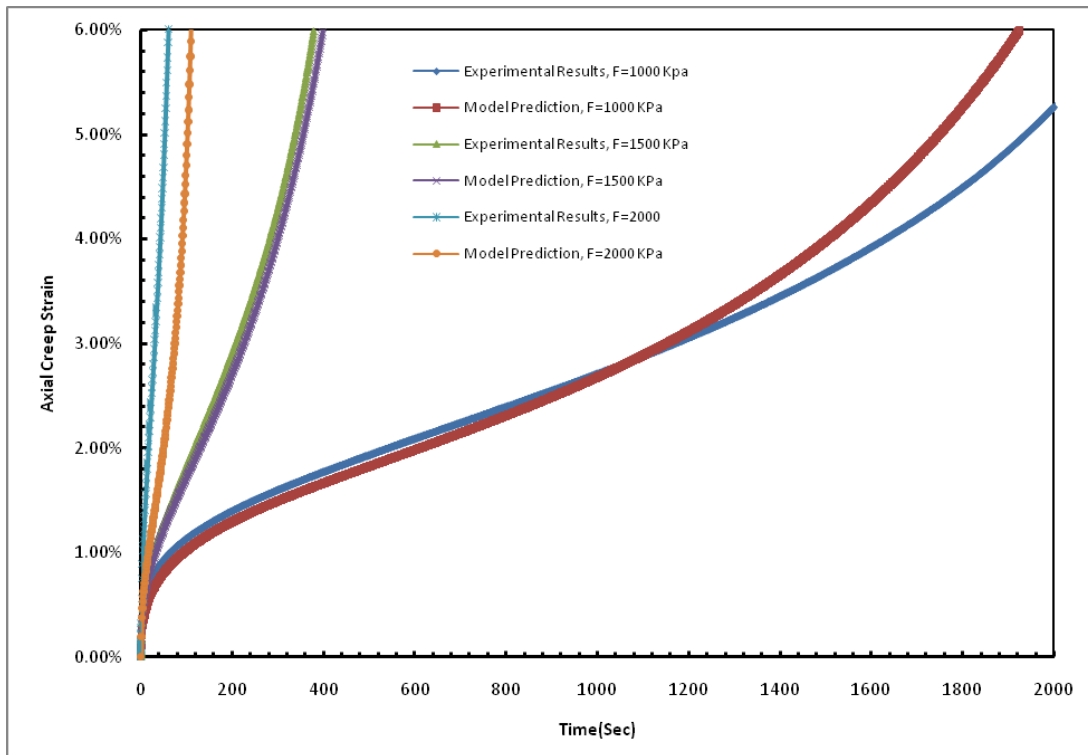


Figure F3c-7. Experimental Results and model predictions for the model proposed in equations (5) and (6).

### Significant Results

The temperature effect and damage model are incorporated within the material constitutive model. The results show that the constitutive model has the ability to represent the temperature effect and damage behavior.

### Significant Problems, Issues and Potential Impact on Progress

There has been a delay in receiving the ALF compression data from NCState. We will start the task of validating the model against the ALF performance once the data are acquired.

### Work Planned Next Quarter

Finite element simulations of wheel tracking experiments that were conducted at the University of Nottingham will be conducted in order to verify the model.

### Journal Papers during This Quarter

Chien-Wei Huang, Rashid K. Abu Al-Rub, Eyad A. Masad, Dallas N. Little, and Golden D. Airey, "Numerical Implementation and Validation of a Nonlinear Viscoelastic and Viscoplastic Model for Asphalt Concrete Mixes", journal of Mechanics of Materials, submitted, 2009.

Chien-Wei Huang, Rashid K. Abu Al-Rub, Eyad A. Masad, and Dallas N. Little, "Three-Dimensional Simulations of Asphalt Pavement Permanent Deformation Using a Nonlinear Viscoelastic and Viscoplastic Model", Journal of Materials in Civil Engineering, submitted, 2009.

### **Work Element F3d: Calibration and Validation**

This work element is planned to start later in the project.

Fatigue Year 3		Year 3 (4/09-3/10)											
		4	5	6	7	8	9	10	11	12	1	2	3
<b>Material Properties</b>													
<b>F1a</b>	<b>Cohesive and Adhesive Properties</b>												
F1a-1	Critical review of literature												
F1a-2	Develop experiment design												
F1a-3	Thermodynamic work of adhesion and cohesion												
F1a-4	Mechanical work of adhesion and cohesion			JP				JP			D		F
F1a-5	Evaluate acid-base scale for surface energy calculations												
<b>F1b</b>	<b>Viscoelastic Properties</b>												
F1b-1	Separation of nonlinear viscoelastic deformation from fracture energy under cyclic loading												JP
F1b-2	Separation of nonlinear viscoelastic deformation from fracture energy under monotonic loading												JP
<b>F1c</b>	<b>Aging</b>												
F1c-1	Critical review of binder oxidative aging and its impact on mixtures												
F1c-2	Develop experiment design		F										
F1c-3	Develop transport model for binder oxidation in pavements						P	JP				P, JP	D
F1c-4	Effect of binder aging on properties and performance						P	JP	D		F		
F1c-5	Polymer modified asphalt materials											P	D
<b>F1d</b>	<b>Healing</b>												
F1d-1	Critical review of literature												
F1d-2	Select materials with targeted properties												
F1d-3	Develop experiment design												
F1d-4	Test methods to determine properties relevant to healing												JP
F1d-5	Testing of materials												
F1d-6	Evaluate relationship between healing and endurance limit of asphalt binders				DP				JP		DP		
F1d-7	Coordinate with AFM analysis												
F1d-8	Coordinate form of healing parameter with micromechanics and continuum damage models												
<b>Test Methods</b>													
<b>F2a</b>	<b>Binder tests and effect of composition</b>												
F2a-1	Analyze Existing Fatigue Data on PMA												
F2a-2	Select Virgin Binders and Modifiers and Prepare Modified Binder												
F2a-3	Laboratory Aging Procedures												
F2a-4	Collect Fatigue Test Data							P					P
F2a-5	Analyze data and propose mechanisms										P		
<b>F2b</b>	<b>Mastic testing protocol</b>												
F2b-1	Develop specimen preparation procedures												
F2b-2	Document test and analysis procedures in AASHTO format												
<b>F2c</b>	<b>Mixture testing protocol</b>												
<b>F2d</b>	<b>Tomography and microstructural characterization</b>												
F2d-1	Micro scale physicochemical and morphological changes in asphalt binders								JP				
<b>F2e</b>	<b>Verify relationship between DSR binder fatigue tests and mixture fatigue performance</b>												
F2e-1	Evaluate Binder Fatigue Correlation to Mixture Fatigue Data												
F2e-2	Selection of Testing Protocols				DP	D		F					
F2e-3	Binder and Mixture Fatigue Testing												
F2e-4	Verification of Surrogate Fatigue Test												
F2e-5	Interpretation and Modeling of Data						JP					P	
F2e-6	Recommendations for Use in Unified Fatigue Damage Model												
<b>Models</b>													
<b>F3a</b>	<b>Asphalt microstructural model</b>												
<b>F3b</b>	<b>Micromechanics model</b>												
F3b-1	Model development												
F3b-2	Account for material microstructure and fundamental material properties												
<b>F3c</b>	<b>Develop unified continuum model</b>												
F3c-1	Analytical fatigue model for mixture design												
F3c-2	Unified continuum model				JP						JP		
F3c-3	Multi-scale modeling												

**LEGEND**

**Deliverable codes**

- D: Draft Report
- F: Final Report
- M&A: Model and algorithm
- SW: Software
- JP: Journal paper
- P: Presentation
- DP: Decision Point
- [x]

-  Work planned
-  Work completed
-  Parallel topic

**Deliverable Description**

- Report delivered to FHWA for 3 week review period.
- Final report delivered in compliance with FHWA publication standards
- Mathematical model and sample code
- Executable software, code and user manual
- Paper submitted to conference or journal
- Presentation for symposium, conference or other
- Time to make a decision on two parallel paths as to which is most promising to follow through
- Indicates completion of deliverable x

Fatigue Year 2 - 5		Year 2 (4/08-3/09)				Year 3 (4/09-3/10)				Year 4 (04/10-03/11)				Year 5 (04/11-03/12)				
		Q1	Q2	Q3	Q4	Q1	Q2	Q3	Q4	Q1	Q2	Q3	Q4	Q1	Q2	Q3	Q4	
<b>Material Properties</b>																		
<b>F1a</b>	<b>Cohesive and Adhesive Properties</b>																	
F1a-1	Critical review of literature			JP														
F1a-2	Develop experiment design																	
F1a-3	Thermodynamic work of adhesion and cohesion																	
F1a-4	Mechanical work of adhesion and cohesion					JP	JP	D	F									
F1a-5	Evaluate acid-base scale for surface energy calculations														JP			
<b>F1b</b>	<b>Viscoelastic Properties</b>																	
F1b-1	Separation of nonlinear viscoelastic deformation from fracture energy under cyclic loading			D,JP	M&A, F				JP		JP		P		JP, M&A, D		F	
F1b-2	Separation of nonlinear viscoelastic deformation from fracture energy under monotonic loading			JP	M&A, F	P, JP			JP		JP		P		JP, M&A, D		F	
<b>F1c</b>	<b>Aging</b>																	
F1c-1	Critical review of binder oxidative aging and its impact on mixtures																	
F1c-2	Develop experiment design			D		F												
F1c-3	Develop transport model for binder oxidation in pavements		P		P, JP			P		P, JP		P		P, JP		D, M&A	F	
F1c-4	Effect of binder aging on properties and performance				JP, P			JP	D	F					JP	D	F	
F1c-5	Polymer modified asphalt materials							P				P				D	F	
<b>F1d</b>	<b>Healing</b>																	
F1d-1	Critical review of literature																	
F1d-2	Select materials with targeted properties																	
F1d-3	Develop experiment design																	
F1d-4	Test methods to determine properties relevant to healing				JP				JP	D	F							
F1d-5	Testing of materials							JP						M&A, D	JP, F			
F1d-6	Evaluate relationship between healing and endurance limit of asphalt binders	DP				DP	JP	DP				JP		P	JP	D	F	
F1d-7	Coordinate with AFM analysis																	
F1d-8	Coordinate form of healing parameter with micromechanics and continuum damage models												JP			JP, D	F	
<b>Test Methods</b>																		
<b>F2a</b>	<b>Binder tests and effect of composition</b>																	
F2a-1	Analyze Existing Fatigue Data on PMA			DP														
F2a-2	Select Virgin Binders and Modifiers and Prepare Modified Binder			DP														
F2a-3	Laboratory Aging Procedures																	
F2a-4	Collect Fatigue Test Data		P		JP			P		P				JP, D, F				
F2a-5	Analyze data and propose mechanisms				P				P				P			P	D	F
<b>F2b</b>	<b>Mastic testing protocol</b>																	
F2b-1	Develop specimen preparation procedures			D														
F2b-2	Document test and analysis procedures in AASHTO format			D														
<b>F2c</b>	<b>Mixture testing protocol</b>			D, JP	F													
<b>F2d</b>	<b>Tomography and microstructural characterization</b>																	
F2d-1	Micro scale physicochemical and morphological changes in asphalt binders							JP				JP	M&A, D	F				
<b>F2e</b>	<b>Verify relationship between DSR binder fatigue tests and mixture fatigue performance</b>																	
F2e-1	Evaluate Binder Fatigue Correlation to Mixture Fatigue Data																	
F2e-2	Selection of Testing Protocols						DP	D, F										
F2e-3	Binder and Mixture Fatigue Testing																	
F2e-4	Verification of Surrogate Fatigue Test													D	F, DP			
F2e-5	Interpretation and Modeling of Data		JP		P			JP		P		JP		M&A				
F2e-6	Recommendations for Use in Unified Fatigue Damage Model																D	F
<b>Models</b>																		
<b>F3a</b>	<b>Asphalt microstructural model</b>								JP					JP			M&A	F
<b>F3b</b>	<b>Micromechanics model</b>																	
F3b-1	Model development				JP				JP				M&A	D	DP	F, SW		
F3b-2	Account for material microstructure and fundamental material properties											JP			D		F	
<b>F3c</b>	<b>Develop unified continuum model</b>																	
F3c-1	Analytical fatigue model for mixture design															M&A, D		F
F3c-2	Unified continuum model				JP		JP		JP					M&A	D	DP	F, SW	
F3c-3	Multi-scale modeling												JP	M&A	D		F	

**LEGEND**

**Deliverable codes**

- D: Draft Report
- F: Final Report
- M&A: Model and algorithm
- SW: Software
- JP: Journal paper
- P: Presentation
- DP: Decision Point

[x]

Work planned

Work completed

Parallel topic

**Deliverable Description**

- Report delivered to FHWA for 3 week review period.
- Final report delivered in compliance with FHWA publication standards
- Mathematical model and sample code
- Executable software, code and user manual
- Paper submitted to conference or journal
- Presentation for symposium, conference or other
- Time to make a decision on two parallel paths as to which is most promising to follow through
- Indicates completion of deliverable x

## **PROGRAM AREA: ENGINEERED MATERIALS**

### **CATEGORY E1: MODELING**

#### **Work element E1a: Analytical and Micro-mechanics Models for Mechanical Behavior of Mixtures (TAMU)**

##### Work Done This Quarter

The problem of aggregate absorption was further investigated in this quarter. A number of aggregate samples were photographed under the natural light and ultraviolet light to visually observe the absorption of asphalt binder by aggregates. These aggregate samples included:

1. A cylindrical limestone sample with a diameter of 2 in and height of 3 in, which was freshly cored from a limestone rock;
2. A cylindrical limestone sample with a diameter of 2 in and height of 3 in, which was soaked in an AAD binder for 32 hours at the mixing temperature of making an asphalt mixture;
3. A cylindrical limestone sample with a diameter of 2 in and height of 3 in, which was soaked in an AAD binder for 64 hours at the mixing temperature of an asphalt mixture;
4. A regular aggregate used in Hot Mix Asphalt (HMA) after mixing;
5. An HMA field core sample from Loop 368 in San Antonio, Texas; and
6. A warm mix field core from Loop 368 in San Antonio, Texas.

Figures E1a.1 through E1a.6 show the pictures of aggregate samples under the natural light and ultraviolet light. These pictures clearly demonstrate that certain asphalt components diffused into aggregates coated with asphalt binder. The aggregates in HMA showed more absorption of asphalt binder than those in the warm mix.



(a) Natural Light

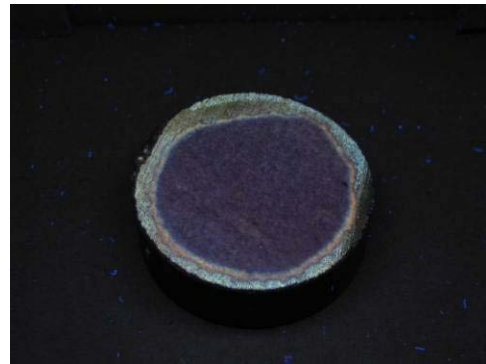


(b) Ultraviolet Light

Figure E1a.1. Fresh limestone sample under natural light and ultraviolet light.



(a) Natural Light

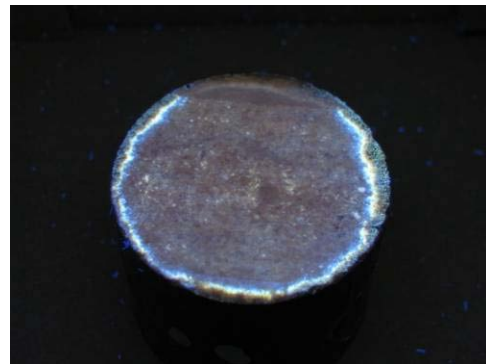


(b) Ultraviolet Light

Figure E1a.2. Limestone sample after 32 hour soaking in AAD binder under natural light and ultraviolet light.



(a) Natural Light



(b) Ultraviolet Light

Figure E1a.3. Limestone sample after 64 hour soaking in AAD binder under natural light and ultraviolet light.

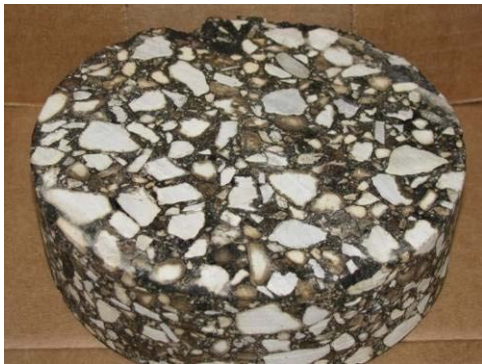


(a) Natural Light

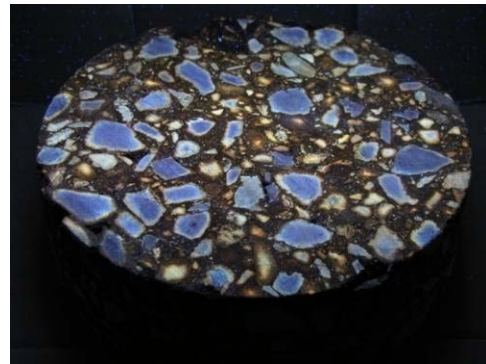


(b) Ultraviolet Light

Figure E1a.4. Limestone aggregate in HMA after mixing under natural light and ultraviolet light.



(a) Natural Light



(b) Ultraviolet Light

Figure E1a.5. HMA field core under natural light and ultraviolet light.



(a) Natural Light



(b) Ultraviolet Light

Figure E1a.6. Warm mix field core under natural light and ultraviolet light.

In order to further identify the asphalt components absorbed into the aggregates, the limestone sample shown in figure E1a.2 was cut into 1 mm thick slices. One of these slices was tested using the technique of Laser Desorption Ionization – Ion Mobility – Mass Spectrometry (LDI-IM-MS) by Dr. Fernandez-Lima in the Department of Chemistry at Texas A&M University. A schematic illustration of the LDI-IM-MS is shown in figure E1a.7 (Becker et al. 2009). During the test, a laser was used to desorb and ionize the sample, which was called “laser desorption-ionization (LDI)”. After the LDI process, ions from the sample were separated in a 15 cm long drift cell with periodic electrical voltage gradient field since heavier ions and lighter ions have different mobility in an electrical voltage gradient field. The field strengths were  $10 - 20 \text{ V.cm}^{-1} \text{ torr}^{-1}$ . This ion separation technique is referred to as ion mobility spectroscopy (IMS). After the IMS separation process was finished, ions were focused in the ion optics and were mass analyzed using a reflectron time-of-flight (TOF) mass spectrometer (MS). In the LDI-IM-MS testing, both the LDI source and the drift cell had the same pressure, which was approximately 3 torr (1 torr = 1,333 Pa), using helium gas. They also both had the same temperature that was approximately 297 K.

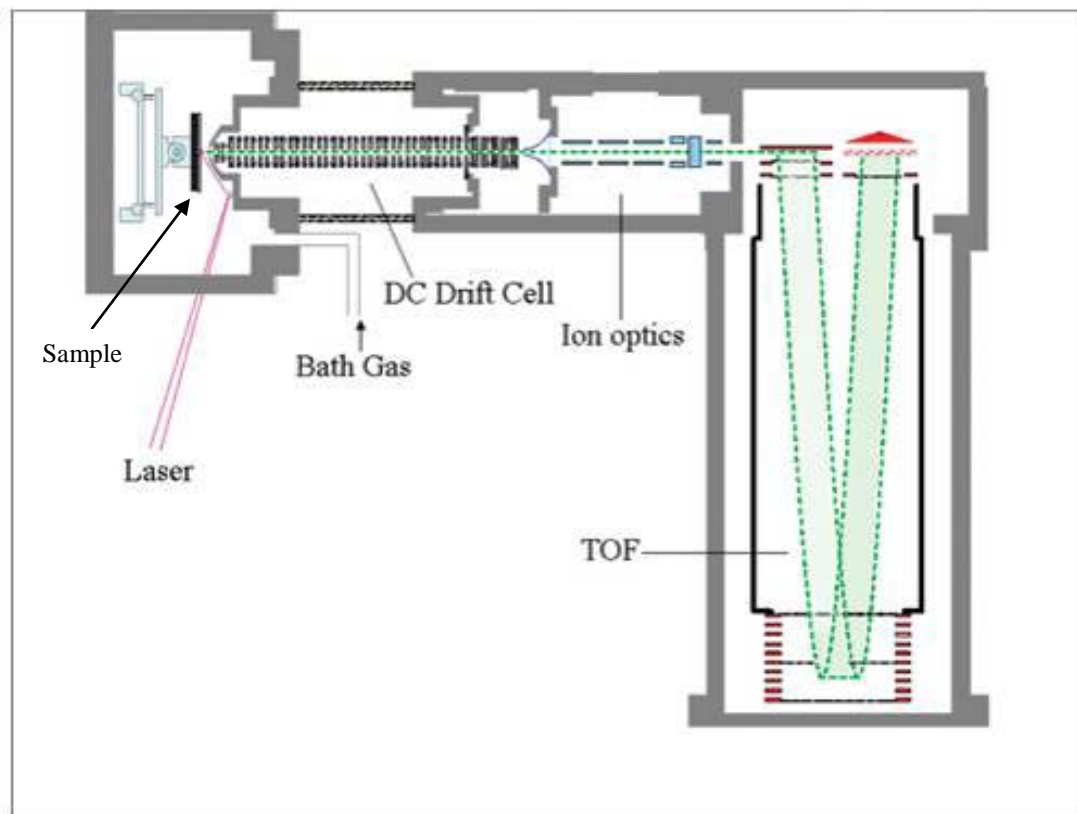


Figure E1a.7. Schematic of IM-MS instrument utilizing an LDI ion source, periodic drift cell, and a reflectron time-of-flight (TOF) (Becker et al. 2009).

Two spots on the limestone slice were tested using the LDI-IM-MS: one was close to the edge of the slice, which had a higher density of asphalt components; the other spot was in the center of the limestone slice that had a lower density of asphalt components. The IM-MS spectrums of both spots are presented in figures E1a.8 and E1a.9, which plot the drift time of the ions (arrival time distribution) versus the ion mass ( $m/z$ ). The two figures also show significant differences in concentration between the edge spot and the center spot. This indicates that the edge spot has more asphalt components than the center spot. The IM-MS spectrum of the edge spot was then magnified at a nominal ion mass level of approximately 308 – 320  $m/z$ , as shown in figure E1a.10. The trend lines in the magnified spectrum correspond to heteroatom hydrocarbons, where the complexity of the sample was significantly high, as indicated by figure E1a.10 in which more than one peak existed at a nominal mass level. This is a normal phenomenon in crude oils and asphaltene samples.

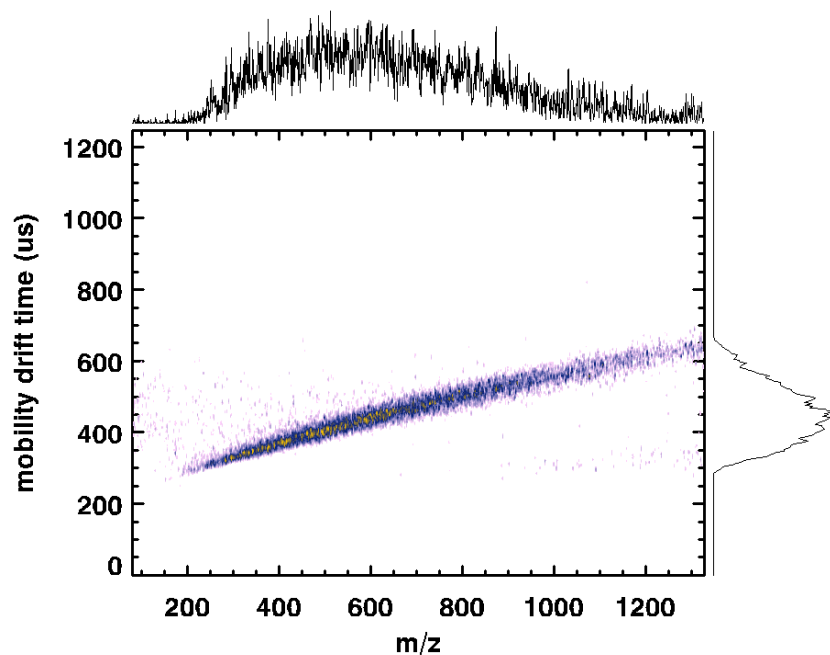


Figure E1a.8. IM-MS spectrum of the edge spot on the limestone slice soaked in AAD binder for 32 hours.

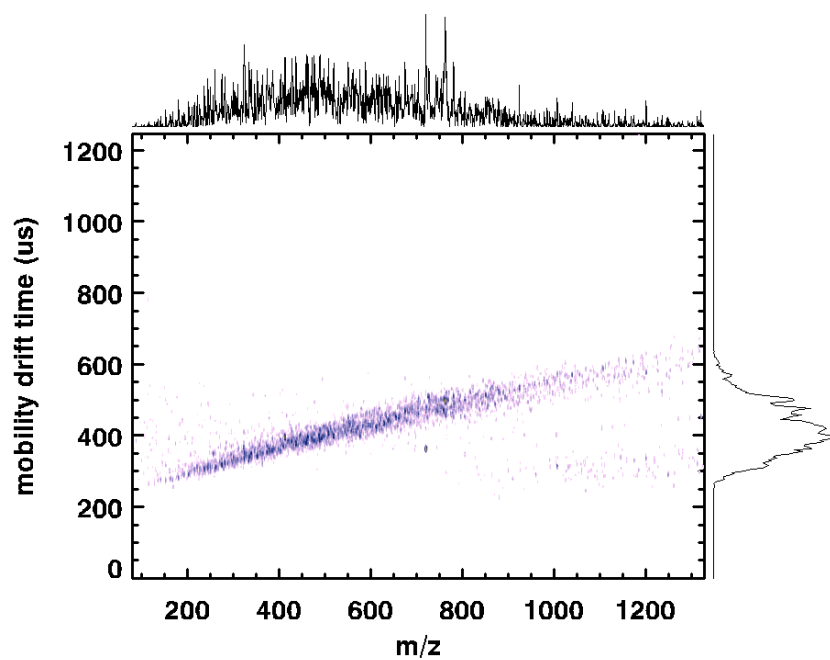


Figure E1a.9. IM-MS spectrum of the center spot on the limestone slice soaked in AAD binder for 32 hours.

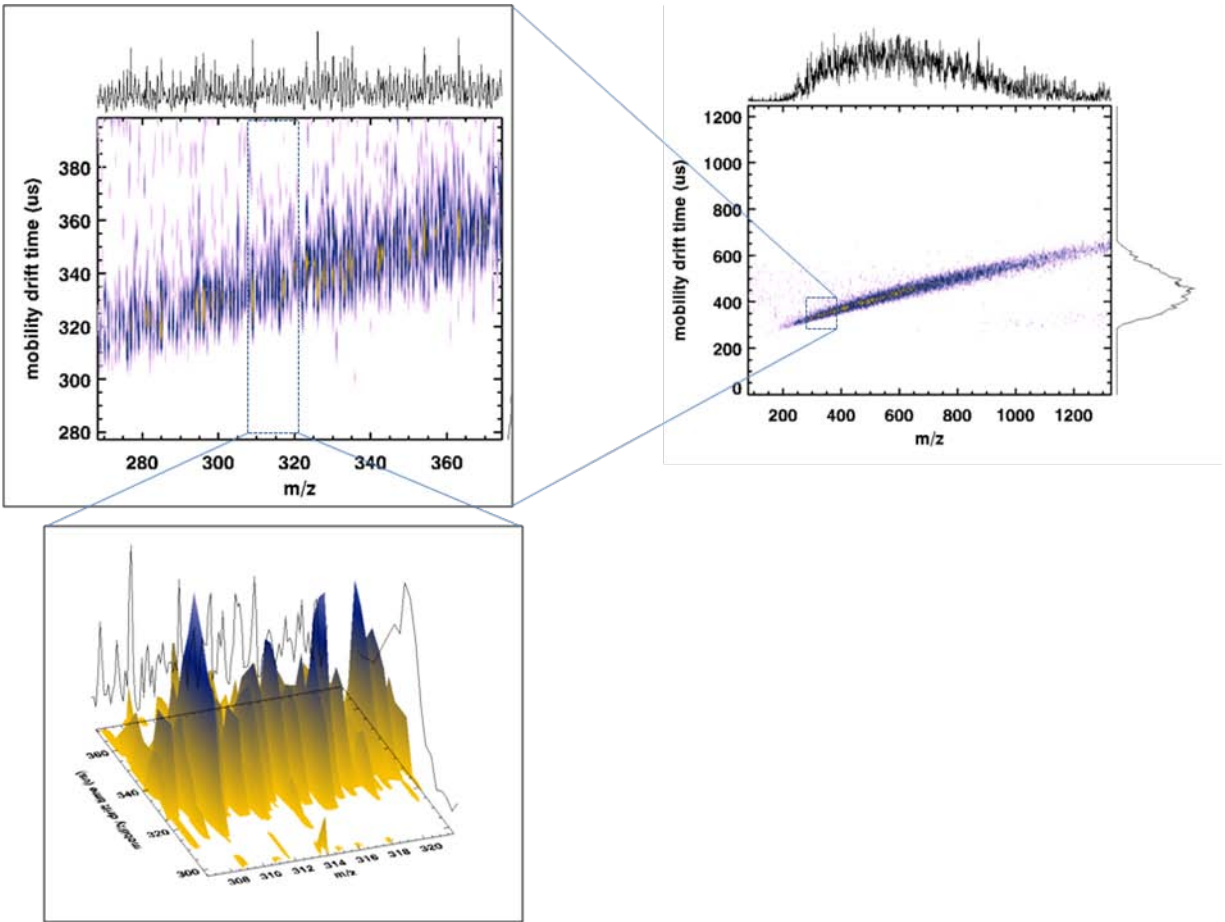


Figure E1a.10. IM-MS spectrum of the edge spot at a nominal mass level around 310 m/z.

After identifying the absorption of asphalt binder by aggregates, a further investigation was made to quantify the effect of absorption on the mechanical properties of aggregates. The mechanical property of the most interest was the viscoelastic property of the aggregates. As a result, a creep test was conducted on the fresh limestone sample shown in figure E1a.1 and the limestone sample soaked in AAD binder shown in figure E1a.2. The test set-up is shown in figures E1a.11 and E1a.12. In the creep test, a load of 4,000 lb was applied to the test samples for 7200 sec (2 hr). Three linear variable differential transformers (LVDTs) were mounted on the surface of the samples to measure the vertical deformation, as shown in figures E1a.11 and E1a.12. The vertical strains of both samples were calculated and plotted in figure E1a.13 versus the creep time. Figure E1a.13 clearly illustrates that the limestone soaked in AAD binder is less stiff than the fresh limestone. In addition, the magnitude of the vertical strain of the limestone soaked in AAD binder is increasing with the elapse of time, which demonstrates that the absorption of asphalt binder by limestone significantly increases the viscoelasticity of the limestone sample.



Figure E1a.11. Configuration of creep test on fresh limestone sample.



Figure E1a.12. Configuration of creep test on limestone soaked in AAD binder.

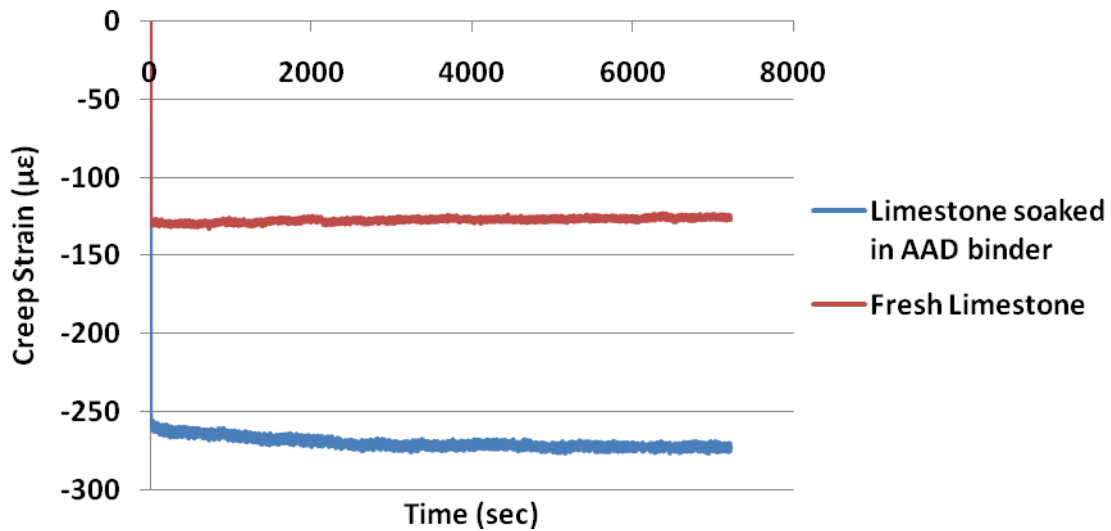


Figure E1a.13. Creep test results of fresh limestone and limestone soaked in AAD binder.

### Significant Results

The inverse micromechanics model that was developed in this work element has shown that aggregates have a frequency dependent complex modulus in the intermediate frequency range between 0.01 and 10 Hertz where the aggregate phase angle is apparently non-zero. There has been skepticism about aggregates being viscoelastic in this frequency range and we have shared in that skepticism. However, the aggregate tests that we have seen show a greater compliance with aggregates that have absorbed asphalt. This indicates that the quantity and stiffness of the absorbed asphalt will affect the stiffness of the aggregate, exactly as the micromechanics model predicted.

The predicted response was that as an asphalt mixture ages, the frequency dependence of the aggregate stiffness decreases (it becomes more elastic). The tests we have run on these aggregates have shown that absorbed asphalt does make an aggregate more compliant. The tests we will make in the next quarter will show clearly what these effects are.

These findings about the selective absorption of asphalt by aggregates have implications for aging and moisture damage, fatigue and thermal cracking, and mix design. Because aggregates in warm mixes do not absorb as much asphalt, this implies that with the same aggregates, the resistance of warm mixes to these types of damage will be different than for hot mix.

The completion of the undamaged, viscoelastic, compressive anisotropic characterization testing and analysis protocol which is reported under Work Element F2c, opens the way for running destructive tests on the same mixtures using our ability to determine  $W_{R2}$ , the dissipated pseudo-strain energy that is related to permanent deformation, to measure and determine the anisotropic compressive viscoplastic properties of an asphalt mixture.

### Significant Problems, Issues and Potential Impact on Progress

Availability of testing equipment, specifically the MTS, UTM, and DMA testing equipment to perform the characterization tests on mixtures, fine aggregate mixtures, binders, and aggregates, is foreseen as being a likely problem in this coming quarter.

### Work Planned Next Quarter

The critical frequencies of loading for the viscoelastic response of aggregates are between 0.01 and 10 Hertz. It is in this frequency range that the micromechanics model indicates a frequency dependence of aggregate stiffness and in which the phase angle is nonzero. Monotonic loading tests will be run on a variety of aggregates with loading times from 0 to 60 seconds and the Laplace transform formulation will be used to determine the frequency dependence of the complex modulus and phase angle of natural aggregates and those which have been soaked in heated binders.

The forward and inverse micromechanics model will be applied to the University of Wisconsin DSR data to determine the accuracy of this method to predict the mastic properties from the properties of the binder and its additives and modifiers.

DMA tests are planned to be run on fine aggregate mixtures which have been equilibrated to different levels of relative humidity. Undamaged and damaged properties will be evaluated using the VEC and torsional repeated loading tests to evaluate and quantify the effects of relative humidity on these properties of a fine aggregate mixture.

Now that undamaged viscoelastic, anisotropic, compressive characterization analysis has been completed and the analysis of mixture test data has proven to be accurate and repeatable, it is time to begin the determination of anisotropic, compressive viscoplasticity properties making use of our newly developed method of measuring  $W_{R2}$ , the dissipated pseudo-strain energy that is related to permanent deformation.

### Cited References

Becker, C., Fernandez-Lima, F., and Russell, D. H. (2009) "Ion Mobility-Mass Spectrometry: A tool for Characterizing the Petroleum." Available online: <http://spectroscopyonline.findanalytichem.com/spectroscopy/Featured+Flash+Component/Ion-Mobility-Mass-Spectrometry-A-Tool-for-Characte/ArticleStandard/Article/detail/592282>

### **Work element E1b: Binder Damage Resistance Characterization (DRC) (UWM)**

#### ***Subtask E1b-1: Rutting of Asphalt Binders***

### Work Done This Quarter

Laboratory testing followed the approved work plan. The initial plan for binder testing includes frequency sweep, Repeated Creep and Recovery (RCR), and Multiple Stress Creep and Recovery

(MSCR) using the Dynamic Shear Rheometer (DSR). The research team postponed frequency sweep testing for the remaining binders because the initial data did not add significant information to repeated creep data. The data collected to date will be used to further validate the relationship between frequency sweep and repeated creep, and a decision on continuing to test will be made later.

The research team noticed irregularities in the results when testing mastics with cone-and-plate geometry. An evaluation of the effect of geometry on mastic testing was conducted, which included a literature search to identify recommendations and laboratory testing to compare cone-and-plate geometry with parallel-plate geometry. At this time, it is clear that complications of cone-to-plate spacing results in major difficulties in testing mastics, and parallel-plate geometry is a more reliable test procedure.

Aggregate of granite mineralogy was selected as the primary source for mixture preparation. The research team will wash the aggregate over the No. 200 sieve prior to batching. After washing, the aggregate blends will be batched and filler added in the amount specified in the mix design. This allows for the addition of different filler types to evaluate the effect of different fillers on HMA. This work is being coordinated with the NCHRP 9-45 testing program.

The asphalt binder testing plan has been prioritized to allow for selection of two binders to be used in mastic and mixture testing to complete a full set of tests. These tests will be used to identify any potential issues and appropriately address them before proceeding to the entire testing matrix. This prioritization has led researchers to focus on binders modified to achieve similar nonrecoverable creep compliance (Jnr) but differing elastic properties.

The selected materials include two modified binders, two fillers and two aggregate gradations using the granite source. The materials selected are:

- Binders: elastomer- and plastomer-modified.
- Mineral filler: hydrated lime and granite.
- Aggregate gradation: coarse and fine.

Testing for the binder and mastic will focus on the MSCR procedure, with increased levels of stresses; testing for the mixtures will focus on the Simple Performance Test (SPT) flow number test. The research team acquired the materials during the last quarter. Testing of binders and mastics was completed this quarter, and batching, mixing and compacting of HMA specimens began.

## Significant Results

### *Effect of Testing Geometry*

All binders in this study are tested using cone-and-plate geometry. However, unreasonable results were observed when testing mastics using the same geometry. The literature recommends conducting tests of viscoelastic particulate composites such as mastics using parallel-plate geometry (Carreau et al. 1997; Rothon 2003; Macosko 2006). Macosko recommends against

using cone-and-plate geometry for materials with relatively high viscosity. Carreau notes that highly erroneous results could be obtained for particulate composites and polymer blends where the particles are of the same order of magnitude of the gap size. In fact, Carreau specifically recommends using parallel-plate geometry for testing particulate composites.

To investigate the effect of the geometry on mastic properties, a frequency sweep test was conducted to observe the change in  $G^*$  with respect to time. The frequency sweep was conducted at 64 °C and 3% strain. Testing was conducted on mastics blended from unmodified binder of PG 64-22 and a limestone binder. Specimens of this mastic were tested using the three geometries indicated below:

- Parallel-plate: gap = 1.0 mm
- Cone-and-plate: gap = 0.105 mm with 4° angle
- Parallel-plate: gap = 0.843 mm to test the same volume of mastic as in cone-and-plate geometry (called “effective gap”)

The absolute values of the measured  $G^*$  at each frequency for the different geometries are shown in figure E1b-1.1.

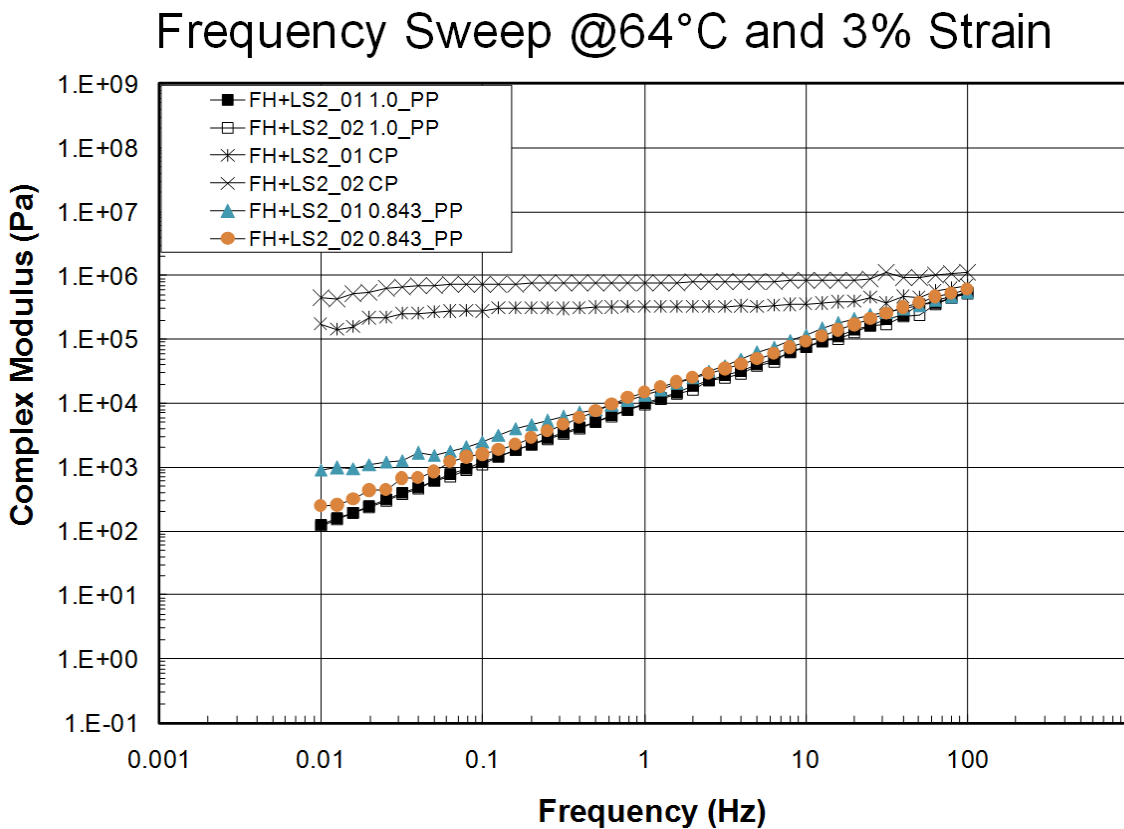


Figure E1b-1.1. Graph. Frequency sweep results for parallel-plate and cone-and-plate geometry. (PP = parallel-plate geometry. CP = cone-and-plate geometry.)

Figure E1b-1.1 clearly shows that testing at the standard gap and effective gap in a parallel-plate geometry yields the same measured values of  $G^*$  as a function of frequency. On the other hand, the cone-and-plate geometry indicates an almost constant value for  $G^*$  at any given frequency, which is unreasonable. The results suggest that the measurements of the cone-and-plate geometry do not yield different behavior due to the change in the sample volume; rather, the different behavior is due to the change in the plate geometry. Therefore, parallel-plate geometry is used for testing mastics in this project, while cone-and-plate geometry is used only for binders.

*Binder and Mastic MSCR Testing*

The research team is attempting to evaluate the significance of measuring the percent recovery from the MSCR test. This work is being coordinated with NCHRP 9-45 activities. Tests have been conducted on the different modified binders to select two binders that demonstrate the same  $J_{nr}$ , but with contradicting percent recovery (%R). The modified binders tested ranged from plastomeric-modified to elastomeric-modified binders. The tests resulted in selecting two binders. The selection criteria are satisfied because both binders demonstrate a value of  $J_{nr}$  less than or equal to 1.0 (1/kPa). According to FHWA recommendations, binders that meet this criterion are considered to be suitable for very heavy traffic volume. Both binders are blended with two fillers: hydrated lime and granite. A summary of the selected fillers' properties measured in the laboratory is shown in table E1b-1.1.

Table E1b-1.1. Physical and chemical properties of selected fillers.

Filler Type	Rigid Voids (%)	Water Solubility (%)	Organic Content (%)	Specific Gravity	Fineness Modulus	Methylene Blue	CaO (%)
Granite	42.60	2.29	0.36	2.66	4.06	2.35	3.50
Hydrated Lime	38.10	-0.96	0.54	2.79	4.15	1.05	32.20

For preparation of mastics, the asphalts selected will be mixed with fillers of pulverized granite and hydrated lime at a dust-to-binder ratio (DTBR) of 1:1. The 1:1 ratio was chosen for consistency between asphalt mastic testing and asphalt mixture testing, and is not expected to have a significant effect on mix design. Results for the binders and mastics tested are summarized in table E1b-1.2.

Table E1b-1.2. Measured percent recovery and nonrecoverable compliance for the selected materials.

Binder/Mastic	%Recovery			Jnr (1/kPa)		
	0.1kPa	3.2kPa	10kPa	0.1kPa	3.2kPa	10kPa
A*	70.1	57.9	40.8	0.27	0.57	0.66
B**	39.1	7.2	1.6	0.10	0.68	1.51
A+Granite	79.9	73.6	62.2	0.04	0.05	0.08
B+Granite	88.1	30.4	5.0	0.01	0.06	0.13
A+Hydrated Lime	72.4	66.7	53.9	0.08	0.09	0.14
B+Hydrated Lime	73.8	17.1	0.2	0.04	0.15	0.29

\* Elastomer binder.

\*\* Plastomer binder.

FHWA recommends an empirical equation between the value of Jnr and the %R; the relationship is shown in figure E1b-1.2. Using the equation, binders can be divided into high-elastic and low-elastic based on their measured %R for a given Jnr at 3.2 kPa. Both binders were tested at 64 °C. As shown in figure E1b-1.2, the values measured for the %R and Jnr for Binders A and B are clearly distinguishing between their levels of elasticity based on the FHWA recommendation. It is important to note that the binders were tested using cone-and-plate geometry.

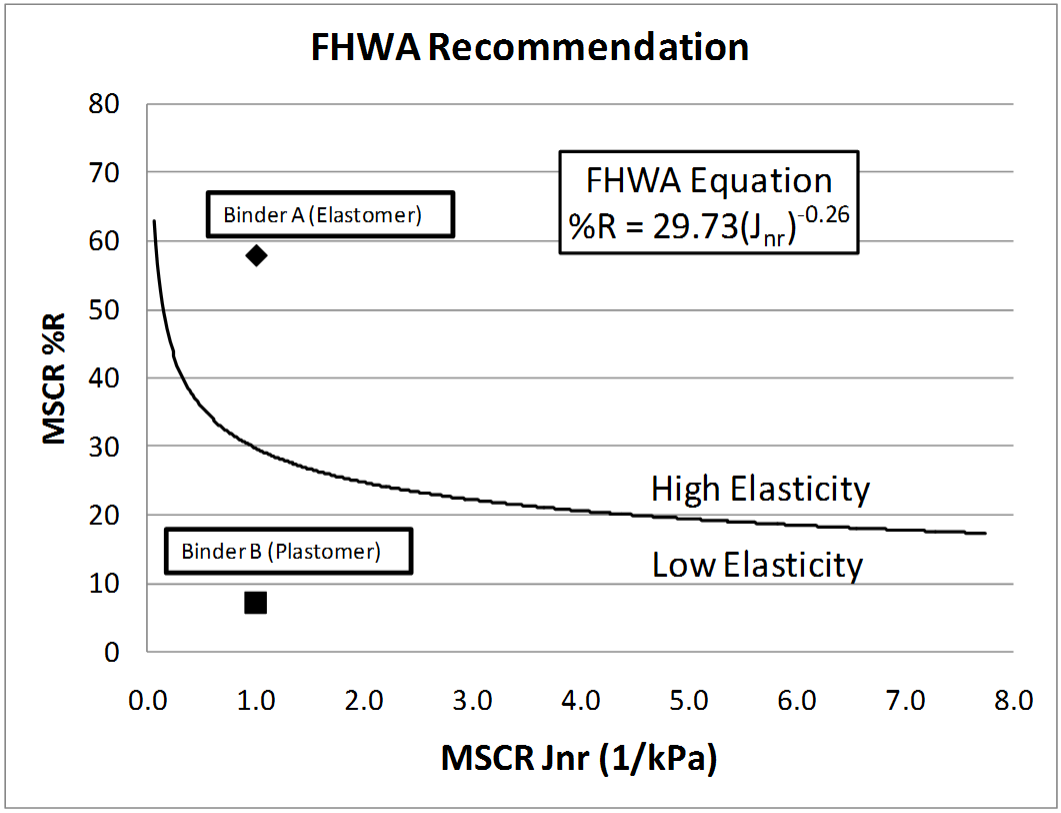


Figure E1b-1.2. Graph. Selection of binders based on the FHWA’s proposed equation.

The research team generated the plots shown in figure E1b-1.3 to examine the effect of stress on the results obtained and reported in table E1b-1.2. Figure E1b-1.3 shows the sensitivity of the nonrecoverable compliance to testing at different stresses. As can be noted in figure E1b-1.3, the research team expanded the range of stresses in the MSCR to include a third stress of 10 kPa.

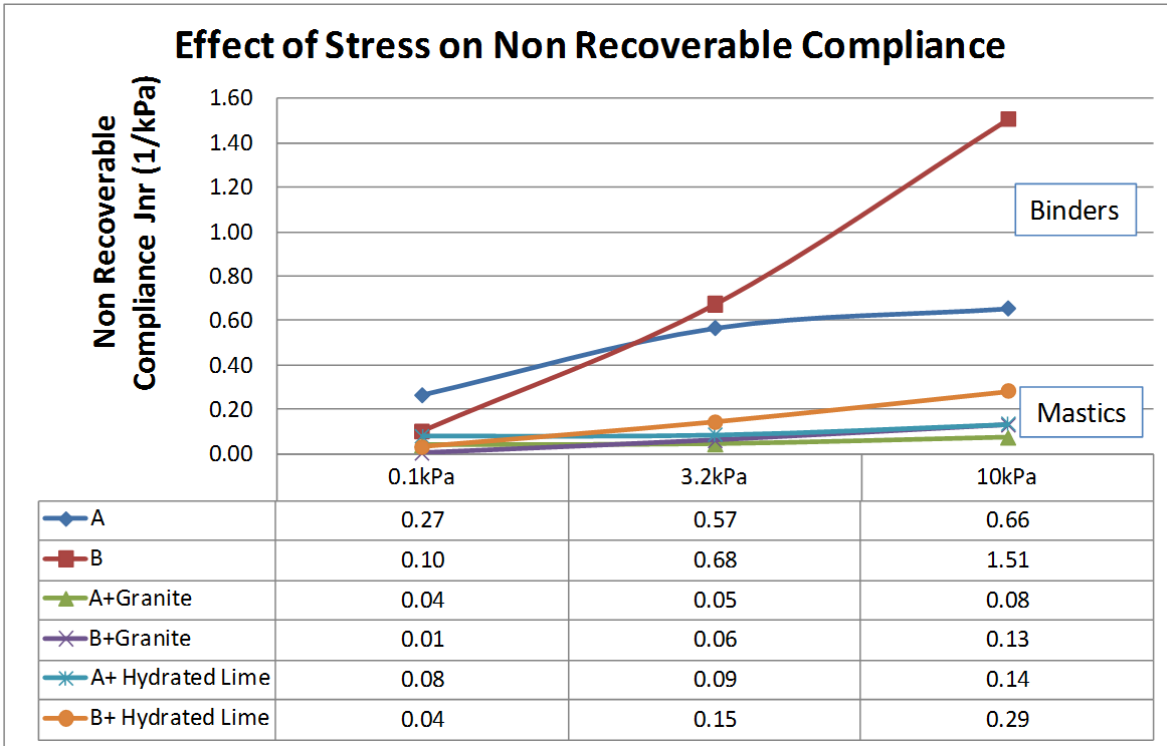


Figure E1b-1.3. Graph. Effect of stress level on Jnr value from the MSCR test. (Binder A = elastomer. Binder B = plastomer.)

At first glance, the Jnr can be seen to distinguish between mastics and binders. On the other hand, although the Jnr of the binders are of similar values at 3.2 kPa, when the stress increases to 10k Pa, the value of the Jnr clearly shows a separation between the performances of both binders. For the mastics, the Jnr does not show enough sensitivity for stress level, binder or filler. Results are evaluated from the percent recovery point of view in figure E1b-1.4.

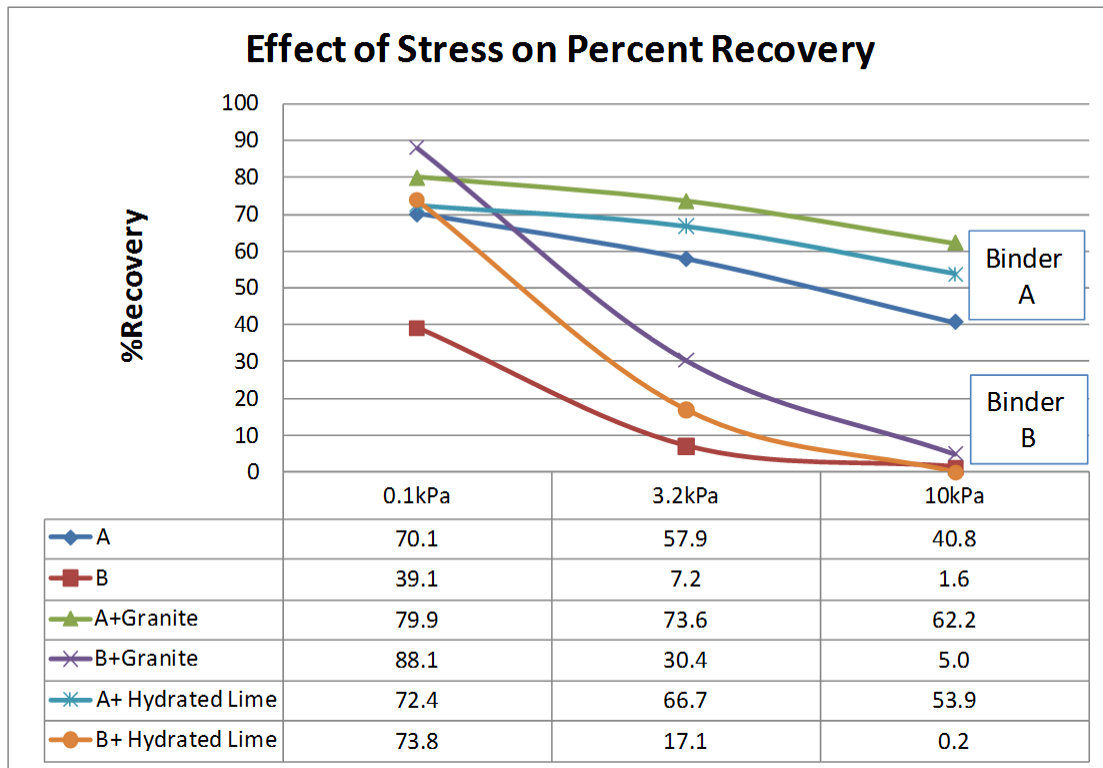


Figure E1b-1.4. Graph. Effect of stress level on measured %R from the MSCR test.

Figure E1b-1.4 clearly shows that %R is successful in distinguishing between the different binders. In addition, mastics show an improved performance with respect to %R compared to binders. With respect to stress level, the plastomeric binder and mastics show much higher sensitivity in contrast to the elastomeric binder and mastics.

Results presented in figures E1b-1.3 and E1b-1.4 indicate that the use of %R provides a more complete evaluation of the tested binders and/or mastics. On the other hand, the stress levels included in the MSCR procedure (0.1 kPa and 3.2 kPa) do not seem to provide enough power to distinguish between the different binders and/or mastics.

#### Significant Problems, Issues and Potential Impact on Progress

None.

#### Work Planned Next Quarter

Next quarter, binder testing will continue according to the test plan. Mixture data for the selected materials will be generated to complement the results obtained from the binders and mastics tested. RCR data will be evaluated in terms of available modeling tools presented in previous quarterly reports.

## Cited References

Carreau, P. J., Daniel De Kee, and Raj Chhabra, 1997, *Rheology of Polymeric Systems: Principals and Applications*. Hanser/Gardner Publications Inc., Cincinnati, OH.

Macosko, C. W., 2006, *Rheology: Principals, Measurements and Applications*. Wiley-VCH, New York, NY.

Rothon, R. N, ed., 2003, *Particulate-Filler Polymer Composites*. Rapra Technology Limited, United Kingdom.

### ***Subtask E1b-2: Feasibility of Determining Rheological and Fracture Properties of Thin Films of Asphalt Binders and Mastics using Simple Indentation Tests***

#### Work Done This Quarter

A brief literature review was compiled and is attached to this report as Appendix A. The review focused on the literature that reports advances in testing viscoelastic material, with a specific interest in asphalt. The review also included the available models proposed to calculate the creep and recovery behavior of tested materials. The laboratory testing setup was adjusted to match the recommendations found in the literature review.

Testing was conducted on two binders: a neat binder of PG-64, and a styrene-butadiene-styrene (SBS)-modified binder of PG-70. Preliminary testing was conducted to evaluate the testing device with respect to changing the temperature and binder type.

#### Significant Results

The testing setup was modified such that the specimen depth and diameter are more than five times the diameter of the indenter, as recommended by the literature. (Refer to Appendix A.) The tests were conducted with a spherical indenter of 17 mm in diameter. Figure E1b-2.1 shows the results of testing the unmodified neat binder at 25 °C, 30 °C and 40 °C. The intent of this testing is to identify the maximum possible testing temperature that can allow enough time to gather enough data points for analysis.

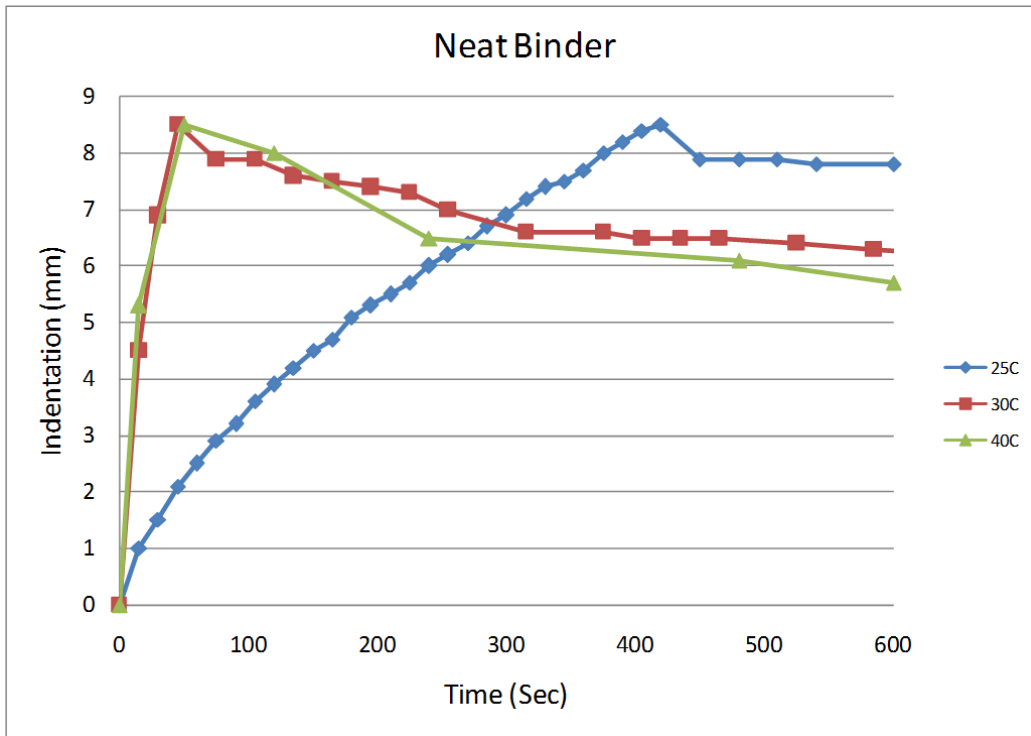


Figure E1b-2.1. Graph. Comparison of indentation and relaxation at different temperatures for neat binder PG-64.

The results reflected in figure E1b-2.1 clearly show that above 25 °C, the rate of indentation is very rapid. Figure E1b-2.2 compares the behavior of different binders at 40 °C.

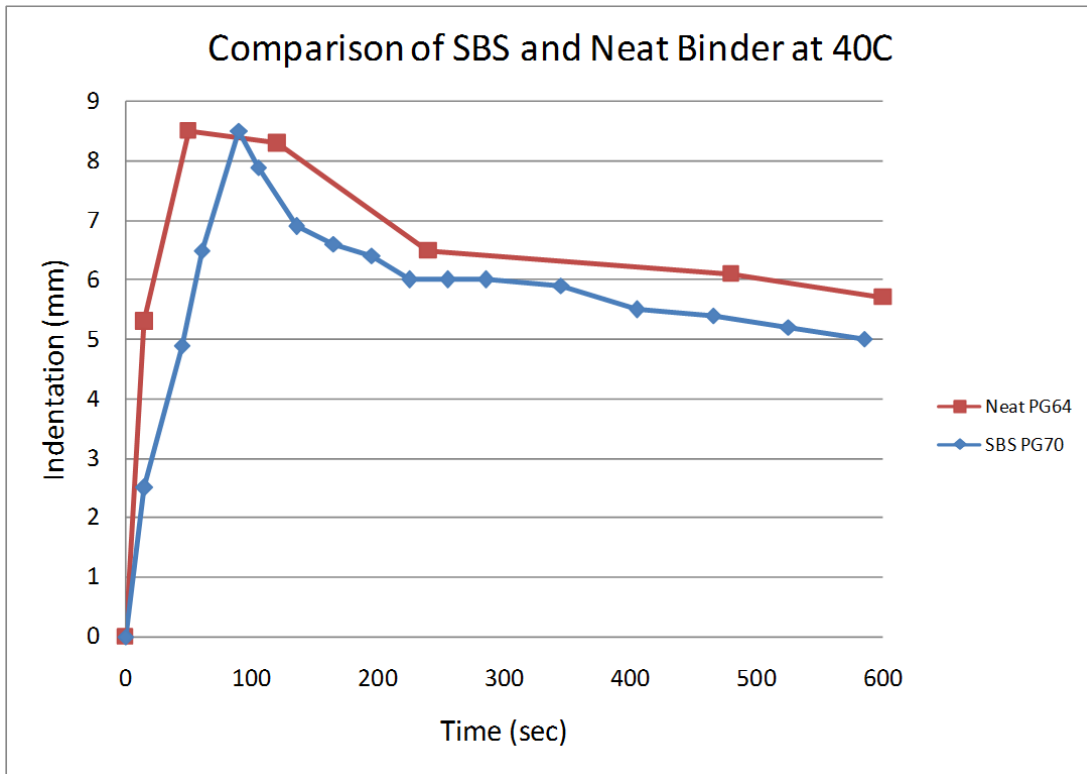


Figure E1b-2.2. Graph. Indentation and relaxation of neat binder and SBS-modified binder.

The results shown in figure E1b-2.2 indicate that the SBS PG-70 binder is more resistant to creep deformation, as it takes about double the time needed by the neat PG-64 binder to reach the maximum deformation (90 seconds for SBS compared to 50 seconds for the neat binder). On the other hand, the SBS binder shows much quicker relaxation. Thus far, data match expectations well.

The main challenge in this test is that it cannot be applied at elevated temperatures (e.g., high PG temperature), although the main intention is to correlate results to rutting behavior of binders. A potential solution to this problem is to test the binder at multiple temperatures, at and below 25 °C, and generate a relaxation modulus master curve to predict behavior at elevated temperatures. The other alternative is to change the diameter of the indenter by increasing it enough to allow for testing at higher temperatures.

#### Significant Problems, Issues and Potential Impact on Progress

The testing setup is not suitable for testing binders at high PG temperatures.

#### Work Planned Next Quarter

Next quarter, the research team will select two binders to generate relaxation modulus master curve for further evaluation of testing potential. Work will be finalized on developing a viscoelastic constitutive model to predict Dynamic Shear Rheometer (DSR) rheological results

from indentation testing. The research team will continue to evaluate the testing assembly to allow for gathering information about binder rheological properties at high PG temperatures.

## **Work Element E1c: Warm and Cold Mixes**

### ***Subtask E1c-1: Warm Mixtures***

#### Work Done This Quarter

Work focused on further evaluation of the effects of warm mix asphalt (WMA) on binder rheological properties and mixture workability. Specific activities included evaluating the effects of foaming on asphalt binder viscosity and rutting resistance. Significant progress was made in the development of a new test to quantify the effects of WMA additives on asphalt binder workability. Previous work by the University of Wisconsin–Madison and others determined that viscosity is inadequate to measure the effects of WMA additives. A literature search was conducted on the fundamental concepts of tribology and existing standards used to measure the lubrication. Based on this review, the testing protocol presented in ASTM D5183-05, “Standard Test Method for Determination of the Coefficient of Friction of Lubricants Using the Four-Ball Wear Test Machine,” was selected for modification for use in the Dynamic Shear Rheometer (DSR) to evaluate the effects of WMA additives. A schematic and photographs of the testing apparatus are provided in the “Significant Results” section of this report.

Efforts related to mixture workability included the use of the Wirtgen WLB10 foaming machine to produce foamed mixes with 1.0%, 1.5% and 2.0% water content. The foamed mixes were used to compare the performance of conventional HMA and WMA produced with other additives at the same compaction temperature with regard to air voids and Construction Force Index (CFI). All mixes were compacted at 110°C. Previously measured mixture data for both a fine-graded (65% passing No. 4) and coarse-graded (45% passing No. 4) mix were analyzed using the workability protocols presented in the NCHRP 9-43 project. A strong relationship was found between the results reported by NCHRP 9-43 researchers and the CFI measurements taken using the Pressure Distribution Analyzer (PDA) at UW–Madison.

Significant effort was put toward coordinating field projects and materials procurement and sharing with the University of Nevada, Reno. Efforts focused on evaluating mixture performance at the University of Nevada, Reno using the mix designs and materials produced at UW–Madison. The following field trial sections have been identified:

- *City of Reno*: Marshall Mix Design (50 blows). Sections include an HMA control section with 15% recycled asphalt pavement (RAP) and a WMA prepared with Ultrafoam technology and 15% RAP. Both mixes include the use of hydrated lime.
- *Manitoba Infrastructure and Transportation*: Construction of two 500-foot sections using each of the following materials: HMA, HMA compacted at lower temperatures, Sasobit, Advera and Evotherm.
- *NCHRP 9-43*: Preliminary contact has been made to work with the NCHRP 9-43 research team in evaluating foamed mixes for some of their field projects.

Detailed experimental plans and/or results of the laboratory evaluation of these field trials will be provided in subsequent quarterly reports.

### Significant Results

#### *Lubricity Testing*

The ASTM D5183-05 standard, “Standard Test Method for Determination of the Coefficient of Friction of Lubricants Using the Four-Ball Wear Test Machine,” was selected for use to attempt to quantify the effects of WMA additives using lubrication. The machine consists of three lower balls that are clamped with a fourth ball, which is held in a chuck and loaded against the clamped ball assembly. The chuck is rotated in one direction with resistance provided by the fixed balls in the cup below. The entire assembly can be placed in a temperature-controlled bath where all the balls can be immersed in the lubricant. The frictional forces are estimated from the torque applied to maintain a constant speed. A schematic of the machine is provided in figure E1c-1.1.

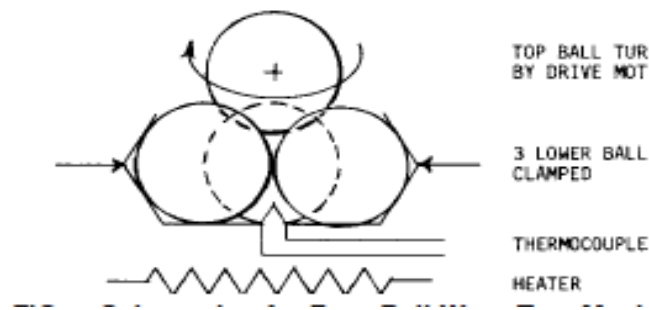


Figure E1c-1.1. Illustration. Schematic of ASTM D5183-05.

The dimensions provided in the ASTM standard were scaled down to fit the dimensions of the Paar-Physica DSR available in the UW–Madison Asphalt Lab. Photographs of the testing assembly are provided in figure E1c-1.2. The DSR was selected to allow for control of normal force as the chuck is rotating across the surface of the balls restrained in the cup.

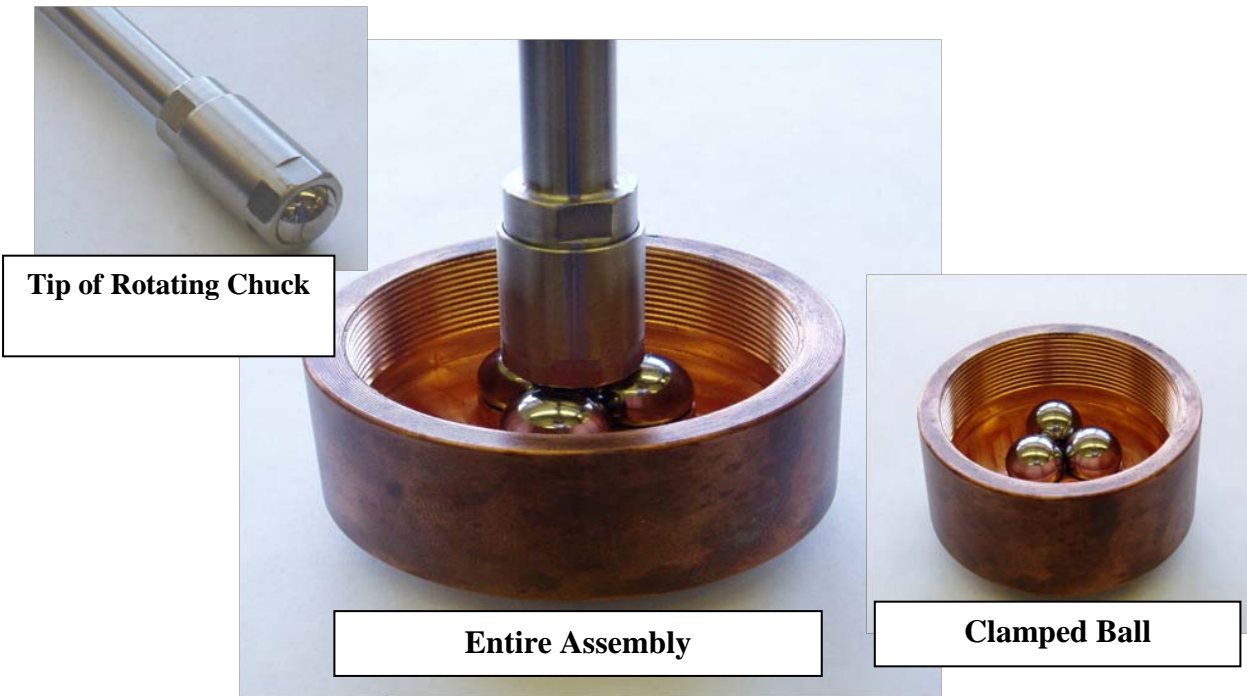


Figure E1c-1.2. Photographs. Photographs of UW–Madison lubricity tester.

Not shown in the photos is the threaded cover that is screwed into the cup to hold the three balls in the cup in place.

The testing procedure is still under development, but the concept is to fill the cup in the clamped ball assembly so asphalt just covers the clamped balls. The chuck is then rotated at a constant speed and the DSR is used to measure torque. Because of the limitations of the peltier plate heating system used in the DSR, all materials will be tested at 100°C. Efforts will be made to allow for higher testing temperatures if development testing shows promise. A normal force of 20 N was selected and a speed sweep was conducted from 1 to 300 rpm to determine the appropriate speed to produce a constant torque. Based on this testing, a speed of 50 rpm was selected. Further testing will involve finalizing a testing procedure and evaluating the response to temperature, binder grade and WMA additive type.

#### *Evaluation of Foamed Asphalt: Effects on Viscosity and High-Temperature Performance*

The Wirtgen WLB10 machine was used to attempt to simulate the Ultrafoam or Double Barrel Green processes currently in use in the laboratory. Based on presentations given for various field projects (Smith 2007, Van Kirk 2009), a range of 1.0% to 2.0% water content by weight of the binder was selected. Asphalt was also foamed with a concentration of 1.5% water. Material at the 1.5% and 2.0% concentrations was immediately sampled and tested. Viscosity temperature profiles were developed by testing at temperatures of 150°C, 125°C and 105°C. Speed was held constant at 20 rpm. Results are presented in figure E1c-1.3.

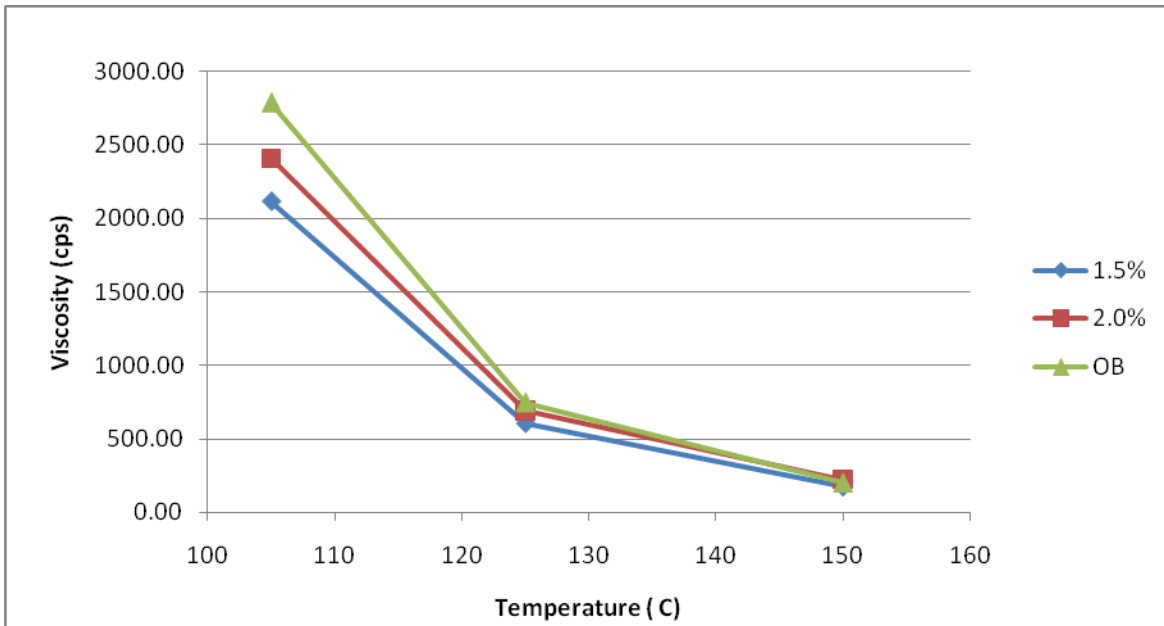


Figure E1c-1.3. Graph. Temperature viscosity profile of foamed asphalts at different water contents with PG 64-22 base binder.

Results presented in figure E1c-1.3 show little difference in viscosity between the neat asphalt (OB) and the foamed asphalts until low temperatures. Testing at 105°C displays a reduction in viscosity of 14% and 24% for asphalts foamed at a concentration of 2.0% and 1.5% water content, respectively. The effects of foaming at the previously stated concentrations on high-temperature performance were evaluated using the high-temperature true grade, which is an approximation of the actual high-temperature grade of the binder using interpolation between the Superpave binder rutting parameter ( $G^*/\sin(\delta)$ ) measured at two different temperatures. Results are presented in figure E1c-1.4.

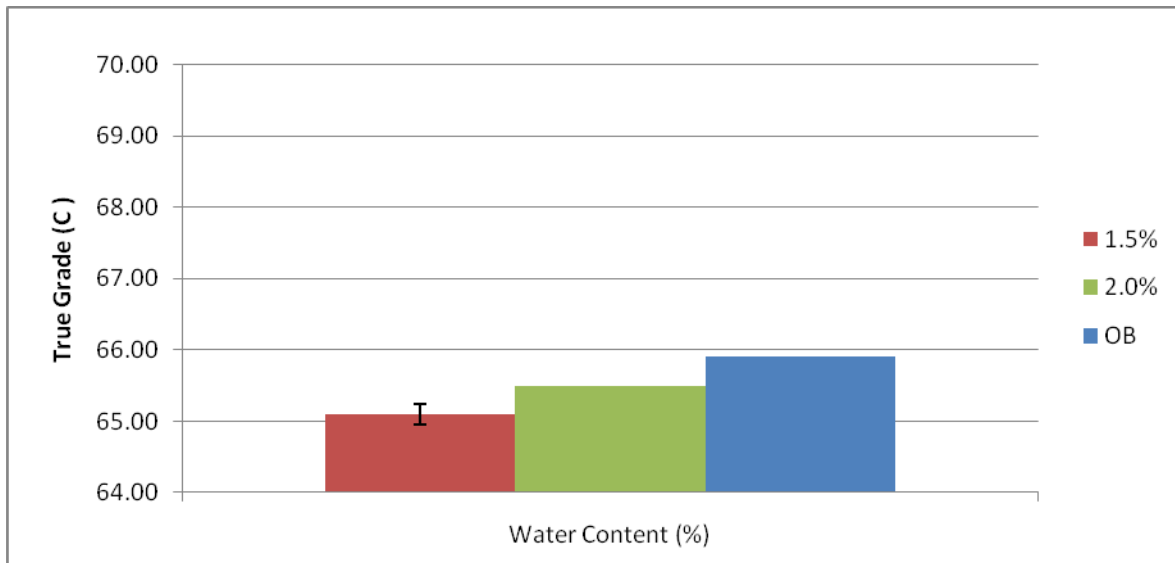


Figure E1c-1.4. Graph. Comparison of high-temperature true grade–foamed asphalt versus original binder.

Results presented in figure E1c-1.4 show true grades within 1°C, indicating that there is no effect of foaming at the concentrations tested on high-temperature binder rheological properties.

*Evaluation of Foamed Asphalt Mixes: Workability Comparison to HMA and Other WMA Additives*

The E10 ( $N_{des} = 160$ ) fine-graded (65% passing No. 4) granite mix with a nominal maximum aggregate size (NMAS) of 19.0 mm used in previous evaluations of mixture workability was prepared using the WLB10 foaming machine at mixing and compaction temperatures of 125°C and 110 °C, respectively. Mixes were prepared using all three previously provided water contents (1.0% to 2.0%). Because the asphalt must be at 165°C to operate the WLB10, the mixing temperature was controlled using the temperature of the aggregates.

Aggregates were placed in the mixing bucket and the prescribed amount of foamed asphalt was shot into the mixing bucket. Samples were cured at the compaction temperature for two hours and compacted at 300 kPa. Weight was recorded immediately after mixing and after one hour curing. Results showed no change, indicating there was no remaining moisture. Results showed that mixture workability in terms of both air voids and CFI were not dependent on the concentration of water used for foaming. The mixes prepared with a water content of 1.5% were compared to HMA and WMA prepared with Advera and Revix compacted under the same conditions, and mixture workability was evaluated in terms of both air voids and CFI. Little difference between the air voids for the mixes at the compaction levels of  $N_{ini}$ ,  $N_{des}$  and  $N_{max}$  were observed. Results for the CFI are presented in figure E1c-1.5.

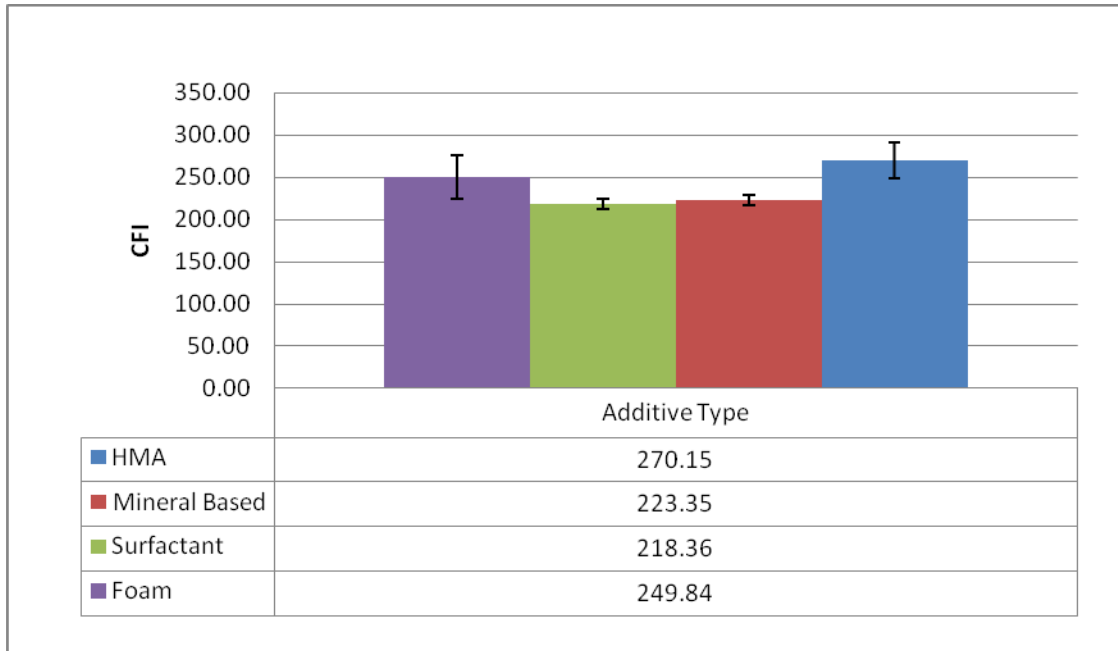


Figure E1c-1.5. Graph. Comparison of CFI for various WMA technologies. Samples compacted at 110°C and 300 kPa.

The CFI values measured for the different material types demonstrate that the foamed mix results in a CFI are marginally lower than that of the HMA, with an overall reduction of about 7% in CFI. More improvement in workability was observed for the Advera and Revix WMA technologies with 17% and 20% reductions in CFI, respectively. However, further analysis is needed to determine if these differences are statistically significant at a reasonable level of confidence.

*Comparison of ARC Workability Testing to NCHRP 9-43 Criteria*

The following criteria have been proposed by the NCHRP 9-43 research team to evaluate mixture workability (Bonaquist 2009):

- Mix compacted at proposed compaction temperature: gyrations to 92% < 0.35 N<sub>des</sub>.
- Mix compacted at proposed compaction temperature – 30°C: gyrations to 92% < 125% increase.

As presented in a publication by Guler et al., the CFI is measured as the energy required to densify the mix from N<sub>ini</sub> to 92% G<sub>mm</sub> (maximum specific gravity). This parameter is very similar to the gyrations to achieve 92% G<sub>mm</sub> proposed by the NCHRP team. As expected, comparison of gyrations to 92% G<sub>mm</sub> to CFI for the mixes compacted for this project showed a very strong correlation (R<sup>2</sup> = 96%). This strong relationship resulted in similar predictions of minimum compaction temperature for the HMA mixes prepared with both PG 64-22 and PG 76-22. Results for the PG 64-22 and PG 76-22 HMA mixes are presented in table E1c-1.1.

Table E1c-1.1. Comparison of workability evaluation using NCHRP 9-43 criteria (gyrations to 92%  $G_{mm}$ ) versus CFI.

Mix	Minimum Compaction Temp –Gyrations to 92% $G_{mm}$ (°C)	Minimum Compaction Temp – CFI (°C)	Difference (°C)
HMA – PG 64-22	125	130	5
HMA – PG 76-22	132	137	5

The CFI had a higher predicted compaction temperature for both binder types. Similar predictions were not available for the warm mixes because they had not failed the proposed compaction criteria after compaction at 90°C, indicating that the minimum compaction temperatures for mixes prepared with both Advera and Revix are below 120°C. Specific temperatures will be determined next quarter.

#### Significant Problems, Issues and Potential Impact on Progress

Submittal of the interim report was delayed to allow the research team to present and analyze a more complete data set. Specifically, the report was delayed to allow for updated information related to lubricity testing, binder low-temperature fracture properties, and mixture workability considering coarse mix design and foaming. This additional information has delayed submittal of the interim report by approximately two months.

Initial trials of an experiment related to the effect of production temperature on binder aging were delayed due to difficulties in rolling thin film oven (RTFO) aging of the materials at temperatures below 135 °C. At these lower temperatures, especially with the styrene-butadiene-styrene (SBS)-modified material, the binder would creep out of the RTFO bottles during aging. To remedy this, the research team elected to age the asphalt binders using the German Flask to evaluate change in high-temperature performance properties as a function of aging temperature. The change in aging procedure has not caused any significant delays in testing.

#### Work Planned Next Quarter

Work next quarter will focus on the following tasks:

- Submit interim report to include preliminary results of testing of foamed mixes and mixture workability using the lubricity tester.
- Continue work on binder and mixture workability testing matrix presented in the Year 3 work plan. Work includes incorporation of newly developed binder tests into the WMA experiment, including the lubricity test and tests to measure and evaluate a coarse mixture gradation and incorporation of foamed asphalts into the testing matrix. The research team will continue to compare the evaluation of workability based on the CFI measurements taken at UW–Madison and the gyrations to 92%  $G_{mm}$  used by the NCHRP 9-43 project.

- Coordinate with the University of Nevada, Reno with regard to testing and planning for the Manitoba and city of Reno field projects. Coordinate with the University of Nevada, Reno to develop and begin to execute a testing matrix that quantifies the effects of lower production temperatures on mixture performance. This will be used in conjunction with data generated at UW–Madison to determine if the effect on mixture performance is the same as that observed in the binder.

#### Cited References

Bonaquist, Ramon, 2009, Mix Design Procedures for Warm Mix Asphalt. Presented at the 88th Transportation Research Board Annual Meeting, Washington, D.C.

Guler, Murat, Hussain U. Bahia, Peter J. Bosscher, and Michael E. Plesha, 2000, Development of a Device for Measuring Shear Resistance of HMA in the Gyratory Compactor. Presented at the 79th Transportation Research Board Annual Meeting, Washington D.C.

Smith, Norm, 2007, Double Barrel Green WMA Process. Presented at the FHWA Warm Mix Asphalt Technical Working Group, Baltimore, MD,  
<http://www.warmmixasphalt.com/wmatwg07.aspx>.

Van Kirk, Jack, 2009, Contractor’s Perspective: RHMA Warm Mix Asphalt Project. Presented at the 2009 California Warm Mix Asphalt Conference, Sacramento, CA,  
[http://www.californiapavements.org/WMA\\_presentations.html](http://www.californiapavements.org/WMA_presentations.html).

#### ***Subtask E1c-2: Improvement of Emulsions’ Characterization and Mixture Design for Cold Bitumen Applications***

##### Work Done This Quarter

##### *Emulsion Construction Properties*

Efforts focused on further development of the test to quantify adhesion as a function of aggregate type, curing time and curing conditions. In previous quarterly reports, this test was called the Pneumatic Adhesion Tensile Testing Instrument (PATTI) test. However, to avoid confusion between previous work by the University of Wisconsin–Madison and others, and to reflect the significant changes made to the device, the test was renamed the Bitumen Bond Strength (BBS) test.

The research team discovered and purchased a commercially available instrument that included many of the changes previously made on the existing instrument. The PATTI Quantum Gold<sup>®</sup> testing device allows for better control of loading rate and includes a data acquisition system to allow for monitoring pressure over time. More details related to the testing equipment are available upon request. To evaluate the BBS equipment, testing was conducted on a CRS-2 emulsion and two aggregate types. The evaluation consisted of three separate experiments to screen factors previously proposed in the experimental design and examine optimum loading rates using samples cured for 24 hours for use in further testing. Results of these experiments

were used to define the experimental factors and appropriate loading rates for use in evaluating the effect of curing conditions on development of bond strength. Details related to these experiments are provided in the “Significant Results” section of this report.

As reported previously, a parallel activity undertaken by the research team is the use of the Dynamic Shear Rheometer (DSR) to evaluate development of emulsion rheological properties. Efforts this quarter involved developing a final testing procedure and related evaluation parameters. The research team decided that the emulsion would be evaluated using the  $G^*/\sin(\delta)$  parameter at 12% and 40% strain to reflect material properties in both the linear and nonlinear ranges of behavior, respectively. Furthermore, a full data set will include testing at 2, 6 and 24 hours curing for two aggregate types (granite and limestone), two levels of curing temperature (15 °C and 35 °C) and two levels of curing humidity (30% and 70%). Completion of the data set allows for statistical analysis to identify significant factors that can be compared to the results of the BBS testing. Completion of a similar test matrix for a modified emulsion will allow the research team to decide which of these candidate test methods is most appropriate for recommendation as a future specification test.

The sweep test as specified by ASTM D7000 was used to evaluate the relationship of the BBS and DSR tests conducted on the components of a chip seal to actual system performance. However, work conducted in NCHRP 14-17, Manual for Emulsion-Based Chip Seals for Pavement, and other projects found that sweep test results are highly dependent on emulsion film thickness and the amount of aggregate applied to the test sample (Schuler and Lord 2009). An experimental plan was developed to determine the significance of these effects and define the most appropriate procedure to use moving forward in chip seal performance testing using the sweep test. Aggregate type and curing conditions will be held constant in this experiment to isolate the effects of different design procedures on percent aggregate loss. The initial experiment will be conducted on CRS-2 and LMCRS-2 emulsions supplied by HG Meigs.

### *Emulsion Residue Properties*

Efforts related to emulsion residue properties involved evaluating the feasibility of replacing the Bending Beam Rheometer (BBR) with estimates provided by frequency sweep data collected at intermediate temperatures in the DSR, and modeling to predict stiffness and m-value at low temperatures. In the previous quarter, models from the original SHRP report A-369 (Anderson et al. 1994) were used to establish an equivalent frequency for oscillation testing in the DSR to relate to the creep testing at 60 seconds in the BBR, and to convert extensional stiffness to shear stiffness. Estimates of m-value were derived using a relationship defined in a viscoelastic properties of polymers textbook by Ferry (Ferry 1980). Evaluation of the model involved the use of one binder at four aging conditions—original binder (OB), rolling thin film oven (RTFO)-aged, pressure aging vessel (PAV)-aged, and twice-PAV-aged—and results from the emulsion residue testing conducted as part of the Federal Lands’ Polymer Modified Emulsions (PME) Technology Deployment Study. Initial correlations showed promise and will be presented in subsequent sections of this report. Activities in the next quarter will involve definition of how the research team will move forward in pursuit of this task.

## *Energy Analysis*

Substantial progress was made in developing a framework for conducting a pavement energy analysis. The purpose of the ongoing investigation is to identify gaps in scientific knowledge regarding asphalt pavement sustainability. Rapid deployment of sustainable paving methods, rating systems and technologies depends on understanding where the industry currently stands in key sustainability indicators such as energy consumption, emissions and environmental impact. In the past quarter, the research team identified the following challenges in implementing a framework that considers the social, financial and environmental impacts of asphalt pavement technologies:

- Reaching consensus on what sustainability means for asphalt pavements.
- Collecting and analyzing data that represent current practice and emerging technologies.
- Defining system boundaries that are consistent among studies and robust enough to handle different locations, road types and projects.

Based on results of a literature review and discussions with industry stakeholders, the current focus of the energy analysis was defined as follows:

- Conduct energy analysis for HMA plants. Real-time production data may be captured and analyzed using advanced systems control and monitoring technologies.
- Target the manufacturing process in the pavement life cycle as the process critical to reducing energy consumption.
- While analysis of plant emissions may be possible in the future, maintain an initial focus of conducting an energy analysis.

The research team has worked to coordinate activities with a number of stakeholders. The team is working with representatives from the Institute for Sustainability to develop a sustainability framework for asphalt pavements. The manufacturing process energy analysis is expected to help define such a framework. The team is also collaborating with systems control companies, pavement associations and contractors to collect and analyze production data.

The following meetings/presentations were held in the last quarter:

- ARC Emulsion Advisory Group Meeting, May 1, conference call. Meeting was held to provide the Project Advisory Group with an update of the ARC research team's progress, discussion of the Year 3 work plan and identification of critical research needs. The next meeting will be scheduled in late summer/early fall.
- Emulsion Task Force Meeting, May 14-15, New Orleans, Louisiana. Andrew Hanz attended the meeting, participating in the Quality Control and Acceptance Subgroup and presenting an update of ARC research activities to the task force.

## Significant Results

### Bitumen Bond Strength Testing

As previously noted, three separate experiments were conducted for BBS testing. The first test screened the experimental factors defined by the research team in the Year 3 work plan. Testing involved evaluation of samples prepared at both levels of curing temperature and curing humidity for the selected aggregate preparation, with testing at curing times of 2, 6 and 24 hours, for a CRS-2 emulsion. Results indicate that loading rate, curing conditions and aggregate type should be investigated further, while aggregate surface roughness and moisture condition (dry versus saturated-surface-dry (SSD)) are insignificant.

The second experiment examined how the response of pullout tension measured by the BBS varied with different loading rates. The goal of the experiment was to select an optimum range of loading rates to evaluate in the full-scale execution of the experimental design. Testing was conducted on granite and limestone substrates after 24 hours of curing. Curing conditions were held constant at 35 °C and 30% relative humidity (RH). Loading rates evaluated ranged from approximately 5 psi/s to 1000 psi/s. Results are presented in figure E1c-2.1.

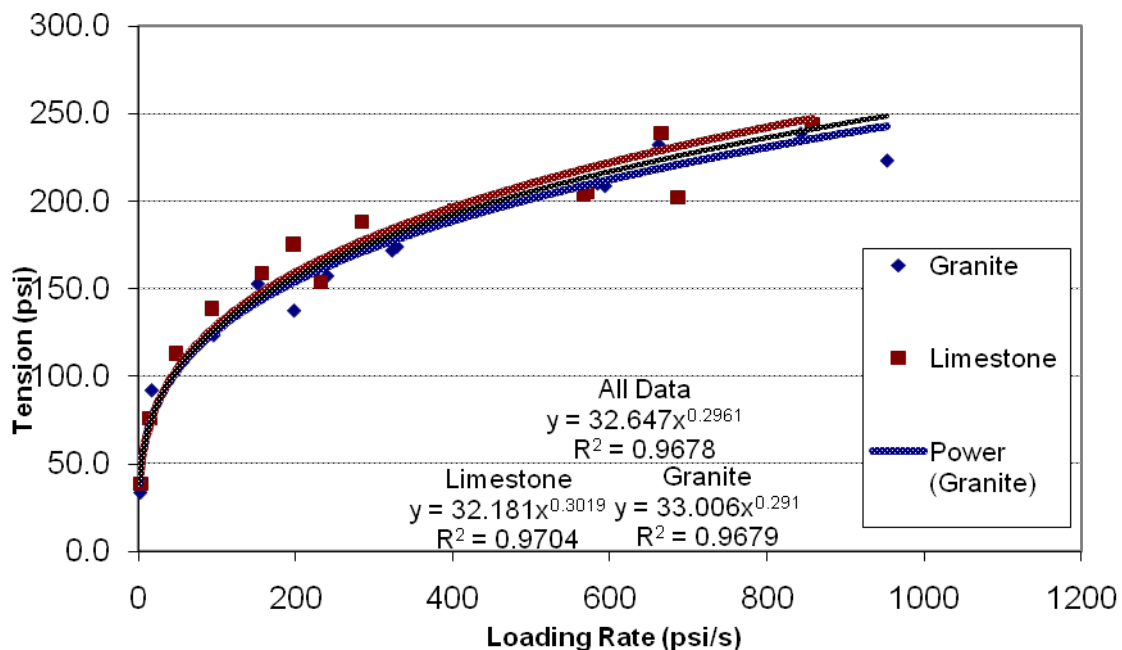


Figure E1c-2.1. Graph. Effect of loading rate on pullout tension.

Results from the study suggest that a strong relationship exists between the pullout tension response (in psi) and the pullout rate (in psi/s). As expected, both pullout tension and loading rate increase with higher flow controller settings. Results show that a strong power relationship exists between loading rate and pullout tension, with an  $R^2$  value of 0.9678 for all data points. The relationship between loading rate and pullout tension appears to be approximately linear above

pullout tensions of 100 psi. Furthermore, high variability was observed at high loading rates. Based on these results, the research team selected loading rates of 100 psi/s and 150 psi/s for further evaluation.

The curing condition experiment was developed to investigate the effects of mineralogy, curing conditions and curing interval on the development of bond strength between a CRS-2-type emulsion and aggregate plates. Factors investigated in the experiment are shown in table E1c-2.1.

Table E1c-2.1. Factors under investigation in the curing condition experiment.

Variable Factors		Level	
		+	-
A	Aggregate Type	granite	limestone
B	Curing Temp (C)	35	15
C	Curing RH (%)	70	30
D	Curing Interval	2 - 6 hr	6 - 24 hr
E	Loading Rate (psi/s)	100	150

RH = relative humidity.

These factors were selected based on results of previous testing in the development of the BBS system. The granite and limestone aggregates represent two very different aggregate types in terms of mineralogy and porosity. Two curing intervals were used in an effort to differentiate between initial and final development of bond strength. These factors were presented to the Project Advisory Group at the May 1 meeting and generally approved. The only comment received was that a higher curing temperature (up to 50 °C to 60 °C) should be investigated. The results of the experiment are presented in table E1c-2.2.

Table E1c-2.2. Increase in pullout tension for selected curing intervals.

Increase in Pullout Tension (psi)				
Curing Conditions	Granite		Limestone	
	2 - 6 HR	6 - 24 HR	2 - 6 HR	6 - 24 HR
35 C - 30 % RH	84.7	15.9	58.0	51.8
35 C - 70 % RH	54.7	126.5	28.6	152.3
15 C - 30 % RH	50.4	32.3	46.8	10.2
15 C - 70 % RH	51.0	32.5	26.5	11.1

It was observed during testing that at 2 hours of curing time, bond strengths for both aggregates under all four curing conditions are relatively constant at 50 psi. With the exception of the samples cured at 35 °C and 70% RH, the greatest gains in bond strength are seen in the 2- to 6-

hour curing interval, with curing on the granite substrate showing more gain in bond strength relative to samples tested on limestone. It is expected that the results at 35 °C and 70% RH do not follow this trend due to testing error; the samples will be re-tested in the next quarter. Gains between 6 and 24 hours of curing time are generally less, with the exception of the 35 °C and 30% RH curing condition on the limestone substrate, which exhibits virtually equal gains across both curing time intervals. Bond strength results for the samples at the previously defined curing intervals for the granite and limestone substrates are presented in figures E1c-2.2 and E1c-2.3, respectively.

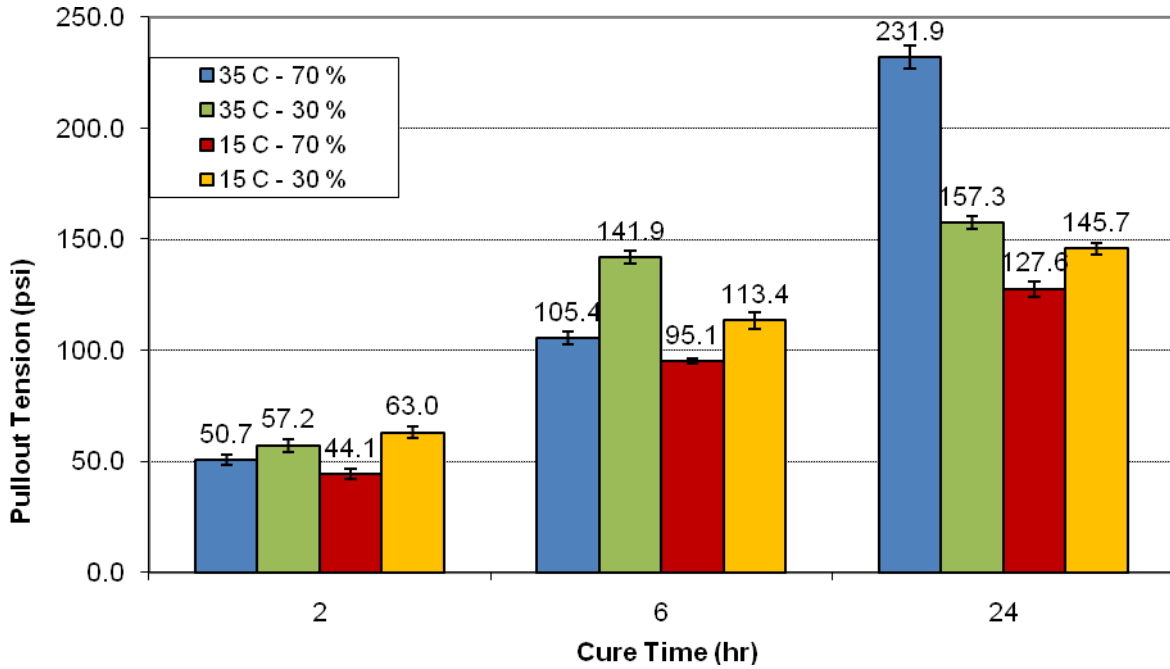


Figure E1c-2.2. Graph. Development in bond strength of CRS-2 emulsion cured on a granite substrate at various curing conditions.

Data presented in figures E1c-2.2 and E1c-2.3 demonstrate that the samples cured for 24 hours at 35 °C and 70% RH are erroneous and need to be re-tested because it is illogical to believe they would exhibit such a drastic increase in bond strength relative to samples cured at the same temperature and lower humidity. However, samples cured at the other conditions show logical trends and, based on the error bars presented in the figures, it is clear that the procedure developed produces repeatable results. Each test was replicated three times.

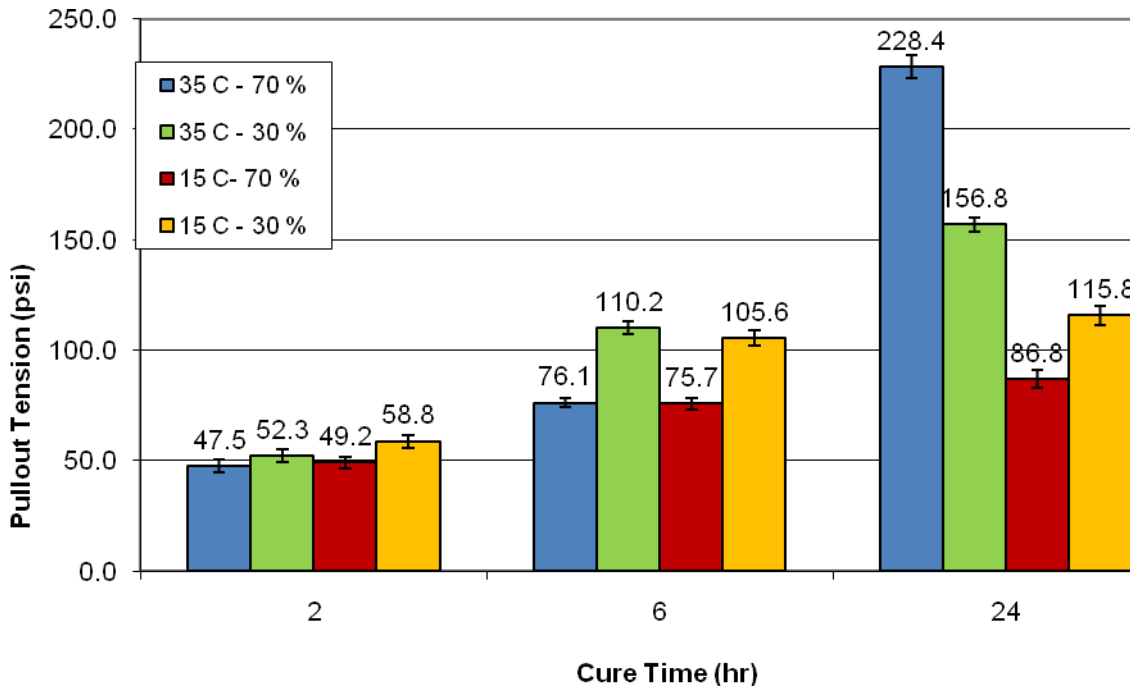


Figure E1c-2.3. Graph. Development in bond strength of CRS-2 emulsion cured on a limestone substrate at various curing conditions.

*Measurement of Emulsion Rheological Properties during Curing Using the DSR*

An experiment similar to the BBS testing was conducted using strain sweep testing in the DSR. Sample preparation and curing procedures are similar to those presented in previous quarterly reports and publications. However, the test evaluation parameter in the nonlinear range of behavior was modified from use of the strain associated with a 50% reduction in the Superpave rutting parameter ( $G^*/\sin(\delta)$ ) to the value of  $G^*/\sin(\delta)$  at 40% strain. This modification was made to allow for more consistent analysis of the data. It was found that especially with modified emulsions, the torque limit of the machine did not allow for the sample to experience the 50% reduction in  $G^*$ . In summary, the new test procedure includes the following evaluation criteria:

- Linear range of behavior:  $G^*/\sin(\delta)$  at 12% strain.
- Nonlinear range of behavior:  $G^*/\sin(\delta)$  at 40% strain.

In this quarter, testing was completed on a full data set that included the aggregate types, curing times and curing conditions used in the BBS testing. To maintain consistency and for future comparison to BBS testing data, analysis of variance (ANOVA) was conducted using a 95% level of confidence for the difference in response between the curing intervals of 2 to 6 hours and 6 to 24 hours for each evaluation criterion. Two replicates were conducted for each test with coefficients of variation between most testing results less than 10%. The  $R^2$  values of the ANOVA models for  $G^*/\sin(\delta)$  at 12% and 40% strain were 88% and 92%, respectively, indicating that the experimental factors selected account for the majority of the change in

response. ANOVA analysis for the  $G^*/\sin(\delta)$  at 12% identified no significant main effects. Conversely, the analysis of the nonlinear evaluation parameter identified the following main effects and two-way interactions as significant:

- Main effects: Aggregate Type and Curing Temperature.
- Two-way interactions: Aggregate Type\*Cure Temp and Aggregate Type\*Cure Interval.

An example of the data generated is provided in figure E1c-2.4. Based on the results of the ANOVA, the plot provides comparison of  $G^*/\sin(\delta)$  at 40% strain as a function of time for curing at 15 °C and 35 °C and an RH of 30%.

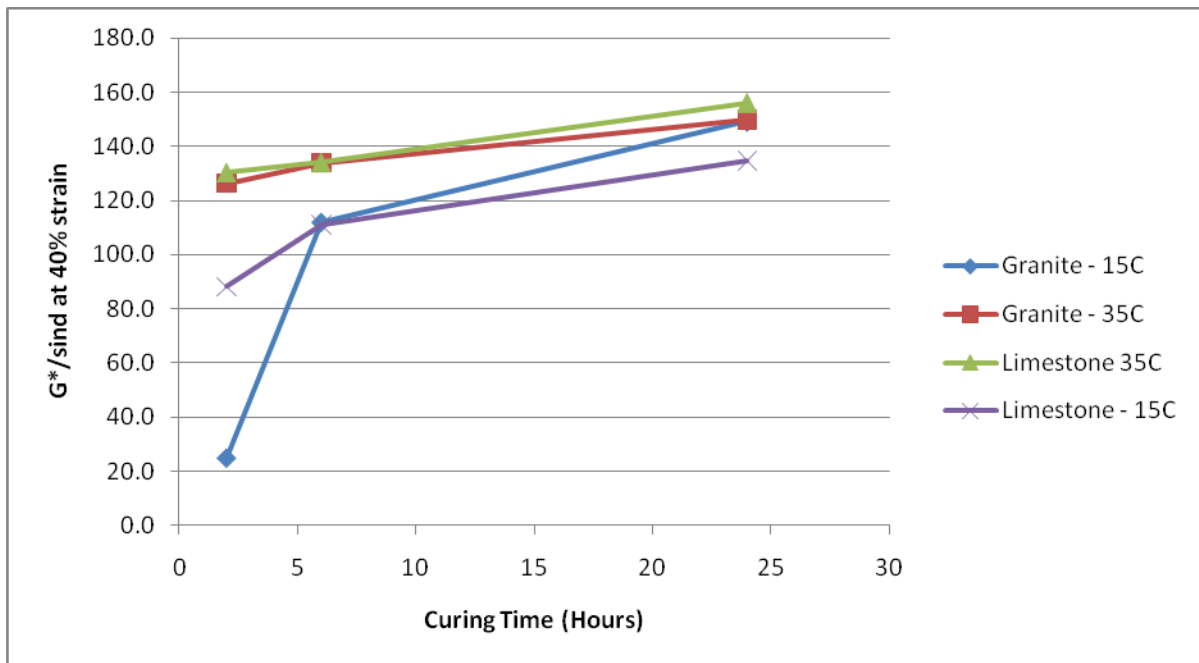


Figure E1c-2.4. Graph. Comparison of  $G^*/\sin(\delta)$  at different curing times on limestone and granite substrates for different curing temperatures at an RH of 30%.

Results presented in figure E1c-2.4 demonstrate an effect of temperature on development of rheological properties for both aggregate types. The emulsion cured on the granite substrate at 15 °C does not attain the rheological properties of the emulsion cured at the higher temperature until 24 hours of curing time. A significant difference in performance is still evident after 24-hour curing for the emulsion cured on limestone substrates. A distinct effect of aggregate type is also noted at low curing temperatures, with the emulsion cured on the limestone aggregate exhibiting significantly higher stiffness relative to the granite substrate. These results are contrary to the BBS testing results, which showed no effect of curing conditions or aggregate type on samples cured for two hours. These differences will be further evaluated in the next quarter.

*Using the DSR to Predict Low-Temperature Performance*

Basic rheological models were applied to frequency sweep data collected at 10 °C. Preliminary analysis of the data showed that the shear modulus ( $G^*$ ) and phase angle ( $\delta$ ) at 10 Hz is most appropriate for comparison to extensional stiffness and m-value at 60 seconds in BBR testing. As previously noted, the models were evaluated using a conventional asphalt subjected to four different levels of aging and four emulsion residues tested through the Federal Lands project.

The work completed in SHRP A-369 established an equation to convert the extensional stiffness to shear stiffness by considering the difference in modulus and compliance for the two types of loading (Anderson et al. 1994). This relationship is provided in the following equation:

$$S(t) \approx \frac{3G^*(\omega)}{[1+0.2\sin(2\delta)]}$$

$$t \rightarrow \frac{1}{\omega}$$

where

$S(t)$  = creep stiffness at time,  $t$ , Pa

$G^*(\omega)$  = complex modulus at frequency  $\omega$ , Pa

$\delta$  = phase angle at frequency  $\omega$ , Pa

Estimates of stiffness ( $S(60)$ ) from the equation above are compared to BBR measurements in figure E1c.2.5. The line of equality is included to provide a reference point for evaluation of the quality of the estimate.

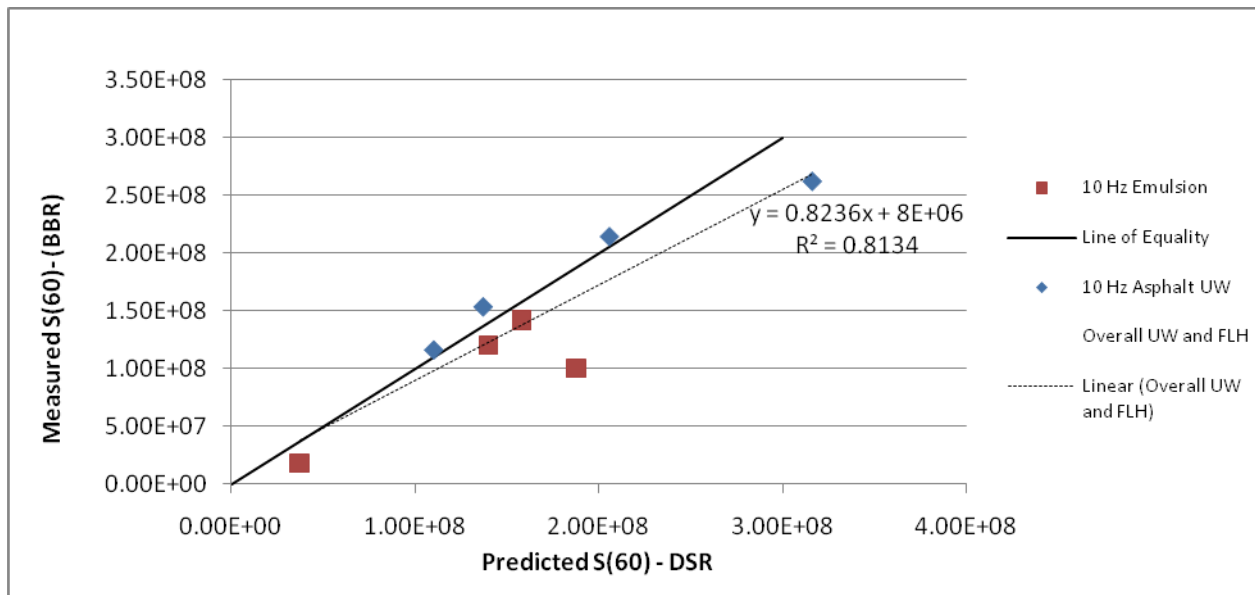


Figure E1c-2.5. Graph. Measured versus predicted values, with stiffness at 60 s.  
FLH = Federal Lands Bureau.

Figure E1c-2.5 demonstrates that prediction of BBR data using DSR measurements taken at 10°C and 10 Hz are promising. Six out of the eight data points plot along the line of equality, with both outliers overpredicting the actual value of S(60). Outliers include both a conventional asphalt PAV aged twice and a polymer-modified emulsion residue. Data from the conventional asphalt and emulsion residues were grouped to develop a linear trend line for the data collected. Trends are very similar, as noted by the slope of the trend line of 0.8236. This value is biased by the two outliers.

For replacement of the BBR with DSR data in any specification, strong correlation between estimates developed using DSR data and the m-value as measured by the BBR is needed. The m-value at 60-second testing time in the BBR (m(60)) was estimated using the following relationship provided by Ferry (Ferry 1980):

$$m = \frac{d(\log G^*)}{d(\log \omega)}$$

where

m = slope of G\* versus frequency plot at a given frequency

δ = phase angle

G\* = complex modulus

ω = frequency (rad/s)

The equation above represents direct evaluation of the derivative of the log G\* versus log frequency function at a given frequency. For this case, the derivative is evaluated at 10 Hz (62.8 rad/s). The log G\* versus log frequency function for each material tested was developed by fitting a second-order polynomial trend line to the data. The resulting first-order derivative was then evaluated at the appropriate frequency to obtain an estimate of m-value. These estimates are compared to measurements in the BBR in figure E1c-2.6.

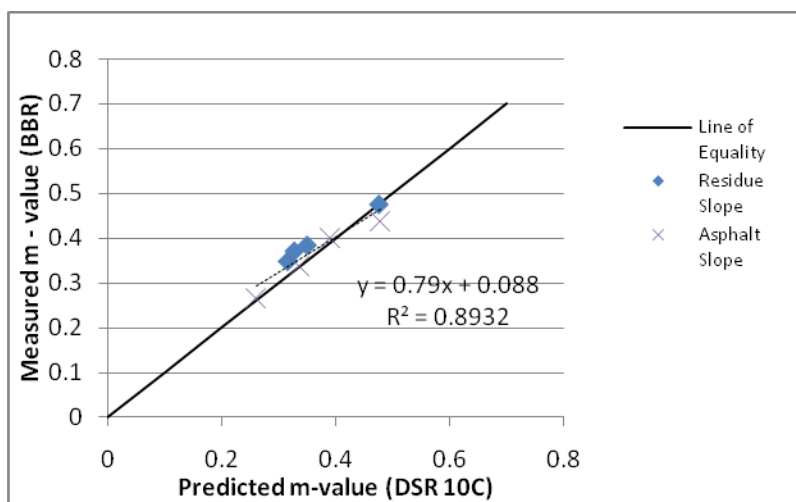


Figure E1c-2.6. Graph. Measured versus predicted using  $\frac{d(\log G^*)}{d(\log \omega)}$ , with m-value at 60 s.

Figure E1c-2.6 shows a strong relationship between measured and predicted values. The accuracy of these initial estimates of stiffness and m-values indicates that using DSR frequency sweep data at intermediate temperatures can provide a strong prediction of low-temperature properties measured by the BBR.

### Significant Problems, Issues and Potential Impact on Progress

The literature review report for this work element has been delayed to allow for investigation and generation of preliminary data related to the different aggregate and emulsion application rates provided in the ASTM D7000 and McLeod design methods. The literature review will be incorporated into an interim report next quarter and include a white paper with the experimental test results and analysis.

Selection of the DSR or BBS test for use in quantifying emulsion curing rate was delayed to accommodate use of the PATTI Quantum Gold apparatus. Now that a full data set has been generated for each method, the research team feels a decision can be made in the next quarter.

Due to the extra efforts dedicated to evaluating the new BBS testing machine and finalizing the procedure, no testing was completed for evaluation of emulsion viscosity and storage stability. Test methods have been identified and will be pursued in the next quarter.

### Work Planned Next Quarter

Work next quarter will focus on the following tasks:

- *Construction properties of emulsions.* The research team will define procedures and begin evaluating candidate tests for emulsion viscosity and storage stability. The DSR strain sweep and BBS will be used on more emulsion types and test methods will be selected for further development. The team will also develop the BBS in draft ASTM format, and submit a paper for publication proposing a framework for more advanced evaluation of emulsions. The paper will serve as a framework for an interim report.
- *Sweep test procedures.* The research team will execute the experimental plan developed this quarter to select optimum emulsion application and aggregate spread rates. The final procedure will be used to evaluate the relationship between chip seal performance measured by the sweep test and the BBS/DSR tests on the chip seal components that have been developed thus far.
- *Field projects.* The research team will collaborate with HG Meigs to develop a plan for two field projects this construction season. The projects will involve sampling of emulsion, large aggregate for processing into plates, and chip seal aggregate to evaluate how the research team's laboratory procedures relate to field condition and performance.
- *Emulsion residue properties.* The research team will continue evaluation of the ability of DSR testing to be used as a surrogate for BBR testing. Evaluation of the models proposed will be conducted on hot applied binders. Conventional binders were selected because there is currently no accepted long-term aging procedure for emulsion residues.

- *Energy analysis.* The research team will continue to develop a strategy for life-cycle comparison of HMA and the impact of using emulsion applications in maintenance cycles.
- *ARC Project Advisory Group and Emulsion Task Force activities.* The research team will continue to hold advisory group meetings and support Emulsion Task Force activities.

### Cited References

Anderson, D. et al., 1994, Binder Characterization and Evaluation, Volume 3: Physical Characterization. SHRP-A-369, Strategic Highway Research Program, National Research Council.

Ferry, J., 1980, Viscoelastic Properties of Polymers. University of Wisconsin–Madison, Madison, WI.

Shuler, S., and A. Lord, 2009, A New Laboratory Test for Predicting Very Early Chip Seal. *Journal of the Association of Asphalt Paving Technologists*, 78.

## **CATEGORY E2: DESIGN GUIDANCE**

### **Work element E2a: Comparison of Modification Techniques (UWM Year 2 start)**

#### Work Done This Quarter

The research team focused on collecting modified materials from manufacturers. At the date of this report, materials had been received from three manufacturers; three more producers are shipping materials. The material library for this study is expected to include 17 materials from six sources, including five base binder grades and 12 modified binder grades.

Work began on characterizing the materials received from producers, and preparations were made to begin testing according to the approved testing matrix.

#### Significant Results

The review of ongoing work clearly indicates that the method of producing polymer-modified asphalts plays a significant role in defining the critical performance of binders. However, information reviewed to date does not clarify the importance of cross-linking and whether the elasticity resulting from cross-linking is important for damage resistance.

To bring more knowledge to this domain, the materials library for this work element is designed to encompass a wide range of modifiers, and includes polymeric and small molecule modifiers with both elastomeric and plastomeric properties. Modified materials received to date span the range of modification available and commonly used throughout the United States, including binders modified with polyphosphoric acid (PPA), styrene-butadiene-styrene (SBS), ethylene

terpolymer, plastomers and combinations of these modifiers. This group of materials includes modifiers with small and large molecular weights, and modifiers with high, intermediate and no elasticity. Elastomeric-behaving modifiers included both reactive and nonreactive types of additives. Comparing the properties of these binders is expected to shed more light on an area that is not very well understood today.

Table E2a.1 shows the status of the contacts made to manufacturers invited to participate in this research effort. Table E2a.2 shows the types of modifiers and the grades that are expected to be included in the testing. The research team expresses its gratitude to those who have pledged their support for this work element and looks forward to their continued involvement.

Table E2a.1. Manufacturers invited to participate in this research effort.

<b>Company</b>	<b>Sent e-mail</b>	<b>Accepted</b>
Nustar	X	X
Holly Asphalt	X	delivered
Seneca Chicago	X	X
United Refining	X	
ConocoPhillips	X	
Kraton	X	
Marathon	X	
Bit Mat	X	
Mathy Construction	X	delivered
Paramount Petroleum	X	
Payne & Dolan	X	X
Valero Oil	X	
Honeywell	X	X
Vance Brothers	X	X

Table E2a.2. Types of modifiers and grades expected from participating manufacturers.

<b>Material #</b>	<b>Base</b>	<b>Modifier</b>	<b>Class of Modifier</b>	<b>Expected Grade</b>
1	A	None	None	PG 64
2	A	Functionalized PE	Plastomer: Nonreactive	PG 70
3	A	Functionalized PE	Plastomer: Nonreactive	PG 76
4	A	SBS with cross-linking	Elastomer: Reactive	PG 70
5	A	SBS with cross-linking	Elastomer: Reactive	PG 76
6	B	None	None	PG 58
7	B	Terpolymer	Elastomer: Reactive	PG 64
8	B	Terpolymer	Elastomer: Reactive	PG 70
9	C	None	None	PG 58
10	C	PPA	Chemical: Reactive	PG 64
11	C	PPA+SBS+cross-linking	Elastomer: Reactive	PG 70
12	D	None	None	PG 58
13	D	Functionalized PE+SBS	Hybrid: Reactive	PG 64
14	D	Functionalized PE+SBS	Hybrid: Reactive	PG 70
15	E	None	None	PG 70
16	E	SBS with cross-linking	Elastomer: Reactive	PG 76
17	E	SBS with cross-linking	Elastomer: Reactive	PG 82

(PE = polyethylene.)

Significant Problems, Issues and Potential Impact on Progress

Because of the current economic environment, building the material library needed for the success of this work element proved to be a bigger challenge than expected. However, the research team believes that significant delays in this research effort can be avoided by maintaining its focus on building the material library.

Work Planned Next Quarter

Next quarter, the research team will continue gathering materials and begin testing materials already in the library. The team will coordinate a meeting with researchers conducting similar work at FHWA and other organizations to discuss possible collaboration.

## **Work element E2b: Design System for HMA Containing a High Percentage of RAP Material (UNR)**

### Work Done This Quarter

This work element is a joint project between University of Nevada, Reno and University of Wisconsin–Madison. The ARC research team presented the impact of current extraction techniques on the specific gravities of extracted aggregates and the newly proposed recycled asphalt pavement binder analysis (RAPBA) at the RAP ETG meeting in Manchester, New Hampshire, on April 22, 2009.

A meeting on the RAP research was held in Sacramento, California on June 8, 2009. The meeting was attended by Drs. Jon Epps, Adam Hand, Hussain Bahia, Randy West, Peter Sebaaly, and Elie Hajj. The meeting is part of the cooperation effort between ARC and NCAT. The attendees discussed the ARC and NCAT work plans for mix design of HMA containing RAP material. An experimental plan for the ARC research was developed to evaluate the mixing procedure for HMA containing RAP.

Testing methods and methods of mortar preparation and specimen molding were adjusted based on new findings. The recycled asphalt pavement binder analysis (RAPBA) spreadsheet developed to analyze test results was changed to accommodate the new methods. The changes are:

1. To prepare the mortar, instead of using selective recycled asphalt pavement (SRAP) retained on Nos. 30, 50 and 100 sieves according to maximum density gradation line, SRAP passing No. 50 sieve and retained on No. 100 sieve was selected. This change was accepted after significant testing of mortars with varying sizes and combination of sizes. The one-size approach was found to give the optimum molding and testing conditions of mortars.
2. For the asphalt content of mortar, instead of controlling new added binder at 25% of SRAP, the asphalt content was controlled to ensure the aged binder in SRAP was 20% of the total binder in mortar. This change was made to achieve a more consistent blending ratio of new and aged binders.
3. Instead of adding pressure aging vessel (PAV)-aged binder mixed with SRAP, rolling thin film oven (RTFO) binder was blended with SRAP to get mortar; then the PAV test for mortar was conducted to get aged mortar. To compare the aging extent between mortar PAV test and binder PAV test, burned aggregate was blended with regular PAV-aged binder to get PAV-binder mortar, while the same burned aggregate was blended with regular RTFO binder to get RTFO-binder mortar. PAV tests with different aging times were conducted for RTFO-binder mortar and compared to the PAV-binder mortar. Finally, a 24-hour PAV test is proposed for a mortar PAV test to achieve a similar aging extent for binder in mortar as compared to a 20-hour binder PAV test.
4. Instead of the modified Bending Beam Rheometer (BBR) mold with 9.35-mm-thick end pieces, the regular BBR mold with 6.35-mm-thick end pieces was used.

5. Instead of one test temperature of 0°C, different test temperatures were chosen to analyze the response time dependency. Testing at a minimum of two temperatures is suggested for RAP mortars. The temperature selection depends on the PG grade of fresh binder used for test and the target PG grade. It is suggested that testing is done at 0°C and another temperature that is one grade higher or lower than the PG grade of fresh binder. The test procedure for mortar at 0°C is the same as that used for binders with no RAP. For the lower test temperature, the only modification is increasing the test load from 980 mN to 4000 mN.

The results from the two test temperatures are used to calculate the two limit percentages of RAP binder. The estimated linear relationship between limit percentage and target PG grade is used to calculate the limit percentages at different target PG grades of blended binder consisting of RAP binder and fresh binder.

### Significant Results

The following experimental plan will be conducted as part of the ARC Work Element E2b-3: Develop a Mix Design Procedure.

The objective of this experiment is to develop a laboratory mixing process that closely simulates the actual conditions in the field under which the RAP materials are incorporated into the mixing of HMA mixtures. Typically, field production of HMA mixtures containing RAP materials follows the process of superheating the virgin aggregates and introducing the RAP materials at ambient temperature. This process relies on the heat transfer between the superheated virgin aggregates and the RAP materials to achieve the required mixing temperature for the entire mix while in the meantime avoiding the heating/aging of the RAP binder.

The following experiment will be conducted to assess the most effective laboratory process to mix virgin aggregates and binder with RAP materials for the purpose of conducting mix design. The following three laboratory mixing methods will be evaluated:

- Heat the virgin aggregates and RAP materials to the appropriate mixing temperature of the virgin binder grade.
- Superheat the virgin aggregates to the appropriate temperature based on NAPA's recommendations and add the RAP materials at their dry condition.
- Superheat the virgin aggregates to the appropriate temperature based on NAPA's recommendations and add the RAP materials at their wet condition.

The three mixing methods will be evaluated on the following materials:

- Select four field projects with the following characteristics:
  - Two projects from the east (NCAT) and two projects from the west (UNR)
  - Superpave mix designs
  - Un-modified asphalt binders
  - RAP percent greater or equal to 25%

- Obtain virgin aggregates, virgin binders, and RAP materials from the four projects: NCAT will sample the east projects and UNR will sample the west projects.
- Obtain loose HMA samples from the four projects at 5 days throughout the construction of each project: NCAT will sample the east projects and UNR will sample the west projects.
- Ship all the virgin, RAP, and loose HMA samples to the UNR laboratory. UNR will cover the cost of shipping the materials.
- The UNR researchers will conduct the following evaluations:
  - Mix laboratory samples for all four projects following the mixing procedures: A, B, and C.
  - Monitor the temperature of the total mix during the mixing process to assess the heat transfer between the virgin aggregates and RAP materials.
  - Short term oven age the laboratory produced mixtures.
  - Extract/recover and test the binder properties of the laboratory and field produced mixtures.
  - Measure the volumetric properties of the lab mixed lab compacted (LMLC) and field mixed lab compacted (FMLC) mixtures.
  - Measure the E\* property of the LMLC and FMLC mixtures (subject the E\* samples to 4 hours of short term aging).
- The measured properties of the LMLC mixtures prepared with mixing methods A, B, and C will be compared to the measured properties of the FMLC samples.

On the other hand, a finalized mortar sample preparation and test procedure has been developed. Tables E2b.1 and E2b.2 show the results of estimating the limit percentage of RAP that can be used as a function of the target PG grade (first column) and the size of the selective RAP (top row). Rall was tested using all RAP passing No. 8 sieve; R351 was the selected RAP of three sieves (Nos. 30, 50 and 100); and R16 was tested using RAP passing No. 16 and retained in No. 30, etc. The note in table E2b.1 indicates the RAP size used.

The results show that there is only limited influence of RAP gradation in SRAP on the allowable percentage. Based on these results and the workability observed during sample molding, the SRAP passing No. 50 sieve and retained on No. 100 sieve has been selected. The total mortar asphalt content was controlled by adding enough fresh binder such that the aged binder in SRAP was 20% of the total binder. This procedure was chosen to ease the mortar preparation.

The effect of the change in percentage of binder content on the maximum limit of the RAP used in an HMA without exceeding the stiffness limit of the PG grading is shown in table E2b.2.

Table E2b.1. Calculated results from RAPBA spreadsheet for different SRAP gradations.

Target of PG grade	Limit percentage by stiffness (%)									CV
	R <sub>all</sub>	R351	R16	R30	R50	R100	R200	<R200	Average	
-16	37.0	35.2	33.8	39.5	31.0	32.6	35.0	34.8	34.9	7.5
-19	30.0	28.5	27.7	31.4	25.4	26.2	27.7	27.9	28.1	6.9
-22	22.0	20.9	20.5	22.7	18.7	19.1	20.0	20.4	20.5	6.6
-25	13.4	12.6	12.5	13.6	11.5	11.5	11.9	12.3	12.4	6.4
-28	4.3	4.1	4.1	4.3	3.7	3.7	3.8	4.0	4.0	6.1
Target of PG grade	Limit percentage by m-value (%)									CV
	R <sub>all</sub>	R351	R16	R30	R50	R100	R200	Filler	Average	
-16	24.0	18.6	21.8	20.1	20.6	19.9	20.5	21.2	20.8	7.6
-19	18.7	14.5	17.0	15.7	16.1	15.5	16.0	16.5	16.2	7.6
-22	13.4	10.4	12.2	11.2	11.5	11.1	11.5	11.8	11.6	7.5
-25	8.1	6.3	7.4	6.8	6.9	6.8	6.9	7.1	7.0	7.4
-28	2.8	2.2	2.6	2.4	2.3	2.4	2.4	2.5	2.5	7.2

**Note:** R<sub>all</sub> represents the RAP material passing No.8 sieve mixed together; R351 represents the RAP material retained on Nos. 30, 50 and 100 sieves mixed together; R16 to <R200 represent single-sieve RAP material retained on Nos. 16, 30, 50, 100, 200 and <200 sieve separately. CV = Coefficient of variation.

Table E2b.2. Calculated results from RAPBA spreadsheet for different SRAP binder percentages in total mortar binder.

Limit Percentage by Stiffness (%)				CV	Limit Percentage by m-value (%)				CV
25%	20%	15%	Average		25%	20%	15%	Average	
32.6	31.0	33.4	32.3	3.7	19.9	19.6	20.7	20.1	2.9
26.2	25.0	26.8	26.0	3.5	15.5	15.3	16.1	15.6	2.9
19.1	18.3	19.6	19.0	3.4	11.1	10.9	11.6	11.2	2.9
11.5	11.1	11.8	11.5	3.2	6.8	6.6	7.0	6.8	2.9
3.7	3.6	3.8	3.7	3.3	2.4	2.3	2.4	2.4	3.6

Figure E2b.1 shows BBR test results of PAV mortar at different PAV aging times. By comparing with PAV binder aging, it can be seen that using a 24-hour PAV aging test for mortar can result in a similar aging extent for binder in mortar when compared with the 20-hour binder PAV test. It should be mentioned that when using mortar for PAV aging, the total volume is larger than the conventional binder PAV sample in each PAV pan. The mortar amount is selected such that the net binder content is kept at 50 grams, which is required in regular PAV aging.

The RAPBA spreadsheet has been adjusted to reflect the BBR data obtained from testing mortar samples. Results of testing PAV mortar and PAV SRAP mortar at two temperatures are shown in table E2b.3 and figure E2b.2. Test results indicate that the limit percentage of RAP binder used

in blended binder can be determined by the new approach when the target low temperature PG grade of blended binder consisting of PAV binder and RAP binder is given.

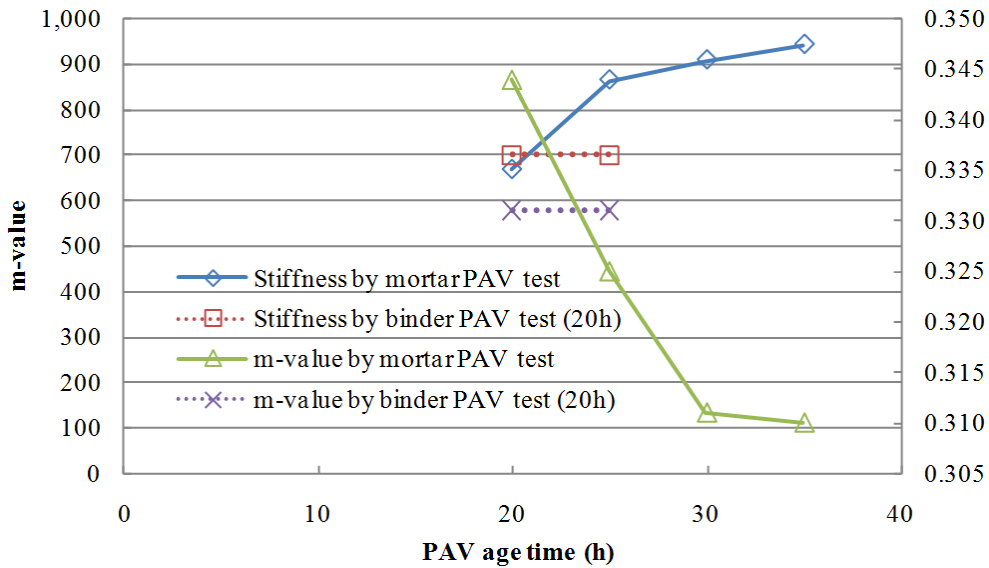


Figure E2b.1. Graph. BBR test results for mortar PAV tests at different aging times and regular binder PAV test.

### Significant Problems, Issues and Potential Impact on Progress

The new test method and RAPBA spreadsheet require verification by more materials, which could delay sharing the spreadsheet with other researchers.

### Work Planned Next Quarter

The research team will conduct a complete experimental design with three binders and three RAP sources, analyze data using the new approach and finalize the RAPBA spreadsheet. An experimental design will also be run for Dynamic Shear Rheometer (DSR) and Asphalt Binder Cracking Device (ABCD) testing.

### **Work element E2c: Critically Designed HMA Mixtures (UNR)**

#### Work Done This Quarter

The UNR team developed generalized equations for estimating the triaxial deviator and confining stresses and pulse time for a given pavement structure and temperature and under a given vehicle speed. The effect of the mixture type on the predicted stresses was accounted for through the corresponding asphalt mixture's stiffness at the effective pavement temperature and loading frequency at 2 inch below the pavement surface.

A preliminary investigation was carried out in an attempt to evaluate the applicability of the recommended deviator and confining stresses. Repeated load flow number testing was performed for the WesTrack Cell 55 plant mixture. The coarse-graded mixture was manufactured with an unmodified PG64-22 asphalt binder and has an optimum binder content of 6.4% and in-place air voids of 4%. The pavement section at WesTrack consisted of a 6-inch HMA layer on top of a 12-inch aggregate base on top of the subgrade. The pavement was subjected to four driverless tractor/triple-trailers with three single-axle semi-trailer followed by two trailers, each with two singles dual axles travelling at a speed of 40 mph.

### Significant Results

During the two year period of the WesTrack project, pavement temperature was recorded at four different depths in the pavement: 0.5, 1.5, 3.5, and 5.5 inch. Figure E2c.1 shows the maximum and minimum recorded temperatures as a function of applied ESALs at a depth of 1.5 inch from the pavement surface. Additionally, figure E2c.1 shows the rut depths for the Cell 55 mixture at various ESAL levels. A strong correlation between pavement temperature and rate of rutting is observed. The rut depth increased from 0.45 inch to 0.60 inch (a 33% increase) when the maximum pavement temperature increased during seven consecutive days from a 40°C to a maximum of 46°C. This correlation indicates that, even under constant loading conditions, HMA pavements will experience significant increases in rutting once their temperature reaches a critical level. In this field case, the critical temperature is expected to be between 40 and 46°C. Consequently, flow number tests were carried out at four different temperatures: 40, 45, 50, and 55°C.

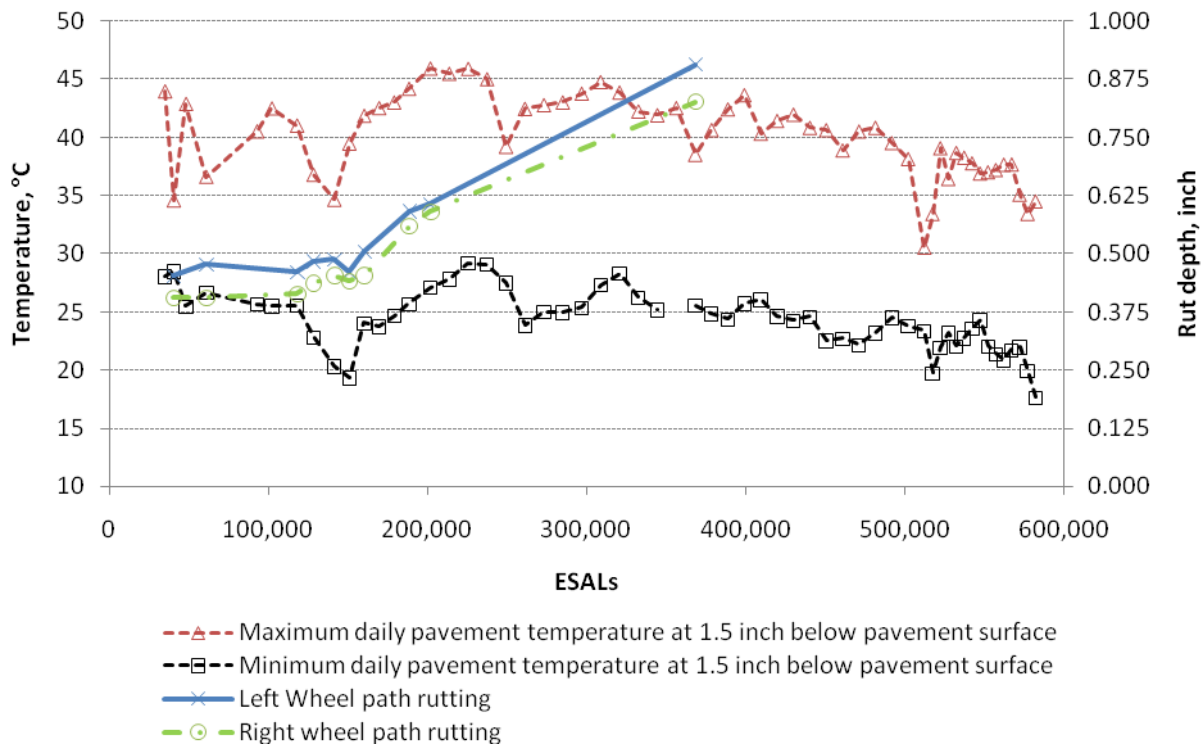


Figure E2c.1. Temperature profile and rut depths in Cell 55 as a function of applied ESALs

At each temperature, the corresponding deviator and confining stresses were determined using the developed equations. The equations require the knowledge of the stiffness of the mix at 2 inches below the pavement surface. Hence, a series of dynamic modulus ( $|E^*|$ ) tests were conducted on the WesTrack HMA mixture and the variations of  $|E^*|$  were estimated at each of these temperatures using the master curve and shift factors. A loading frequency of 30 Hz was used to determine the representative dynamic moduli values at these temperatures. The loading frequency was selected from the analysis of the deviator stress pulse time at the corresponding temperature and vehicle speed. Using the determined  $|E^*|$  along with the corresponding temperature and the vehicle speed (40 mph), deviator and confining stresses were determined. Table E2c.1 summarizes the testing conditions. A deviator stress of 77 psi was found at all temperatures. The confining stress was found to decrease with the increase in temperature.

Table E2c.1 Flow Number Testing Conditions and Results.

Testing Temperature (°C)	Dynamic Modulus (psi)	Deviator Stress (psi)	Confining Stress (psi)	Replicates	Flow Number (3 Stage Approach)		Flow Number (Stepwise Increase)	
					Results	Average	Results	Average
40	258,000	77	42	1	No FN*	No FN*	19,900	19,250
				2	No FN*		18,600	
45	182,000	77	39	1	11,400	11,950	9,700	10,200
				2	12,500		10,700	
50	130,000	77	37	1	7,100	6,900	6,900	6,450
				2	6,700		6,000	
55	95,600	77	35	1	4,000	4,050	3,200	3,100
				2	4,100		3,000	

\* A flow number was not found

The FN test was conducted using the determined stress conditions at the four temperatures for 20,000 cycles. Two replicates were conducted at each temperature. The flow number was calculated using the three stage permanent deformation method (Zhou et al. 2004) and the stepwise increase method (Goh and You 2008).

The three-stage permanent deformation method consists of determining the primary, secondary, and tertiary deformation stages in the flow number test. The method consists of first determining the initial point of the secondary stage using the power-law model to fit the curve. Then, a linear regression model is used to obtain the flow number by evaluating the absolute ratio ( $R_d < 1\%$ ) of the model's intercept to the current maximum adjusted cumulative permanent deformation. Finally an exponential model is used to characterize the tertiary stage, and thus the FN is defined as the maximum number of cycles of the secondary stage with an  $R_d$  less than 1%.

The stepwise increase approach consists of obtaining the minimum point of the permanent strain divided by the loading cycle number ( $\epsilon_p/N$ ) versus the cycle number ( $N$ ). In addition, Goh et al. suggested minimizing the flow number calculation error by smoothing the cumulative permanent strain curve through a modification of the entire non-uniform discontinuous data points and shifting each point forward along the x-axis (cycle number) and not changing the strain level to provide a stepwise increasing trend. In other words, the FN is determined as the minimum point of  $\epsilon_p/N$  versus load cycle number using the new modified data points.

Table E2c.1 and figure E2c.2 summarize the FN test results. In general, comparable results for the FN were found between the two FN analysis methods. No flow number was found at 40°C when the test results were analyzed using the three-stage method. On the other hand the stepwise method showed an average FN of 19,250 at 40°C. A closer look at the data shows no initiation for the tertiary stage at 40°C and after 20,000 cycles.

For a temperature greater than 40°C, the mixture exhibited a tertiary stage. A linear increase in the FN was observed at temperatures greater than 40°C. The data indicate that the 45°C temperature is the mixture specific critical temperature under the loading testing conditions. The critical temperature is consistent with the field observation of the mix, thus indicating the general applicability of the procedures and generalized equations presented in the paper. Though this is a

promising result, additional investigations with different mixes from the WesTrack and other similar projects are needed for further validation.

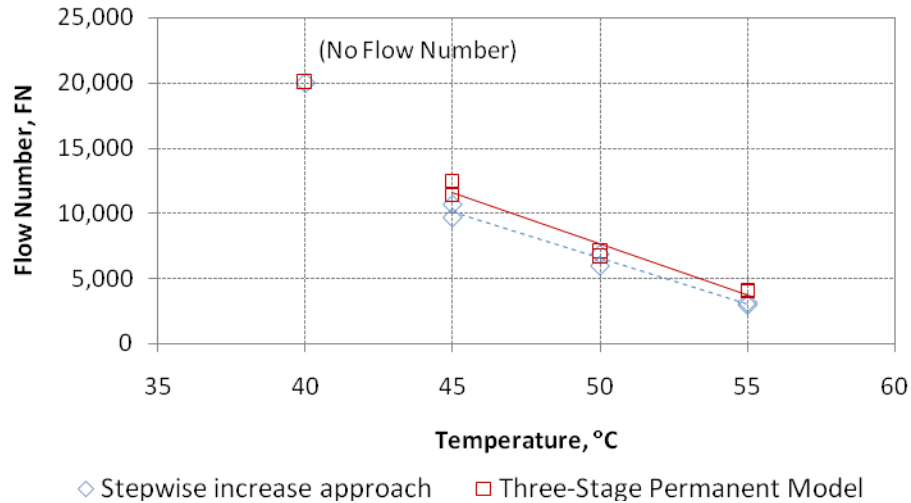


Figure E2c.2. Flow number test results

### Significant Problems, Issues and Potential Impact on Progress

The 3D-Move runs are taking more time than what was anticipated because of limitations in the number of computers that can be used. The extra time needed to complete all the 3D-Move runs described in the experimental plan of this work element will delay the original schedule.

### Work Planned Next Quarter

The calculations of the 3D-Move model will continue to cover all the loading conditions that were described in the experimental plan for this work element.

Evaluate additional mixtures from WesTrack project in the laboratory for permanent deformation characteristics under the repeated load triaxial test.

### Cited References

Zhou, F., Scoullion, T., Pellinen, and Sun, L., “Verification and Modeling of Three-stage Permanent Deformation Behavior of Asphalt Mixes”, *Journal of Transportation Engineering*, ASCE, 2004.

Goh, S. W., and You., Z.,”A Simple Method to Determine the Tertiary Flow in the Repeated Load Test”, *Proceedings of the Mid-Continent Transportation Research Forum*, University of Wisconsin-Madison, Madison, Wisconsin, 2008.

## **Work element E2d: Thermal Cracking Resistant Mixes for Intermountain States (UNR & UWM)**

### Work Done This Quarter

This work element is a joint project between University of Nevada Reno and University of Wisconsin–Madison. Efforts at UNR this quarter include parts of Subtask E2d-1, “Identify Field Sections,” and Subtask E2d-3, “Identify an Evaluation and Testing System.” These are described below.

The long-term oven aging process continued for the following binders as described in the experimental plan for this work element:

- Unmodified PG64-22
- Polymer modified PG64-28 (using the same PG64-22 crude source) that meets the specs of UT, NV, and CA.
- PG64-22 + 3% SBS
- PG64-22 + 10% hydrated lime
- PG64-22 + 20% hydrated lime

Additionally, the aged binders are under testing for their rheological properties.

The experimental plan to evaluate the impact of aggregate absorption and aggregate gradation on the long-term aging properties of the binder in the HMA mix is undergoing. HMA mixes are prepared and aged in the ovens. Current progress of the aggregate absorption portion is focused around obtaining the remainder of the aggregate sources (California and WesTrack), as well as developing mix designs for the materials on hand (Utah).

A meeting on the thermal cracking research was held at Granite Construction in Reno Nevada on April 20, 2009. The meeting was attended by Drs. Jon Epps, Adam Hand, Hussain Bahia, Charles Glover, Claine Petersen, Peter Sebaaly, Elie Hajj, and Mrs. Edward Cortez and Nathan Morina. The attendees evaluated the progress to date of work element E2d and the work plan for the coming years.

The existing TSRST equipment set-up at UNR was upgraded with a chiller and a control unit based on compressed air to replace the liquid nitrogen cooling agent. The TSRST is now capable of applying different cooling and warming rates during the test.

Efforts at UW–Madison this quarter include parts of Subtask E2d-2, “Identify the Causes of the Thermal Cracking,” and Subtask E2d-3, “Identify an Evaluation and Testing System.” These are described below.

The Single-Edge Notched Bending (SENB) data acquisition software is finished and working well. The research team tested the frame and discovered issues when testing very stiff materials that are similar to those encountered in the case of normal binder SENB testing; for example, the deformation speed imposed could not be maintained. Further investigation indicated that this problem is caused by several factors that synergistically prevented the deformation speed from being constant. These factors include:

- Compliance in motor coupling.
- Loss of torque due to friction in defective bearings.
- Friction between metal pieces that were not supposed to touch.
- Locking of the air bearing when subjected to side-loading.

The frame was sent to the machine shop for repairs and upgrades, which should be completed at the beginning of next quarter.

The data acquisition system and sensors are being upgraded to obtain better data from the glass transition temperature instrument. The upgraded version will allow the research team to perform three types of tests using this instrument: glass transition temperature measurements for binders, glass transition temperature measurements of mixes, and Thermal Stress Restrained Specimen Test (TSRST) measurements of mixes. The new dilatometric cells are being tested with different gasket materials to minimize or eliminate leaks.

### Significant Results

Under the absorption experiment, significant progress has been made in sample production and aging. All the  $E^*$  samples for the intermediate gradations (task E2d.3.b) for three sources (Nevada, Colorado, and Utah) have been prepared and are currently in the aging process (3, 6, and 9 months). The unaged  $E^*$  samples have been tested and are ready for the binder extraction process.

Progress has been made in the  $E^*$ -tension area, however final results and methods are not yet determined. It does appear at this point that full  $E^*$ -tension master curves will not be practical (without significant software upgrades). Therefore, the current plan includes limited frequencies (10 and 1 Hz). The 10 Hz testing is also expected to be run through a full cycle of fatigue testing, though the exact testing protocols have not been established.

Efforts have also been put forth to establish which mixture from which test sections at WesTrack will be included and replicated in this and the next task.

Under the gradation experiment, significant progress has been made in the area of sample preparation and  $E^*$  testing. Currently Nevada and Utah have both had intermediate gradation samples (4 and 11% air voids) that have been tested for  $E^*$  in compression. Similarly both have nearly all the samples in the aging process. The Utah Fine mixture has also been tested and is undergoing the required aging at 7% air voids. The Nevada fine mixture is in the finishing stages of the mix design, and will begin sample production shortly.

A sample of the revised testing matrix is included below in reference to the mixtures mentioned above.

Table E2d.1 Impact of Aggregate Absorption Experiment

Source	Gradation	Asphalt Binder	Film Thickness Levels	Air Voids
Nevada	Intermediate	64-22	2	7.0%
		64-28		
Colorado	Intermediate	64-22	2	7.0%
		64-28		
California	Intermediate	64-22	2	7.0%
		64-28		

Table E2d.2 Impact of Gradation Experiment

Source	Gradation	Asphalt Binder	Film Thickness (microns)	Air Voids (%)
Nevada	Intermediate	64-28	9	4.0, 7.0, 11.0
	Fine	64-28		7.0
Utah	Intermediate	64-28	9	4.0, 7.0, 11.0
	Fine	64-28		7.0
California	Intermediate	64-22	9	4.0, 7.0, 11.0
	Fine	64-22		7.0
WesTrack	Intermediate	64-22	--	4.0, 7.0, 11.0
	Fine	64-22	--	4.0, 7.0, 11.0

The SENB data acquisition software is developed and functional, as shown in figure E2d.1. The software allowed the research team to test functionality of the frame and motor combination. A preliminary report is provided in Appendix E2d.A.

Based on the testing results highlighted in Appendix E2d.A, the research team recommends:

- Replacing the current ball-screw drive with a finer one. The current ball-screw drive has a pitch of 3 mm/turn. Changing it with another drive that has a smaller pitch will allow for use of the motor at higher feedback loop.
- Conducting tests at slower deformation rate (suggesting 0.05 mm/s).
- Obtaining a better data acquisition card to minimize noise.

Figure E2d.2 shows examples of the results for glass transition temperature ( $T_g$ ) measurements with a new type of gasket for an aluminum disk. Results include both cooling and heating cycles.

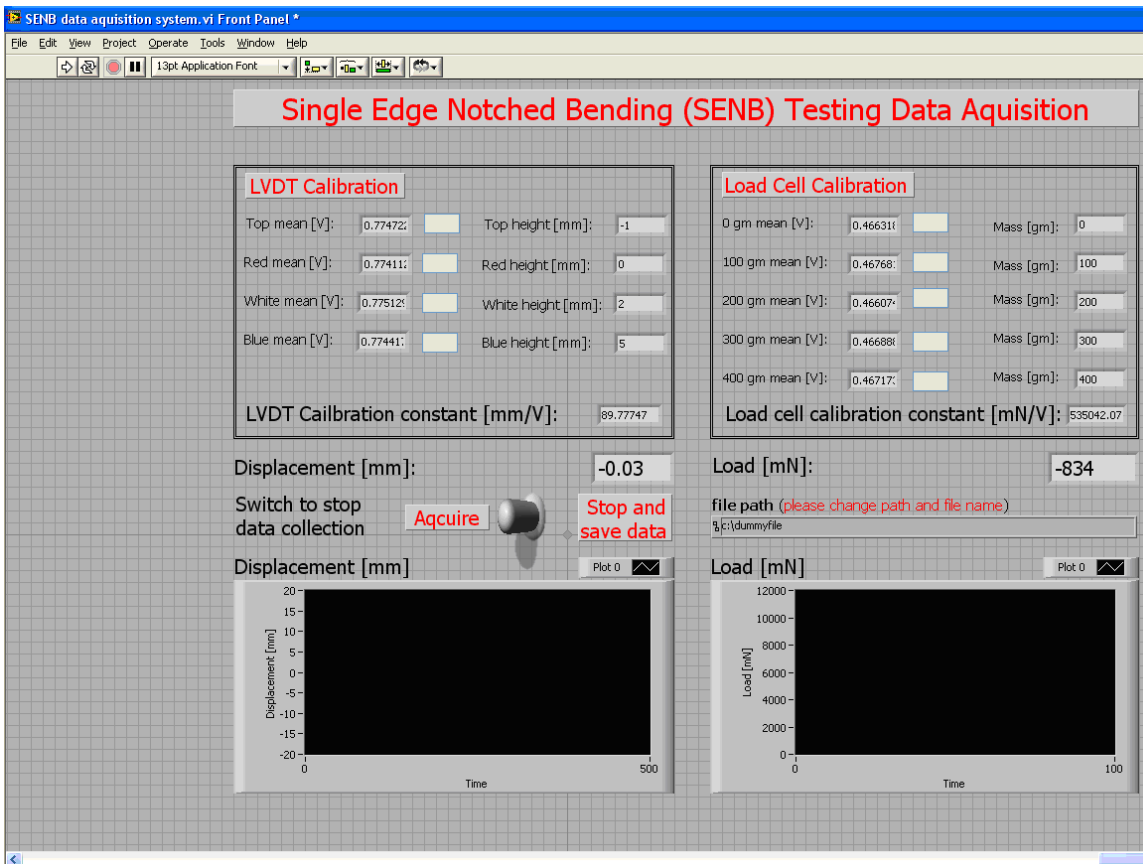


Figure E2d.1. Screen shot. Application window of the SENB data acquisition software.

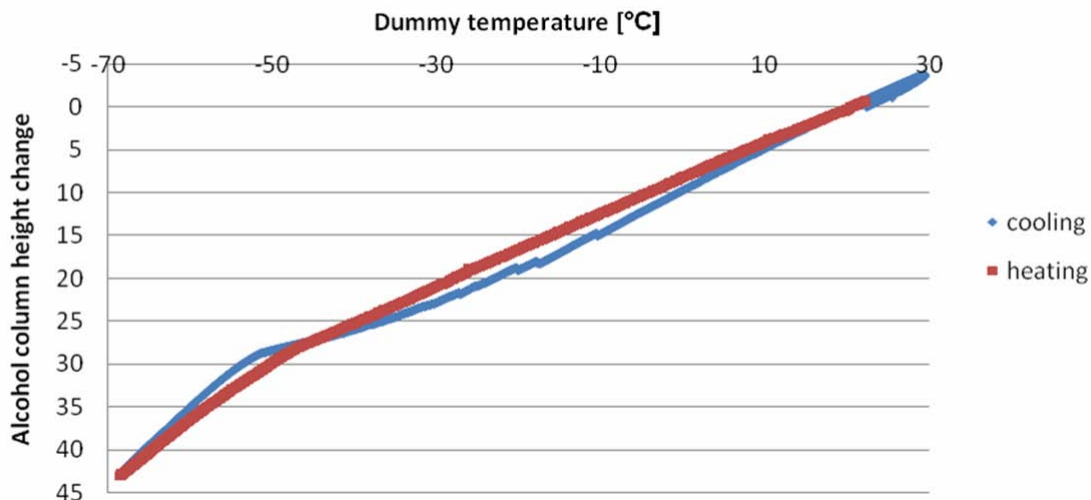


Figure E2d.2. Graph. Calibration curve of a dilatometric cell with aluminum dummy. Two aspects of figure E2d.2 are important to highlight:

- There are no alcohol leaks by the end of the test, as the column height goes back to the original starting level.
- The heating cycle provides more uniform data than the cooling cycle.

The research team proceeded with Buna gaskets based on information collected with the new cells and recommended running tests above  $-50\text{ }^{\circ}\text{C}$  to minimize interference with uniformity of volume change.

Results of an experiment conducted on a polypropylene sample were collected, as shown in figure E2d.3, to calibrate the new system. Polypropylene was chosen as a sample because of its known glass transition temperature ( $-13\text{ }^{\circ}\text{C}$ ), which is within the common range of glass transition temperatures for asphalts.

In figure E2d.3, the plot shows a glass transition temperature of approximately  $-12\text{ }^{\circ}\text{C}$ , which is a typical value for the glass transition of polypropylene. This result encourages the research team to believe this testing setup is suitable for the current experiment.

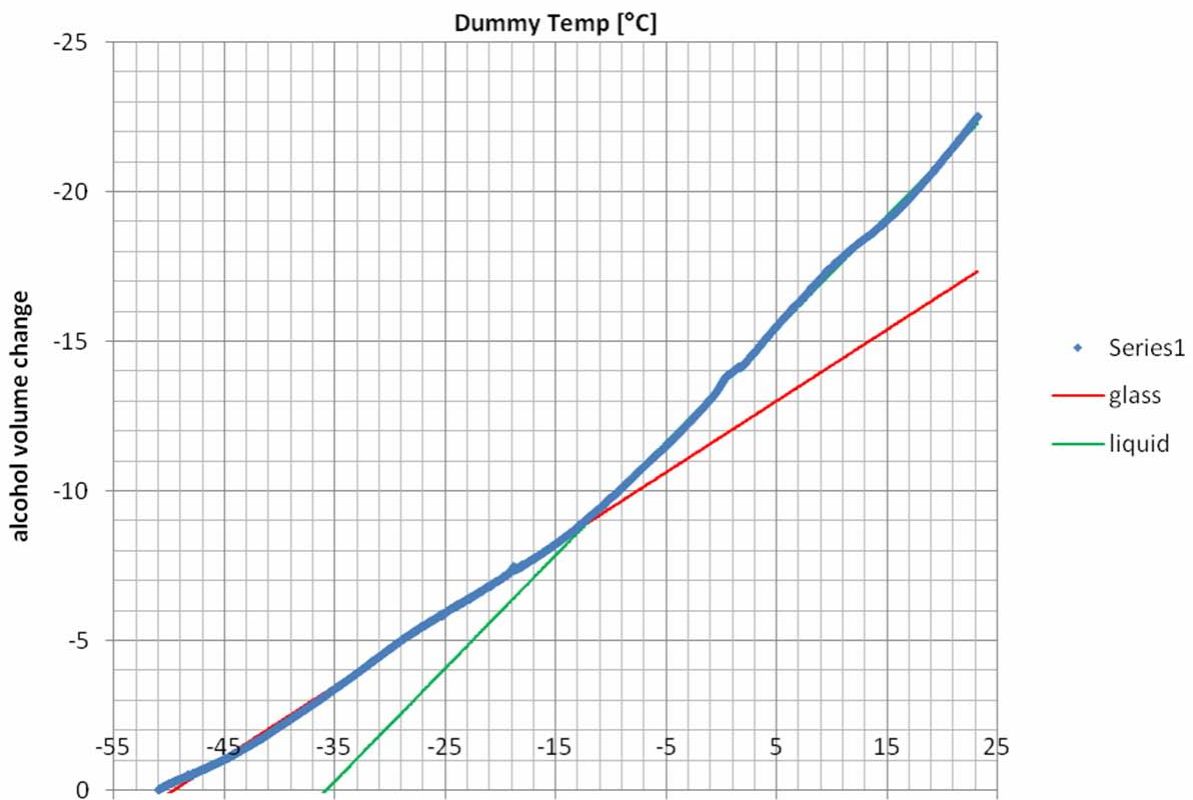


Figure E2d.3. Graph. Glass transition temperature measurement of a polypropylene sample.

### Significant Problems, Issues and Potential Impact on Progress

Results obtained thus far, though encouraging, are only preliminary results. Further testing is needed to prove that meaningful repeatable results can be obtained with the current system. The research team estimates that a fully updated measuring system will be determined early next quarter, which will allow the team to start testing binders and gathering sufficient data to assess the repeatability of test results.

### Work Planned Next Quarter

Continue the aging process of binders and continue measuring the properties of the aged binders.

Continue the work on the impact of aggregate absorption and gradation on the aging of the asphalt binder.

The research team will complete upgrade of the  $T_g$  testing system and start gathering data to prove the functionality of the instrument. The team will also continue collecting data for the carbonyl growth Fourier transform infrared spectroscopy (FTIR) measurements.

### **Work element E2e: Design Guidance for Fatigue and Rut Resistance Mixtures (AAT)**

#### Work Done This Quarter

Dr Christensen developed a detailed plan for further refinement of the continuum damage fatigue model. This plan includes temperatures, strain levels, loading cycles and rest periods for preliminary tests. Plans for final tests are also included, which will be refined on the basis of preliminary tests. As an aid in developing this work plan, a spreadsheet was developed which can be used to predict the response of any HMA under complex fatigue loading histories, once the continuum damage model parameters for the mixture have been determined.

#### Significant Results

A detailed plan, including test plans, for refinement of the continuum damage model was developed. A spreadsheet for prediction of the response of HMA mixtures under complex fatigue loading histories was developed.

### Significant Problems, Issues and Potential Impact on Progress

None.

### Work Planned Next Quarter

Final experimental designs will be prepared using the final core materials selected by the Asphalt Research Consortium. Preliminary continuum damage fatigue testing will commence.

Engineered Materials Year 3	Year 3 (4/2009-3/2010)												Team
	4	5	6	7	8	9	10	11	12	1	2	3	
<b>(1) High Performance Asphalt Materials</b>													
E1a: Analytical and Micro-mechanics Models for Mechanical behavior of mixtures													TAMU
E1a-1: Analytical Micromechanical Models of Binder Properties			JP			P			P			JP	
E1a-2: Analytical Micromechanical Models of Modified Mastic Systems			JP			P			P				
E1a-3: Analytical Models of Mechanical Properties of Asphalt Mixtures			JP			P			P			M&A	
E1a-4: Analytical Model of Asphalt Mixture Response and Damage			JP			P			P				
E1b: Binder Damage Resistance Characterization													UWM
E1b-1: Rutting of Asphalt Binders													
E1b-1-1: Literature review													
E1b-1-2: Select Materials & Develop Work Plan													
E1b-1-3: Conduct Testing					JP							P	
E1b-1-4: Analysis & Interpretation					JP							P	
E1b-1-5: Standard Testing Procedure and Recommendation for Specifications													
E1b-2: Feasibility of determining rheological and fracture properties of asphalt binders and mastics using simple indentation tests (modified title)													UWM
E1b-2i: Literature Review					D								
E1b-2ii: Proposed SuperPave testing modifications						P							
E1b-2iii: Preliminary testing and correlation of results												D	
E1b-2iv: Feasibility of using indentation tests for fracture and rheological properties					JP							P	
E2a: Comparison of Modification Techniques													UWM
E2a-1: Identify modification targets and material suppliers													
E2a-2: Test material properties					DP								P
E2a-3: Develop model to estimate level of modification needed and cost index													
E2a-4: Write asphalt modification guideline/report on modifier impact over binder properties													
E2c: Critically Designed HMA Mixtures													UNR
E2c-1: Identify the Critical Conditions					JP			D					F
E2c-2: Conduct Mixtures Evaluations													D
E2c-3: Develop a Simple Test													
E2c-4: Develop Standard Test Procedure													
E2c-5: Evaluate the Impact of Mix Characteristics													
E2d: Thermal Cracking Resistant Mixes for Intermountain States													UWM/UNR
E2d-1: Identify Field Sections													
E2d-2: Identify the Causes of the Thermal Cracking								F					
E2d-3: Identify an Evaluation and Testing System		DP	D			JP			DP		D		
E2d-4: Modeling and Validation of the Developed System													
E2d-5: Develop a Standard													
E2e: Design Guidance for Fatigue and Rut Resistance Mixtures													AAT
E2e-1: Identify Model Improvements													
E2e-2: Design and Execute Laboratory Testing Program												P	
E2e-3: Perform Engineering and Statistical Analysis to Refine Models													
E2e-4: Validate Refined Models													
E2e-5: Prepare Design Guidance													
<b>(2) Green Asphalt Materials</b>													
E2b: Design System for HMA Containing a High Percentage of RAP Material													UNR
E2b-1: Develop a System to Evaluate the Properties of RAP Materials		D				JP				F	P		
E2b-2: Compatibility of RAP and Virgin Binders												D	
E2b-3: Develop a Mix Design Procedure													
E2b-4: Impact of RAP Materials on Performance of Mixtures													
E2b-5: Field Trials													
E1c: Warm and Cold Mixes													UWM
E1c-1: Warm Mixes													
E1c-1i: Effects of Warm Mix Additives on Rheological Properties of Binders													
E1c-1ii: Effects of Warm Mix Additives on Mixture Workability and Stability													
E1c-1iii: Mixture Performance Testing						JP					P		DP
E1c-1iv: Develop Revised Mix Design Procedures													
E1c-1v: Field Evaluation of Mix Design Procedures and Performance Recommendations													
E1c-2: Improvement of Emulsions' Characterization and Mixture Design for Cold Bitumen Applications													UWM/UNR
E1c-2i: Review of Literature and Standards		D1						D3					
E1c-2ii: Creation of Advisory Group													
E1c-2iii: Identify Tests and Develop Experimental Plan		D1									D5		
E1c-2iv: Develop Material Library and Collect Materials													
E1c-2v: Conduct Testing Plan						JP		D4			P		
E1c-2vi: Develop Performance Selection Guidelines													
E1c-2vii: Validate Performance Guidelines						D2							
E1c-2viii: Develop CMA Mix Design Guidelines													
E1c-2ix: Develop CMA Performance Guidelines													

**Deliverable codes**  
D: Draft Report  
F: Final Report  
M&A: Model and algorithm  
SW: Software  
JP: Journal paper  
P: Presentation  
DP: Decision Point

**Deliverable Description**  
Report delivered to FHWA for 3 week review period.  
Final report delivered in compliance with FHWA publication standards  
Mathematical model and sample code  
Executable software, code and user manual  
Paper submitted to conference or journal  
Presentation for symposium, conference or other  
Time to make a decision on two parallel paths as to which is most promising to follow through

 Work planned  
 Work completed  
 Parallel topic

Engineered Materials Year 2 - 5	Year 2 (4/08-3/09)				Year 3 (4/09-3/10)				Year 4 (04/10-03/11)				Year 5 (04/11-03/12)				Team
	Q1	Q2	Q3	Q4	Q1	Q2	Q3	Q4	Q1	Q2	Q3	Q4	Q1	Q2	Q3	Q4	
<b>(1) High Performance Asphalt Materials</b>																	
E1a: Analytical and Micro-mechanics Models for Mechanical behavior of mixtures																	
E1a-1: Analytical Micromechanical Models of Binder Properties																	
E1a-2: Analytical Micromechanical Models of Modified Mastic Systems																	
E1a-3: Analytical Models of Mechanical Properties of Asphalt Mixtures																	
E1a-4: Analytical Model of Asphalt Mixture Response and Damage																	
E1b: Binder Damage Resistance Characterization																	
E1b-1: Rutting of Asphalt Binders																	
E1b-1-1: Literature review																	
E1b-1-2: Select Materials & Develop Work Plan																	
E1b-1-3: Conduct Testing																	
E1b-1-4: Analysis & Interpretation																	
E1b-1-5: Standard Testing Procedure and Recommendation for Specifications																	
E1b-2: Feasibility of Determining rheological and fracture properties of asphalt binders and mastics using simple indentation tests (modified title)																	
E1b-2i: Literature Review																	
E1b-2ii: Proposed SuperPave testing modifications or new testing devices																	
E1b-2iii: Preliminary testing and correlation of results																	
E1b-2iv: Feasibility of using indentation tests for fracture and rheological properties																	
E2a: Comparison of Modification Techniques																	
E2a-1: Identify modification targets and material suppliers																	
E2a-2: Test material properties																	
E2a-3: Develop model to estimate level of modification needed and cost index																	
E2a-4: Write asphalt modification guideline/report on modifier impact over binder properties																	
E2c: Critically Designed HMA Mixtures																	
E2c-1: Identify the Critical Conditions																	
E2c-2: Conduct Mixtures Evaluations																	
E2c-3: Develop a Simple Test																	
E2c-4: Develop Standard Test Procedure																	
E2c-5: Evaluate the Impact of Mix Characteristics																	
E2d: Thermal Cracking Resistant Mixes for Intermountain States																	
E2d-1: Identify Field Sections																	
E2d-2: Identify the Causes of the Thermal Cracking																	
E2d-3: Identify an Evaluation and Testing System																	
E2d-4: Modeling and Validation of the Developed System																	
E2d-5: Develop a Standard																	
E2e: Design Guidance for Fatigue and Rut Resistance Mixtures																	
E2e-1: Identify Model Improvements																	
E2e-2: Design and Execute Laboratory Testing Program																	
E2e-3: Perform Engineering and Statistical Analysis to Refine Models																	
E2e-4: Validate Refined Models																	
E2e-5: Prepare Design Guidance																	
<b>(2) Green Asphalt Materials</b>																	
E2b: Design System for HMA Containing a High Percentage of RAP Material																	
E2b-1: Develop a System to Evaluate the Properties of RAP Materials																	
E2b-2: Compatibility of RAP and Virgin Binders																	
E2b-3: Develop a Mix Design Procedure																	
E2b-4: Impact of RAP Materials on Performance of Mixtures																	
E2b-5: Field Trials																	
E1c: Warm and Cold Mixes																	
E1c-1: Warm Mixes																	
E1c-1i: Effects of Warm Mix Additives on Rheological Properties of Binders																	
E1c-1ii: Effects of Warm Mix Additives on Mixture Workability and Stability																	
E1c-1iii: Mixture Performance Testing																	
E1c-1iv: Develop Revised Mix Design Procedures																	
E1c-1v: Field Evaluation of Mix Design Procedures and Performance Recommendations																	
E1c-2: Improvement of Emulsions' Characterization and Mixture Design for Cold Bitumen Applications																	
E1c-2i: Review of Literature and Standards																	
E1c-2ii: Creation of Advisory Group																	
E1c-2iii: Identify Tests and Develop Experimental Plan																	
E1c-2iv: Develop Material Library and Collect Materials																	
E1c-2v: Conduct Testing Plan																	
E1c-2vi: Develop Performance Selection Guidelines																	
E1c-2vii: Validate Guidelines																	
E1c-2viii: Develop CMA Mix Design Procedure																	
E1c-2ix: Develop CMA Performance Guidelines																	

**Deliverable codes**  
D: Draft Report  
F: Final Report  
M&A: Model and algorithm  
SW: Software  
JP: Journal paper  
P: Presentation  
DP: Decision Point

**Deliverable Description**  
Report delivered to FHWA for 3 week review period.  
Final report delivered in compliance with FHWA publication standards  
Mathematical model and sample code  
Executable software, code and user manual  
Paper submitted to conference or journal  
Presentation for symposium, conference or other  
Time to make a decision on two parallel paths as to which is most promising to follow through



## **PROGRAM AREA: VEHICLE-PAVEMENT INTERACTION**

### **CATEGORY VP1: WORKSHOP**

#### **Work element VP1a: Workshop on Super-Single Tires**

This work element is complete.

### **CATEGORY VP2: DESIGN GUIDANCE**

#### **Work element VP2a: Mixture Design to Enhance Safety and Reduce Noise of HMA (UWM)**

##### Work Done This Quarter

Work focused on measuring the surface macrotexture and microtexture (friction properties) of laboratory-prepared gyratory specimens using the sand-patch method and the British Pendulum Skid Resistance Tester, respectively. Measurements were conducted for more than 100 samples. The samples covered a wide range of mix variables, such as aggregate gradation, aggregate type, design equivalent single axle loads (ESALs), compaction pressure and compaction temperature.

Significant effort was also put toward investigating the use of an abrasive rotating disk to simulate the polishing of asphalt pavements by traffic. To achieve this, one gyratory-compacted sample was polished for 15 minutes at different time increments.

##### Significant Results

###### *Macrotexture and Microtexture Measurements*

Surface macrotexture properties of asphalt samples were measured following the ASTM E965 standard (ASTM 2006) to determine the mean texture depth (MTD) in mm. The British Pendulum Skid Resistance Tester was used to determine the friction properties of asphalt mixes by measuring the British Pendulum Number (BPN) in accordance with the ASTM E303 standard. The tested samples covered:

- Three types of aggregates: limestone, gravel and granite.
- Three levels of design ESALs: E-1, E-2 and E-3.
- Two compaction pressures: 300 and 600 kPa.
- Three compaction temperatures: 60 °C, 90 °C and 120 °C.
- A wide range of dense-graded mix designs.

Figure VP2a.1 shows the gradation curves for the limestone and gravel samples; the gradation curves for the granite samples are shown in figure VP2a.2. The gradations ranged from coarse to fine for all three aggregates. However, the granite samples had a more controlled aggregate gradation.

Figure VP2a.3 shows a scatter plot of the MTD and BPN measurements. The figure shows that there is no direct relation between the two measurements. This is expected as the BPN represents a measure of the surface microtexture, while the MTD is more of a surface macrotexture indicator. The plot also shows that each of the three aggregates exhibited a wide range of both BPN and MTD values. This variation is expected as each sample had different mix variables such as gradation and compaction temperature.

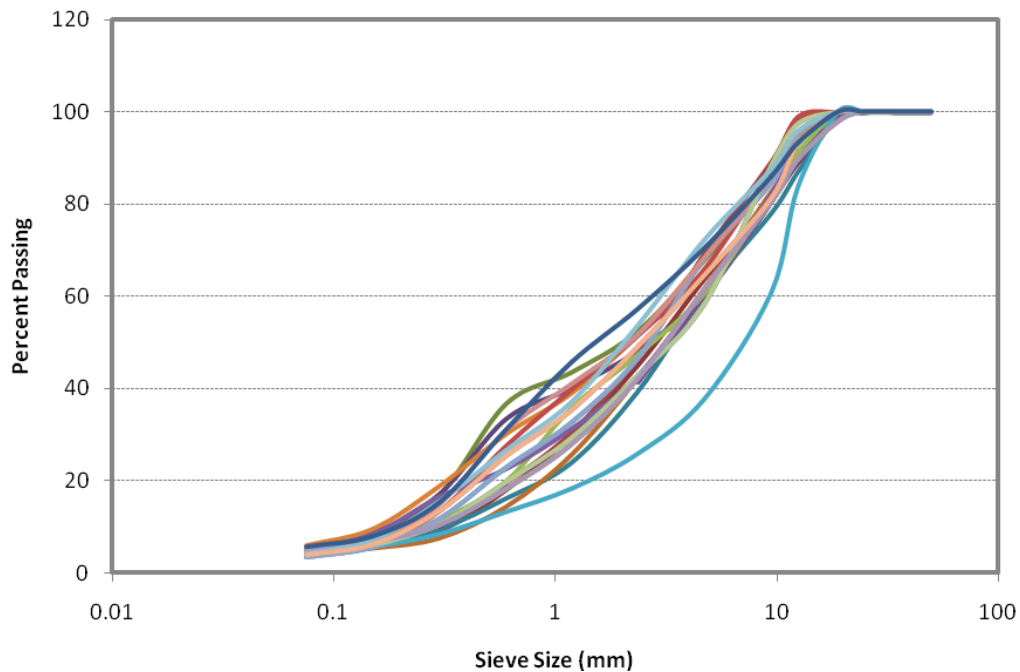


Figure VP2a.1. Graph. Aggregate gradation for limestone and gravel samples.

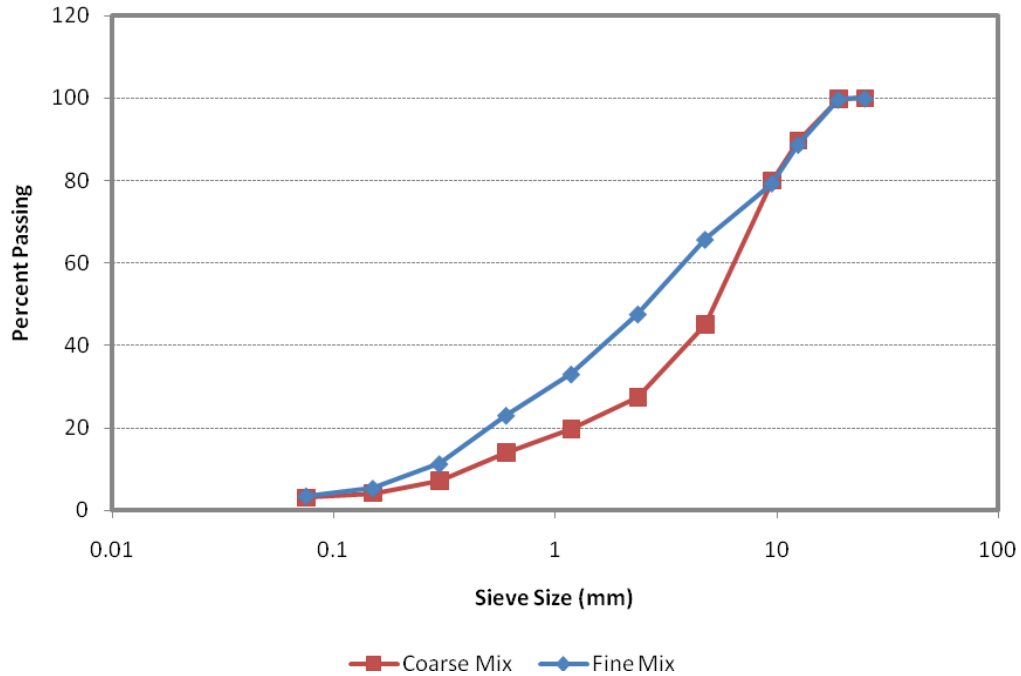


Figure VP2a.2. Graph. Aggregate gradation for granite samples.

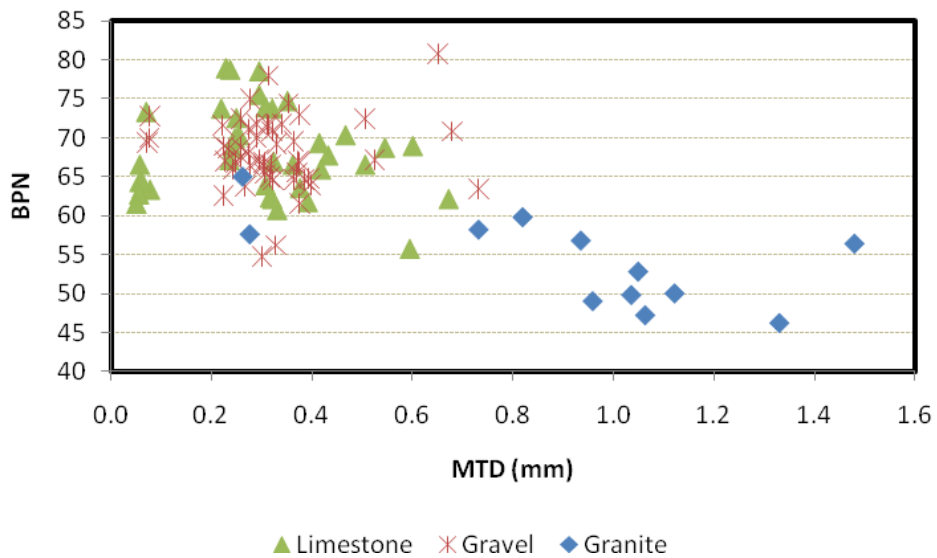


Figure VP2a.3. Graph. Scatter plot of the BPN measurements versus MTD.

The more controlled gradations of the granite samples allowed for classification into two categories: fine mix and coarse mix. Figure VP2a.4 shows a bar chart of the MTD measurements for the granite samples. It can be seen that the coarse mix had higher MTD values when compared to the fine mix case. However, a more thorough analysis will be conducted in subsequent quarters to relate BPN and MTD measurements to the different mix variables.

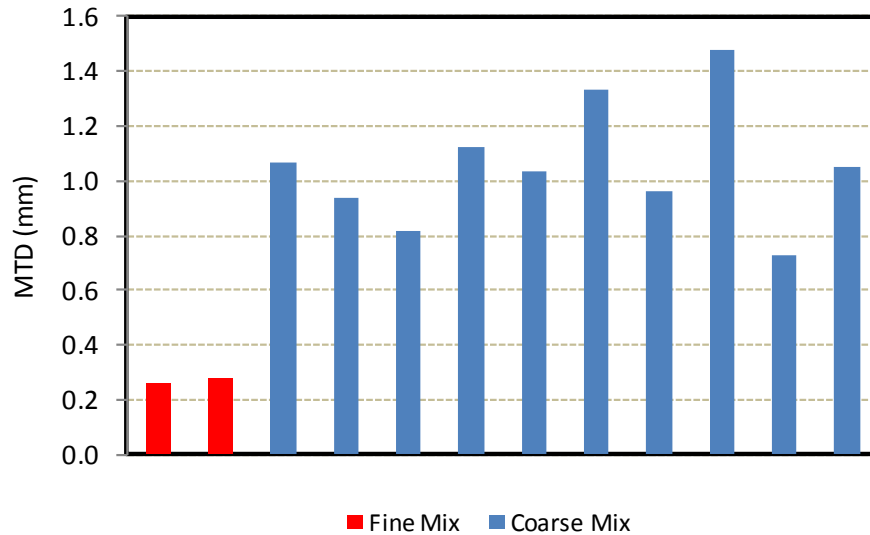


Figure VP2a.4. Graph. MTD measurements for the granite mix samples.

### *Laboratory Polishing of Asphalt Mixes*

Using laboratory-prepared gyratory specimens, the research team used an abrasive rotating disk to abrade/polish the sample surface to simulate the polishing of asphalt pavements by traffic. Polishing time, a crucial element of such a procedure, should be enough to achieve terminal texture condition. The research team decided to polish three samples representing high, medium and low values of BPN. Each sample will be polished for 15 minutes, with the polishing process stopped every 30 seconds for the first 9 minutes, followed by stops at the 12-minute mark and, finally, the 15-minute mark. At each stop, MTD and BPN will be measured. These measurements will capture polishing behavior as a function of time and allow the research team to determine the required polishing time.

Initial testing was completed for one sample. Figure VP2a.5 shows the BPN values at different polishing intervals, with an exponential function fitted to the data points. For this sample, polishing for about 8 minutes achieved the surface terminal texture condition. The other two samples will be tested during the coming quarter to finalize selection of the required polishing time.

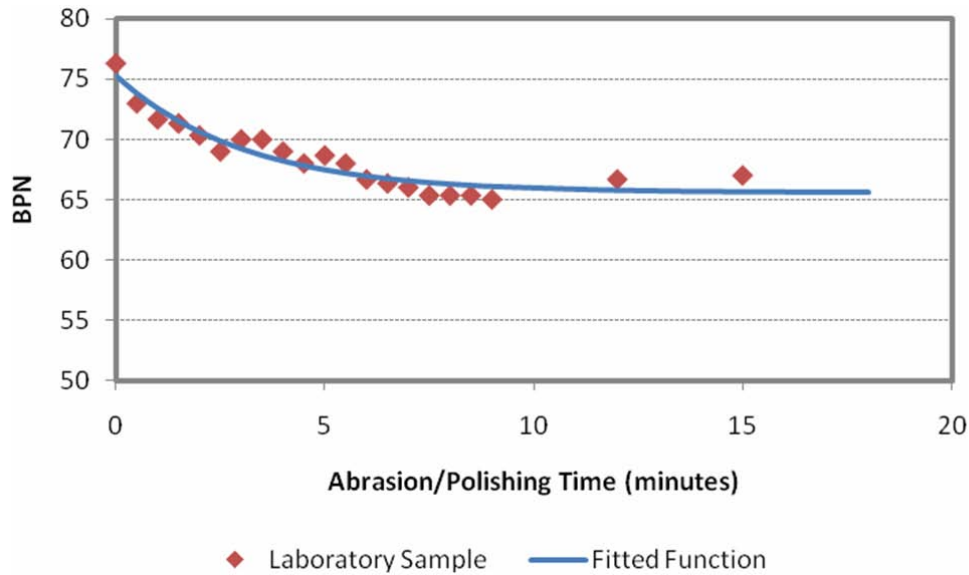


Figure VP2a.5. Graph. BPN measurements at different polishing intervals.

### Significant Problems, Issues and Potential Impact on Progress

More evaluation of the waveguide sound absorption device developed at the University of Wisconsin–Madison is required, with the key point being calibration of the device. The research team is in contact with researchers at the National Center for Asphalt Technology (NCAT) and the University of Kentucky. Both institutes have experience with measuring sound absorption using a similar device. The research team is also reviewing the ISO standard to check the current device’s compliance with the standard.

Contact with Professor Massimo Losa of the University of Pisa, Italy, has been established. Professor Losa is leading a large-scale project funded by the European Union on mapping noise and proposing mixture designs to reduce noise and increase friction. Professor Losa, who visited UW–Madison and delivered a lecture on this subject, will be invited to participate in the project on a cost-share basis to help resolve some of the problems encountered. An outline of a plan for collaboration was developed during his visit to UW–Madison. Samples will be shipped to Professor Losa’s lab in the near future for testing and evaluation.

### Work Planned Next Quarter

Next quarter, the research team will continue macrotexture and microtexture evaluation of laboratory-prepared gyratory specimens. New samples will be tested to achieve balance in covering the different mix variables. This will be followed by a parametric/statistical analysis to identify the relationship between asphalt friction properties and the different mix variables. The research team will also work on finalizing the procedure for the abrasion/polishing of asphalt mix specimens using a circular rotating abrasion device. Two additional samples will be tested in a manner similar to the sample tested in this quarter.

Significant effort will be focused on calibrating and collecting data using the waveguide device, as well as the design and development of laser-based testing equipment for measuring the profile of asphalt mix specimens.

### Cited References

ASTM, 2006 (reapproved), ASTM E965-06 Standard Test Method for Measuring Pavement Macrottexture Depth Using a Volumetric Technique. American Society of Testing and Materials. West Conshohocken, PA.

ASTM, ASTM E303 Standard Test Method for Measuring Surface Frictional Properties Using the British Pendulum Tester. American Society of Testing and Materials. West Conshohocken, PA.

ISO, ISO 13472-2 Acoustics – Measurement of Sound Absorption Properties of Road Surfaces In Situ – Part 2: Spot Method for Reflective Surfaces. International Organization for Standardization. Geneva, Switzerland.

## **CATEGORY VP3: MODELING**

### ***Work element VP3a: Pavement Response Model to Dynamic Loads (UNR Year 2 start)***

#### Work Done This Quarter

The UNR team continued the work on the 3D-Move model to make it a menu-driven software to integrate the measured non-uniform contact stress distributions in the 3D-Move model.

#### Significant Results

One of the important inputs to 3D-Move is the pavement contact stress distribution. It is customary to assume simpler contact stress distributions, for example, circular or elliptical loaded areas with uniform vertical stress. However, the pavement contact stress distributions are non-uniform and more complex. Past studies have revealed that it is important to include the non-uniform stress distributions as the simpler distributions are neither realistic nor conservative.

There have been many studies world-wide (e.g. South Africa, USA, and Japan) where substantial efforts have been expended on measuring the complex tire-pavement interface stress distributions for a number of tires under a variety of loading conditions (Himkeo et al. 1997; de Beer and Fisher, 1997; Sime and Ashmore 1999). Two sets of data, which are the work of de Beer and Fisher (1997) and of Sime and Ashmore (1999) are available in soft copy format and therefore have been the focus here.

De Beer and his co-workers from South African Institute of Roads developed a measurement system called Vehicle-Road Surface Pressure Transducer Array (VRSPTA), which is capable of

measuring vertical ( $\sigma_{zz}$ ), longitudinal shear ( $\tau_{xz}$ ) and transverse shear ( $\tau_{yz}$ ) stresses at a creep vehicle speed of 0.7 mph. A variety of tire types that included single and wide base tires under a tire pressure range of 220 – 1000 kPa and a tire load range of 26 – 106 kN have been reported by de Beer and Fisher (1997). Both highway and also aircraft tires have been considered. There were as many as 159 sets of contact stress distributions of  $\sigma_{zz}$ ,  $\tau_{xz}$ , and  $\tau_{yz}$  are available in the VRSPTA database. On the other hand, the second set of data comes from the Kistler MODULAS Quartz Sensor Array device. Though the Kistler device measures only the vertical stress, this database includes stresses measured at vehicle speeds of up to 40 mph. There are as many as 192 sets of  $\sigma_{zz}$  stress distributions, covering both single and wide base tires with tire pressure range of 420 – 1000 kPa and the tire load range of 4.5 - 62 kN.

These two databases are quite extensive and the selection of the appropriate stress distribution for input to 3D-Move is not straightforward. In many cases only a limited tire pressures and tire loads were covered. For example, VRSPTA reports only one set of data for Goodyear G178/65R22.5 wide base tire and this case is for a tire pressure of 830 kPa and a tire load of 48 kN. On the other hand, it lists as many as seven sets of data for Goodyear 425/65R22.5 wide base tire under 700 kPa tire pressure and the loads varied between 26 and 106 kN. A similar uneven database attributes issues exist with the Kistler device also.

The nature of these databases required an innovative solution to zero-in on to the representative contact stress distribution. The solution adopted in the software developments is illustrated using menus presented below. Figure VP3a.1 shows a menu in which the top left corner shows all the types tires for which the datasets are available. Once a tire type has been selected (shown by highlight on top left corner selection or list box), the measuring devices that have been used for this tire type is subsequently displayed on the top right selection box. Once a selection from this box is taken, the middle box will display the available tire pressures. Subsequently, the bottom decision boxes come to live and the user is prompted to make his/her choices here. The displays within these selection boxes depend on the selection made in the previous boxes. Say for example, in the case with VRSPTA database, only one speed (0.7 mph) will be displayed inside the bottom left selection box, as the VRSPTA database is available only at this speed.

An intermediate tire load and the pavement-tire interface friction can also be considered. A linear interpolation is used for the intermediate tire load and the interpolation is allowed only within the range for which the data is available. For example, Fig. VP3a.2 shows the specification of an intermediate tire load of 28 kN, and in this case the linear interpolation is undertaken between the tire loads 25 and 31 kN, as data are available for these load levels. It may be seen from the illustration that a “dynamic” menu displays, which depend on the selection made previously, are needed because of the nature of the database.

Figure VP3a.3 displays the menu for the selection of axle configuration, once the tire type and contact pressure distributions have been selected. This menu displays at the top the type and other characteristics of the tire that have been selected thus far and at the bottom prompts for axle configuration selections. Many choices, varying from a single tire to tridem axle dual tire configuration can be specified using the axle spacing parameters (S1, L1, and L2) shown.

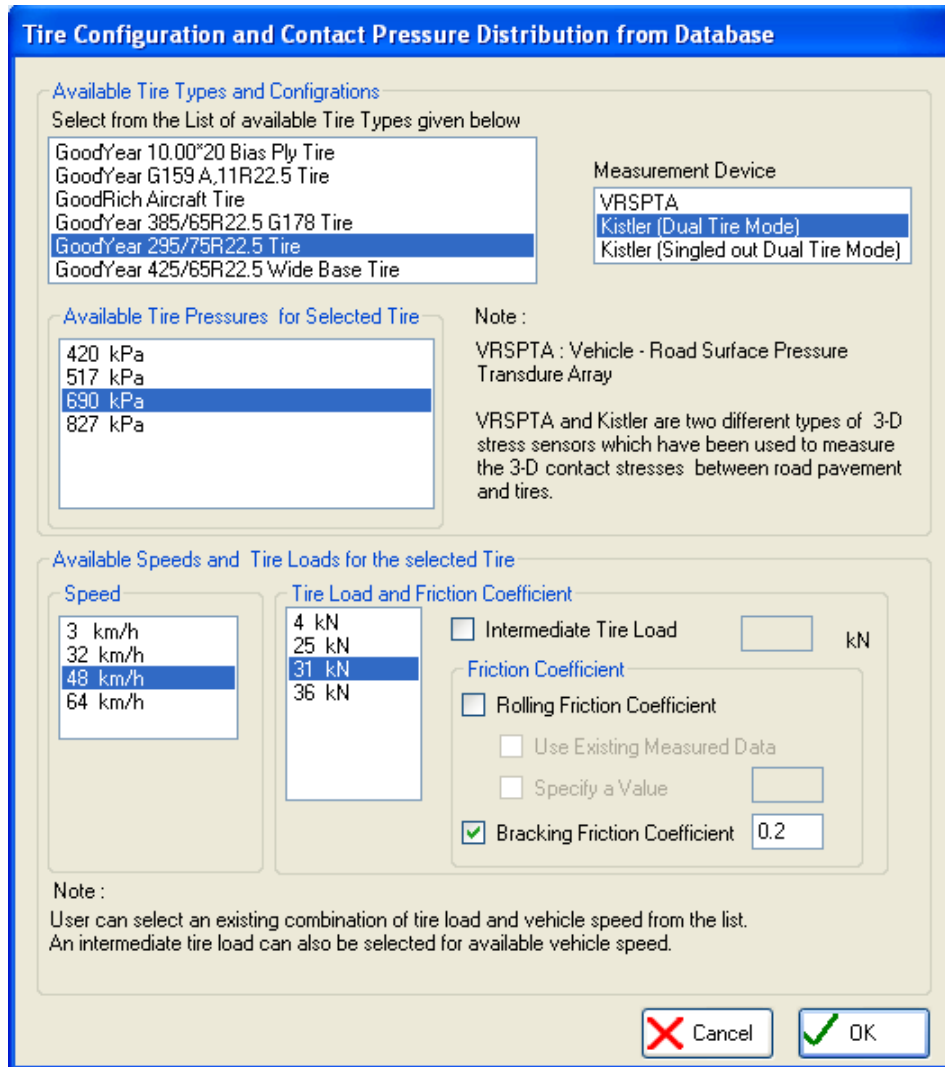


Figure VP3a.1. Menu showing sequence of selections to be made in identifying the contact pressure distribution from VRSPATA and Kistler databases.

**Tire Configuration and Contact Pressure Distribution from Database**

Available Tire Types and Configurations  
 Select from the List of available Tire Types given below

GoodYear 10.00\*20 Bias Ply Tire  
 GoodYear G159 A,11R22.5 Tire  
 GoodRich Aircraft Tire  
 GoodYear 385/65R22.5 G178 Tire  
**GoodYear 295/75R22.5 Tire**  
 GoodYear 425/65R22.5 Wide Base Tire

Measurement Device  
 VRSPTA  
**Kistler (Dual Tire Mode)**  
 Kistler (Singled out Dual Tire Mode)

Available Tire Pressures for Selected Tire  
 420 kPa  
 517 kPa  
**630 kPa**  
 827 kPa

Note :  
 VRSPTA : Vehicle - Road Surface Pressure Transdure Array  
 VRSPTA and Kistler are two different types of 3-D stress sensors which have been used to measure the 3-D contact stresses between road pavement and tires.

Available Speeds and Tire Loads for the selected Tire

Speed  
 3 km/h  
 32 km/h  
**48 km/h**  
 64 km/h

Tire Load and Friction Coefficient  
 4 kN  
 25 kN  
 31 kN  
 36 kN

Intermediate Tire Load 28 kN

Friction Coefficient  
 Rolling Friction Coefficient  
 Use Existing Measured Data  
 Specify a Value 0.1  
 Bracking Friction Coefficient

Note :  
 User can select an existing combination of tire load and vehicle speed from the list.  
 An intermediate tire load can also be selected for available vehicle speed.

Cancel OK

Figure VP3a.2. Interpolation for an intermediate tire load.

**User-Selected Tire Configuration and Contact Pressure Distribution from Database**

Reference Title for Axle

**Selected Tire Type and Tire Pressure**

Type of Tire <input type="text" value="Goodyear 295/75R22.5 Tire"/>	Measuring Device <input type="text" value="Kistler (Dual Tire Mode)"/>
Tire Pressure <input type="text" value="690 kPa"/>	Speed <input type="text" value="48 km/h"/>
Tire Load <input type="text" value="31 kN"/>	Coefficient of Bracking Friction <input type="text" value="0.2"/>

**Axle Spacing**

L1	<input type="text" value="1.22"/>	m	
L2	<input type="text" value="1.22"/>	m	
S1	<input type="text" value="0.37"/>	m	

**Note :**

1. As many as , six Single Loaded Areas can be specified
2. A Single Tire can be represented by using  $S1 = L1 = L2 = 0$
3. A Single Axle Dual Tire can be represented by  $L1 = L2 = 0$  and  $S1 \neq 0$
4. A Tandem Axle Dual Tire can be represented by  $L2 = 0$  and  $S1 \neq 0, L1 \neq 0$

Figure VP3a.3. Selection of axle configuration.

### Significant Problems, Issues and Potential Impact on Progress

Michelin will most likely not share their measured non-uniform contact stress data with the pavement design community.

### Work Planned Next Quarter

Continue working on the 3D-Move model to make it a menu-driven software.

### Cited References

De Beer, M., and C. Fisher, "Contact Stresses of Pneumatic Tires Measured with Vehicle-Road Surface Pressure Transducer Array (VRSPTA) System for University of California (UCB) and the Nevada Automotive Test Center (NATC), June 1991.

Sime, M., and S.C. Ashmore, "Tire-Pavement Interface Pressure Patterns," Final Report DTFH61-96-C-00053, Federal Highway Administration, Washington, D.C., (1999).

Himkeo, K., T. Ikeda, T. Kamijima, and T. Abe, "Distribution of Tire Contact Pressure of Vehicles and its Influence on Pavement Distress," 8<sup>th</sup> Int. Conf. Asphalt Pavements, Vol. I, Seattle, Washington, pp. 129-139.

Vehicle-Pavement Interaction Year 3	Year 3 (4/2009-3/2010)												Team	
	4	5	6	7	8	9	10	11	12	1	2	3		
<b>(1) Workshop</b>														
VP1a: Workshop on Super-Single Tires														UNR
<b>(2) Design Guidance</b>														
VP2a: Mixture Design to Enhance Safety and Reduce Noise of HMA														UWM
VP2a-1: Evaluate common physical and mechanical properties of asphalt mixtures with enhanced frictional skid characteristics														
VP2a-2: Evaluate pavement macro- and micro-textures and their relation to tire and pavement noise-generation mechanisms														
VP2a-3: Develop a laboratory testing protocol for the rapid evaluation of the macro and micro-texture of pavements														
VP2a-4: Run parametric studies on tire-pavement noise and skid response					JP		M&A						D	
VP2a-5: Establish collaboration with established national laboratories specialized in transportation noise measurements. Gather expertise on measurements and analysis														
VP2a-6: Model and correlate acoustic response of tested tire-pavement systems														
VP2a-7: Proposed optimal guideline for design to include noise reduction, durability, safety and costs														
<b>(3) Pavement Response Model Based on Dynamic Analyses</b>														
VP3a: Pavement Response Model to Dynamic Loads														UNR
VP3a-1: Dynamic Loads														
VP3a-2: Stress Distribution at the Tire-Pavement Interface														
VP3a-3: Pavement Response Model							SW, v, β							
VP3a-4: Overall Model														

**Deliverable codes**

- D: Draft Report
- F: Final Report
- M&A: Model and algorithm
- SW: Software
- JP: Journal paper
- P: Presentation
- DP: Decision Point

**Deliverable Description**

- Report delivered to FHWA for 3 week review period.
- Final report delivered in compliance with FHWA publication standards
- Mathematical model and sample code
- Executable software, code and user manual
- Paper submitted to conference or journal
- Presentation for symposium, conference or other
- Time to make a decision on two parallel paths as to which is most promising to follow through

 Work planned  
 Work completed  
 Parallel topic

Vehicle-Pavement Interaction Years 2 - 5	Year 2 (4/08-3/09)				Year 3 (4/09-3/10)				Year 4 (04/10-03/11)				Year 5 (04/11-03/12)				Team
	Q1	Q2	Q3	Q4	Q1	Q2	Q3	Q4	Q1	Q2	Q3	Q4	Q1	Q2	Q3	Q4	
<b>(1) Workshop</b>																	
VP1a: Workshop on Super-Single Tires																	UNR
<b>(2) Design Guidance</b>																	
VP2a: Mixture Design to Enhance Safety and Reduce Noise of HMA																	UWM
VP2a-1: Evaluate common physical and mechanical properties of asphalt mixtures with enhanced frictional skid characteristics				DP													
VP2a-2: Evaluate pavement macro- and micro-textures and their relation to tire and pavement noise-generation mechanisms				DP													
VP2a-3: Develop a laboratory testing protocol for the rapid evaluation of the macro and micro-texture of pavements		M&A		P													
VP2a-4: Run parametric studies on tire-pavement noise and skid response			JP			JP, M&A	D										
VP2a-5: Establish collaboration with established national laboratories specialized in transportation noise measurements. Gather expertise on measurements and analysis																	
VP2a-6: Model and correlate acoustic response of tested tire-pavement systems									JP	D	F						
VP2a-7: Proposed optimal guideline for design to include noise reduction, durability, safety and costs										D	P, F						
<b>(3) Pavement Response Model Based on Dynamic Analyses</b>																	
VP3a: Pavement Response Model to Dynamic Loads																	UNR
VP3a-1: Dynamic Loads			JP							D, F	JP						
VP3a-2: Stress Distribution at the Tire-Pavement Interface										D, F	JP						
VP3a-3: Pavement Response Model						SW, v. β							SW, JP				
VP3a-4: Overall Model													D	F			

**Deliverable codes**

D: Draft Report  
F: Final Report  
M&A: Model and algorithm  
SW: Software  
JP: Journal paper  
P: Presentation  
DP: Decision Point

**Deliverable Description**

Report delivered to FHWA for 3 week review period.  
Final report delivered in compliance with FHWA publication standards  
Mathematical model and sample code  
Executable software, code and user manual  
Paper submitted to conference or journal  
Presentation for symposium, conference or other  
Time to make a decision on two parallel paths as to which is most promising to follow through





## **PROGRAM AREA: VALIDATION**

### **CATEGORY V1: FIELD VALIDATION**

#### **Work element V1a: Use and Monitoring of Warm Mix Asphalt Sections (Year 1 start)**

##### Work Done This Quarter

No work planned.

##### Significant Results

Warm mix sections were placed at the East Entrance to Yellowstone National Park in the Fall of 2007.

##### Significant Problems, Issues and Potential Impact on Progress

None.

##### Work Planned Next Quarter

It is planned to monitor the warm mix sections at the east gate of Yellowstone National Park in the next quarter.

#### **Work element V1b: Construction and Monitoring of additional Comparative Pavement Validation sites (Year 1 start)**

##### Work Done This Quarter

A pre-construction distress survey was conducted on June 16 and 17 on ten areas of the Manitoba PTH 14 highway project where three warm mix additives, a lower temperature compaction hot mix section, and a control hot mix section will be constructed. The pre-construction survey identified two 500 foot sections in each of the five different materials that will be used for future performance monitoring after milling and construction is completed. The areas were accurately located with survey stationing and GPS so that the effect of any previous distress on the new pavements can be analyzed.

A visual survey was also conducted on the new pavement placed at the PTH 8 RAP project in Manitoba. There was no distress noted in the pavement placed in the Fall of 2008. The ARC RAP sections will be placed over the pavement placed last Fall.

##### Significant Results

None.

Significant Problems, Issues and Potential Impact on Progress

None.

Work Planned Next Quarter

It is planned to obtain samples of construction materials at the Manitoba PTH 8 (RAP) and PTH 14 (Warm mix) sections in the next quarter if construction actually occurs.

**CATEGORY V2: ACCELERATED PAVEMENT TESTING**

**Work element V2a: Accelerated Pavement Testing including Scale Model Load Simulation on Small Test Track (Later start)**

Work Done This Quarter

No activity this quarter.

Significant Results

None.

Significant Problems, Issues and Potential Impact on Progress

None.

Work Planned Next Quarter

No accelerated (field) testing is planned.

**Work element V2b: Construction of Validation Sections at the Pecos Research & Testing Center (Later start)**

This work element is included to indicate that this may be a possibility for accelerated pavement testing for ARC research because it is a facility in the TAMU system.

## **CATEGORY V3: R&D VALIDATION**

### **Work element V3a: Continual Assessment of Specifications (UWM)**

#### Work Done This Quarter

Work focused on seeking cooperation with the Western Cooperative Testing Group (WCTG) and the Rocky Mountain Asphalt User/Producer Group (RMAUPG). Cooperation focuses on testing asphalt binders used in building pavements during this construction season. The goal of this cooperation is to build a database that can include binder testing results and pavement performance indicators. The binder testing battery includes conventional Superpave and PG Plus testing. PG Plus tests will be included in such a manner that evaluating the PG Plus tests can be done with respect to pavement performance. At this time, cooperation with WCTG and RMAUPG is restricted to high-temperature performance tests.

The University of Wisconsin–Madison will receive binders that will be used in pavement monitoring and conduct additional PG Plus tests outside the cooperation with WCTG and RMAUPG to evaluate specification test parameters other than high temperatures. These tests include intermediate- and low-temperature tests that are discussed in the next section of this report.

As noted in the last quarterly report, a limited study is under way to evaluate the Multiple Stress Creep and Recovery (MSCR) outputs (percent recovery and nonrecoverable compliance) with respect to testing binders and mastics. Two binders were selected: one modified with an elastomer and the other with a plastomer. Two fillers were selected: hydrated lime and granite. Testing was conducted for the binders, mastics and mixture. It is important to note that this study overlaps with subtask E1b-1. Results to date on the E1b-1 subtask are included in the quarterly report on the E1b-1 subtask.

Work also continued in connection with development of the Single-Edge Notched Bending (SENB) test. The work focused on evaluating the testing frame with respect to compliance issues. The feedback between the controlling software and the loading motor was examined to define the optimum configuration without affecting the loading capacity of the loading frame. To achieve this, two types of materials were selected: a recycled asphalt pavement (RAP) mortar beam of dimensions similar to that of the Bending Beam Rheometer (BBR) beam and a mastic SENB specimen. These two samples were selected to have a deformable specimen (RAP mortar) and a stiff specimen (mastic). Figure V3a.1 shows the standard dimensions for the SENB specimen.

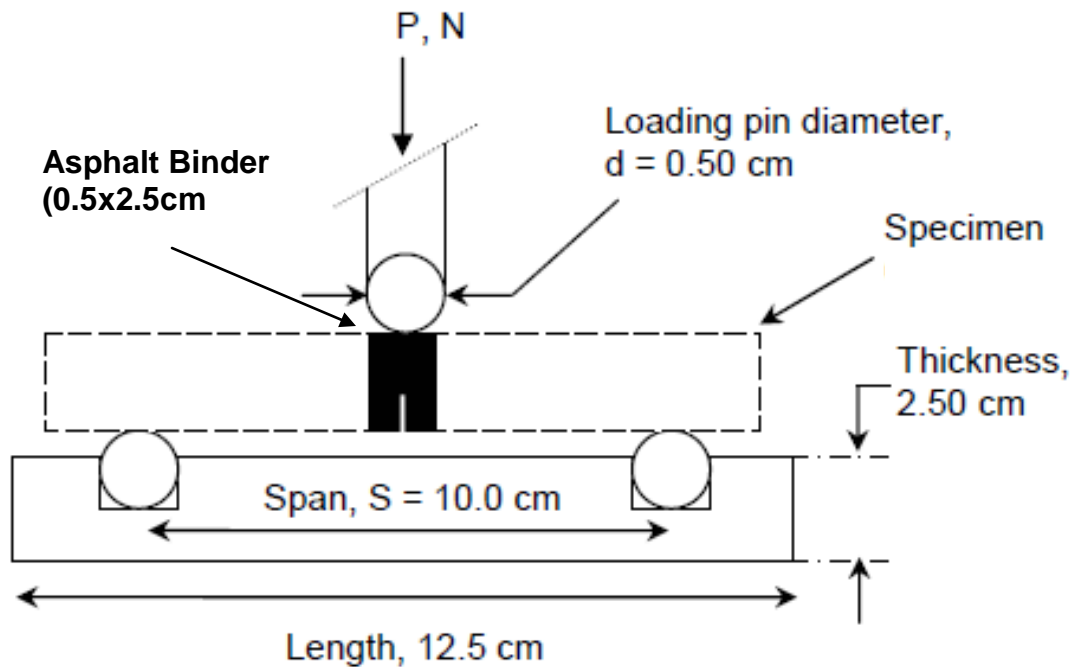


Figure V3a.2. Illustration. Standard dimensions for the SENB specimen.

## Significant Results

### *Cooperation with WCTG and RMAUPG*

After multiple conference calls, the research team reached an agreement with WCTG and RMAUPG. UW–Madison will receive samples from different suppliers as part of WCTG’s regular round-robin testing program. The following summarizes the understanding with WCTG and RMAUPG:

### Material Sampling

- Suppliers are to indicate which projects and/or contractors will use the materials supplied.
- UW–Madison will coordinate with state departments of transportation that are members of WCTG and RMAUPG, as well as contractors, to obtain an extra sample from quality control/quality assurance testing for individual projects.
- UW–Madison will test both the supplier and quality control samples.

### Material Testing

The following summarizes the testing battery accepted by WCTG and RMAUPG:

- $G^*$  and  $\delta$  (AASHTO M320).
- Toughness and tenacity (ASTM D5801-95).

- Elastic recovery (AASHTO T301).
- MSCR (ASTM D7405).
  - Test at two temperatures.
  - Test at 0.1, 3.2 and 10 kPa.
- Ductility (AASHTO T51).
- Direct Tension (DT) (AASHTO M320).

Since the samples procured from WCTG will be tied to paving projects, the overall performance of these pavements will be tracked and reported. Therefore, UW–Madison will conduct and evaluate additional PG Plus tests that address more distresses. These tests are:

- Cracking temperature (Asphalt Binder Cracking Device (ABCD)).
- Fracture evaluation (SENB).
- Repeated Creep and Recovery (RCR).
  - Multiple temperatures.
  - Multiple stresses.
- Indentation creep (refer to subtask E1b-2).
- Binder Yield Energy Test (BYET).

Binders selected (all modified) include:

- PG 58-34.
- PG 64-34.
- PG 70-28.
- PG 76-28.
- PG 64-28.

#### *Single-Edge Notched Bending Test Development*

The SENB testing frame was evaluated by testing two types of materials. The first is a RAP mortar beam, which is similar to the BBR beam to assure deformability while withholding a maximum load compared to that expected from SENB test specimens. The second is a mastic SENB specimen (binder plus mineral filler). The mastic is selected due to its expected high stiffness and load capacity. It is important to note that the test was conducted at -6 °C. Before testing these two specimens, multiple tests were conducted to establish the optimum feedback loop speed that allows for maintaining the maximum control of the deformation speed while not jeopardizing the maximum torque that the motor can impose.

#### RAP Mortar Results

The imposed rate of deformation is 0.01mm/s in testing the RAP specimen. Test results indicate that the actual rate, which was determined to be 0.009mm/s, was close to the imposed rate.

Testing two replicates of RAP show that the test can repeatably control the loading of the specimen with high accuracy. The imposed deformation rate is shown in figure V3a.2.

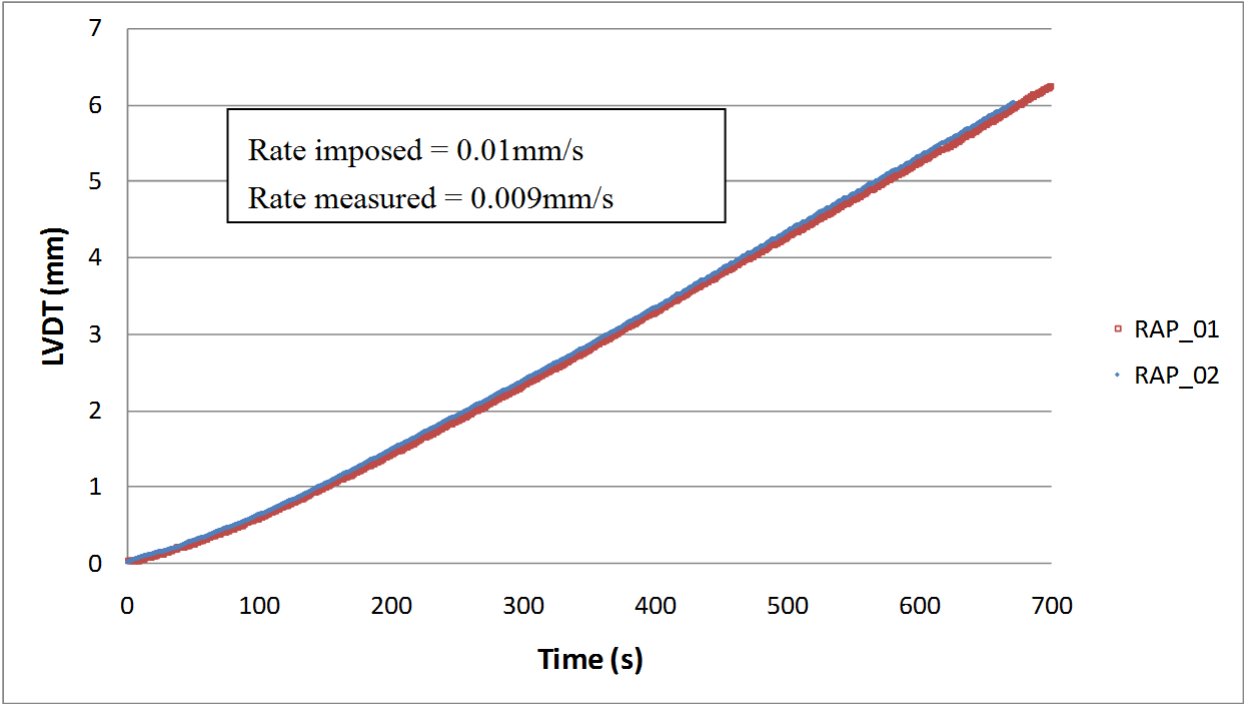


Figure V3a.3. Graph. Applied deformation rate during the test of RAP mortar. (LVDT = linear variable differential transformer.)

The results, as shown in figure V3a.3, indicate that the test is sufficiently repeatable and the replicates are very close to each other. Table V3a.1 shows the measured maximum load and deformation at maximum load.

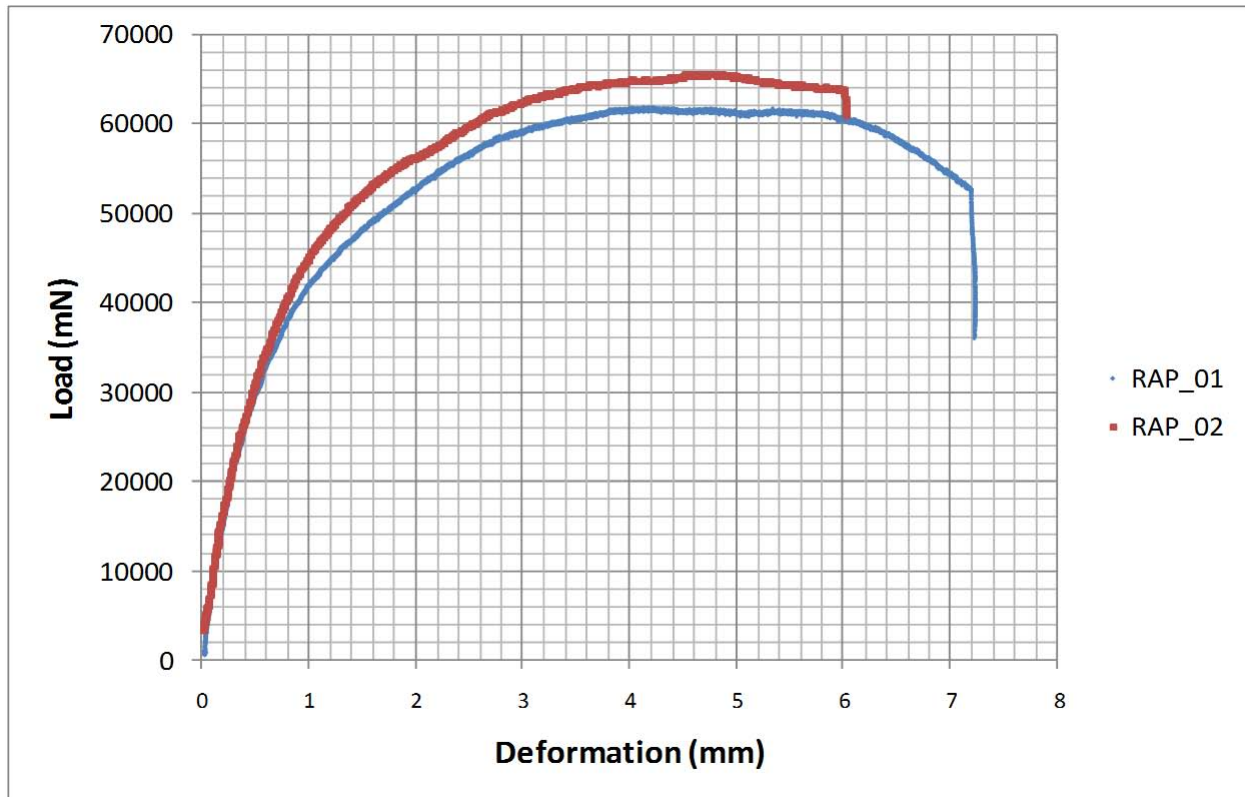


Figure V3a.4. Graph. Load in mN measured during the test of RAP mortar.

TableV3a.3. Measured results from testing RAP mortar.

Specimen	Max Load (mN)	Deformation at Max Load (mm)
1	61894.75	4.13
2	65641.97	4.65
<b>Average</b>	<b>63768.36</b>	<b>4.39</b>
<b>Coefficient of Variation</b>	<b>4.2%</b>	<b>8.4%</b>

Table V3a.1 shows that the measured maximum load and deformation at the maximum load are statistically repeatable with a coefficient of variation less than 10%. This data provide confidence in the testing frame, as it can maintain the imposed rate of deformation as well as yield highly repeatable results.

## Mastic SENB Specimen Results

Testing the mastic SENB specimen is intended to push frame testing to the maximum capacity. The mastic was tested by imposing the same deformation rate as the RAP mortar (0.01mm/s).

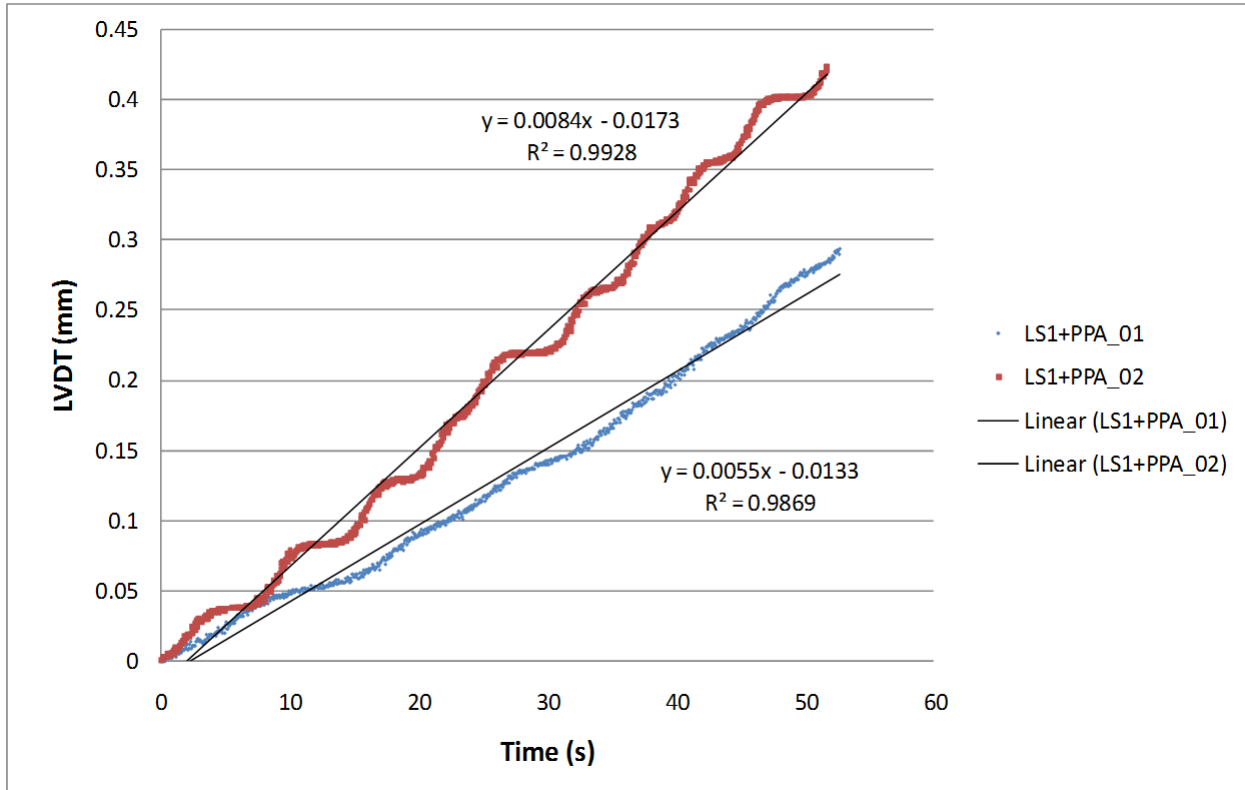


Figure V3a.5. Graph. Applied deformation rate during the test of mastic SENB specimen. (LS = limestone. PPA = polyphosphoric acid.)

Figure V3a.4 shows that the loading setup is unable to achieve the target constant deformation rate. The device is also not capable of providing repeatable control on the deformation rate between both specimens. This is expected to give different results for the two specimens tested, as shown in figure V3a.4.

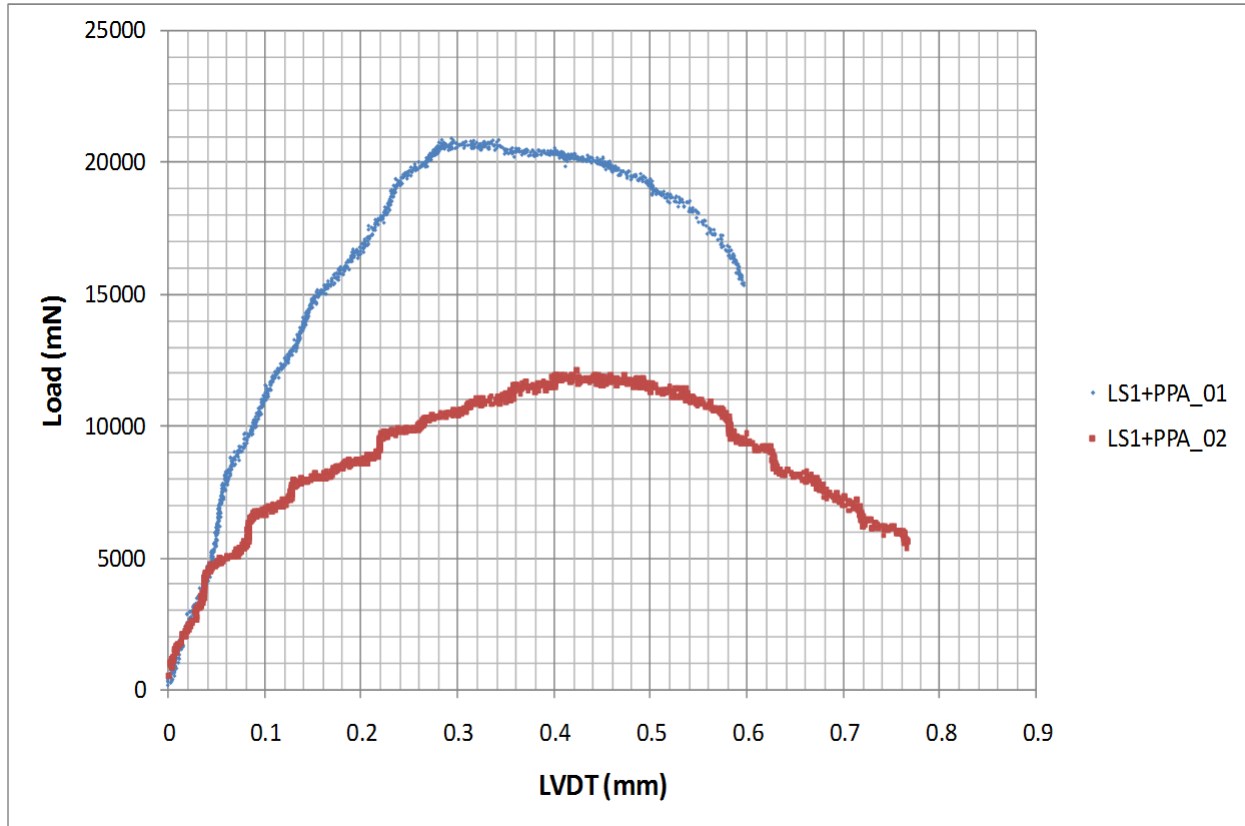


Figure V3a.6. Graph. Load in mN measured during the test of mastic SENB specimen.

The results shown in figure V3a.5 are summarized in table V3a.2. The results clearly indicate that for highly stiff specimens, the test setup is not able to control the loading deformation or produce repeatable results.

Table V3a.4. Measured results from testing the mastic SENB specimen.

Specimen	Max Load (mN)	Deformation at Max Load (mm)
LS1+PPA_01	12104.35	0.42
LS1+PPA_02	20918.88	0.29
<b>Average</b>	<b>16511.62</b>	<b>0.36</b>
<b>Coefficient of Variation</b>	<b>37.7%</b>	<b>25.4%</b>

The research team believes that the deformation rate required was not achieved for the mastic SENB specimen due to the lack of enough torque in the testing motor. On the other hand, as reflected in figure V3a.4, there is a fluctuation in the deformation for both specimens. This is

believed to be due to the feedback loop speed. It seems that the testing setup requires a higher speed to maintain a uniform deformation rate. However, increasing the feedback speed decreases the maximum torque produced by the motor.

Based on these results, the research team recommends the following:

- Install a gear box to increase the torque of the loading device.
  - This will increase the loading capacity of the device.
- Conduct tests at slower deformation rate (suggesting 0.05mm/s).
  - This will allow testing to be conducted at higher feedback loop without requiring much more torque.

#### Significant Problems, Issues and Potential Impact on Progress

None.

#### Work Planned Next Quarter

Next quarter, work will start on specimens received from WCTG according to the testing battery shown in this report. Mixture testing will be conducted on the specimens generated for the E1b-1 subtask, and work will continue on developing the testing setup for the SENB test to study the fracture behavior of specimens. SENB test results will be compared to the ABCD test results reported in the previous quarter.

#### **Work element V3b: Validation of the MEPDG Asphalt Materials Models Using New MEPDG Sites and Selected LTPP Sites (UNR, UWM)**

##### *Subtask V3b-1: Design and Build Sections (Start Year 1, Year 2, and Year 3)*

#### Work Done This Quarter

Arranged with Washoe RTC in northern Nevada to conduct a distress survey of the pavement that was constructed in summer 2008.

#### Significant Results

None.

#### Significant Problems, Issues and Potential Impact on Progress

Only three agencies have committed to the construction of MEPDG sites: the Washoe RTC in northern Nevada in 2008, The South Dakota DOT in 2009/2010, and the Wisconsin DOT in 2009. The researchers are facing significant hesitation from the DOTs to use the MEPDG to design and construct HMA pavements. The level of this work element may have to be reduced.

### Work Planned Next Quarter

Continue discussions with the states to select field sections for the MEPDG validation sites.

### ***Subtask V3b-2: Additional Testing (Start Year 2, Year 3, and Year 4)***

#### Work Done This Quarter

This work element is to provide additional testing for states (or others) that commit to MEPDG validation sites.

#### Significant Results

None.

#### Work Planned Next Quarter

None planned at this time.

### ***Subtask V3b-3: Select LTPP Sections (Start Year 1 thru Year 5)***

#### Work Done This Quarter

Testing began on the LTPP binders listed in the previous quarterly report. Binder Yield Energy Tests (BYETs) were conducted at a rate of 0.01/s at the PG intermediate temperature for each binder. Information for the test materials is as follows:

- 04-B901 PG 76-10 (Arizona)
- 09-0902 PG 64-28 (Connecticut)
- 34-0961 PG 78-28 (New Jersey)
- 37-0962 PG 76-22 (North Carolina)

This quarter, the research team made contact with FHWA's Turner-Fairbank Highway Research Center (TFHRC) asphalt research team, led by Dr. Nelson Gibson, and placed two conference calls to discuss possible collaborative efforts. Presentations of the FHWA and University of Wisconsin-Madison teams were exchanged, and plans for sharing ideas and materials were developed.

#### Significant Results

Results of the BYET at 0.01/s at PG intermediate temperature are shown in figure V3b-3.1. The measured cracking from LTPP monitoring is also given.

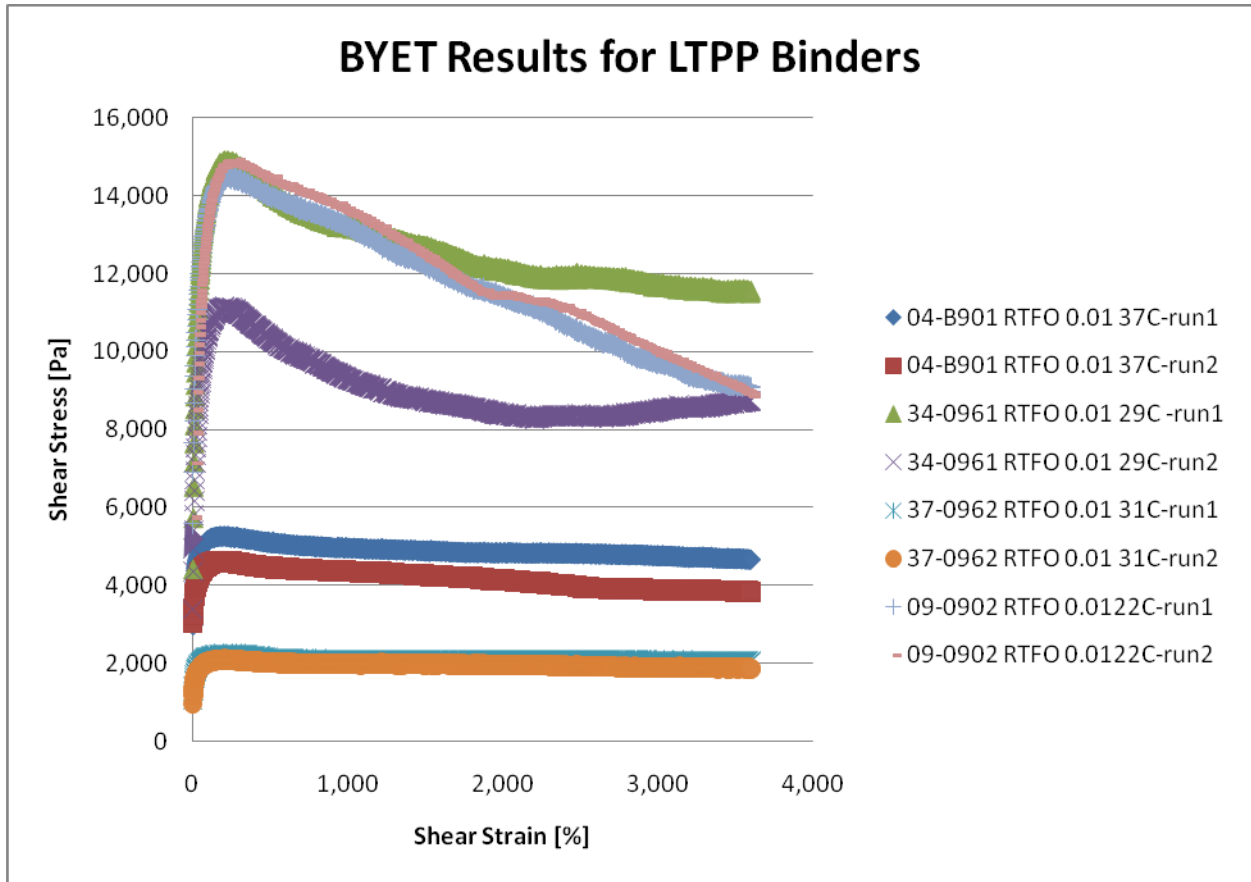


Figure V3b-3.1. Graph. Stress versus strain curves from BYET. (RTFO = rolling thin film oven.)

Tables V3b-3.1 and V3b-3.2 provide yield energy (YE) and gamma at tau max (GTM) results of the BYET.

Table V3b-3.1. LTPP BYET YE results.

Binder	Rate	Temp [°C]	YE Run 1 [Pa]	YE Run 2 [Pa]	Avg [Pa]	Coefficient of Variation	LTPP Fatigue Cracking [m <sup>2</sup> ]
04-B901	0.01	37	11,323	8,770	10,047	18.0%	328
34-0961	0.01	29	26,698	20,043	23,370	20.1%	179
37-0962	0.01	31	4,107	4,034	4,071	1.3%	0
09-0902	0.01	22	33,601	38,143	35,872	9.0%	0

Table V3b-32. LTPP BYET GTM results.

Binder	Rate	Temp [°C]	GTM Run 1 [%]	GTM Run 2 [%]	Avg [%]	Coefficient of Variation	LTPP Fatigue Cracking [m <sup>2</sup> ]
04-B901	0.01	37	225.360	199.720	212.540	8.5%	328
34-0961	0.01	29	205.590	205.380	205.485	0.1%	179
37-0962	0.01	31	199.610	206.740	203.175	2.5%	0
09-0902	0.01	22	255.140	279.340	267.240	6.4%	0

Figures V3b-3.2 and V3b-3.3 show the results when BYET parameters are plotted against cracking.

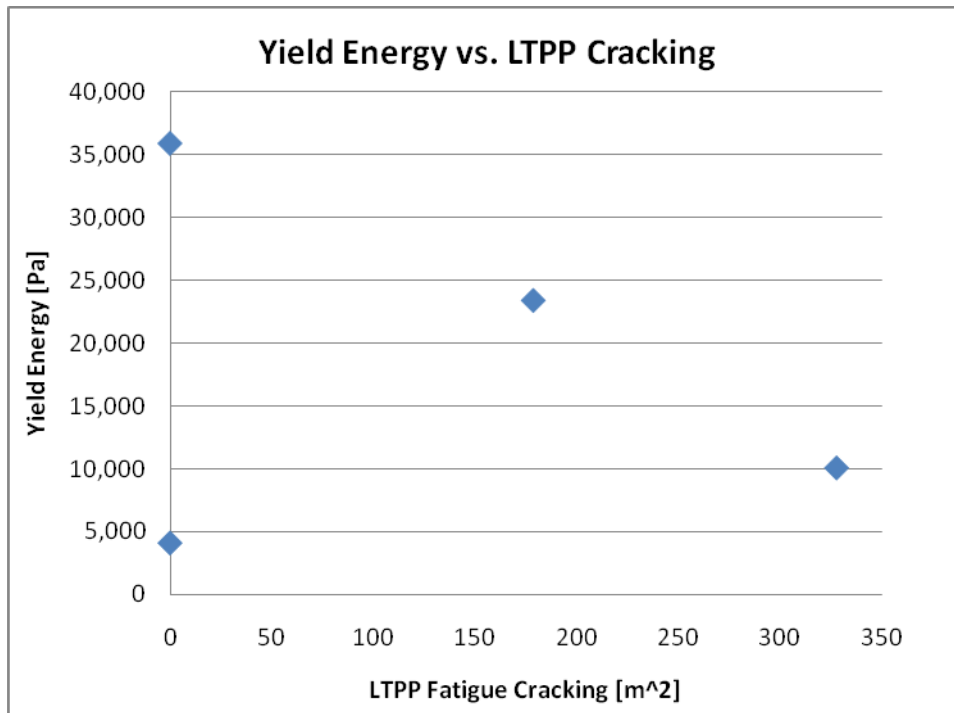


Figure V3b-3.2. Graph. YE versus LTPP fatigue performance.

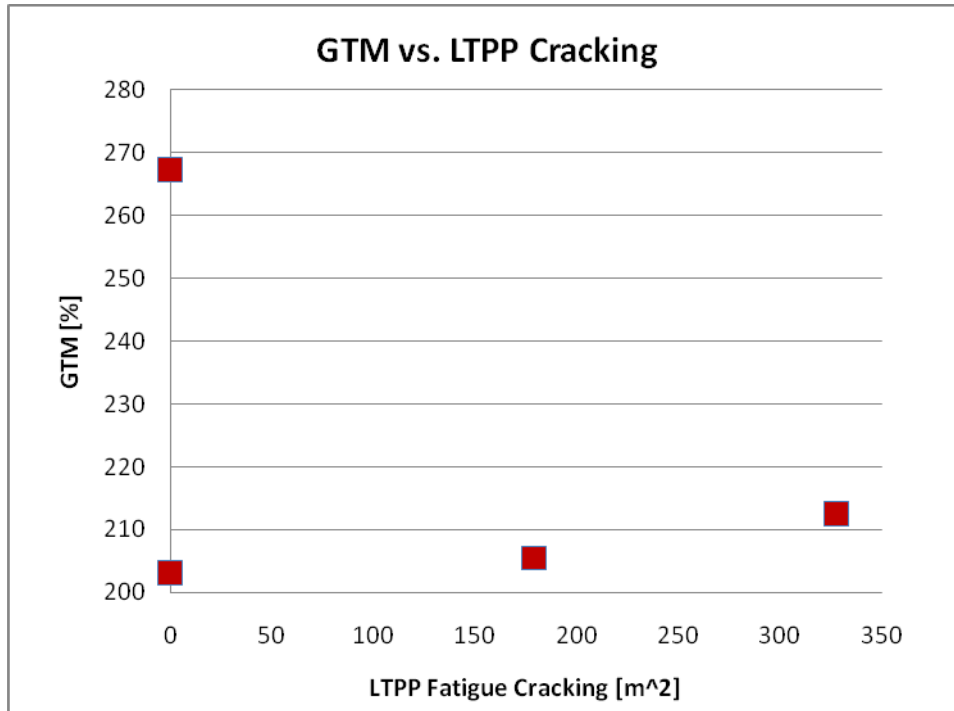


Figure V3b-3.3. Graph. GTM versus LTPP fatigue performance.

As the results show, with the exception of one binder, YE shows a relationship previously found with accelerated pavement testing fatigue performance—with increasing YE values, the amount of fatigue cracking is reduced.

Significant Problems, Issues and Potential Impact on Progress

None.

Work Planned Next Quarter

Further BYET testing will be performed on the other LTPP binders received from the LTPP Materials Reference Library. The research team has begun a Binder Fatigue Working Group with members of the TFHRC team. In addition to BYET testing, selected LTPP materials will be sent to TFHRC for evaluation using the Double-Edged Notched Tension (DENT) test, which has been under investigation by the TFHRC research team for its ability to also indicate fatigue performance. The results of this collaborative effort will be reported next quarter.

***Subtask V3b-4: Testing of Extracted Binders from LTPP Sections (Start Year 1)***

Work Done This Quarter

No work planned

***Subtask V3b-5: Review and Revisions of Materials Models (Start Year 2, Year 3, Year 4, and Year 5)***

Work Done This Quarter

No work planned.

**Subtask V3b-6: Evaluate the Impact of Moisture and Aging (Start Year 3, Year 4, and Year 5)**

Work Done This Quarter

No activity to date.

Validation Year 3	Year 3 (4/2009-3/2010)												Team
	4	5	6	7	8	9	10	11	12	1	2	3	
<b>(1) Field Validation</b>													
V1a: Use and Monitoring of Warm Mix Asphalt Sections													WRI
V1b: Construction and Monitoring of additional Comparative Pavement Validation sites													WRI
<b>(2) Accelerated Pavement Testing</b>													
V2a: Accelerated Pavement Testing including Scale Model Load Simulation on small test track (This work element will include all accelerated pavement testing)													WRI
V2b: Construction of validation sections at the Pecos Research & Testing Center													WRI
<b>(3) R&amp;D Validation</b>													
V3a: Continual Assessment of Specification													UWM
V3a-1: Evaluation of the PG-Plus practices and the motivations for selecting the "plus" tests.													
V3a-2: Detailed analysis of all PG-Plus tests being proposed or in use today, documentation of benefits and costs of these tests, and comparison with new tests			D										
V3a-3: Development of protocols for new binder tests and database for properties measured					JP								
V3a-4: Development of specification criteria for new tests based on field evaluation of construction and performance						D					P		
V3a-5: Interviews and surveys for soliciting feedback on binder tests and specifications													
V3b: Validation of the MEPDG Asphalt Materials Models and Early Verification of Technologies Developed by ARC using new MEPDG Sites and Selected LTPP sites													UNR/UWM/WRI
V3b-1: Design and Build Sections													UNR
V3b-2: Additional Testing (if needed)													
V3b-3: Select LTPP Sites to Validate New Binder Testing Procedures							DP				P		UWM
V3b-4: Testing of Extracted Binders from LTPP Sections													
V3b-5: Review and Revisions of Materials Models													
V3b-6: Evaluate the Impact of Moisture and Aging													

**Deliverable codes**  
D: Draft Report  
F: Final Report  
M&A: Model and algorithm  
SW: Software  
JP: Journal paper  
P: Presentation  
DP: Decision Point

**Deliverable Description**  
Report delivered to FHWA for 3 week review period.  
Final report delivered in compliance with FHWA publication standards  
Mathematical model and sample code  
Executable software, code and user manual  
Paper submitted to conference or journal  
Presentation for symposium, conference or other  
Time to make a decision on two parallel paths as to which is most promising to follow through

 Work planned  
 Work completed  
 Parallel topic

Validation Years 2 - 5	Year 2 (4/08-3/09)				Year 3 (4/09-3/10)				Year 4 (04/10-03/11)				Year 5 (04/11-03/12)				Team
	Q1	Q2	Q3	Q4	Q1	Q2	Q3	Q4	Q1	Q2	Q3	Q4	Q1	Q2	Q3	Q4	
<b>(1) Field Validation</b>																	
V1a: Use and Monitoring of Warm Mix Asphalt Sections																	
V1b: Construction and Monitoring of additional Comparative Pavement Validation sites																	
<b>(2) Accelerated Pavement Testing</b>																	
V2a: Accelerated Pavement Testing including Scale Model Load Simulation on small test track																	
V2b: Construction of validation sections at the Pecos Research & Testing Center																	
<b>(3) R&amp;D Validation</b>																	
V3a: Continual Assessment of Specification																	
V3a-1: Evaluation of the PG-Plus practices and the motivations for selecting the "plus" tests.		P	D,F														
V3a-2: Detailed analysis of all PG-Plus tests being proposed or in use today, documentation of benefits and costs of these tests, and comparison with new tests				P	D												
V3a-3: Development of protocols for new binder tests and database for properties measured						JP			P								
V3a-4: Development of specification criteria for new tests based on field evaluation of construction and performance						D		P	P			JP	P		JP		
V3a-5: Interviews and surveys for soliciting feedback on binder tests and specifications									P			JP	P		D	F	
V3b: Validation of the MEPDG Asphalt Materials Models and Early Verification of Technologies Developed by ARC using new MEPDG Sites and Selected LTPP sites																	
V3b-1: Design and Build Sections										D, F							
V3b-2: Additional Testing (if needed)																	
V3b-3: Select LTPP Sites to Validate New Binder Testing Procedures								DP		P		JP	P		D	F	
V3b-4: Testing of Extracted Binders from LTPP Sections																	
V3b-5: Review and Revisions of Materials Models																D, F	
V3b-6: Evaluate the Impact of Moisture and Aging																D, F	

**Deliverable codes**

D: Draft Report  
 F: Final Report  
 M&A: Model and algorithm  
 SW: Software  
 JP: Journal paper  
 P: Presentation  
 DP: Decision Point

**Deliverable Description**

Report delivered to FHWA for 3 week review period.  
 Final report delivered in compliance with FHWA publication standards  
 Mathematical model and sample code  
 Executable software, code and user manual  
 Paper submitted to conference or journal  
 Presentation for symposium, conference or other  
 Time to make a decision on two parallel paths as to which is most promising to follow through

 Work planned  
 Work completed  
 Parallel topic



## **PROGRAM AREA: TECHNOLOGY DEVELOPMENT**

### **Work element TD1: Prioritize and Select Products for Early Development (Year 1)**

#### Work Done This Quarter

None. This work element has been completed.

#### Significant Results

Six early technology development projects have been identified and all have received favorable ratings from the ETGs.

#### Significant Problems, Issues and Potential Impact on Progress

None

#### Work Planned Next Quarter

None

### **Work element TD2: Develop Early Products (Year 2)**

#### Work Done This Quarter

The procedure for FAM testing (from Work Element F2b) is complete and available in AASHTO format. It is being reviewed for final edits. It is planned to submit the draft procedure to the Binder and Mix & Construction ETG's in September 2009 for review of the procedure and advice/recommendations on conducting the ruggedness testing and sensitivity analysis for the test procedure.

Work continued on the Simplified Continuum Damage Fatigue project. The draft standard method is essentially complete.

The research team is working with Interlaken Technology Corporation (ITC) to modify NCHRP's Asphalt Mixture Performance Tester (AMPT) to perform the continuum damage fatigue testing. This equipment was purchased by NCHRP in NCHRP Project 9-29. It is being used by AAT on Phase VI of NCHRP Project 9-29. The software for continuum damage fatigue testing has been installed on the device and is now being remotely shaken down by ITC engineers.

### Significant Results

Software for performing continuum damage fatigue tests has been installed on the Interlaken simple performance tested at AAT's Sterling laboratory.

A spreadsheet for the predication of fatigue response of HMA mixtures under complex loading was developed. This spreadsheet is extremely useful in developing and evaluating test protocols for characterizing HMA mixtures using continuum damage test methods.

### Significant Problems, Issues and Potential Impact on Progress

None.

### Work Planned Next Quarter

The test method and equipment will be applied to fatigue data from several mixtures. A ruggedness testing plan for the simplified continuum damage fatigue test will be developed.

## **Work element TD3: Identify Products for Mid-Term and Long-Term Development (Years 2, 3, and 4)**

### Work Done This Quarter

The research team continued to review interim research products to identify potential mid-term and long-term development projects.

### Significant Results

None

### Work Planned Next Quarter

The research team will continue to review interim research products to identify potential mid-term and long-term development projects.

## **Work Element TD4: Develop Mid-Term and Long-Term Products (Years 3, 4, and 5)**

This activity is planned for later in the project.

## **PROGRAM AREA: TECHNOLOGY TRANSFER**

### **CATEGORY TT1: OUTREACH AND DATABASES**

#### **Work element TT1a: Development and Maintenance of Consortium Website (Duration: Year 1 through Year 5)**

##### Work Done This Quarter

The ARC website was maintained and updated. The ARC quarterly technical progress report, Jan 1- Mar 31, were uploaded to the ARC website.

##### Significant Results

None.

##### Significant Problems, Issues and Potential Impact on Progress

None.

##### Work Planned Next Quarter

Continue maintaining and updating the ARC website.

#### **Work element TT1b: Communications (Duration: Year 1 through Year 5)**

##### Work Done This Quarter

No work planned.

##### Work Planned Next Quarter

The fifth ARC Newsletter is planned for August 2009.

#### **Work element TT1c: Prepare Presentations and Publications**

##### **Publications**

Bullard, J.W., A.T. Pauli, E.J. Garboczi, and N.S. Martys, 2009, A Comparison of Viscosity-Concentration Relationships for Emulsions. *Journal of Colloid and Interface Science*, 330 (1), 186-193.

ASTM D4124-01, 2010, Standard Test Method for Separation of Asphalt into four Fractions. *Annual Book of ASTM Standards, Road and Paving Materials; Vehicle-Pavement Systems*, Section 4, vol. 04.03. ASTM International, West Conshohocken, PA. Troy Pauli-Technical Contact. (ACCEPTED FOR PUBLICATION 2001).

Caro, S., E. Masad, A. Bhasin, and D. Little, 2009, "A Coupled Micromechanical Model of Moisture-Induced Damage in Asphalt Mixtures." *Journal of Materials in Civil Engineering* (ASCE), (in press).

Caro, S., E. Masad, A. Bhasin, D. Little, and M. Sanchez-Silva, 2009, "Analysis of the Effect of the Internal Air Void Structure on the Moisture Sensitivity of Asphalt Mixtures." *Journal of the Association of Asphalt Paving Technologists* (AAPT), (submitted for evaluation).

Luo, X., R. Luo, R. L. Lytton, and Y. Koohi, 2009, "Characterization of Damage in Asphalt Mixture Using Dissipated Pseudo-Strain Energy." To be submitted to *Journal of Transportation Engineering*, American Society of Civil Engineers.

Luo, R., and R. Lytton, 2009, "Distribution of Crack Size in Asphalt Mixtures." To be submitted to *Journal of Transportation Engineering*, American Society of Civil Engineers.

Y. Kim, J. Lee, and J. Lutfi, 2009, "Geometrical Evaluation and Experimental Verification to Determine Representative Volume Elements of Heterogeneous Asphalt Mixtures." *Journal of Testing and Evaluation*, submitted.

F. Aragão, Y. Kim, and J. Soares, 2009, "Dynamic Modulus Prediction of Asphalt Concrete Mixtures through Various Methods: Analytical, Phenomenological, and Numerical Methods." *Transportation Research Record*, submitted.

F. Aragão and Y. Kim, 2009, "Modeling of Asphalt Mixtures Subjected to Nonlinear Viscoelastic Fracture." *2010 GeoFlorida Conference: Advances in Analysis, Modeling, and Design*, submitted.

F. Aragão, Y. Kim, J. Lee, and J. Soares, 2009, "A Micromechanical Finite Element Model for Predicting the Dynamic Modulus of Heterogeneous and Rate-Dependent Asphalt Concrete Mixtures." *2009 ABPV Conference*, accepted.

Chien-Wei Huang, Rashid K. Abu Al-Rub, Eyad A. Masad, Dallas N. Little, and Golden D. Airey, "Numerical Implementation and Validation of a Nonlinear Viscoelastic and Viscoplastic Model for Asphalt Concrete Mixes", *Journal of Mechanics of Materials*, submitted, 2009.

Chien-Wei Huang, Rashid K. Abu Al-Rub, Eyad A. Masad, and Dallas N. Little, "Three-Dimensional Simulations of Asphalt Pavement Permanent Deformation Using a Nonlinear Viscoelastic and Viscoplastic Model," *Journal of Materials in Civil Engineering*, submitted, 2009.

## **Presentations**

Kringos, N., T., Pauli, A., Scarpas and R., Robertson, A Thermodynamical Approach to Healing in Bitumen, 7th RILEM Conference on Advanced Testing and Characterization of Bituminous Materials, May 2009, Rhodes, Greece.

Schmets, A.J.M., N. Kringos, A. Scarpas, C.P. Duif, G. Schitter and T. Pauli, First-principles investigation of the multiple phases in bituminous materials: the case of asphaltene stacking, 7th RILEM Conference on Advanced Testing and Characterization of Bituminous Materials, May 2009, Rhodes, Greece.

Pauli, T., Studies of the Physico-Chemical Nature of the SHRP Asphalts: PART-I. Chemomechanics of Bituminous Materials Workshop, Delft, June 10-12, 2009.

Pauli, T., Studies of the Physico-Chemical Nature of the SHRP Asphalts: PART-II. Chemomechanics of Bituminous Materials Workshop, Delft, June 10-12, 2009.

Pauli, T., A. Beemer, J. Miller, W. Grimes, J. Beiswenger, and J. F. Branthaver Physico-Chemistry of the SHRP Asphalts. Petersen Asphalt Research Conference, July 13<sup>th</sup> - 15<sup>th</sup>, 2009 Laramie, Wyoming.

F. Aragão, Y. Kim, J. Lee, and D. H. Allen. "A Micromechanical Fracture Model for Heterogeneous and Rate-Dependent Asphalt Concrete Mixtures Using the Finite Element Method." *10<sup>th</sup> U.S. National Congress on Computational Mechanics*, presented.

F. T. S. Aragão and Y. Kim. "Modeling Fracture and Failure of Nonlinear, Inelastic Asphalt Concrete Mixtures." *2009 Joint ASCE-ASME-SES Conference on Mechanics and Materials*, presented.

## **Work element TT1d: Development of Materials Database (Duration: Year 2 through Year 5)**

### Work Done This Quarter

Work progressed on the design and implementation of the database to store research results collected from the ARC project. In addition, development and unit testing is underway on a Web-based application allowing ARC members to enter data into the database, query research results, and collaborate with other researchers.

### Significant Results

During the quarterly period, an SQL Server 2005 database has been implemented to store materials, material properties, and material measurements. The database design and structure allows for the following:

- Material properties are divided into quantitative and qualitative properties for the purposes of validation. Quantitative properties must fall between a range of valid numeric values. Qualitative properties consist of known descriptive values. The validation of properties is extensible. That is, ARC users can define hard and soft limits for numeric property values and the valid qualitative values.
- The system allows materials to be categorized into different types (aggregates, fillers, mastics, asphalts, binders, etc...) for the purposes organization and grouping. Material types are dynamic and can be created by ARC users, as necessary.
- Composite materials can be created from core materials. Furthermore, new composite materials can be created from existing composite materials. The database design supports tracking of a composite material back to its original source material.
- The framework for a role-based security system has been created. Roles have been defined for administrative ARC users, consortium users, and general (public) users. As work progresses, this framework will restrict allowable tasks based on a user's role. Given the current framework implementation, additional roles can be easily created.

Change management policies and procedures have been defined such that both test and production versions of the database are maintained. Regular backups of both test and production databases and software are also being performed. Off site database backups are also maintained.

Implementation is underway for the following:

- The structure of selected tables is not yet complete. For example, a prototype for validation sections has been created. However, the full complement of fields has not been defined. Similar prototypes exist for material samples and material sources.
- Tables have been created to log database access and database changes. The goal is to provide a complete audit trail of all database activity.
- While the role-based framework is complete, work is in-progress to determine which application features are available to each role.

Significant progress has been made on the Web-based application allowing ARC users to create materials, define material types, and identify material properties. The Web-based application and database are being hosted at the University of Nevada, Reno. Microsoft ASP.NET was chosen as the primary technology to implement this application. The latest version of ASP.NET and the .NET Framework (3.5) is being used for software development. The following user interface elements have been completed and unit testing is underway for these user interface elements.

- The user interface to create and edit core and composite materials has been completed and unit testing is underway. ARC users can select specific types of materials and material categories. The user-interface has also been completed to create and edit material details and the sources of each material. Figure TT1d.1 shows the user interface for this application form.
- The user interface to create and edit material properties has been completed and unit testing is underway. ARC users can create and edit both quantitative and qualitative

properties along with creating and managing property groups. Figure TT1d.2 shows the user interface for quantitative and qualitative properties for a core aggregate.

- Work is underway for a Material Browser form. This form allows the user to select materials and browse information about the material, the source of that material, and the properties applicable to the material. Because of the large volume of information available, sections containing the material source, properties, measures, and details about the material can be expanded or collapsed. Development continues on this form to support material measures. Figure TT1d.3 shows the Material Browser form.

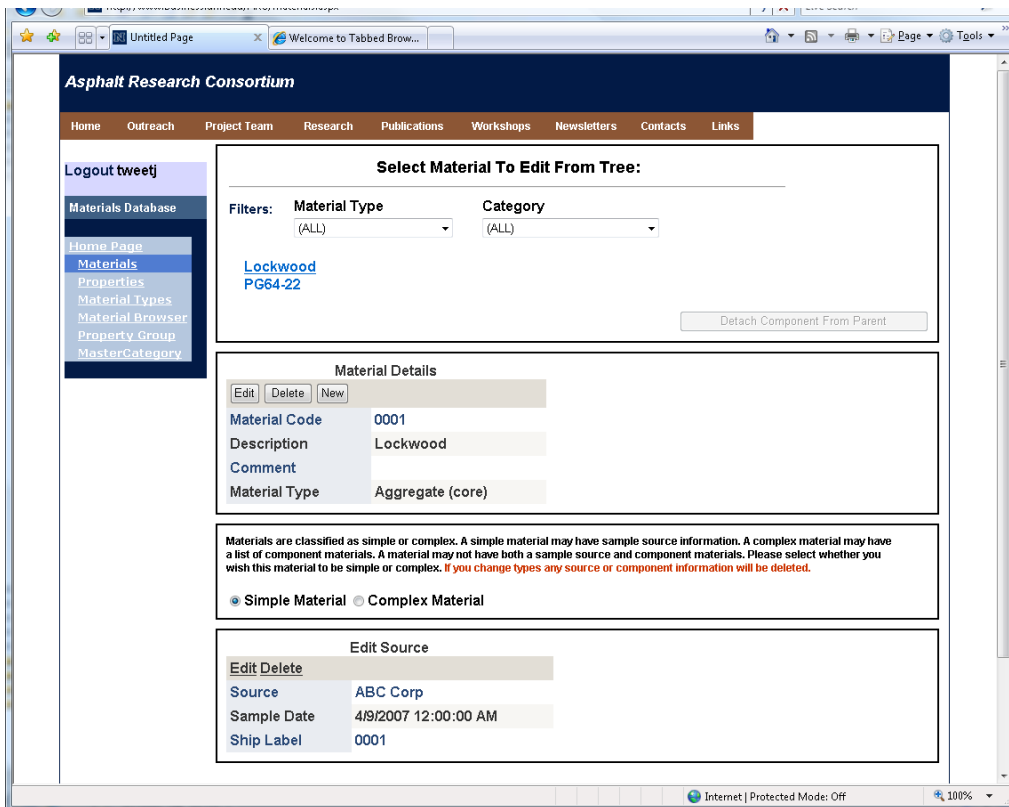


Figure TT1d.1. Material editing form.

Asphalt Research Consortium

Home Outreach Project Team Research Publications Workshops Newsletters Contacts Links

Logout tweetj

Select Material Type: Aggregate (core) Views:  Quantitative  Qualitative  Unit Editor

Materials Database

Home Page  
Materials  
Properties  
Material Types  
Material Browser  
Property Group  
MasterCategory

**Quantitative Properties**

**Aggregate Gradation**

Property Name	Unit	Soft Min	Soft Max	Hard Min	Hard Max	Comment
Passing #4	%			0	100	<input type="button" value="Delete"/>
Passing #8	%			0	100	<input type="button" value="Delete"/>
Passing 1"	%			0	100	<input type="button" value="Delete"/>
Passing 1/2"	%			0	100	<input type="button" value="Delete"/>
Passing 3/4"	%			0	100	<input type="button" value="Delete"/>

**Aggregate Durability**

Property Name	Unit	Soft Min	Soft Max	Hard Min	Hard Max	Comment
CA Durability	%			0	100	<input type="button" value="Delete"/>

Aggregate Gradation

**Qualitative Properties**

**Aggregate Composition**

Property Name	Comment	Valid Values
Composition Type		Crushed Gravel <input type="button" value="Edit Values"/> <input type="button" value="Delete"/>
Texture		Coarse <input type="button" value="Edit Values"/> <input type="button" value="Delete"/>

**Aggregate Geology**

Property Name	Comment	Valid Values

Figure TT1d.2. Material properties form.

Asphalt Research Consortium

Home Outreach Project Team Research Publications Workshops Newsletters Contacts Links

Logout tweetj

Materials Database

Home Page  
Materials  
Properties  
Material Types  
Material Browser  
Property Group  
MasterCategory

**Material Selection Tree**

Filters: Material Type (ALL) Category (ALL)

[Lockwood PG64-22](#)

Views:  Source  Properties  Measures  Material Details

**Material Details**

Property Name	Value
fidMaterialID	16
fidDescription	Lockwood
fidComment	
fidMaterialCategoryID	1
fidValSectionID	
fidMaterialName	0001
fidSourceID	1
fidSampleDate	4/9/2007 12:00:00 AM
fidShipLabel	0001
fidMaterialCategoryName	Aggregate (core)

[Add/Edit Materials](#)

Figure TT1d.3. Material Browser form.

### Significant Problems, Issues and Potential Impact on Progress

None.

### Work Planned Next Quarter

Continue the work on the database and the dynamic web site. Implementation of the following application features is currently underway:

- The design and implementation of application features that will log all database transactions is currently under development, along with the necessary user interface elements to provide ARC users a complete history of all record additions, changes, and deletions. Administrative users will be able to view all record changes and determine the user who made those changes.
- The forms and code that will manage validation sites is in progress.
- The forms and code to create and edit property groups and property categories are under development.
- The forms and code to manage users and user access are currently under development.

### **Work element TT1e: Development of Research Database (Duration: Year 2 through Year 5)**

#### Work Done This Quarter

Uploaded the Quarterly Technical Progress Report to the ARC website.

#### Significant Results

None.

### Significant Problems, Issues and Potential Impact on Progress

None.

### Work Planned Next Quarter

Upload the ARC Quarterly Technical Progress Report for the period April 1 to June 30, 2009 to the ARC website.

## **Work Element TT1f: Workshops and Training**

### Work Done This Quarter

No activity this quarter.

### Significant Results

None.

### Significant Problems, Issues and Potential Impact on Progress

None.

### Work Planned Next Quarter

A plan will be prepared for a workshop to describe and explain the differences of the various continuum damage analysis methods. The plan will be delivered to the ETG meetings in September 2009.

The Texas A&M team and TU Delft are conducting a training course on Modeling and Characterization of Asphaltic Materials on September 21-25, 2009 at Texas A&M University.

Technology Transfer Year 3	Year 3 (4/2009-3/2010)												Team	
	4	5	6	7	8	9	10	11	12	1	2	3		
<b>(1) Outreach and Databases</b>														
TT1a: Development and Maintenance of Consortium Website														UNR
TT1b: Communications														UNR
TT1c: Prepare presentations and publications														ALL
TT1d: Development of Materials Database														UNR
TT1d-1: Identify the overall Features of the Web Application														
TT1d-2: Identify Materials Properties to Include in the Materials Database														
TT1d-3: Define the Structure of the Database														
TT1d-4: Create and Populate the Database										SW, v. β			SW	
TT1e: Development of Research Database														UNR
TT1e-1: Identify the Information to Include in the Research Database														
TT1e-2: Define the Structure of the Database														
TT1e-3: Create and Populate the Database														
TT1f: Workshops and Training														UNR

**Deliverable codes**

- D: Draft Report
- F: Final Report
- M&A: Model and algorithm
- SW: Software
- JP: Journal paper
- P: Presentation
- DP: Decision Point

**Deliverable Description**

- Report delivered to FHWA for 3 week review period.
- Final report delivered in compliance with FHWA publication standards
- Mathematical model and sample code
- Executable software, code and user manual
- Paper submitted to conference or journal
- Presentation for symposium, conference or other
- Time to make a decision on two parallel paths as to which is most promising to follow through

 Work planned  
 Work completed  
 Parallel topic

Technology Transfer	Year 2 (4/08-3/09)				Year 3 (4/09-3/10)				Year 4 (04/10-03/11)				Year 5 (04/11-03/12)				Team
	Q1	Q2	Q3	Q4	Q1	Q2	Q3	Q4	Q1	Q2	Q3	Q4	Q1	Q2	Q3	Q4	
<b>(1) Outreach and Databases</b>																	
TT1a: Development and Maintenance of Consortium Website																	UNR
TT1b: Communications																	UNR
TT1c: Prepare presentations and publications																	ALL
TT1d: Development of Materials Database																	UNR
TT1d-1: Identify the overall Features of the Web Application																	
TT1d-2: Identify Materials Properties to Include in the Materials Database																	
TT1d-3: Define the Structure of the Database																	
TT1d-4: Create and Populate the Database																	
TT1e: Development of Research Database																	UNR
TT1e-1: Identify the Information to Include in the Research Database																	
TT1e-2: Define the Structure of the Database																	
TT1e-3: Create and Populate the Database																	
TT1f: Workshops and Training																	UNR

**Deliverable codes**

D: Draft Report  
 F: Final Report  
 M&A: Model and algorithm  
 SW: Software  
 JP: Journal paper  
 P: Presentation  
 DP: Decision Point

**Deliverable Description**

Report delivered to FHWA for 3 week review period.  
 Final report delivered in compliance with FHWA publication standards  
 Mathematical model and sample code  
 Executable software, code and user manual  
 Paper submitted to conference or journal  
 Presentation for symposium, conference or other  
 Time to make a decision on two parallel paths as to which is most promising to follow through

 Work planned  
 Work completed  
 Parallel topic